1

A STUDY OF EXTERNAL PNEUMATIC COMPRESSION FOR THE PREVENTION OF DEEP VENOUS THROMBOSIS

by

ROGER D. KAMM

B.S., Northwestern University
(1972)

S.M., Massachusetts Institute of Technology
(1973)

SUBMITTED IN PARTIAL FULFILLMENT
OF THE REQUIREMENTS FOR THE
DEGREE OF

DOCTOR OF PHILOSOPHY

at the

MASSACHUSETTS INSTITUTE OF TECHNOLOGY

May, 1977

ARCHIVES
MASS. INST. TECH.
AUG 18 1977
LIBRARIES

Signature of Author . . . . . .
Department of Mechanical Engineering, May 18, 1977

Certified by . . . . . May 18, 1977
Thesis Supervisor

Accepted by . . . . . .
Chairman, Department Committee on Graduate Students

A STUDY OF EXTERNAL PNEUMATIC COMPRESSION FOR THE PREVENTION OF DEEP VENOUS THROMBOSIS

by

ROGER D. KAMM

Submitted to the Department of Mechanical Engineering on May 18, 1977 in partial fulfillment of the requirements for the Degree of Doctor of Philosophy.

ABSTRACT

A technique involving intermittent external compression of the legs is used as prophylaxis against the occurrence of thrombi in the deep veins of the calf. The collapse of the veins produced by compression eliminates venous stasis and introduces a pulsatile component to the normally sluggish blood flow during and subsequent to surgery.

A theoretical model was developed to simulate unsteady flow in a system of branching vessels, and was validated by hydraulic experiments using a single, thin-walled latex tube.

The theory was applied to the prediction of venous flow parameters resulting from leg compression with a variety of pressure cycles and modes of pressurization. The results suggest the possibility of considerable improvements over the currently used method by either of two means:

- applying a spatially non-uniform external pressure which is maximum at the ankle;
- compression of the leg with a wave-like motion starting at the ankle and proceeding toward the knee.

Thesis Supervisor: Ascher H. Shapiro
Title: Professor of Mechanical Engineering

ACKNOWLEDGEMENTS

I have many to thank for their help and encouragement during the past several years. Without my friends, this would have been a much more difficult and much less rewarding endeavor.

The advice and assistance I received from Professor Shapiro exceeded by far my expectations of an advisor. His patient guidance helped me to develop the art of applying classroom knowledge to the very tangible needs of scientific research and engineering.

Many other members of the Fluid Mechanics Laboratory helped through their willingness to discuss problems and topics of all sorts and in providing a congenial atmosphere in which to work. In particular, I want to thank Dr. Peter Scherer and Professors Huber, Kenyon, and Dewey for their helpful suggestions along the way. To Dick Fenner, who makes everything work often in spite of our help, to Cindy Polansky who did many things including type this thesis, and to Marj Joss, I owe many thanks. The work of two undergraduates, Charles Kaye and Ping Chiu Hui, is also appreciated.

Support of a less technical sort came from many, but particularly from my wife, Judy, who helped in more ways than could be imagined.

Finally, I am indebted to the NIGMS Training Grant Program in Biomedical Engineering (Grant No. 5TOIGM02136), the National Heart, Lung, and Blood Institute (HEW Grant No. HL17974) and the Fluid Mechanics Program of the National Science Foundation (Grant No. ENG76-08924), all which provided financial support for my studies and research.

TABLE OF CONTENTS

		Page
CHAPTER I.	Overview of the Investigation	5
CHAPTER II.	Introduction	20
CHAPTER III.	Venous Physiology as it Pertains to the Pathogenesis and Prevention of DVT	24
CHAPTER IV.	Theory: Unsteady Flow Through a Network of Collapsible Tubes	39
CHAPTER V.	A Modified Method of Characteristics	58
CHAPTER VI.	Solution by the Method of Finite Differences . . .	71
CHAPTER VII.	Scaling Parameters	83
CHAPTER VIII.	Structural Properties of the Tube	91
CHAPTER IX.	Flow Experiments	108
CHAPTER X.	Numerical Simulation of Flow Experiments	124
CHAPTER XI.	A Model of the Venous Network	149
CHAPTER XII.	Simulating Venous Hemodynamics for the Purpose of Understanding and optimizing the Techniques of EPC	166
CHAPTER XIII.	Recommendations for Future Research	190
References	. . . . .	200
Tables	. . . . .	206
List of Figures	. . . . .	214
APPENDIX A.	Uniform Collapse of a Single Vessel	259
APPENDIX B.	A Similarity Solution for Viscous Dominated Flow . .	266
APPENDIX C.	Computer Program for Numerical Calculations	273
APPENDIX D.	Experiments for Determining the Structural Properties of Collapsing Vessels	295
Biographical Note	. . . . .	304

CHAPTER I:

OVERVIEW OF THE INVESTIGATION

This chapter has been included primarily for the benefit of those who, although interested in the study, would not have time to read the entire document. It presents, in highly condensed form, the most important features of the present investigation avoiding the cumbersome details which are necessary in the more complete form.

Our primary goal is this: to understand the fluid dynamics associated with external compression of the lower leg and to apply this knowledge to the task of optimizing the technique of External Pneumatic Compression for the prevention of Deep Vein Thrombosis (DVT). By way of introduction we first discuss the disease, its relationship to anatomical and hemodynamic effects, and the methods currently being used to prevent it.

Introduction

The incidence of deep venous thrombosis and pulmonary embolism has been increasing in recent years in spite of the development and wide implementation of new preventative procedures. The methods currently used require either administering one of many different anti-coagulants or applying some physical means of enhancing those characteristics of venous blood flow which act to limit thrombus grwoth. Of this latter group the method of External Pneumatic Compression (EPC) has received

considerable attention due to the impressive results of recent clinical studies. In these clinical trials EPC has proven itself to be at least competitive with the more widely accepted anti-coagulant therapies, causing a reduction in the incidence of DVT of at least 60% in most groups of high-risk patients. The success of the method is somewhat surprising when one recognizes that the mechanism by which EPC prevents thrombosis is not at all well understood. The lack of knowledge concerning the relationship between flow properties and the onset of the disease, in addition to the potential of making significant improvements in the method, provide the motivation for this study.

The underlying goal of this work is to develop, from the point of view of a fluid dynamicist, a fundamental understanding of the role of EPC in altering venous flow. The steps taken to reach this goal are, however, applicable to a much broader range of investigations, with implications for any system of branching vessels which, under some circumstances, may undergo collapse. These would include the venous and arterial circulations and the airways of the lung.

Venous Physiology and Deep Vein Thrombosis

To understand the process of thrombus formation, one must first understand the physiology and pathophysiology of normal venous hemodynamics of the lower limb. By anatomical considerations these vessels can be divided into two categories, the deep and superficial veins. Both groups, but primarily the deep veins, are extensively valved, allowing a significant reduction in the mean venous pressure due to

muscular activity when one stands erect. Of particular interest to this study are the muscular veins of the calf because of the tortuous path they follow and because of the large blood volumes they contain which might in some circumstances become trapped. These muscular veins constitute the pumping chamber for the calf muscle pump which, in the case of rhythmic muscular activity, pumps blood from the deep veins toward the heart.

In venous thrombosis the vessels become partially or totally obstructed by a layered thrombus, slowing or preventing completely the normal flow of blood through these veins. Virchow first postulated three conditions which, by themselves or in conjunction with others, are thought to initiate the thrombotic process. These are:

- a lesion in the intima of a vessel involving the endothelium, invoking an inflammatory response;
- venous stasis, i.e., a slowing or other abnormality of blood flow, permitting the adhesion of aggregated platelets to the intima;
- an increase of the tendency of the blood to coagulate due to either chemical or physical processes.

Investigations since the time of Virchow have provided additional evidence to support the role of the latter two mechanisms. In accordance with these concepts the prophylactic methods mentioned above act upon either the fluid dynamic or chemical properties of the blood.

EPC, in very general terms, is thought to act by limiting venous stasis. However, its role in enhancing mixing, shear rates, or even

fibrinolytic activity might be equally or more important. The technique currently used has been "optimized" on the basis of either measurements of femoral vein flow rate or the emptying of a radio-opaque dye from the deep veins. The cycle of external compression has been examined only in view of its rate of pressurization, pressure amplitude, and frequency. The complexity of the overall process, as we shall see, cannot be viewed in such simple terms.

As a guide line for our investigations, we have examined the literature pertaining to the relationship between venous hemodynamics and the onset of thrombosis. The results of our survey are summarized in the following set of criteria which we propose for the prevention of DVT:

- high flow pulsatility
- increased volume flow rate
- increased flow velocity
- increased shear stresses
- clearance of valve sinuses
- mechanical stressing of vessel walls
- complete periodic emptying of the veins.

Our objective is, then, to investigate this set of criteria as they relate to flows in a network of collapsible vessels subjected to periodic external compression.

Theoretical Framework

We start our analysis with the fundamental equations governing fluid flow in a collapsible-distensible vessel with the appropriate boundary conditions. Our hydraulic model (shown in Fig. 1) contains, in a rough sense, all the essentials for a simulation of external compression of the calf veins. Flow originates in a high pressure reservoir (arterial pressure), flows through a high resistance (capillary bed) into the collapsible tube test section (leg veins), and out through a lumped parameter model of resistance, inductance, and capacitance (iliac vein and vena cavae), ending in a constant pressure reservoir (the right heart). The theory permits the rest cross-sectional area, A_0 , wave speed in the unstressed vessel, c_0 , external pressure, p_e , and a friction parameter, C_f , each to vary with distance along a system of symetrically branching collapsible vessels with a variable influx of fluid per unit length, Q_L .

To describe flow in the collapsible segment of tubing we have developed a theoretical model which assumes the flow to be one-dimensional and unsteady, and includes the effect of viscous flow resistance. The form of the flow resistance function is a function of the local flow characteristics and can approximate laminar, turbulent, and developing boundary layer situations.

The governing equations are:

- the mass conservation equation;
- the equation of motion;
- the "tube law" (a functional relationship between the local

cross-sectional area and the transmural pressure).

This set of equations is highly non-linear and hyperbolic and, in complete form, must be solved numerically.

Two cases can be analyzed somewhat more simply, however. These are (1) uniform tube collapse and (2) viscous dominated flow. In the first case, the non-linear partial differential equations can be reduced to a set of ordinary differential equations that can be solved easily by the Runge-Kutta method. The second case can be shown to reduce to an ordinary differential equation with the introduction of the appropriate similarity variable. Each case is useful for providing insights into the more complicated real flow situations.

Although these two approximate solutions are highly instructive, the original set of equations must be solved numerically to simulate non-ideal flows.

Numerical Methods

The numerical method combines the techniques of the method of characteristics and finite differences. The flow field is divided into two parts, the moving boundary is the point of minimum cross-sectional area. Computations upstream of the "throat" (point of minimum area) follow a modified method of characteristics which permits direct calculation of the solution at a set of fixed grid points. Downstream, we use an alternating point, implicit, finite difference formulation into which is incorporated a term to account for head loss due to flow separation in the region of a rapidly diverging vessel wall.

The boundary conditions are as described for the hydraulic model and the initial condition is one of uniform steady flow.

Flow Experiments and the Corresponding Numerical Simulations

The first phase of our investigation was devoted to the development and verification of the theoretical model and the numerical methods. A series of laboratory experiments were conducted using the hydraulic model of Fig. 1 with the test section as shown in Fig. 2. The test chamber is divided into two parts. One part is exposed to the cyclic variations in external pressure while the other is vented to the outside. The two chambers are separated from each other by a flexible plastic pressurizing sleeve. This sleeve surrounds a piece of compliant latex tubing which extends through both sections. This design allowed us to pressurize only the upstream portion of the collapsible tube, thereby eliminating a troublesome boundary artifact at the point of attachment between the downstream rigid duct and the latex tube.

The experiments and the corresponding computer simulations covered a wide range of values for the various parameters of the system including, for example:

- rate of pressurization;
- maximum external pressure;
- fluid viscosity;
- initial flow rate;
- downstream capacitance;
- downstream resistance and inertance;
- downstream pressure.

In general, the agreement between experiment and theory was quite good as seen in Figs. 10-13 in which volume flow rate as measured at the outlet (downstream end) of the collapsible tube is plotted versus time.

The collapse process proceeded consistently in each of the experiments. We can describe the main features of tube emptying qualitatively with the aid of Figs. 3 and 4.

The top graph in Fig. 3 shows a typical pressure cycle, the applied pressure reaching a maximum value of from 20 to 70 mm Hg in a period of up to about 7 seconds. On the bottom of this same figure is a corresponding plot of volume flow rate at the exit of the collapsible tube versus time. The flow rate accelerates rapidly at first, reaching a maximum often before the pressure maximum. It then decays, rapidly at first, but more and more slowly as the tube empties.

Figure 4 shows the successive states of collapse when a vessel is compressed by a spatially uniform external pressure. The process is fundamentally the same for a vein (shown here schematically) as for the latex tube used in our experiments. (a) shows the tube before compression begins. When pressure is first applied, fluid empties from the downstream end forming a narrow throat as seen in (b) which impedes further emptying. (c) and (d) show later stages that illustrate that as the vessel empties the collapsed region propagates upstream more and more slowly.

One of the primary inputs to the model was the functional form of the tube law. A considerable part of our work centered about first

scanning the literature for theory and experiments describing the collapse characteristics of an initially circular or elliptical tube, then conducting a series of experiments on tubes of our own. The procedure for obtaining precise measurements of tube cross-sectional area as a function of pressure is extremely difficult, owing to the necessity of connecting the flexible vessel to rigid supports and to the fact that tubes obtained commercially are highly non-uniform.

A Model of the Venous System

The problems associated with obtaining a tube law for latex tubes are relatively minor, however, compared to those for estimating the characteristics of a vein in its normal environment. Here again, when beginning to formulate a model of the physiologic system, we looked first to the literature, then used our fundamental understanding of the process of vessel collapse to fill in the considerable gaps. From the literature we found information, mostly for veins filled to a positive transmural pressure, from such diverse sources as plethysmography, radiology, and experiments on excised veins. Although much of this information was highly qualitative and somewhat contradictory, we were able to construct from it a tube law for the region of pressures greater than approximately zero transmural pressure. We managed to extend these results to negative pressures by using estimates of the vessel wall structural properties and an approximate model of the effect of surrounding tissue, thus completing the tube law.

The remaining features of the physiologic model consist of the spatial variations in total vessel cross-sectional area, A_0 , wave speed, c_0 , a friction parameter, C_f , and the distribution of tributary inflow per unit length, Q_L . A_0, c_0, and C_f are each plotted as a function of distance along the leg in Fig. 5. A_0 is the sum of the areas of all the vessels at each location at normal physiologic pressures. c_0 is a measure of the stiffness of these vessels, again at normal physiologic pressures. C_f takes into account the difference between flow resistance in a single tube and that in a system of vessels having the same total cross-sectional area. Introducing this friction parameter allows us to use our single tube model to predict flows in a symmetrically branching system.

The need for C_f was found through scaling arguments in which we compared the normalized form of the governing equations for a two-vessel junction and for a single tube having the same total cross-sectional area and flow rate. We can see why C_f was necessary if we compare the pressure drop per unit length in these systems: the bifurcated system will have a higher viscous pressure drop unless some parameter (C_f) is introduced to the term representing viscous flow resistance in the single tube analogue.

Venous Flow Simulations

The simulations of venous flows can be classified in terms of the pressure cycle used in each case. The three categories are illustrated in Fig. 6. (A) shows the current method which we call the uniform

pressure application. As shown in the left-hand plot, the applied pressure reaches a maximum in a period of several seconds and is held there for a period of 5-10 seconds, then released. The spatial distribution is plotted on the right. Pressure is uniform over the calf but falls off at the knee at the edge of the pressurizing cuff. The pressure falls gradually because of the smearing effect of the muscular tissue surrounding the veins.

Chart (B) illustrates a linear pressure application. Again the applied pressure rises, then remains constant. The spatial distribution is different, however. The pressure drops linearly from a maximum value at the ankle to zero at the knee. This type of pressurization was motivated by the results of the investigation of uniform vessel collapse mentioned earlier. The advantage of applying pressure in this fashion is that it helps to eliminate the narrow throat which forms at the knee in the case of uniform compression.

The third means of compression [case (C)] is a wave-like pressure application. Again, the pressure-time curve can either be the same as in (A) and (B), or might rise instantaneously to the maximum value. However, in contrast to the previous methods, the spatial distribution of pressure varies with time. The front of the pressure distribution propagates from the ankle toward the knee, effectively milking the blood from the veins as it moves.

Using the criteria mentioned earlier for optimal protection from DVT, we simulated each of these three modes of compression, finding distinct differences. As in the single tube experiments of the same type,

when the system of veins was pressurized as in (A) with a uniform external pressure, a highly constricted throat soon developed. Due to the high flow resistance at the throat and the constant influx of blood from the upstream points, it was observed that much of the system never did empty. Some improvements were made by either reducing the rise time of the cycle or increasing the maximum pressure, but the mode of collapse remained relatively unchanged.

One of the main objectives in simulating the linear pressure application [Case (B)] was to explore various means of eliminating the restrictive throat. This method was highly successful and resulted in much more rapid and complete emptying of the entire system. The peak values of volume flow rate, flow velocity, and shear rate were much higher than in Case A and the peak values were more uniform throughout most of the system.

The wave-like pressure application [Case (C)] had results quite comparable to those in (B). The collapse proceeded at the same speed as the front of the compression wave, except at the highest wave speeds. Emptying was accomplished, then, in the time required for the wave to travel from the ankle to the knee. With a pressure wave propagation speed of 50 cm/sec (the highest simulated) the peak flows were as much as 10 times as great as those achieved with the current cycle. If further flow enhancement is desired, this method could be extended to still higher wave speeds with yet greater induced flows.

Our most significant observations are summarized below:

- The current method of spatially uniform compression along the calf causes a necked-down region at the edge of the pressure cuff which severely impedes further emptying of the vessels located distal to the point of collapse.

- Using the method of uniform compression the effectiveness of the method generally increases with decreasing rise times.

- The effectiveness also improves as the applied pressure is increased, but only marginally for pressures greater than 30 mm Hg.

- The upstream constriction can be eliminated by either of the two newly proposed methods: linear or wave-like pressure application.

- With either method, flow rates, flow velocities, and shear rates at points inside the calf can be increased significantly above what is attainable with uniform compression.

- Both new methods provide collapse of the entire deep venous system.

- The time required to empty the system can be reduced to approximately 1 to 2 seconds using these methods.

- In the linear mode of compression, the method is made more effective either by increasing the maximum applied pressure or by reducing rise time.

- For wave-like compression, both Q_{max} and u_{max} increase with increasing pressure wave propagation velocities.

- Filling time might be reduced by applying an occlusion cuff at the thigh during the refilling phase of the cycle.

- The mean flow rate through the calf might actually be increased if $\frac{p_e}{p_v}\frac{t_c}{t_R} < 1$.

Proposals for Future Efforts

In view of these findings, we propose that either the linear or wave-like pressure application be subjected to the following trial procedure. Following construction of a compression device and pressurizing sleeve capable of reproducing these cycles, these methods should be tested on volunteers using indirect means of evaluating the theoretical predictions. These methods might include plethysmography or measurements that could be incorporated into routine venographic or surgical procedures. With the appropriate refinements, the method might then be subjected to an extensive clinical trial comparing it with one of the more successful anti-coagulant methods.

The theoretical background developed here lends itself well to an investigation of a variety of processes occurring in collapsible tube systems. Of the possible research areas, two seem particularly appropriate. The first involves a method of circulation assist that acts through periodic collapse of the arteries by means of external leg compression. The method, called External Cardiac Assist, works on a principle similar to the aortic balloon pump and could, if perfected, provide

an effective non-invasive means of providing the same patient benefit.

The lung airways constitute another system of vessels which may, under some circumstances, collapse due to elevated external pressures and/or reduced internal pressures. An understanding of how and why airway collapse occurs in the lung could lead to the development of useful new diagnostic methods.

As mentioned earlier, this has been a brief survey of those topics which are covered in more detail in the following text. The reader is encouraged to refer to the more complete version for any topic of particular interest or for further clarification.

CHAPTER II:

INTRODUCTION

A surprisingly large number of people are unaware of the high incidence of Deep Vein Thrombosis (DVT) or of the fact that thousands die each year due to its complications. The risks associated with DVT are well recognized by physicians, however, and as a result, nearly all hospitals take some precautionary measures in patients undergoing surgery which requires either long periods of anesthesia or extended post-operative bedrest.

DVT is the development and growth of red thrombi in the deep veins of the leg. The thrombi, if they remain in these vessels, constitute an impediment to normal perfusion of the limb and can eventually lead to a condition referred to as phlebitis or thrombophlebitis which is characterized by localized inflammation and edema. Although this condition itself is sufficient justification for the physician's concern, an even greater danger is posed by the threat of pulmonary embolism (PE). This occurs in the event that one of these leg thrombi dislodges and travels through the heart to the pulmonary artery where it occludes blood flow to the lung.

By various estimates as many as 50,000[1] - 150,000[2] individuals die each year due to PE. Approximately 73-90% of these thrombi originate in the deep veins of the lower leg.[3,4] It has been suggested that the actual number of deaths directly attributable to PE is much higher than this figure indicates. By any accounting procedure, the cost of DVT in

terms of loss of life, severe discomfort, and monetary expense is very significant. And, indications are that, in spite of increased efforts to protect against DVT, its incidence rate has been rising steadily. The most probable cause of the increasing mortality rate is the expanding list of inflictions which can now be treated surgically and, as a direct result, the increasing probability that any one individual will undergo surgery of some kind.

Because of its recognized prevalance, particularly among surgical patients, various prophylactic procedures have been developed over the years to combat venous thrombosis. In very broad terms, these methods can be thought of as either physical or chemical in nature. The physical methods act by altering the sluggish blood flow through the deep veins (often referred to as venous stasis) which accompanies surgery and the imposed period of immobility afterward. Chemical methods act on blood chemistry to decrease the tendency of the blood to coagulate in the veins. The advantages and disadvantages of both of these categories will be described in detail in Chapter III. In short, some methods from each classification have met with considerable, but not complete, success, and are not altogether free of other complicating factors.

One of several physical methods of prophylaxis is the technique of External Pneumatic Compression (EPC) of the patient's lower leg by means of an inflatable boot or cuff. (Again, more details will be provided in Chapter III.) The method, although already quite effective, may not be providing optimum protection from DVT given the criteria that have been

set forth in past investigations.

Our main objective in this study is to analyze current methods and, by way of careful analysis, suggest alternate means of limb compression which may prove to be more optimal for the prevention of thrombosis. The steps along the way are goals in themselves and are enumerated below:

- develop a useful model of venous blood flow under the application of externally-applied pressures;
- use this model to aid in understanding the role of EPC in preventing DVT;
- investigate normal physiologic venous flows in rest and exercise;
- apply these tools to an analysis and optimization of the technique of EPC;
- propose potential improvements in the method which can be tested clinically.

The approach is as follows. Our first step was to develop a model of the processes occurring in the veins during intermittent external compression. We conducted a series of hydraulic experiments in the laboratory designed to simulate the dynamics associated with unsteady flow in a collapsible vessel such as the veins of the lower leg. We next developed a completely general theoretical description that could be applied both to the experimental apparatus and to the system of veins, the simulation of collapsible tube flows being performed by numerical procedures. Then, as a means of evaluating the range of validity of the various assumptions and approximations made in the development of the theoretical model, we applied our model to the task of simulating the experiments. Having

learned the capabilities and limitations of the theory, we turned to the physiologic case.

The model of the venous network used in the simulations is described in Chapter XI. It was necessarily a very approximate model owing to the many unknown characteristics of this part of the circulation. We subjected this model of the venous system to a variety of types of pressure cycles in an attempt to determine which of the many possibilities was most successful in satisfying the set of criteria set forth in the next chapter.

Our conclusions, which can be found in Chapter XII, offer a sharp contrast to the current method. It is our hope that, through the additional steps discussed in Chapter XIII we can test and further refine our recommendations and provide a much improved method of protection against DVT.

CHAPTER III:

VENOUS PHYSIOLOGY AS IT PERTAINS TO THE PATHOGENESIS AND PREVENTION OF DVT

The purpose of this chapter is to acquaint the reader with those aspects of venous anatomy and physiology which are relevant to the initiation and growth of deep vein thrombi. These basic concepts lead to the several theories which have been proposed to explain the relationship between venous hemodynamics and thrombosis. An understanding of the underlying mechanisms aids us in establishing a more complete set of criteria which can, in turn, be used to guide us in optimizing the efficiency of any preventative technique. We begin by describing the complicated anatomical configuration of the deep veins of the lower leg.

Venous Anatomy of the Lower Limbs

The veins of the leg, particularly those of the lower leg, contain numerous valves (spaced at from 2 to 4 cm) permitting blood to flow only in the proximal direction and preventing the hydrostatic head from exerting its full effect when one stands erect. These veins can be divided into three general categories: (1) deep veins, those well below the surface of the calf; (2) superficial veins, those running outside of the leg muscles just beneath the surface of the skin; and (3) perforating or lateral veins, those which connect the veins of the deep and superficial systems. The valves within the laterals generally permit flow only in the direction of the deep veins.

In addition to their different anatomical location, deep veins also differ from superficial veins in terms of their wall structure. The walls of the deep vessels contain proportionately more collagenous and less smooth muscle tissue than their superficial counterparts.[5] The wall-to-diameter ratio is smaller in deep veins, producing a vessel which has relatively little tone and whose walls might be considered inextensible when undergoing collapse. For this reason the deep veins can be thought of as passive vessels which, in the range of small positive and negative transmural pressures, are composed of an essentially inextensible but very flexible material. It follows that the pressure-area relationship for these vessels would be strongly influenced by the degree of tethering to surrounding tissue.

The muscular veins are distinguishable from other deep veins because of significant structural differences. Although it has been reported that they contain no valves,[6] they actually are valved nearly as extensively as are other leg veins.[7-9] They are often tortuous and may vary considerably in cross-sectional area. Blood contained in these muscular veins must flow through a series of dilated sinuses before emptying, usually into the proximal end of the posterior tibial veins. These sinuses can be as large as 1 cm in diameter and 5 cm in length[10] and, therefore, contain a significant portion of the total venous blood volume of the leg.

The course of blood flow is generally in the direction of the deep veins and toward the heart. Due to the interconnecting nature of, for example, the posterior tibial and muscular veins, it is thought that blood may flow into the muscular veins from the distal portion of a deep

vein and back into the same vessel at a more proximal point.[11] The tibial and peroneal veins generally occur in pairs which have numerous cross-over points. The details of the geometrical configuration of these deep veins are subject to a large degree of variability.

Many factors can alter the flow of blood through this network of interconnecting vessels. It can be affected by either external or internal influences and the effect can be either desirable, as in the case of the normal functioning muscle pump, or undesirable, as in varicose veins, valve incompetency, or thrombosis.

Pressures in the calf veins vary greatly depending on posture and muscle activity. The pressure drop between the large veins of the calf and the right heart due to wall shear stresses is between 2 and 10 mm Hg by calculation[12] and measurement.[13] A change in posture, however, from supine to erect, can raise venous pressure in the calf to nearly 100 mm Hg due to the effect of hydrostatic pressure gradients.[13]

These pressures must be viewed in relation to the intramuscular pressure surrounding the vessels which can range from several mm Hg when the muscles are relaxed to 250 mm Hg under maximal muscle contraction.[14] These large pressures which act on the muscular veins form the basis of the "muscle pump" which serves both to lower the mean venous pressure in the leg veins during exercise and to alter the amount of blood flow perfusing the calf muscles. Because the muscle pump is one of the most significant natural means of prophylaxis against DVT, we will consider it in some detail.

Functioning of the Calf Muscle Pump

As an aid in understanding how the muscle pump functions, we can think of the vessels of the lower leg as being divided into several parts: a pumping chamber, inlets for fluid supply from a high pressure source, and one or more discharge ducts leading into a low pressure system. The pumping chamber consists of the intramuscular veins and venules and the intermuscular veins, primarily those of the soleus and gastrocnemius muscles. Fluid flowing into the pump may enter either directly from the arterial circulation via the capillaries in the calf, or from the veins perfusing the ankle and foot. Upon muscular contraction pressures inside the pumping chamber rise considerably and, aided by the venous valves, blood is discharged primarily through the popliteal vein by way of the posterior tibial and peroneal veins. As noted, intramuscular pressures as high as 250 mm Hg have been measured under extreme muscular contraction. Normal walking, however, generally produces pressures on the order of only 100 mm Hg. The stroke volume of this pump is difficult to estimate and no doubt varies considerably depending on the degree of muscle development. It is known, however, that up to 130 mm[15] of additional blood can be accommodated in the calf and this entire volume could conceivably be expelled during a single contraction.

Mean venous pressures in veins considered to lie within the pumping chamber tend to fall during rhythmic exercise by more than 50 mm Hg, accompanied by a decrease in calf volume.[15] Thus, assuming no inlet flow restrictions such as might be caused by muscular constriction of arterioles, there exists at least one mechanism tending to increase the

mean A-V pressure gradient and consequently the total limb perfusion rate. Allwood[16] investigated this mechanism by applying an intermittent compression to the calf while measuring mean flow rate at the foot. In healthy individuals in the sitting posture using a cycle of 1 sec of pressurization to 110-120 mm Hg and 4 sec rest applied to the calf only, he observed an increase in mean flow rate of approximately 60%. This mechanism is explored in some detail in Chapter XII.

One particularly thorough investigation of the calf pump was conducted by Arnoldi *et al.*[11] In a series of well-controlled experiments on healthy subjects, simultaneous recordings of venography (both A-P and lateral views) and venous pressures were obtained during systematically performed leg exercise. Observations were made with the subject inclined 60° from the horizontal during a series of four or five muscular contractions of one-second duration at one-second intervals.

They observed that during the first compression, the muscular veins emptied completely, apparently into the tibial veins. The tibial veins themselves decreased slightly in cross-sectional area, the greatest degree of collapse occurring at the proximal end. The popliteal vein underwent an increase in diameter and internal pressure, a fact attributable to the increased blood flow entering this vein from the collapsing regions. Other veins experienced more modest pressure increases and, in general, increased in cross-sectional area if located outside the "pumping chamber," and decreased if located inside.

Upon relaxation for a period of only one second, the muscular veins returned nearly to their original cross-sectional areas, filling primarily

from the distal end of the posterior tibial veins. It appeared, therefore, that there was a sort of shunting action in which the blood, rather than passing directly up the posterior tibial veins, flowed out into the distal portions of the muscular veins during relaxed states, and into the proximal posterior tibial veins during muscular contraction. In addition to this shunting action, the muscular veins are constantly fed by capillary blood flow from regions in the calf itself. These two blood sources apparently provide for extremely rapid filling of the muscular veins, at least following short periods of compression.

The effectiveness of the muscle pump in removing blood from the muscular veins was demonstrated radiographically by Nicolaides *et al.*[17] Measuring the clearance time of dye from the soleal and tibial veins they observed that

(i) resting clearance from the tibial veins was much more rapid than from the soleal veins, and

(ii) that active plantar flexion against a resistance decreased soleal clearance times from 9.6 minutes to the time of two plantar flexions.

We provide this background material on the muscle pump because of the apparent success of this pumping action in preventing the onset of thrombosis. We should stress "apparent" because it cannot be proven that the reason most individuals who are healthy and active do not develop thrombosis is due to the continuous flushing of the deep veins provided by the muscle pump. During sleep, for example, the pump does not function, yet the risk of thrombosis is still very low. Most physicians

will agree, however, that the muscle pump is one very important mechanism and certainly plays a role in preventing thrombosis. The relationship between fluid dynamic effects and thrombosis will be explored in the next section.

Deep Vein Thrombosis

As noted in the Introduction, the consequences of DVT and the resulting pulmonary emboli are extremely lethal and the morbidity associated with it has shown a consistent increase in recent years. This trend can be partly attributed to the rise in the range of surgical procedures now possible, particularly in the area of elective surgery. During this same period, the extent of prophylaxis has also risen but obviously without total effectiveness.

The thrombi which, when dislodged from their source and carried through the circulation to the lung to produce a pulmonary embolism, most often originate in the deep veins of the leg, and especially the lower leg. Many factors have been found that increase the tendency for DVT but the process by which the thrombin clot first forms and how external factors affect its formation are still unclear.

The actual cause of venous thrombosis has been a topic of much debate and is still not entirely understood. It was Virchow[18] who first postulated the three conditions which, by themselves or in conjunction with others, might initiate the thrombotic process. These are:

(1) a lesion in the intima of a vessel involving the endothelium, invoking an inflammatory response;

(2) venous stasis, i.e., a slowing or other abnormality of blood flow, permitting the adhesion of aggregated platelets to the intima;

(3) an increase of the tendency of the blood to coagulate due to either chemical or physical processes.

Venous thrombosis, although not exclusively a disease of the thigh and lower leg, most often originates there.[3,4] Six primary sites have been identified by Sevitt[19] where thrombi are most likely to be found. These include the following:

(1) intramuscular calf veins (soleal plexus);

(2) posterior tibial veins;

(3) popliteal vein (particularly just below the adductor ring at the site of a large valve);

(4) at the termination of the deep femoral vein;

(5) common femoral vein;

(6) iliac vein.

Among these the soleal and posterior tibial veins are the most common locations. Thrombi tend to originate at particular anatomical points such as in valve pockets, vessel junctions, or dilated sinuses. Each of these have in common either lower mean flow velocities or stagnated or separated flow regions.

The soleal veins are particularly prone to stasis because of their complex structure. The situation is further complicated when the patient is in the supine position and gravity tends to pool the blood in these sinuses causing filling and emptying to take place very slowly.

There seems to be little agreement on the pathogenesis of venous thrombosis. One likely schema,[20] however, postulates a local accumulation of thrombin due either to blood stagnation, microscopic lesion, or abnormalities in blood chemistry. This leads to the formation of platelet aggregates which, in slowly flowing blood, can settle out much more rapidly than non-aggregated platelets. Associated with platelet aggregation is a release of platelet contents which further promotes platelet adhesion and initiates the fibrinogen-fibrin process. Once initiated in this manner, the process can continue, producing the successive layers of fibrin and platelets which comprise most vein thrombi. With continued growth, the thrombi become long tubular structures which exhibit this layered construction throughout.

Numerous factors have been associated with a higher risk of venous thrombosis and are discussed extensively in the literature. A list of predisposing factors and literature reference is provided in Table 1. The relationship between these factors and the initial thrombotic response is, in general, poorly understood. Many, however, can be directly related to one of the three primary causes expounded by Virchow. In addition to those listed, other correlations have been proposed but the evidence is often inconclusive or contradictory.

Associated with many of these predisposing factors is the possible existence of purely anatomical effects on the blood flow. And, as it was shown earlier, the locations and postulated mode of thrombus formation also indicate strong fluid mechanical effects.

Sevitt[22] has stated in a recent article that, in the development of

venous thrombi, "venous stasis and eddying of flow are the main predisposing mechanisms." The presence of a trapped or slow-moving eddy, as might be found in valve sinuses, at junctions or at points of sudden area change can have several deleterious effects. First, since dilution with fresh blood takes place over a very long time scale, the clearance of clotting factors or activated products which may be present in the blood is greatly reduced. Also, the endothelial cells are likely to become undernourished and may, as a result, release some of their contents which are capable of initiating thrombus growth. Experiments have shown that in platelet-rich plasma, stirring or mixing the solution accelerates aggregation[20] and the circulating eddy may have the same effect. It has also been postulated that eddying promotes wall deposition, bringing any activated complexes present in the blood in contact with the vessel wall where they can accumulate over time.

The effects of venous stasis are quite similar to those just discussed in relation to trapped eddies. The slowing of blood flow, particularly at stagnation points, has the effect of:

(1) preventing the removal by the liver of activated clotting factors released locally or brought from other sites;

(2) slowing the arrival of inhibiting agents, such as anti-thrombin and ADP-ase;

(3) permitting ADP (a platelet aggregation inducement) to accumulate locally;

(4) producing an hypoxic condition in the endothelium;

(5) increasing particle deposition on vessel walls at specific points;

(6) increasing the degree of rouleaux formation and platelet adhesiveness;

(7) silting into valve sinuses of platelets, leucocytes, and red blood cells resulting in a local accumulation of ADP.

This evidence strongly suggests that the fluid dynamic effects play a significant, if not dominant role in all stages of thrombus development, and prevention of stasis would seem to be of definite prophylactic value.

There are many methods purporting to increase either the velocity or pulsatility of blood flow in the legs. Among these methods are electrical stimulation, leg wrapping, elevation of the legs, exercise, and external pneumatic compression (EPC). Each of these techniques has been evaluated by numerous clinical studies and do provide varying degrees of protection, but are far from being totally successful. The next section provides a discussion of the more popular methods of prophylaxis and a critical evaluation of each based on published clinical results.

Methods of Prophylaxis Against DVT

Primarily because no preventative measure has been proven to be entirely successful, there is little agreement among physicians as to the "best" method. Those which have received considerable attention in recent years and which are commonly used can be divided into two general categories based on their mode of attack.

The first category includes the various types of anti-coagulant therapy. These methods are probably the most widely used and accepted means of prophylaxis for those classified as high-risk patients.

Although each of the various anti-coagulants used act in a slightly different fashion, the objective is the same: to alter the chemical composition of the blood in such a way as to lessen the tendency of the blood to coagulate. These drugs normally act by inhibiting or blocking one or more of the reactions in the complex process of thrombus growth. One clear objection that can be raised to this type of therapy is that, while inhibiting the growth of deep vein thrombi, these drugs also interfere with the normal clotting process and as a result, patients undergoing anti-coagulant therapy run the additional risk of hemorrhage or other bleeding complications accompanying surgery. For these reasons treatment cannot begin prior to surgery which further compromises the overall effectiveness of the technique. Several of the anti-coagulants used are listed in Table 2 along with the clinical tests in which each has been evaluated. Of those listed, low dose heparin is probably the most effective and has been the focus of many of the more recent studies.

The second category of preventative methods which are collectively referred to as "physical" methods, act by altering the behavior of blood flow in the veins. These methods range from simple bandaging or elevation of the lower limbs to electrical stimulation of the calf muscles. Several of these are listed along with the corresponding clinical trials in Table 2. They all aim at some rather vague goal of "eliminating venous stasis" and all that that implies. Possibly one reasons these methods have often been overlooked by physicians is that the relationship between first, venous hemodynamics and thrombus growth and second, the physical method used and the accompanying changes in venous blood flow, are poorly understood and have not been carefully and completely

examined. The connection between treatment with anti-coagulants and decreasing the tendency toward thrombosis is clear; the connection between, for example, elevating a patient's leg and inhibiting thrombus growth is not. In fact, one might argue, and justifiably so, that some of these methods might actually impede blood flow and thereby worsen the tendency toward thrombosis.

For whatever reasons, these methods have in general been slow to find acceptance. One possible exception is the use of elastic stockings which, in spite of recent publications[36] disclaiming the value of the procedure, continues to be common practice in many hospitals, particularly among patients with only a slight danger of developing DVT. A recent investigation[38] has determined that, with careful application of the elastic stockings, flow velocity can actually be increased somewhat. But it is doubtful that the procedure is performed with the necessary care in routine situations.

One of the physical methods listed in the table shows considerable promise as evidenced by the highly successful clinical trials. This is the method of External Pneumatic Compression (EPC). Unlike electrical stimulation which has also met with some success, EPC involves little patient discomfort and can be performed continuously, beginning even before surgery, on nearly all patients.

The procedure followed and the details of the technique of EPC differ depending on the individual hospital and the commercial device being used. However, we can describe the method in rather general terms which would apply almost universally. Treatment would begin just prior to surgery

by placement of an inflatable plastic boot or cuff on the patient's lower legs covering the calf and, in some cases, the foot as well. By means of periodically inflating this boot, the blood flow through most of the leg veins becomes highly pulsatile, creating a situation in these vessels which, in many ways, mimics the action of the muscle pump. Typically, this cycle consists of a rapid pressure rise from zero to 30-50 mm Hg, after which the pressure is held constant for approximately 10 seconds. The pressure is then released and a rest period of about 45 seconds follows before the next pressure pulse is applied.

The means by which intermittent external compression prevents thrombosis can only be postulated. However, several likely mechanisms have been proposed. These mechanisms can be thought of in terms of the set of criteria for optimal protection from DVT listed below.

- high flow pulsatility;
- increased volume flow rate;
- increased flow velocity;
- increased shear stresses;
- clearance of valve sinuses;
- mechanical stressing of the vessel walls;
- complete periodic emptying of the vessels.

Each criterion can be seen to relate directly to one or more of the hemodynamic effects mentioned before which influence thrombus initiation and growth, with the possible exception of mechanical stressing of the vessel walls. Recently, Knight[39] has shown that intermittent compression of the arm can actually lead to a reduction of DVT in the

leg veins. The only obvious conclusion one might draw from this observation is that fibrinolytic activity is somehow enhanced by compression and may be related to a mechanical stressing or to bringing the opposing walls of a vessel in the arm into contact with each other. This may be only one of several mechanisms which give rise to the effectiveness of the technique, but it is certainly one which deserves further investigation.

It should be stressed that the stage of knowledge concerning the pathogenesis of thrombosis and how it relates to the various fluid mechanical or mechanical events accompanying EPC are poorly understood. The results of the study presented in this thesis provide a necessary, but incomplete picture of the role of EPC in preventing thrombosis. Additional research into the intricate biochemical relationship between local fluid dynamics and thrombus growth is needed. Our approach has been to first identify those flow properties which, based on present knowledge, are likely to affect the onset of thrombosis, then to carefully and systematically explore different pressure cycles and modes of pressurization in terms of their effect on these properties. We begin this process, in the next chapter, by developing a theoretical model for flow in a collapsible tube.

CHAPTER IV:

THEORY: UNSTEADY FLOW THROUGH A NETWORK OF COLLAPSIBLE TUBES

In this chapter we derive a theoretical description of unsteady flow through a collapsible vessel or a symmetric network of vessels. The expressions are written in the most general form in all cases so as to permit any of the following variations:

(i) variable cross-sectional area of the unstressed tube, A_0 ;

(ii) variable wave speed, c_0 (and consequently variable tube stiffness);

(iii) variable external pressure, p_e ;

(iv) symmetric branching.

The results are used in two ways. In Chapters V and VI a numerical scheme is described which permits the solution of the governing equations yielding a detailed picture of the flow behavior for any given set of parameters. Secondly, in Chapter VII, we determine the important scaling parameters of the system to aid in the design of an experimental model which, although lacking the detailed characteristics of the real venous system, will exhibit the correct general flow features.

The Theoretical Model

The proposed model consists of one or more collapsible vessels which are subjected to external pressurization. The complete theoretical description consists of the equations governing flow in the

collapsible vessel, two boundary conditions, an initial condition, the prescribed variations in p_e , A_0 and c_0 , and what we call a tube law, which is simply a relationship between the transmural pressure and the local cross-sectional area.

The boundary and initial conditions are designed to accurately model the actual physiological environment they are intended to represent. Briefly, they are:

(1) Upstream boundary condition: A high pressure reservoir kept at a constant pressure is located at the upstream end of the system. It drains through a linear resistance, into the collapsible vessels.

(2) Downstream boundary condition: Fluid drains through two rigid vessels having both resistance and inertance which are separated by a capacitance tank. Fluid eventually empties into a constant pressure reservoir.

(3) Initial condition: Initially there exists a steady flow of fluid determined by the pressure drop from inlet to outlet and the resistances in between.

The Governing Equations

The one-dimensional equations governing flow in the collapsible duct are obtained by applying the principles of conservation of mass and momentum to a small control volume of length dx . Mass continuity states that the change in flow rate over a distance dx is balanced by the decrease in volume of the element. This is written as

$$\frac{\partial(uA)}{\partial x} + \frac{\partial A}{\partial t} = Q_L \quad , \tag{1}$$

where u is the mean flow velocity and A is the cross-sectional area. Q_L represents the added flow rate per unit length which in this model can be thought of as passing through the vessel walls.

Denoting the internal pressure by p, and the external pressure by p_e, the equation of momentum conservation can be expressed as follows:

$$\rho\left(\frac{\partial u}{\partial t} + u\frac{\partial u}{\partial x}\right) + \frac{\partial}{\partial x}(p - p_e) + \frac{\partial p_e}{\partial x} + \frac{P\tau_w}{A} = 0 \quad . \tag{2}$$

Here, τ_w is the wall shear stress acting in the negative x-direction, and P is the wetted perimeter.

For the purpose of defining characteristic curves which we will eventually need, it is useful to introduce the wave speed, c, into these equations. The relationship between c and the other variables is obtained by considering the propagation of an infinitesimal pressure wave in a flexible walled tube of arbitrary cross-section. Without loss of generality we can assume that the incompressible fluid is initially at rest. Associated with this pressure wave will be a change in cross-sectional area as illustrated below.

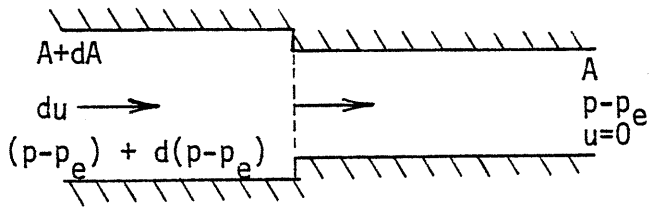

We can effectively freeze the motion of this wave by adopting a reference frame traveling to the right at the same speed, c , as the pressure pulse. With respect to this new frame of reference, the momentum equation for a control volume including the area transition (neglecting the effects of friction, viscoelasticity of the wall, and longitudinal bending) can be written as

$$A\, d(p - p_e) = \rho c A\, du \quad .$$

Combining this with the continuity expression across the transition,

$$\frac{du}{c} = \frac{dA}{A}$$

yields a relationship which will serve as the definition of c ,

$$c \equiv \left[\frac{A}{\rho} \frac{d(p - p_e)}{dA} \right]^{\frac{1}{2}} \quad . \tag{3}$$

Equations (1)-(3) can be made dimensionless by substitution of the normalized variables listed below:

$$U \equiv \frac{u}{c_0(0)} \quad ; \qquad \alpha \equiv \frac{A}{A_0(\xi)} \quad ; \qquad \xi \equiv \frac{x}{L}$$

$$\tau \equiv \frac{t c_0(0)}{L} \quad ; \qquad P \equiv \frac{p - p_e}{K_p(\xi)} \quad ; \qquad C \equiv \frac{c(\xi)}{c_0(\xi)} \tag{4}$$

$$Q \equiv \frac{Q}{A_0(0) c_0(0)} = U\alpha \frac{A_0(\xi)}{A_0(0)} \quad .$$

Introducing these variables into Eq. (2) and dividing the result by $\rho c_0^2(0)/L$ yields

$$\frac{\partial U}{\partial \tau} + U\frac{\partial U}{\partial \xi} + \frac{K_p(\xi)}{\rho c_0^2(0)}\frac{\partial P}{\partial \xi} + \frac{P}{\rho c_0^2(0)}\frac{dK_p(\xi)}{d\xi} + \frac{1}{\rho c_0^2(0)}\frac{\partial p_e}{\partial \xi} + \frac{C_f(\xi)PL}{\rho c_0^2(0)A_0(\xi)}\frac{\tau_w}{\alpha} = 0 \quad . \tag{5}$$

Here $C_f(\xi)$ has been introduced to the friction term. For the present we can assume that $C_f(\xi) = 1$. The reason for its inclusion will be revealed at a later time in Chapter VII.

We can eliminate $\partial P/\partial \xi$ and K_p from this expression by means of the following relationships derived with the aid of Eq. (3):

$$\left(\frac{\partial P}{\partial \xi}\right)_\tau = \frac{dP}{d\alpha}\left(\frac{\partial \alpha}{\partial \xi}\right)_\tau = \frac{C^2}{\alpha\beta}\left(\frac{\partial \alpha}{\partial \xi}\right)_\tau \quad .$$

Then,

$$K_p(\xi) = \rho c_0^2(\xi)\beta \quad \text{where} \quad \beta \equiv \left(\frac{d\alpha}{dP}\right)_{\alpha=1} \quad .$$

Thus, we can write the momentum equation in final form as

$$\frac{\partial U}{\partial \tau} + U\frac{\partial U}{\partial \xi} + \left[\frac{c_0(\xi)}{c_0(0)}\right]^2 \frac{C^2}{\alpha}\frac{\partial \alpha}{\partial \xi} + 2P\beta\frac{c_0(\xi)}{c_0^2(0)}\frac{dc_0(\xi)}{d\xi} + \frac{1}{\rho c_0^2(0)}\frac{\partial p_e}{\partial \xi} + C_f(\xi)F = 0 \quad , \tag{6}$$

where $F \equiv \dfrac{[PL/\rho c_0^2(0)A_0(\xi)]\,\tau_w}{\alpha}$.

The continuity equation can be normalized in a similar manner and reduced to

$$\frac{\partial \alpha}{\partial \tau} + \frac{\partial (U\alpha)}{\partial \xi} + U\alpha \frac{1}{A_0(\xi)} \frac{dA_0(\xi)}{d\xi} - Q_L \frac{L}{c_0(0)A_0(\xi)} = 0. \quad (7)$$

In addition to Eqs. (6) and (7) we have the normalized form of (3),

$$C^2 = \alpha\beta \frac{dP}{d\alpha} \quad , \quad (8)$$

and a known relationship between P and α which, for the present discussion, can be assumed to be expressed as

$$\alpha = \text{fn}(P) \quad . \quad (9)$$

The functional dependence of α on P is actually quite complicated and is left as the topic of Chapter VIII. For now, we turn to a derivation of the equations for the boundary and initial conditions.

Upstream Boundary Conditions. As mentioned in the introductory remarks, the supply of fluid entering the collapsible network (at ξ=0) flows from a high pressure reservoir at a pressure, p_A , through a linear resistance R_A . This represents, for example, the total resistance of all the vessels of the capillary bed. Flow is governed by the equation:

$$(uA)_{\xi=0} = \frac{p_A - p_{\xi=0}}{R_A} \quad .$$

In terms of normalized quantities this can be written as

$$(U\alpha)_{\xi=0} = \left[\frac{p_A - K_p(0)P - p_e}{c_0(0)A_0(0)R_A} \right]_{\xi=0} \quad . \tag{10}$$

Downstream Boundary Condition. The system into which the collapsible tube empties can be represented by the following lumped parameter model:

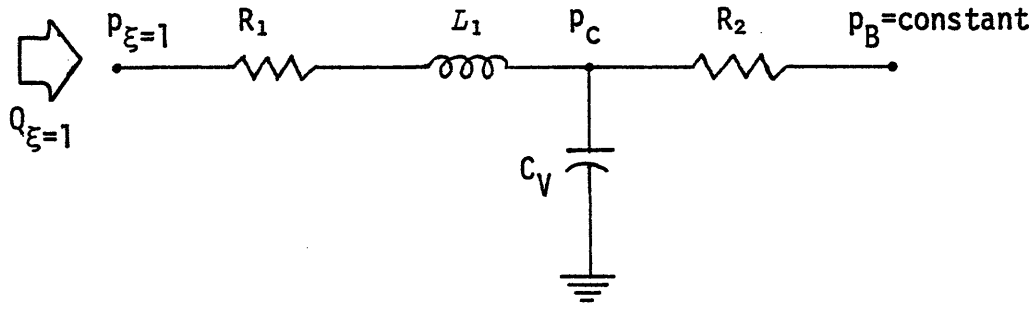

The equations for such a system can be expressed in terms of pressures at the various nodes:

$$p_{\xi=1} - p_c = Q_{\xi=1}R_1 + L_1 \frac{dQ_{\xi=1}}{dt} + h_L \rho \left(\frac{Q}{A}\right)^2_{\xi=1} \tag{11}$$

$$p_c - p_B = Q_B R_2 + L_2 \frac{dQ_B}{dt} \tag{12}$$

$$p_c - p_{c_{t=0}} = \frac{1}{C_V} \int_0^t (Q_{\xi=1} - Q_B)\, dt \quad , \tag{13}$$

where

$$L_1 \equiv \frac{\rho L_1}{A_1} \qquad R_1 \equiv \frac{8\pi\mu L_1}{A_1^2}$$

$$L_2 \equiv \frac{\rho L_2}{A_2} \qquad R_2 \equiv \frac{8\pi\mu L_2}{A_2^2}$$

$$C_V \equiv \frac{dV}{dp}$$

and Q_B is the flow rate through R_2, p_c is the pressure in the capacitance tank, and p_B is the outlet pressure. The normalization of Eqs. (11)-(13) will be left for the next chapter where the equations will be combined in a way that allows a convenient computation at the boundary. The last term in Eq. (11) has been introduced to account for inertial losses due to abrupt changes in vessel diameter such as at a junction between two tubes. In these equations it takes the form of a constant times the square of the flow velocity.

Initial Conditions.* In the initial state, we assume that all acceleration terms (both convective and temporal) in the governing equations and boundary conditions are zero. Furthermore, since the collapsible network in normal initial states will be open, the dominant resistance is assumed to be located upstream of the collapsible system. As a reasonable approximation we assume that the initial flow resistance in the collapsible tubes can be estimated assuming $A = A_0(\xi)$. The initial flow rate, then, is defined in the following equation:

$$Q_i = \frac{p_A - p_B}{R_A + R_1 + R_2 + 8\pi \int_{x=0}^{x=L} C_f(x) \frac{u}{A_0^2} \, dx} \quad . \tag{13}$$

To obtain an estimate of the actual cross-sectional area of the collapsing tubes we can first compute the pressure at $\xi = 1$ from the expression,

$$p_{\xi=1} = p_B + (R_1 + R_2)Q_i \quad .$$

Introducing normalized variables we have:

$$P_{\xi=1} = \frac{p_B + (R_1 + R_2)Q_i}{\rho c_0^2(1)\beta} \quad . \tag{14}$$

---

*Q_L is assumed to be zero in this discussion. A nonzero Q_L can be introduced with minor modifications to the equation.

Based on the assumptions that

(i) fully developed laminar flow exists throughout the vessel;

(ii) $p_e(\xi) \equiv 0$ for $\tau = 0$; and

(iii) inertial effects can be neglected,

we can write the momentum equation in the following simplified form:

$$\frac{d(p - p_e)}{dx} = \frac{-8\pi\mu C_f(x)Q_i}{A^2} ,$$

from which we obtain the normalized equivalent,

$$\alpha\, d\alpha = -Q_i \frac{8\pi\mu c_0(0)A_0(0)C_f(\xi)L}{\rho c_0^2(\xi)A_0^2(\xi)C^2} d\xi - \frac{4\beta P\alpha^2}{c_0(\xi)C^2} \frac{dc_0(\xi)}{d\xi} d\xi . \qquad (15)$$

In the general case when C_f , c_0 , and A_0 are arbitrary functions of ξ , the RHS of Eq. (15) must be integrated numerically.

The resistance function F can exhibit a variety of features depending on the local flow conditions. The flow can be either laminar or turbulent or, if laminar, can be either fully developed or in a state of boundary layer growth. Each of these will be considered in the following discussion.

Selection of Resistance Functions

Let us assume that the flow at any point in the collapsing vessel satisfies the criteria for one of the following conditions:

(1) laminar flow with a developing boundary layer;

(2) fully developed laminar flow;

(3) turbulent flow.

Case 1. Two necessary but not sufficient conditions for laminar developing boundary layer flow are (i) that the Reynolds number (based on hydraulic diameter) must be less than the critical value, Re_{cr}, which marks the transition to turbulent flow, and (ii) that the boundary layer thickness, δ, be less than r, where r is a characteristic radius of the cross-section ($r \cong$ hydraulic diameter/2 = 2A/P). One means of approximating δ is by analogy to Stokes' first problem, that of an infinite flat plate suddenly accelerated to a velocity u_0 in a semi-infinite fluid. In the collapsing tube, the real situation is complicated by the time varying nature of the flow and by the convection of vorticity from points upstream where the flow conditions may differ considerably from those locally. We will assume these effects to be negligible since their inclusion would introduce much complexity to a problem of minor significance. It is quite probable that the boundary layers will fill the collapsed tube before viscous resistance becomes a significant factor so a more complete analysis is not warranted.

The errors introduced by this assumption will be most pronounced in the case of oscillating flow. For sufficiently high frequencies, the boundary layer is confined to a small region close to the tube wall and the viscous damping of such oscillations is much greater than would be predicted using this approach.

In the absence of significant flow oscillations we can make an

estimate of the boundary layer thickness,

$$\delta \approx 4\sqrt{\nu t} \quad .$$

As one criterion for assuming the existence of developing boundary layer flow we will require that $\delta < r$.

Returning to the problem of an impulsively started plate, the velocity distribution can be shown to be

$$\frac{u}{u_0} = \operatorname{erfc}\left(\frac{y}{\sqrt{4\nu t}}\right) \quad ,$$

where y is the distance from the wall and u_0 is the plate velocity. We can superimpose the solutions for a series of impulsive accelerations in the following manner:

$$u(y,t) = \lim_{\substack{\Delta t \to 0 \\ \Delta u \to 0}} \left[\Delta u_0(0) \operatorname{erfc}\left(\frac{y}{\sqrt{4\nu t}}\right) + \Delta u_0(\tau_1) \operatorname{erfc}\left(\frac{y}{\sqrt{4\nu t}}\right) + \ldots \right] .$$

This limit can be expressed in integral form permitting the use of a continuously varying plate velocity, $u_0(t)$:

$$u(y,t) = \int_0^t \frac{du_0}{d\tau} \operatorname{erfc}\left[\frac{y}{\sqrt{4\nu(t-\tau)}}\right] d\tau \quad . \qquad (17)$$

From the velocity profile, we can compute the wall shear stress:

$$\tau_w = -\mu \left.\frac{\partial u}{\partial y}\right|_{y=0} = -\left(\frac{\rho\mu}{\pi}\right)^{\frac{1}{2}} \int_0^t \frac{du_0(\tau)}{d\tau} \frac{d\tau}{\sqrt{t-\tau}} \quad . \tag{18}$$

If we assume that the velocity-time profile can be approximated as linear during this initial period an expression can be derived for τ_w :

$$\tau_w = 2\left(\frac{\rho\mu}{\pi}\right)^{\frac{1}{2}} \frac{\Delta u_0}{\Delta t} \sqrt{t} \quad . \tag{19}$$

In terms of our previous notation the corresponding resistance function for open tubes is written

$$\frac{\tau_w P}{A_0(\xi)\alpha} = 4\left[\frac{\rho\mu c_0{}^3(0)}{L\tau A_0(\xi)}\right]^{\frac{1}{2}} \frac{U}{\alpha}$$

or

$$F = 4\left[\frac{\mu L}{\rho c_0(0)\tau A_0(\xi)}\right]^{\frac{1}{2}} \frac{U}{\alpha} \quad , \quad \alpha > 0.27 \tag{20}$$

and for the collapsed tube, assuming the configuration ⋈ [i.e., $P = 2(4\pi A/2)^{\frac{1}{2}}$] ,

$$\frac{\tau_w P}{A_0(\xi)\alpha} = 4\left[\frac{2\rho\mu c_0{}^3(0)\alpha}{L\tau A_0(\xi)}\right]^{\frac{1}{2}} \frac{U}{\alpha}$$

or

$$F = 4\left[\frac{2\mu L}{\rho c_0(0)\tau A_0(\xi)\alpha}\right]^{\frac{1}{2}} U \qquad \alpha < 0.27 \quad . \tag{21}$$

$\alpha = 0.27$ was chosen as the point of transition from one shape to the other because it corresponds, roughly, to the area at which the walls first come into contact.

Case 2. When $\delta > r$ and $Re < Re_{cr}$, fully developed laminar flow results. This too must be an approximation in unsteady flow since, with a time-varying flow rate, the velocity profile is never truly "fully developed."

Derivation of resistance functions for the collapsing tube are possible only by numerical techniques. Assuming Poiseuille flow, Flaherty *et al.*[40] have computed the shape of the collapsed cross-section and the velocity profiles from which the resistance functions can be determined. For cross-sectional areas less than $\simeq 0.21$, a similarity solution exists (see Chapter VIII) for the relationship between transmural pressure and cross-sectional area. The resistance function in the collapsed tube can be determined simply by knowing the resistance at one state and imposing the similarity condition. This results in the following relationship which is found by way of the same numerical investigation to be reasonably accurate up to $\alpha \cong 0.36$:

$$\frac{\tau_w P}{A_o(\xi)\alpha} = \frac{70\mu c_o(0)}{A_o(\xi)} \frac{U}{\alpha} \tag{21}$$

$$F = \frac{L}{\rho c_o^2(0)} \frac{70\mu U}{A_o(\xi)\alpha} \qquad \alpha \leq 0.36 \quad .$$

For cross-sectional areas greater than $\alpha = 0.36$ but less than 1.0, the numerical solution follows closely that of Poiseuille flow through an elliptical cylinder (see Milne-Thompson[41]). For a cylinder of major and minor radii a and b the perimeter and area are defined as

$$P \cong 2\pi \left(\frac{a^2 + b^2}{2} \right)^{\frac{1}{2}}$$

$$A = \pi a b \quad .$$

The momentum equation for slow, steady flow of a viscous liquid through this cylinder is

$$Q = - \frac{dp}{dx} \frac{1}{4\mu} \frac{a^2 b^2}{a^2 + b^2} A$$

or

$$uA = - \frac{dp}{dx} \frac{1}{4\mu} \frac{2A^3}{P^2} \quad . \tag{22}$$

If we convert to the previously defined dimensionless variables, Eq. (22) can be rewritten as

$$\frac{K_p}{L} \frac{dP}{d\xi} = - \frac{c_0(0)}{A_0(\xi)} P \pi \mu \frac{U}{a^2} \quad , \tag{23}$$

where P = constant $= 2\pi[A_0(\xi)/\pi]^{\frac{1}{2}}$. This result when expressed in our standard form is

$$\frac{\tau_w P}{A_0(\xi)\alpha} = \frac{8\pi\mu c_0(0)U}{A_0(\xi)\alpha^2}$$

or

$$F = \frac{1}{\rho c_0^2(\xi)} \frac{8\pi\mu c_0(0)U}{A_0(\xi)\alpha^2} , \quad 1.0 > \alpha > 0.36 . \quad (24)$$

If $\alpha > 1.0$, the tube is circular in cross-section. The resistance in laminar, fully-developed flow is given by the following expressions:

$$\frac{\tau_w P}{A_0(\xi)\alpha} = \frac{8\pi\mu c_0(0)U}{A_0(\xi)\alpha}$$

or

$$F = \frac{L}{\rho c_0^2(0)} \frac{8\pi\mu c_0(0)U}{A_0(\xi)\alpha} \quad \alpha > 1.0 .$$

Case 3. When the local Reynolds number exceeds Re_{cr} , we will assume that fully developed turbulent flow exists. Turbulent wall stress in the case of a hydraulically smooth pipe of circular cross-section has been found to obey the relationship

$$\tau_w = C_t(\tfrac{1}{2}\rho u^2) \frac{u}{|u|} , \quad (25)$$

where $C_t = (0.3164/4)Re^{-0.25}$ with Re based on hydraulic diameter (see Schlichting[42]).

As was true for Case (1), velocity gradients are essentially confined

to narrow zones close to the wall. Therefore, the shape of the cross-section is relatively unimportant in terms of computing the shear stress. If we make the assumption that Eq. (17) is a valid expression regardless of tube shape, the previously defined resistance functions can be easily written, for pre-collapse states:

$$\frac{\tau_w P}{A_0(\xi)\alpha} = \frac{0.3164}{4}\left[\frac{\pi}{A_0(\xi)}\right]^{\frac{1}{2}} \frac{\rho c_0^2(0)\ \mathrm{Re}^{-0.25}}{\alpha}\frac{U^3}{|U|}$$

or

$$F = \frac{0.3164}{4}\left[\frac{\pi}{A_0(\xi)}\right]^{\frac{1}{2}} \frac{L\ \mathrm{Re}^{-0.25}}{\alpha}\frac{U^3}{|U|}\ ,\quad 1.0 > A > 0.27 \qquad (26)$$

and for the collapsed tube,

$$\frac{\tau_w P}{\alpha A_0(\xi)} = \frac{0.3164}{4}\left[\frac{2\pi}{A_0(\xi)\alpha}\right]^{\frac{1}{2}} \rho c_0^2(0)\ \mathrm{Re}^{-0.25}\frac{U^3}{|U|}$$

or

$$F = \frac{0.3164}{4}\left[\frac{2\pi}{A_0(\xi)\alpha}\right]^{\frac{1}{2}} L\ \mathrm{Re}^{-0.25}\frac{U^3}{|U|} \qquad A < 0.27\ . \qquad (27)$$

The previously obtained equations for mass and momentum conservation, the tube law, the expressions for the friction parameter F, the conditions at the boundaries, and the initial condition comprise a complete formulation for flow in a collapsible tube. The system of equations is hyperbolic and, clearly, cannot be solved analytically.

Two cases have been explored, however, in which the complexity of the equations can be reduced to a more soluble form. These are the cases of

- uniform vessel collapse;
- viscous dominated collapse,

and are discussed in detail in Appendices A and B, respectively.

We found in Appendix A that the tube collapses uniformly in the specific instance where the external pressure varies as

$$p_e = a + bx^2$$

where x is measured from the outlet of the vessel. Using a spatially varying compression of this type it was found that the tube could be emptied much more rapidly than in the case of uniform external pressure. This difference can be accounted for, primarily, by the absence of a highly constrictive throat at the downstream end which generally occurs in the case of uniform external pressure.

In Appendix B we demonstrated the existence of a similarity variable which reduces the governing partial differential equations to a single ordinary differential equation in the instance of highly viscous collapsible tube flow. The true boundary condition, however, cannot be expressed precisely in terms of the similarity variable due to the existence of an initial period during which inertial effects must be important. The results, although illustrative, probably apply only for either very late stages of collapse or for extremely viscous fluids.

The complete set of equations can only be solved numerically. Being

hyperbolic, the applicable numerical methods can be divided into two categories:

(1) methods employing the equations in characteristic form;

(2) methods in which the governing equations are written directly as difference equations.

Both techniques have been studied and the method used in our computations did, in fact, incorporate both solution procedures. These methods, as they relate to our analysis, will be discussed in the next two chapters.

CHAPTER V:

A MODIFIED METHOD OF CHARACTERISTICS

The pair of equations governing flow in the collapsible segment [Eqs. (7) and (8)] are well suited to solution by the method of characteristics whereby the solution is found along curves of possible discontinuities. For the purpose of numerical calculations, the equations can be formulated along these characteristic curves.

Derivation of Characteristic Equations

First we multiply the continuity equation by an undefined parameter, λ and add Eq. (6) and to the resulting form of Eq. (7):

$$\frac{\partial U}{\partial \tau} + (U+\lambda\alpha)\frac{\partial U}{\partial \xi} + \lambda\frac{\partial \alpha}{\partial \tau} + \left(\delta_c{}^2\frac{C^2}{\alpha} + \lambda U\right)\frac{\partial \alpha}{\partial \xi} + H + \lambda G = 0 \quad , \qquad (28)$$

where

$$H = \frac{1}{\rho c_0{}^2(0)}\frac{\partial (p_e)}{\partial \xi} + 2P\beta\delta_c\frac{1}{c_0(0)}\frac{dc_0(\xi)}{d\xi} + C_f(\xi)F$$

$$G = \alpha U\frac{1}{A_0(\xi)}\frac{dA_0(\xi)}{d\xi}$$

$$\delta_c = \frac{c_0(\xi)}{c_0(0)} \quad .$$

Multiplying Eq. (28) by $d\xi$ and substituting the identities,

$$dU = \frac{\partial U}{\partial \xi} d\xi + \frac{\partial U}{\partial \tau} d\tau$$

$$d\alpha = \frac{\partial \alpha}{\partial \xi} d\xi + \frac{\partial \alpha}{\partial \tau} d\tau$$

results in this reduced expression:

$$(U \pm \delta_c C)dU + \left(\frac{C^2}{\alpha} \delta_c{}^2 \pm \frac{\delta_c CU}{\alpha}\right) d\alpha + H\, d\xi \pm \frac{\delta_c C}{\alpha} G\, d\xi = 0 \qquad (29)$$

if

$$(U + \lambda\alpha) = \frac{d\xi}{d\tau} \quad \text{and} \quad \left(\delta_c{}^2 \frac{C^2}{\alpha\lambda} + U\right) = \frac{d\xi}{d\tau} \qquad (30)$$

or equivalently, if

$$\lambda = \pm \frac{C}{\alpha} \delta_c \ .$$

By rearranging Eq. (29) and substituting the derived expression for λ into Eq. (30), we obtain the final form of the characteristic equations,

$$dU \pm \delta_c C \left[d(\ell n\ \alpha) + \frac{G}{\alpha} d\tau\right] + H\, d\tau = 0 \qquad (31a)$$

$$(U \pm \delta_c C)_{\substack{R \\ L}} = \frac{d\xi}{d\tau} \ . \qquad (31b)$$

Here R and L denote the rightward and leftward running characteristic curves, respectively (for subcritical velocities, i.e., $U < C$). This analysis has provided a pair of physical characteristics defined by (31b) on which the solution reduces to that of a pair of ordinary differential equations, (31a). Equivalently, these equations define the characteristic curves [Eq. (31a)] and their projections on the physical (ξ,τ) plane [Eq. (31b)].

The solution carried out in this fashion breaks down in certain situations encountered during the course of the computation. Significant errors are introduced at a position where large area changes take place between two adjacent grid points. The source of these truncation errors are discussed in Chapter X.

In the true method of characteristics the solution is carried out strictly along the curves defined by Eq. (31b) using Eq. (31a). This procedure has the disadvantage of yielding a result that must be interpolated in both ξ and τ to obtain results on a uniform grid. Furthermore, as the computation proceeds, the characteristic mesh must be periodically adjusted as the characteristic curves become more concentrated in some regions than in others. The advantage of this technique, however, lies in the more precise location of shock-like discontinuities which may develop during the computation as a result of characteristic curves of the same family coalescing. Due to the hyperbolic nature of the equations, shocks encountered using this procedure are true discontinuities. In reality both in gas dynamic shocks or the quasi-shocks that may occur in collapsing tubes, some mechanism acts to prevent the

creation of a true discontinuity. The nature of these mechanisms in collapsible tube flow and the method by which we chose to take them into account will be discussed in Chapter VI.

The modified method of characteristics used in our calculations was first introduced by Hartree[43] to circumvent the complicated interpolation associated with the original method. Using the modified technique, the solution is found on a predetermined ξ-τ grid along characteristic curves which intersect with the fixed network of points. Since the curve along which the solution is computed changes with each time step, the procedure might be considered to be a sort of step-wise characteristic method. It lacks, however, the more satisfying nature of continuous characteristic curves. In the following discussion, this method is described in some detail.

Computational Procedure Using the Characteristic Method

As mentioned, the numerical calculation involves marching the solution forward in time along an essentially predetermined ξ-τ grid. The solution at each point is computed along the physical characteristics passing through it using finite difference approximations to the characteristic equations. In general, these expressions are second order approximations. Equations written in this manner can be used both for the initial calculation and for subsequent iterations should they be necessary.

Assuming that U and α are known at time τ_0 for all ξ, the

procedure for computing interior points (i.e., those not on the boundary) at time $\tau_0+\Delta\tau$ is outlined below. The notation follows the general rule that subscripts involving "n" refer to position and superscripts with "m" refer to time. Therefore, U^{m+1}_{n-1} is the velocity at position n-1 and time m+1. Subscripts R and L denote variables at the intersection of the rightward or leftward running characteristic curves (see diagram) with the $\tau = \tau_0$ line.

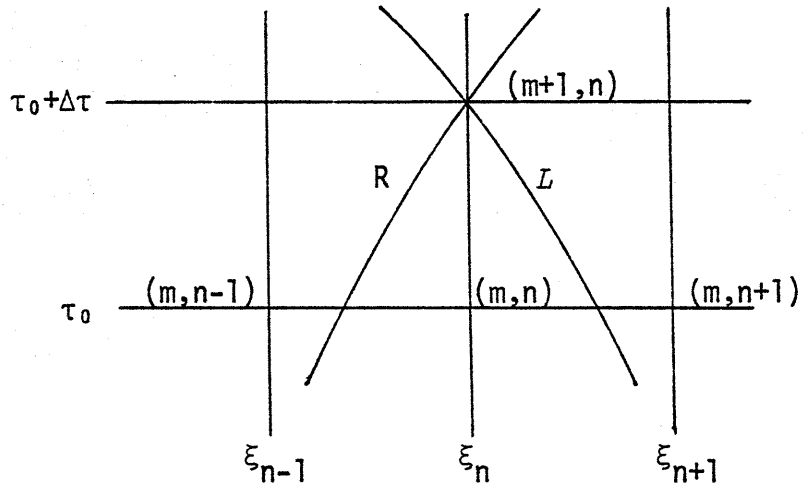

(1) As a first approximation equate each variable at points R, L, and (m+1, n) to the corresponding variable at (m,n); i.e.,

$$U_R = U_L = U^{m+1}_n = U^m_n \quad .$$

(2) Using a second order approximation to Eq. (31b), solve for ξ_L and ξ_R:

$$\xi_{\substack{R\\L}} = \xi_n - \frac{\Delta\tau}{2}\left[\left(U^{m+1}_n \pm \delta_c C^{m+1}_n\right) + \left(U_{\substack{R\\L}} \pm \delta_c C_{\substack{R\\L}}\right)\right]. \qquad (32)$$

(3) Interpolate to obtain estimates for α, Q, $\frac{\partial p_e}{\partial \xi}$, δ_c, etc. at points ξ_R and ξ_L. The linear approximations are, for example,

$$Q_R = {}^{m}Q_{n-1} + \frac{(\xi_R - \xi_{n-1})}{\Delta\xi}\left({}^{m}Q_n - {}^{m}Q_{n-1}\right) \tag{33a}$$

and the quadratic expression:

$$\begin{aligned} Q_R = {}^{m}Q_{n-1} & \frac{(\xi_n - \xi_R)}{2\Delta\xi}\left({}^{m}Q_{n+1} - {}^{m}Q_{n-1}\right) \\ & + \frac{(\xi_n - \xi_R)}{2\Delta\xi^2}\left({}^{m}Q_{n+1} - 2{}^{m}Q_n + {}^{m}Q_{n-1}\right) . \end{aligned} \tag{33b}$$

The linear approximation was often used for two reasons. First, for supercritical flow, only it truly isolates upstream points from the flow behavior downstream. Secondly, the second order equation would sometimes yield negative values for α in regions where the cross-sectional area was undergoing rapid change.

(4) Using the interpolated variables, solve for each variable or group of variables needed in the characteristic expressions including F, H, G, etc.

(5) By means of the characteristic equation (31a) we can write the following finite difference approximations, once again of second order:

$$\ell n\ \alpha_n^{m+1} = \ell n\ \alpha_{\substack{R\\L}} \mp \tfrac{1}{2} K_{\substack{R\\L}} \left(U_n^{m+1} - U_{\substack{R\\L}} \right)$$

$$\mp \frac{1}{2} \left[\left(\frac{H}{\delta_c C} \right)_n^{m+1} + \left(\frac{H}{\delta_c C} \right)_{\substack{R\\L}} \pm \left(\frac{G}{\alpha} \right)_n^{m+1} \pm \left(\frac{G}{\alpha} \right)_{\substack{R\\L}} \right] d\tau \tag{34}$$

where

$$K_{\substack{R\\L}} \equiv \left[(\delta_c C)_n^{m+1} \right]^{-1} + \left[(\delta_c C)_{\substack{R\\L}} \right]^{-1} .$$

Solving for U_n^{m+1} between the rightward and leftward expressions yields

$$U_n^{m+1} = \frac{1}{K_R + K_L} \left\{ 2\ \ell n \frac{\alpha_R}{\alpha_L} + K_R U_R + K_L U_L \right.$$

$$\left. - \Delta\tau \left[2 \left(\frac{H}{\delta_c C} \right)_n^{m+1} + \left(\frac{H}{\delta_c C} \right)_R + \left(\frac{H}{\delta_c C} \right)_L + \left(\frac{G}{\alpha} \right)_R + \left(\frac{G}{\alpha} \right)_L \right] \right\} \tag{35}$$

Either of Eqs. (34) can be used to solve for α_n^{m+1}; e.g.,

$$\alpha_n^{m+1} = \alpha_L \exp \left\{ \frac{K_L}{2} \left(U_n^{m+1} - U_L \right) \right.$$

$$\left. + \frac{1}{2} \left[\left(\frac{H}{\delta_c C} \right)_n^{m+1} + \left(\frac{H}{\delta_c C} \right)_L - \left(\frac{G}{\alpha} \right)_n^{m+1} - \left(\frac{G}{\alpha} \right)_L \right] \Delta\tau \right\} . \tag{36}$$

Upon completing step (5), the solution either returns to step (2) continuing the iterative process, or proceeds to the next computation at point (n+1, m+1).

Computations at the Boundaries

At the boundaries the solution takes on a slightly different form. At the upstream and downstream boundaries, the equations derived earlier involving flow conditions outside of the collapsible duct are combined with either the leftward or rightward running characteristic equation.

Upstream Boundary. At the inlet ($\xi = 0$), Eq. (10) and one form of Eq. (31a) are solved simultaneously. The second of these can be written so that Q and P are the differential quantities,

$$dQ - \frac{A_0(\xi)}{A_0(0)} \frac{\alpha\beta}{C^2} (U + \delta_c C)\, dP + \alpha \frac{A_0(\xi)}{A_0(0)} \left(H - \frac{\delta_c C}{\alpha} G \right) d\tau - \frac{U}{A_0(0)} \alpha\, dA_0(\xi) = 0 \quad . \tag{37}$$

For the purpose of the numerical calculation, Eq. (37) can be expressed in difference form as

$$P_1^{m+1} = P_L + \frac{1}{X_B} \left(Q_1^{m+1} - Q_L + X_A \right) \tag{38}$$

where

$$X_A \equiv \frac{1}{2}\left[(H\alpha - \delta_c CG)_1^{m+1} + \frac{A_0(\xi)_L}{A_0(0)}(H\alpha - \delta_c CG)_L\right]\Delta\tau$$

$$- \frac{1}{2}\left[Q_1^{m+1} + Q_L\frac{A_0(0)}{A_0(\xi)_L}\right]\left[1 - \frac{A_0(\xi)_L}{A_0(0)}\right]$$

and

$$X_B \equiv \frac{\beta}{2}\left\{\left[\frac{\alpha(U - \delta_c C)}{C^2}\right]_1^{m+1} + \frac{A_0(\xi)_L}{A_0(0)}\left[\frac{(U + \delta_c C)}{C^2}\right]_L\right\} .$$

Between Eqs. (10) and (38) we can eliminate P_1^{m+1} and solve for Q_1^{m+1} :

$$Q_1^{m+1} = \left(\frac{1}{X_B} + X_C\right)^{-1}\left[\frac{p_A - p_e}{K_p} - P_L + \frac{1}{X_B}(Q_L - X_A)\right] \qquad (39)$$

where $X_C \equiv c_0(0)A_0(0)R_A/K_p(0)$.

Having obtained an estimate for Q_1^{m+1} from Eq. (39) we return to Eq. (38) to solve for P_1^{m+1} and subsequently, α_1^{m+1} . An accurate result requires one or more iterations.

Downstream Boundary Condition. The flow at $\xi = 1$ is governed by Eqs. (11)-(13) from the previous chapter. These can be converted to difference form with the following result. Equations (11)-(13) become

$$p_{\xi=1}^{m+1} - p_c^{m+1} = R_1 Q_{\xi=1}^{m+1} + L_1 \frac{Q_{\xi=1}^{m+1} - Q_{\xi=1}^{m}}{\Delta t} + h_L \rho u_A^2 \tag{40}$$

$$p_c^{m+1} - p_B^{m+1} = R_2 Q_B^{m+1} + L_2 \frac{Q_B^{m} - Q_B^{m-1}}{\Delta t} \tag{41}$$

$$p_c^{m+1} - p_c^{1} = \frac{1}{C_V} \left[V^m + \frac{\Delta t}{2} \left(Q_{\xi=1}^{m+1} + Q_{\xi=1}^{m} - Q_B^{m+1} - Q_B^{m} \right) \right] \tag{42}$$

where

$$V^m \equiv \frac{\Delta t}{2} \sum_{i=1}^{m} \left(Q_{\xi=1}^{i} + Q_{\xi=1}^{i-1} - Q_B^{i} - Q_B^{i-1} \right) .$$

With some algebraic manipulation, we can eliminate p_c^{m+1} and Q_B^{m+1} from these equations resulting in an expression in which $P_{\xi=1}^{m+1}$ and $Q_{\xi=1}^{m+1}$ are the only unknowns:

$$p_{\xi=1}^{m+1} = p_B + L_2 \frac{Q_B^{m} - Q_B^{m-1}}{\Delta t} + \frac{1}{1 + \frac{\Delta t}{2R_2 C_V}} \left\{ p_c^1 - p_B - L_2 \frac{Q_B^{m} - Q_B^{m-1}}{\Delta t} + \frac{1}{C_V} \left[V^m + \frac{\Delta t}{2} \left(Q_{\xi=1}^{m} - Q_B^{m} \right) \right] \right\} + \left(R_1 + \frac{L_1}{\Delta t} + \frac{1}{\frac{2C_V}{\Delta t} + \frac{1}{R_2}} \right) Q_{\xi=1}^{m+1}$$

$$- \frac{L_1}{\Delta t} Q_N^m + h_L \rho u_A^2 \quad .$$

Upon normalization, this becomes

$$P_N^{m+1} = X_1 + X_2 Q_{\xi=1}^{m+1} - X_3 \quad , \tag{43}$$

where

$$X_1 \equiv \frac{1}{\rho c_0^2(0)\beta}\left(p_B + \bar{\psi} + \frac{1}{1 + \frac{L\Delta\tau}{2R_2 C_V c_0(0)}}\left\{p_c^1 - p_B - \bar{\psi} + \frac{A_0(0)L}{C_V}\left[\bar{V}^m + \frac{\Delta\tau}{2}\left(Q_{\xi=1}^m - Q_B^m\right)\right]\right\}\right)$$

and $p_{e_{\xi=1}}$ has been assumed to be zero.

$$X_2 \equiv \frac{A_0(0)c_0(0)}{\rho c_0^2(1)\beta}\left\{R_1 + \frac{c_0(0)L_1}{L\Delta\tau} + \left[\frac{2C_V c_0(0)}{L\Delta\tau} + \frac{1}{R_2}\right]^{-1}\right\}$$

$$X_3 \equiv \frac{L_1 c_0^2(0)A_0(0)}{L\Delta\tau\rho c_0^2(1)\beta} Q_{\xi=1}^m - \frac{h_L}{\beta}\left[\frac{U_A}{\delta_c(1)}\right]^2$$

In X_1, $\bar{\psi}$ has replaced $L_2 \frac{c_0^2(0)A_0(0)}{L}\left(Q_B^m - Q_B^{m-1}\right)\frac{1}{\Delta\tau}$.

The additional equation is supplied by the rightward running characteristic expressed in terms of Q and P :

$$dQ = \frac{A_0(\xi)}{A_0(0)}\left[\frac{\alpha\beta}{C^2}(U - \delta_c C)dP - (\alpha H + \delta_c CG)d\tau + \frac{U\alpha}{A_0(\xi)}\,dA_0(\xi)\right]. \tag{44}$$

We can write this equation in difference form and solve for Q_N^{m+1} ("N" denotes the point at which $\xi = 1$):

$$Q_N^{m+1} = Q_R + \frac{\Lambda}{2}\left(P_N^{m+1} - P_R\right) - \Gamma \tag{45}$$

where

$$\Lambda \equiv \left[\frac{A_0(\xi)\alpha\beta}{A_0(0)C^2}(U - \delta_c C)\right]_N^{m+1} + \left[\frac{A_0(\xi)\alpha\beta}{A_0(0)C^2}(U - \delta_c C)\right]_R$$

$$\Gamma \equiv \frac{\Delta\tau}{2}\left\{\left[\frac{A_0(\xi)}{A_0(0)}(\alpha H + \delta_c CG)\right]_N^{m+1} + \left[\frac{A_0(\xi)}{A_0(0)}(\alpha H + \delta_c CG)\right]_R\right\} \tag{46}$$

$$- \frac{1}{2}\left(Q_N^{m+1} + Q_R\right)\ell n\,\frac{A_{0_N}}{A_{0_R}} \quad .$$

Between Eqs. (43) and (46) we can eliminate $Q_{\xi=1}^{m+1}$ with the result

$$P_N^{m+1} = \frac{X_1 + X_2\left(Q_R - \frac{\Lambda}{2}P_R - \Gamma\right) - X_3}{1 - \frac{X_2\Lambda}{2}} \quad . \tag{47}$$

The calculation of the boundary parameters using Eqs. (46) and (47) is performed by way of an iterative procedure to any desired precision.

Initial Condition

The initial condition requires solving for Q_i and $P_{\xi=1}$ in Eqs. (13) and (14), then using these results in a numerical integration of Eq. (15). We used Simpson's Rule for this purpose which can be expressed, in this particular case, as

$$\alpha_{\xi_n} = \left\{ \alpha_{\xi_N}{}^2 + \frac{\Delta\xi}{3}\left[\psi(\xi_N) + 4\psi(\xi_{N-1}) + 2\psi(\xi_{N-2}) + \ldots \right.\right. \tag{45}$$

$$\left.\left. \ldots + 4\psi(\xi_{n+3}) + 2\psi(\xi_{n+2}) + 4\psi(\xi_{n+1}) + \psi(\xi_n)\right]\right\}^{\frac{1}{2}}$$

where

$$\psi(\xi_n) = X_D \frac{\mu C_f(\xi_n)}{c_0{}^2(\xi_n) A_0{}^2(\xi_n) C_n{}^2} Q_i + \frac{4\beta P \alpha^2}{c_0(\xi) C^2} \frac{dc_0(\xi)}{d\xi}$$

$$X_D = \frac{16\pi c_0(0) A_0(0) L}{\rho} \quad .$$

In obtaining Eq. (45) we have integrated both sides of Eq. (15) (the left hand side exactly) between $\xi = \xi_N$ and $\xi = \xi_n$ and have expressed the integral containing the unknown functions of ξ in terms of its numerical approximation.

The next chapter describes an alternate procedure, that of finite differences.

CHAPTER VI:

SOLUTION BY THE METHOD OF FINITE DIFFERENCES

The set of equations derived in Chapter III are hyperbolic and, as such, their solution may give rise to shock-like discontinuities in the flow field such as are commonly found in the analogous situation of one-dimensional flow of a compressible fluid in a duct of varying cross-sectional area. If the characteristic method described in the previous chapter is used to obtain the solution, and if the solution tends toward the development of a flow discontinuity (which is characterized by many characteristic curves of the same family coalescing) large errors will result and, by experience, the solution will go unstable.

Two reasons can be given for the failure of the numerical calculation using the method of characteristics. First, in the solution method described in Chapter V, the results are obtained at fixed grid points and the possibility exists of integrating along a characteristic curve which passes through a discontinuity of the type described above. Right at the discontinuity, the slope of the characteristic curve changes abruptly, but the difference equations use a slope which is estimated as the average of the slopes evaluated at the two endpoints of the curve. Thus the integration is subject to considerable error.

Secondly, an error can result at the point of smooth transition from super- to subcritical flow, should it exist. Close to the transition point, u approaches c and the slope of the leftward running characteristic ($dt/dx = 1/u-c$) approaches infinity. Within practical

limitations on grid size, the difference equations will not be able to follow the exact nature of these upstream running characteristics. Again, the averaging features of the computational procedure produce increasingly large errors as the slope of the curve approaches infinity.

The traditional procedure used to circumvent the first of the two problems mentioned above is called shock fitting. Basically, this involves computing up to the shock from both sides using the characteristic equations following along characteristic curves. The equations across the shock (called the Rankine-Hugoniot jump conditions) are determined by satisfying the requirements of mass, momentum, and energy conservation. Needless to say, this method can be extremely cumbersome and is prone to stability problems particularly in the case of embedded shocks which arise at later times in the solution.

The other methods used in gas dynamics to compute conditions across a shock wave involve the use of the difference equations corresponding directly to Eqs. (6) and (7) of the earlier formulation. These methods can be divided into two categories:

(1) pseudo-viscosity methods;[44]

(2) conservation-law formulations.[45]

In Case (1), an artificial dissipative mechanism is introduced to the governing equations which becomes large only in instances where a shock would develop. The resulting dissipation tends to "smear" the shock, generally over 3 or 4 grid spacings, and allows the use of the difference equations straight through the transition zone.

The second case effectively introduces the Rankine-Hugoniot jump

conditions into the solution scheme automatically. Using what is called the conservation-law form of the governing equations,[46] the requirements of mass, momentum, and energy conservation are incorporated directly into the corresponding difference equations.

In spite of the numerous similarities, there are significant differences between the flow of a compressible fluid and the fluid flow in a collapsible tube in the immediate region of an actual discontinuity, and these differences should be reflected in the numerical procedure. In gas dynamics, the shock wave is very nearly a true discontinuity, having a thickness on the order of the mean free path. Viscous dissipation prevents the shock from narrowing further, giving rise to an increase in entropy across the shock. In collapsible tube flow, the numerical discontinuity is smeared over a much larger distance, primarily due to two effects. These are:

(i) When flow passes from a region of small to large cross-sectional area boundary layer separation occurs and, as a result, dissipation in the form of head loss is observed.

(ii) The tube itself, due to its structural integrity, cannot physically undergo a step change in area. The combined effects of tube tension and longitudinal bending moments tend to induce an effective pressure which acts to smooth out the sharply defined transition zone of the shock.

Of these two shock spreading mechanisms, only the first affects the

mass and momentum conservation equations in any way.* If the dissipation associated with flow separation is accounted for in our governing equations and if we use the conservation law form, then the basic physical requirements are satisfied. In terms of the numerical procedure the important point is this: if we can obtain a stable solution through the region of difficulty using the conservation equations, then the solution on one side must be consistent with the solution on the other based on the physical requirements of mass and momentum conservation. In our solution, any possible discontinuities are spread out mainly by the averaging of the numerical procedure. Trial-and-error led us to the particular computational scheme which provided stable, consistent solutions with the aid of this numerical averaging. The details of this method are described in what follows.

The Governing Equations in Conservation-Law Form

The governing equations, since they include a term for wall shear stress, cannot be expressed in true conservation-law form, which would be:

$$\frac{\partial \overline{U}}{\partial \tau} + \frac{\partial}{\partial \xi} F(\overline{U}) = 0 \quad .$$

They can, however, be expressed in a form such that if $F \equiv 0$, the

---

*Tube tension effects may produce locally significant effects but it should not alter the conditions on the two sides of the shock as in the case of flow separation.

equations reduce to the form shown above. If Eqs. (6) and (7) are written in this manner, we obtain

$$\frac{\partial \overline{U}}{\partial \tau} + \frac{\partial}{\partial \xi} F(\overline{U}) = -\overline{K} \quad , \tag{46}$$

where

$$U \equiv \begin{bmatrix} U \\ A_0(\xi)\alpha \end{bmatrix}$$

$$F(\overline{U}) \equiv \begin{bmatrix} \frac{U^2}{2} + \frac{K_p P + p_e}{\rho c_0{}^2(0)} \\ \\ A_0(\xi) U \alpha \end{bmatrix}$$

$$\overline{K} \equiv \begin{bmatrix} C_f(\xi) F \\ \\ -Q_L \frac{L}{c_0(0)} \end{bmatrix} .$$

In the absence of dissipation and fluid influx along the tube, the two quantities contained in F are exactly conserved in the real flow system. We can easily show that integration of Eq. (46) between points $n-1$ and $n+1$ yields a difference equation with the exception of an integral containing the time-derivative and $\overline{K}$,

$$\int_{n-1}^{n+1} \left(\frac{\partial \overline{U}}{\partial \tau} + \overline{K} \right) d\xi + F_{n+1} - F_{n-1} = 0 \quad . \tag{47}$$

If we approximate the integral by

$$2\Delta\xi \left(\frac{\partial \overline{U}}{\partial \tau} + \overline{K} \right)_n \quad ,$$

and replace the time-derivative by the appropriate two-level difference form, we have a difference expression that could be used in place of the previously derived characteristic equations.

Losses at an Abrupt Change in Cross-Sectional Area

We have not yet introduced the losses associated with an abrupt change in duct area. To do so, we must examine the integrated momentum conservation law more closely. If we perform this integration across the transition zone between the points of minimum and maximum cross-sectional area, we obtain an expression analogous to (7):

$$\int_1^2 \left[\frac{\partial U}{\partial \tau} + C_f(\xi) F \right] d\xi + \tfrac{1}{2}(U_2^2 - U_1^2) + \left[\frac{K_p P + p_e}{\rho c_0^2(0)} \right]_2 - \left[\frac{K_p P + p_e}{\rho c_0^2(0)} \right]_1 = 0 \quad . \tag{48}$$

Here, the subscripts refer to the point of minimum (1) and maximum (2) cross-sectional area.

We can compare the above expression to the result for steady, frictionless flow of an incompressible fluid across an abrupt change in cross-sectional area in which the area increases in the direction of flow. The result, expressed in terms of normalized quantities, is

$$\left[K_p P + p_e + \tfrac{1}{2}\rho c_0^2(0) U^2\right]_2 - \left[K_p P + p_e + \tfrac{1}{2}\rho c_0^2(0) U^2\right]_1 = -\tfrac{1}{2}\rho c_0^2(0) U_1^2 \left(1 - \frac{A_{0_1}\alpha_1}{A_{0_2}\alpha_2}\right)^2 . \tag{49}$$

In physical terms, the RHS is the head loss due to incomplete pressure recovery across the expansion.

We can incorporate these losses into the present analysis simply by rewriting Eq. (48) as

$$\int_1^2 \left[\frac{\partial U}{\partial \tau} + C_f(\xi) F\right] d\xi + \frac{\gamma}{2}\left(U_2^2 - U_1^2\right) + \left[\frac{K_p P + p_e}{\rho c_0^2(0)}\right]_2 - \left[\frac{K_p P + p_e}{\rho c_0^2(0)}\right]_1 = 0 , \tag{50}$$

where

$$\gamma \equiv \frac{U_2^2 - \lambda U_1^2}{U_2^2 - U_1^2} \qquad \lambda \equiv 1 - \left(1 - \frac{A_{0_1}\alpha_1}{A_{0_2}\alpha_2}\right)^2 ,$$

or

$$\gamma = 1 - \left[\frac{\left(1 - \frac{A_{0_1} \alpha_1}{A_{0_2} \alpha_2} \right)^2}{1 - \left(\frac{U_2}{U_1} \right)^2} \right] ,$$

where we neglect the error in Eq. (51) in assuming the flow to be steady.

Defining γ in this way, although the point-to-point calculation within the transition is not strictly correct, we should obtain a consistent result on both sides of the expansion which is independent of the grid size. In reality, the process of boundary layer separation and reattachment would occur over a relatively long distance and the results which we have used in the derivation of Eq. (50) would apply strictly only for large control volumes. For the purpose of this analysis, however, we feel that it is sufficient to model the separation mechanism in such a way that the variables at the boundaries of the transition zone are essentially correct even though the details of the transition structure may not be.

Computational Procedure

The difference form for these equations has been set forth in the previous discussion and are written below in the general form used for the numerical solution procedure:

$$\frac{U_n^{m+1} - U_n^{m}}{\Delta\tau} + \frac{\gamma}{4\Delta\xi}\left[\left(U_{n+1}^{m+1}\right)^2 - \left(U_{n-1}^{m+1}\right)^2\right] + \frac{1}{2\Delta\xi}\left\{\left[\frac{K_p P + p_e}{\rho c_0^2(0)}\right]_{n+1}^{m+1} - \left[\frac{K_p P + p_e}{\rho c_0^2(0)}\right]_{n-1}^{m+1}\right\} + F_n^{m+1} = 0 \tag{51a}$$

$$\frac{\alpha_n^{m+1} - \alpha_n^{m}}{\Delta\tau} + \frac{1}{2\Delta\xi A_{0_n}(\xi)}\left\{[A_0(\xi)U\alpha]_{n+1}^{m+1} - [A_0(\xi)U\alpha]_{n-1}^{m+1}\right\} - Q_L\frac{L}{c_0(0)A_{0_n}(\xi)} = 0 . \tag{51b}$$

The above formulation is implicit and requires an iterative method. The procedure found to be stable and convergent involves solving the two Eqs. (51) at alternate points and performing three iterations. Values for α at points where (51a) is used and values for U where (51b) is used are obtained by linear interpolation. For points within the transition zone, γ takes on the value given in Eq. (50) and elsewhere is equal to unity.

In principle, there is no reason why the characteristic equations need be used at all since Eqs. (51) are valid throughout the collapsible tube. We have, in fact, obtained solutions using Eqs. (51) exclusively. The solution obtained in this way exhibits considerable error in the

region of supercritical flow which can be attributed to either a numerical instability or lack of convergence of the equations. To eliminate these oscillations, we use a combination of the procedures described in this chapter and in Chapter V. The collapsible tube is divided into two regions separated by the point of minimum cross-sectional area. The variables at all points upstream are computed using the characteristic equations; the variables at downstream points are computed using Eqs. (51) by means of the alternate point iterative method described above. A complete listing of the program, written in FORTRAN IV, can be found in Appendix C.

The program is divided into three parts: the main program and two subroutines. It incorporates all the generalities described in the theory requiring as input the spatial distributions of A_0 , c_0 , Q_L , p_e , and C_f in addition to the tube law and all the parameters of the two boundary conditions. The output is selectively printed out and stored in a disk data set for later retrieval and subsequent plotting. Included in the Appendix are alternate forms of certain parts of the program which apply to either the laboratory experiments or the venous system. Aside from these modifications, the solution is entirely general and requires only the appropriate input parameters to model any system of collapsible vessels with a wide range of admissible boundary conditions.

There is one limitation, however, on the conditions in which this solution procedure yields valid results. Under normal conditions a pressure is applied externally to a portion of the collapsible tube, and is maintained until the end of the calculation. During this time,

the only disturbances which propagate in the upstream direction toward the compressed zone are relatively small amplitude waves reflected from the downstream boundary. Under these conditions, the upstream propagating disturbances have little effect on the conditions at the throat of the tube and the solution procedure behaves predictably and correctly. If, however, the downstream end of the tube were suddenly blocked, causing a strong compression wave to propagate upstream and if at the time this wave reached the throat the flow was supercritical, then the numerical solution would yield unrealistic results. The compression wave would not cause the "shock" to move upstream and eventually disappear as one would expect. The reason for this lies in the method of computation at the boundary between the two solution methods. Up to and including the point of minimum area, calculations are made by using the characteristic equations which, in the case of supercritical flow, are approximated by one-sided difference equations. Changes in the parameters at downstream points should not and cannot affect the solution computed in this region.

What the numerical procedure lacks is a means of moving the transition zone or "shock" in the upstream direction. Therefore, although a strong compression wave would, in reality, decelerate the flow by pushing the shock further and further upstream, the numerical solution upstream would not change. In gas dynamic calculations, the motion of the shock is normally predicted, in the case of shock fitting, by computing the shock location using both up- and downstream conditions and in the case of finite difference methods, by using two-sided difference equations in

the entire flow field. Our hybrid method does not include either of these mechanisms and as a result cannot account for upstream motion of the shock.

Normally, however, our procedure works perfectly well for the following reason. Due to the form of the tube law, the transition from super- to subcritical flow must occur at the point where the tube goes from a collapsed to an open configuration. This can only happen at the end of the compression zone, a point which, in all our calculations, is either stationary or moves downstream--never upstream. Therefore, even if the shock does become effectively "frozen" at one point in the tube due to the solution procedure, the point at which it freezes cannot be far from the actual transition point and the overall solution is relatively unaffected.

The possibility does exist for the flow to remain supercritical somewhat longer in the numerical solution than in the real case. We can, in fact, observe a slight "glitch" in the solution when the minimum area point does finally go subcritical. This disturbance, though, quickly disappears and does not cause any significant change in the behavior of the tube at other points.

CHAPTER VII:

SCALING PARAMETERS

The scaling parameters of a particular system are generally used to develop a prototype or scaled model of the real system. If all the scaling parameters can be matched between the real and modeled systems, then the normalized test results from the prototype experiment can be used to predict the behavior of the real system.

Due to the complexity of the venous network, it is not practical to construct a true scale model in the laboratory. The scaling parameters can, however, be useful for deriving an appropriate model which can be simulated on the computer as will be shown in this chapter.

A Description of the Dimensionless Groups

In Chapter IV we derived a complete set of normalized equations and boundary conditions for flow in a single collapsible tube. The results of this analysis are expressed in Eqs. (6)-(12), which are all in normalized form. In addition, we must include the numerous expressions which define F under the variety of possible flow conditions [Eqs. (12-(21), (24), (26), (27)]. By inspection of these equations we find that the relevant dimensionless groups are:

$$\delta_c \quad ; \quad \beta \quad ; \quad \frac{1}{c_0(\xi)} \frac{dc_0(\xi)}{d\xi} \quad ; \quad \frac{1}{\rho c_0^2(0)} \frac{\partial p_e}{\partial \xi} \quad ;$$

$$\frac{C_f(\xi)\mu L}{\rho c_0(0)A_0(\xi)}^{\dagger} \quad ; \quad \frac{1}{A_0(\xi)}\frac{dA_0(\xi)}{d\xi} \quad ;$$

$$\frac{\rho c_0^2(0)C_V}{A_0(0)L} \quad ; \quad \frac{p_B - p_e(1)}{\rho c_0^2(0)} \quad ; \quad \frac{p_A - p_e(0)}{c_0(0)A_0(0)R_A} \quad ; \quad \frac{R_A A_0^2(0)}{C_f(0)\ \mu L}$$

$$\frac{L_1 A_0(0)}{\rho L} \quad ; \quad \frac{L_2 A_0(0)}{\rho L} \quad ; \quad \frac{R_1 A_0^2(0)}{C_f(0)\mu L} \quad ; \quad \frac{R_2 A_0^2(0)}{C_f(0)\mu L} \quad .$$

If we were to construct a properly scaled model of a particular system the parameters of the modeled system would have to be such that when combined into the above groups, each would equal its counterpart in the real system. Each of these groups which results from normalization of a boundary condition provides a means of determining one of the boundary parameters of the scaled system. These parameters are: p_A-$p_e(0)$; R_A ; C_V , R_1 , R_2 , L_1 , L_2 , and p_B-$p_e(1)$.

The remaining dimensionless groups describe the collapsible tube. Similarity of the second term, β , is assured if we assume that there exists one universal P-α law which is applicable along the entire length of both collapsible segments. Proper scaling of the first, third, and sixth groups requires that $A_0(\xi)$ and $c_0(\xi)$ be identical functions of ξ for both the model and the modeled system.

The two remaining groups,

---

†Laminar flow only.

$$\frac{1}{\rho c_0^2(0)} \frac{\partial p_e}{\partial \xi} \quad \text{and} \quad \frac{C_f(\xi)\mu L}{\rho c_0(0) A_0(\xi)}$$

pertain to the flow in the collapsible tube itself and will help us later to determine the criteria for modeling a system of branching vessels by a single tube.

An example will help to illustrate the implications of the scaling analysis. Presumably we can model a single venous segment by a single length of uniform collapsible tube with an appropriate choice of conditions at the boundaries of the vessel. If the value of each individual parameter which corresponds to that of the actual venous system is denoted by subscript "v" and that of the model by subscript "m," then we would expect the laws of similarity to hold if $\Pi_v = \Pi_m$ where Π represents any one of the dimensionless groups. If the dimensional parameters of the model are chosen so as to satisfy these criteria then each of the normalized variables (P, U, α, and C) will be identical functions of dimensionless time and distance for the two systems. This is essentially the approach taken, as much as possible, in the design of the flow experiments (see Chapter IX).

The dimensionless groups listed above have further significance with respect to the problem of modeling a collection of branching vessels by a single tube. This problem is taken up in the next section.

A Single Tube Model for a Branching Network of Tubes

In the representation we have adopted, the system of veins in the leg is modeled by a single length of collapsible tubing. The following

discussion will provide the rationale for such a model based on the previous results.

The system to be modeled is shown in schematic form below:

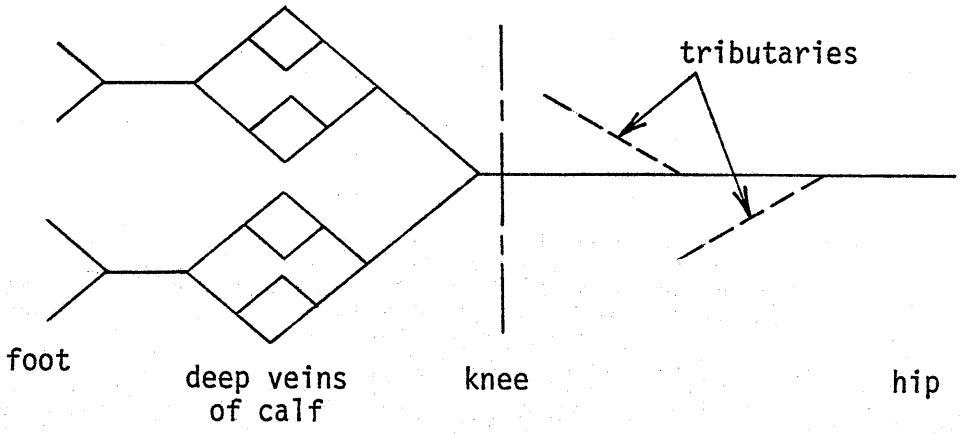

All branches of the deep venous system of the calf (really all vessels which drain through the popliteal vein) are included explicitly in the model. Those vessels which merge with the popliteal (or femoral) vein at points proximal to the knee are included only in terms of the effect they exert on flow in the vessel downstream of the junction.

To illustrate the relationship of this system to a single tube representation we first consider a junction of two vessels at a point distal to the knee.

Vessel Junction Within the Calf. The objective of this analysis is to determine the characteristics of a single tube of unstressed cross-sectional area, $A_{0_S}(\xi)$ which, in terms of the flow into the vessel downstream of a junction, is identical to the two-vessel system. The model

and modeled system are sketched below:

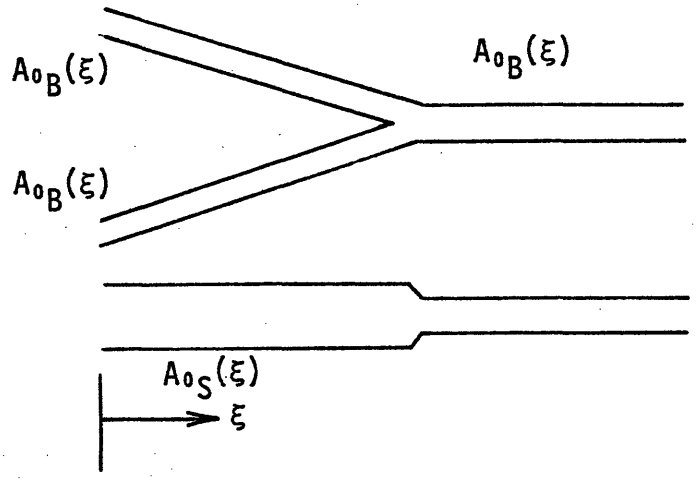

[$A_{0_B}(\xi)$ is the unstressed area of the main vessel. The tributaries are of equal unstressed area, $A_{0_B}(\xi)$.] The dissimilarities in flow at the junction due to the merging of the two tributary flows are neglected in this one-dimensional model. We define our requirements for equivalency of these two systems by stipulating that, at any point ξ upstream of the junction, all variables [u, p, A (in this case the total vessel area at the point ξ, $A = 2A_B$), and c] for the model are equal to their counterpart in the modeled system and that mass continuity is satisfied across the junction. These criteria are satisfied if (i) all the scaling parameters are equal; and (ii) if the normalizing quantities [i.e., $c_0(\xi)$, $\rho c_0^2(\xi)$, $A_0(\xi)$, and L] are equal. (This is not a "scaled" system in the true sense of the word since our intent is to produce a single tube model which is exactly equivalent to the multiple tube arrangement.)

Actually, only those scaling parameters involving the internal flow equations are relevant to the present argument. Those dimensionless groups dealing with the boundary conditions will again only be used in

determining the appropriate scaling of the boundary conditions.

Now we are in a position to define the equivalent system. All the criteria for equivalency are satisfied by the following relationships upstream of the junction:

$$c_{0_S}(\xi) = c_{0_B}(\xi) \quad ; \quad \rho c_{0_S}^2(\xi) = \rho c_{0_B}^2(\xi) \quad ;$$

$$A_{0_S}(\xi) = 2A_{0_B}(\xi) \quad ; \quad L_S = L_B \quad ; \quad \beta_S = \beta_B \tag{52}$$

$$\left(\frac{\partial p_e}{\partial \xi}\right)_S = \left(\frac{\partial p_e}{\partial \xi}\right)_B \quad ; \quad \left[\frac{C_f(\xi)\mu L}{\rho c_0(0) A_0(\xi)}\right]_S = \left[\frac{C_f(\xi)\mu L}{\rho c_0(0) A_0(\xi)}\right]_B \quad .$$

We find that an equivalent single tube model is one which is identical in all respects to the individual branch tubes with two exceptions: $A_{0_S}(\xi) = 2A_{0_B}(\xi)$ and $C_{f_S}(\xi) = 2C_{f_B}(\xi)$.

The extension of this result to numerous bifurcations is obvious. The friction coefficient must double at each bifurcation and the unstressed cross-sectional area of the single tube model at any point ξ must equal the sum of the unstressed cross-sectional areas of all the branch vessels at the same point ξ in the real venous system. This is equivalent to saying that if "n" is the number of bifurcations encountered traveling upstream from the knee joint at a distance ξ in the venous tree, then

$$A_{0_B}(\xi) = 2^n A_{0_B}(\xi) \quad \text{and} \quad C_{f_S}(\xi) = 2^n C_{f_B}(\xi) \quad . \tag{53}$$

Intuition confirms that C_f (which can be thought of as a measure of the magnitude of viscous effects) must increase in the single tube model as compared to the branching system in order for the pressure drop per unit distance to remain the same. This is to say that if a two-vessel system having the same cross-sectional area and total flow rate as a single tube is to have the same pressure drop, the viscosity in the single tube must be twice as large as in the two-branch system.

The weakest of the several assumptions made for this analysis is that of symmetry of the branching system. As will become evident in Chapter XI, the popliteal vein, upon entering the calf, divides into several long, straight conduits which extend to the ankle. In a circuit parallel to these main vessels and concentrated in the upper muscular part of the calf are a tangled mass of vessels of varying stiffness and diameter. Although we can extract very little quantitative information from the literature concerning the exact nature of these vessels, we would expect them to differ from the more direct vessels. This discrepancy will be discussed in Chapter XII.

The Effect of Junctions Proximal to the Calf. In determining the properties of our equivalent single tube model which allow us to mimic the effect of flow tributaries that are not implicitly included in the model we must, at the onset, make a reasonable assumption about the flow from each tributary. The first few junctions which are encountered progressing proximally from the knee are with vessels which primarily drain the lower leg and are either superficial veins (external and internal

saphenous) or are small deep veins (gastroenemeus). Because of the compression, these vessels will exhibit a time varying flow rate but of a much smaller amplitude owing either to their origin (superficial veins) or their size. For this reason, we have chosen to model their effect purely in terms of a leakage flow rate which is a function of ξ but independent of time. This leakage flow, Q_L , was recognized in Chapter IV in the writing of the mass conservation equation. As more is learned concerning the exact nature of flow in these tributaries, we may choose to introduce it as a function of time as well but, for the present, we leave it as a function of ξ only.

This relates to our model in the following way. Since no scaling is involved, all parameters of the vessel proximal to the knee have the same value as the main vessel which, in our case, is the popliteal, femoral, and iliac veins, as you proceed from the knee to the thigh. C_f , then, has a value of unity throughout this part of the system and $A_{0_S} = A_{0_B}$.

CHAPTER VIII:

STRUCTURAL PROPERTIES OF THE TUBE

The formulation of the problem of unsteady flow in a collapsible-distensible tube found in Chapter IV was complete in all but one respect: the form of the constitutive expression or "tube law" relating transmural pressure to normalized area. In this chapter we will complete that analysis by providing a theoretical background for predicting the functional dependence indicated in Eq. (9). To accomplish this we define two distinct phases of tube inflation which are discussed separately below.

The Inflated or Distended Tube

The tube law for the inflated tube is based on several assumptions which combine to make the analysis relatively straightforward. These are:

- the cross-section of the tube is circular
- the vessel is thin-walled ($h/R \ll 1$)
- the vessel wall is uniform and isotropic
- viscoelastic effects are ignored
- either longitudinal tension or total length are constant
- inertial effects are neglected
- the bulk modulus, K, and Young's modulus, E, are both much greater than the transmural pressure, p_{tr}
- E is not a function of p_{tr}
- the surrounding medium exerts negligible radial force on the tube.

The validity of these assumptions will be discussed in conjunction with the similar set of assumptions given later for the collapsed tube.

With acceptance of these conditions we can proceed as many others have to derive the constitutive law for the range of positive transmural pressures for which the assumptions are valid. Using Laplace's law to relate the hoop stress in the wall to the transmural pressure, p_{tr}, we can derive an expression relating normalized area to p_{tr} (for small values of $2p_{tr}r_0/E_{tan}h_0$):

$$\alpha \equiv \frac{A}{A_0(\xi)} \cong \left(1 - \frac{2p_{tr}}{E_{tan}} \frac{r_0}{h_0}\right)^{-1} , \qquad (54)$$

where the subscripts refer to the unstressed or resting state of the tube and E_{tan} is the Young's modulus in the tangential direction. Another result of this analysis is an expression for wave speed:

$$c = \left(\frac{E_{tan}}{2\rho} \frac{h_0}{r_0\alpha}\right)^{\frac{1}{2}} , \qquad (55)$$

which is often referred to as the Moens-Kortweig Equation. For additional information concerning the derivation of these expressions, the reader is reffered to one of a number of papers and texts covering arterial wall mechanical (e.g., McDonald[47] or Strandness and Sumner[48]).

The Fully or Partially Collapsed Tube

In the range of pressures for which the tube is either fully or partially collapsed one must, again, make several simplifying assumptions which can later be verified either by direct observation or indirectly as in the case of experimental verification of results obtained using a particular model. The assumptions are, in some ways, quite different for a collapsed tube and, as a result, the analysis too must differ from that followed for the distended tube. The shape of the tube cross-section varies and the nature of wall stresses have shifted from tension to primarily bending. Because of possible non-uniform wall composition, the effective Young's modulus for bending may differ from that in the previous analysis and will be referred to as E_{bend}. (Think for example of a sheet comprised of laminates of different materials.) Due to these and other differences between the two models, we must now require for the purpose of constructing a theoretical model, that:

- the vessel wall be inextensible (i.e., $E_{tan} \cong \infty$);
- $h/D << 1$;
- $A = A(p_{tr}, x)$ alone;
- E_{bend} be independent of p_{tr} ;
- the tube environment have no effect on the tube law.

Theoretical Description. The methods used for determining the constitutive law for collapsed states rely on the equations of equilibrium for a small element of tube wall acted upon by a transmural pressure,

tension (T), shear (N) and bending moments (M) as illustrated in the figure.

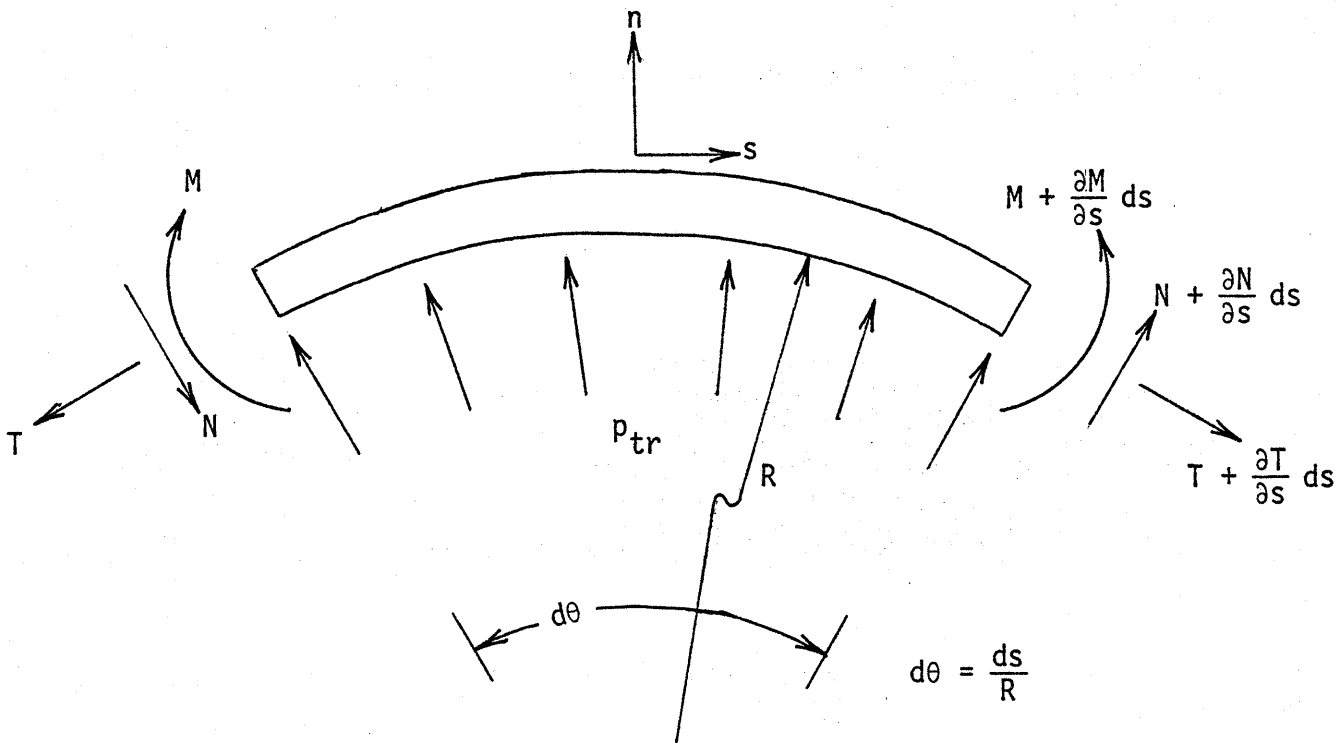

We arrive at the following set of equations from force and moment equilibrium conditions:

$$\sum F_n = 0 \quad ; \quad \frac{dN^*}{ds^*} - T^* \frac{d\theta}{ds^*} + P = 0$$

$$\sum F_t = 0 \quad ; \quad \frac{dT^*}{ds^*} + N^* \frac{d\theta}{ds^*} = 0 \qquad (56)$$

$$\sum M = 0 \quad ; \quad \frac{dM^*}{ds^*} + N^* = 0 \ .$$

In addition, we have the constitutive relation,

$$M^* + \frac{d\theta}{ds^*} - \left(\frac{d\theta}{ds^*}\right)_{P=0} = 0 \quad , \tag{57}$$

where the normalized variables denoted by the asterisk are defined below:

$$P \equiv \frac{p_{tr}}{EI/R^2} \quad ; \quad T^* \equiv \frac{T}{EI/R^2} \quad ; \quad N^* \equiv \frac{N}{EI/R^2}$$

$$s^* \equiv \frac{s}{R} \quad ; \quad M^* \equiv \frac{M}{EI/R} \tag{58}$$

The boundary conditions on one quadrant of the tube depend upon whether or not the tube walls are in contact at $s = \pi/2$. Referring to the following diagram, we can state the boundary conditions for each case as follows.

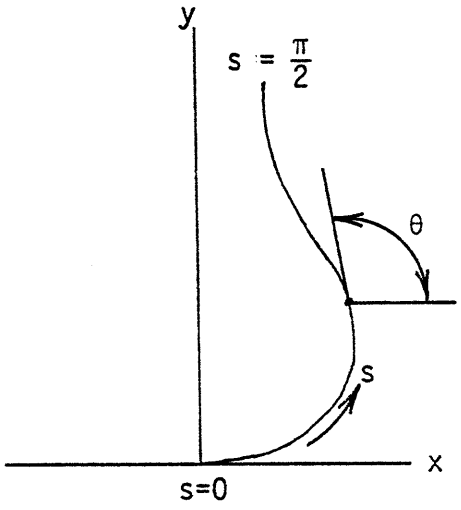

Case I. Tube walls not in contact

$$\theta(0) = 0 \quad , \quad \theta\left(\frac{\pi}{2}\right) = \frac{\pi}{2}$$

$$N^*(0) = 0 \quad , \quad N^*\left(\frac{\pi}{2}\right) = 0 \quad . \tag{59}$$

These last two conditions are based on the necessary condition that N^* be continuous at $s = 0$ and $s = \pi/2$. Using Eq. (4d) and the symmetry assumption, we see that N^* must be zero at these two points.

Case II. Tube walls in point contact

$$\theta(0) = 0 \quad , \quad \theta\left(\frac{\pi}{2}\right) = \frac{\pi}{2}$$

$$N^*(0) = 0 \quad , \quad T^*\left(\frac{\pi}{2}\right) = 0 \quad . \tag{60}$$

The fourth condition has changed because N^* can now be discontinuous at $s = \pi/2$ but, based on the equilibrium of one half of the tube, T^* must be zero.

Case III. Tube walls in line contact

$$\theta(0) = 0 \quad , \quad \theta(s_c) = \frac{\pi}{2}$$

$$N^*(0) = 0 \quad , \quad T^*(s_c) = 0 \quad . \tag{61}$$

where s_c is the value of s at which contact first occurs. This case can be shown to satisfy a similarity solution which, given a solution

at one pressure, permits us to determine all other solutions satisfying these same boundary conditions.

A Similarity Solution for Collapsed States. To illustrate the existence of a similarity solution, we first replace s by $\bar{s}$ in the governing equations where $\bar{s} = s/s_c$, so that the boundary conditions become

$$\begin{aligned} \theta(0) &= 0 \quad , \quad \theta(1) = \frac{\pi}{2} \\ N^*(0) &= 0 \quad , \quad T^*(1) = 0 \quad . \end{aligned} \tag{62}$$

Assume then that we know one solution at $P = P_s$ which satisfies the equations and boundary conditions and that this solution is given by $\bar{N}(\bar{s})$, $\bar{T}(\bar{s})$, $\bar{\theta}(\bar{s})$, and $\bar{M}(\bar{s})$. If we then introduce the following variable transformation,

$$\begin{aligned} N'(s') &\equiv (P/P_s)^{1/3}\ \bar{N}(\bar{s}) \\ T'(s') &\equiv (P/P_s)^{2/3}\ \bar{T}(\bar{s}) \\ \theta'(s') &\equiv \bar{\theta}(\bar{s}) \\ s' &\equiv (P_s/P)^{1/3}\ \bar{s} \\ M'(s') &\equiv (P/P_s)^{2/3}\ \bar{M}(\bar{s}) \end{aligned} \tag{63}$$

into the governing equations, we find that N', T', ... M' is also a solution. In this manner all solutions satisfying the equations and boundary conditions for Case III can be found, thus proving the existence

of a similarity solution. A consequence of this result is that we can express the cross-sectional area as

$$A = A_s(P_s/P)^{2/3} \quad . \tag{64}$$

This same result can be reached through dimensional arguments. If the wall thickness is small compared with the local radius of wall curvature R_c, and since the boundary of the problem is located at s_c which cannot be related to the original perimeter, then we can say there is no characteristic length. The radius of curvature at any point must then depend on the two dimensional qualitites, EI (the tube stiffness) and p_{tr}. Accordingly, we can say that

$$R_c = fn(EI, p_{tr}) \quad . \tag{65}$$

The physical dimensions of each term are given below:

$$[R_c] = L$$
$$[EI] = FL$$
$$[p_{tr}] = FL^{-2} \quad .$$

The only possible combination of these terms which satisfies the above functional relationship is an expression for the wall curvature:

$$R_c = \text{constant} \times \left(\frac{EI}{-p_{tr}}\right)^{1/3} \quad . \tag{66}$$

As this expression can be written for each point along the tube (with different constants), the cross-sectional area can be shown to vary as

R_c^2 ; hence,

$$A = \text{constant} \times \left(\frac{EI}{-p_{tr}}\right)^{2/3} . \qquad (67)$$

This result can be directly compared with Eq. (64) derived on the basis of the governing equations.

Numerical Solutions. The problem remains, however, both of obtaining the solution we assumed known in this analysis and of obtaining solutions for Cases I and II for which no similarity solution exists. This problem has been solved numerically in various degrees by Tadjbakhsh and Odeh,[49] Flaherty, Keller, and Rubinow,[40] and Kresh and Noordergraaf.[50] Of these, the paper by Flaherty *et al.* provides the most complete analysis of tubes which are circular in their initial state. Their results are shown on Figs. 7 and 8 by the line labeled "theory" in the form of a plot between normalized area and normalized transmural pressure. The work of Kresch and Noordergraaf considers the effect of initially non-circular tubes, but their analysis is incorrect for configurations in which the opposing walls are in contact. Their error results from neglecting to take into account the normal forces exerted on the interface between the two walls. The numerical methods were similar in each case and if interested the reader should look to these references for more details. In addition to computing the shapes of the partially collapsed cross-sections, Flaherty *et al.* also solved for the velocity profiles within the vessel assuming fully developed laminar flow. These results

were used in our study to estimate the flow resistance term for Poiseuille flow in a collapsed tube [see Eq. (21)].

Limitations of the Theoretical Description

But, as noted already, numerous assumptions have been made in arriving at these results and we should investigate these in a more critical manner before blindly applying them to veins.

The Effect of Muscular Tissue. One glaring omission is the neglect in the model of any effect of the external muscular tissue which surrounds all deep veins of the calf. Intuitively, we might expect the tissue to have greatest influence in the portion of the P-α curve where large changes in shape occur over relatively small changes in transmural pressure. Although an exact analysis has not been performed and would be extremely difficult, we can get some idea of the order of magnitude of tissue effects by considering the following example.

Assume that the tissue-surrounded vein can be modeled as a small diameter circular hole in a large cylindrical body. This problem is analyzed in any of a number of texts on structural mechanics (e.g., Timoshenko[51]). Following their methods, we consider the deflection, due to a pressure difference between the inside (p_i) and the outside (p_o) of the cylinder:

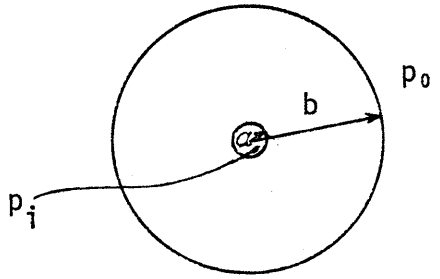

Radial deflection is denoted by u, the Young's modulus by E, and Poisson's ratio by μ. Using the basic equilibrium equations, one can solve for $u(r)$ with the result given below:

$$u(r) = \frac{1-\mu}{E} \frac{a^2 p_i - b^2 p_o}{b^2 - a^2} r + \frac{1+\mu}{E} \frac{a^2 b^2 (p_i - p_o)}{(b^2 - a^2) r} \quad . \tag{68}$$

By assumption, $a \ll b$, giving

$$u(r) = \frac{1 - \mu}{E} r(-p_o) + \frac{1 + \mu}{E} \frac{a^2}{r} (p_i - p_o) \quad . \tag{69}$$

Evaluating the deflection at $r = a$, we have

$$u(a) = \frac{a}{E} \left[(1 + \mu) p_i - 2 p_o \right] \quad . \tag{70}$$

For human tissue, $\mu \cong 0.5$ and, as a rough estimate, we can say that

$$\frac{u(a)}{a} \cong \frac{2 p_{tr}}{E} \quad . \tag{71}$$

This result pertains to the deflections associated with a symmetric hole, i.e., the hole does not change geometry. But, for an order of magnitude estimate of the pressures required to collapse the vessel, we can assume that, in going from the circular to collapsed state, $u \cong a/2$ and the required transmural pressure associated with this shape change can be estimated as indicated above and given by

$$p_{tr} \cong \frac{E}{4} \quad \text{, for collapse.}$$

In other words, tissue with a Young's modulus of $E \cong 6 \times 10^4$ dynes/cm^2 would prevent collapse for transmural pressures less than approximately 1.5×10^4 dynes/cm^2 or, $p_{tr} \cong 11$ mm Hg. In Chapter XI in which we establish the tube law used for the venous calculations we will see that the magnitude of the tissue influence is, indeed, a significant factor in this range of pressures.

When the vessel is either distended or fully collapsed, however, it can be shown by similar estimates that the tissue will exert a much smaller relative effect due to the steeper slope of the P-α law for the tube alone. This will be shown more clearly in Chapter XI. In this later discussion, the tissue is considered to be the dominant influence in the collapsing region while the tube walls themselves provide the observed stiffness in other regions. Thus, in this intermediate zone, the slope of the pressure-area law will be no less than the limit established here, or

$$\frac{dp_{tr}}{dA} \gtrsim \frac{E}{4A} \quad .$$

It should be noted that, in all arterial studies, the effect of surrounding tissue has been entirely neglected. According to our estimates, this oversight is entirely justified as long as the transmural pressures are great enought to insure that the vessels remain filled by pressures well into the distended range.

Viscoelasticity. A second possible influence which deserves consideration is that of viscoelasticity. This topic has received considerable attention in the literature on arterial hemodynamics and is reviewed in most of the recent texts (e.g., McDonald[47]). In the analysis of wall viscosity effects, one approach is to divide the effective Young's modulus into two parts, one real and the other imaginary. The real part, called E_{dyn}, is due to the spring-like nature of the walls and is what we generally think of as the Young's modulus. The imaginary part, $\eta\omega$, is a retarding force exerted as a result of viscous effects within the vessel wall itself where η is the coefficient of viscosity and ω is the radian frequency. It follows then that

$$E_{eff} = \left[E_{dyn}^2 + (\eta\omega)^2 \right]^{\frac{1}{2}} , \qquad (72)$$

and, as a consequence in this model, the faster a tube is either inflated or deflated, the stiffer it will seem. The value of the viscous components has been measured in arteries by Gow and Taylor[52] and Bergel[53] and was found to be approximately 9 to 12 percent of the dynamic component for frequencies in the range of the arterial pulse (1-10 Hz).

Because the veins are generally thinner-walled vessels than arteries and because the range of frequencies of interest in our study is probably much lower than 10 Hz, we feel justified in neglecting the viscoelasticity of the venous wall. Additionally, the primary importance of viscous effects is in their influence on the damping of propagating waves, an effect which has little significance in the general

trends looked for in our study.

There is, however, one possible exception to the argument for neglecting viscous effects. That is in the intermediate region of collapse where large deflections occur in the muscular tissue as previously noted. As this collapse is made to occur more and more rapidly (which is one of the goals of this investigation) viscous effects associated with muscular tissue might become a significant factor, and one which we should attempt to estimate.

A formulation for the effective modulus similar to that expressed in Eq. (72) was derived for muscular tissue with accompanying experimental measurements by von Gierke *et al.*[54] Their results yielded values for E_{dyn} of $\sim 3 \times 10^4$ dynes/cm^2 and for η of $\sim$ 150 dynes/cm^2. Again, for frequencies less than $\sim$ 10 Hz, the viscous effects account for less than 1/3 of the effective modulus. Clearly, if the freuqencies encountered in the calculation of vessel collapse exceed 10 Hz, viscoelasticity will become important and the type of analysis will have to undergo the necessary modifications. One of these modifications lies in the basic nature of the computer simulation. Introducing viscoelasticity changes the equations from hyperbolic to parabolic as noted by Kivity *et al.*[55] Methods such as the Lax-Wendroff method can be used to solve a system of parabolic equations and would be the method of choice if viscoelasticity were added to our analysis.

Longitudinal Tension. A final comment should be made concerning the effect of longitudinal tension. Tension was not included in our

model for several reasons. First, we were unable to find any information in the literature concerning the degree of venous tension *in vivo* other than an occasional comment concerning its existence. Secondly, we should be able to predict what effect, if any, longitudinal tension might have.

In a uniformly collapsing vessel, the effect would be exhibited only in terms of a slight decrease in the wall thickness and, barring any influence of non-isotropy of the vessel wall, a corresponding decrease in stiffness would result. This would be most pronounced in the collapsed tube since K_p varies as h^3. Therefore, a small decrease in h would lead to a considerable increase in vessel compliance. However, it is in this range of pressures that our knowledge of the true venous characteristics is most incomplete and the corrections due to wall tension would be of little value.

The second effect of tension, and probably the most significant, occurs when the vessel undergoes large area changes over relatively small distances. An analysis similar to that of a curved membrane acted upon by tension and a pressure difference would tell us that, where the wall curvature is positive (i.e., $d^2r/dx^2 > 0$), tension would exert an effective positive transmural pressure--a negative pressure being associated with negative curvature. To explore the significance of this effect, we can estimate the magnitude of the effective pressure due to tension, p_t, given a wall tension T and the tube properties and compare it to the applied external pressures. Assuming membrane stresses

$$p_t \cong T \frac{d^2r}{dx^2} \quad , \tag{73}$$

for small deflections. Since

$$A \cong \pi r^2 \quad \text{or} \quad dA = 2\pi r\, dr \quad ,$$

for nearly circular tubes, Eq. (73) can be rewritten as

$$\begin{aligned} p_t &\cong T \frac{d}{dx}\left(\frac{1}{2\pi}\sqrt{\pi/A}\ \frac{dA}{dx}\right) \\ &= \frac{T}{\sqrt{\pi}}\ \frac{d^2A^{\frac{1}{2}}}{dx^2} \quad . \end{aligned} \tag{74}$$

As an order of magnitude estimate, if $T \cong Ap_{mv}/2\pi r = \frac{r}{2} p_{mv}$ (where p_{mv} is the mean venous pressure), then

$$p_t \simeq \frac{p_{mv}}{2\pi}\ \sqrt{A}\ \frac{d^2A^{\frac{1}{2}}}{dx^2}$$

or

$$p_t \simeq \frac{p_{mv}}{2\pi}\ \sqrt{A}\ \frac{\Delta A^{\frac{1}{2}}}{(\Delta x)^2} \quad . \tag{75}$$

And if area changes typically take place over a minimum distance of four diameters,

$$p_t \cong \frac{p_{mv}}{(2)(16)(D^2)}\ \frac{A}{\pi} = 0.008\ p_{mv} \quad . \tag{76}$$

For vessel diameters of approximately 0.7 cm, $p_t/p_e \simeq 0.008(p_{mv}/p_e)$.

This estimate, although derived by way of very crude approximations, seems to lend credence to our assumption of negligible wall tension effects. For some instances in which area changes are found by our calculations to be even more abrupt than these estimates or if T were greater than predicted here, tension would tend to smooth out the area transition with corresponding changes in the local fluid dynamic predictions.

CHAPTER IX:

FLOW EXPERIMENTS

Difficulties in Applying the Scaling Laws to the Design of the Experiment

Using the scaling laws of Chapter VII we could, in principle, design a set of properly scaled experiments to determine the nature of flows in the veins of the lower leg. In attempting to set of these experiments, however, we encounter a number of practical limitations.

The first of these concerns the structural properties of the tube itself. The vein wall has a complicated structure resulting in a highly non-iostropic behavior and a variable Young's modulus depending on the state of tension in the material. Also, there is reason to believe (although this has not yet been observed experimentally) that the modulus in bending differs from that in tension. Add to this the relatively unknown influence of the surrounding viscoelastic muscular tissue and you have an extremely complicated tube behavior, one which would be almost impossible to mimic in the laboratory with any material other than actual veins.

Another difficulty is posed by the complexity of the venous network. Even if the exact geometry of the system could be determined, it would be a major undertaking to create some sort of an elastic replica of the interconnecting structure. The model would have to be one continuous piece completely void of rigid parts because of the nature of wave propagation and vessel collapse at junctions between rigid and compliant tubes.

This requirement would eliminate the possibility of piecing together a system of individual segments.

Finally, we must recognize that the different veins vary considerably in wall stiffness and unstressed cross-sectional area. Although these variations could be approximated by an elastic vessel in which the wall thickness and cross-sectional area are appropriately varied, we are not, at present, capable of manufacturing tubes of this type. Methods are being tested which will eventually allow some flexibility in producing the desired characteristics, but still not to the extent required for the construction of an exact scale model.

Because of these practical limitations, we view the flow experiments primarily as a means of evaluating the computer simulations. Since we naturally want to conduct experiments which are somewhat representative of induced venous flows we have chosen the model parameters to be roughly equivalent to their physiological counterparts using the appropriate scaling laws. And, in the course of experimentation, we have attempted to bracket the actual physiologic range of parameters. After conducting these tests, we then perform the corresponding computations and compare results, looking primarily for the accurate prediction of general trends. The results of this comparison are presented in Chapter X.

Description of the Hydraulic Model

We used the hydraulic model shown in Fig. 1. Basically, it can be divided into three parts: the test section, upstream components, and

downstream components.

Upstream Boundary. A high pressure reservoir is located at the upstream end of the flow circuit which is kept at a constant pressure, approximately equal to the mean arterial pressure. This drains through a resistive element which represents the resistance of the capillary bed and arterioles. The combination of these components acts to maintain a relatively constant inflow to the test section since the pressure downstream of the resistance element varies by only a fraction of the resting Δp even during pressurization of the test section.

Downstream Boundary. Downstream of the test section are two rigid ducts separated by a capacitance tank. The tube adjacent to the test section roughly models the resistance and inductance of vessels distal to the vena cava. The capacitance tank represents the highly distensible vena cava and empties through the second rigid duct, into a constant pressure reservoir (the right heart in this model).

Test Section. Both the upstream and downstream flow components are designed so as to create the proper physiologic environment for the test section. The test section is shown in Fig. 2. It contains a single flexible tube running the entire length of the chamber which is collapsed by various cycles of external pressure. The chamber itself is divided into two parts as shown in the diagram. A plastic sleeve runs the length of the upstream chamber which permits the application of external pressure

over this portion of the collapsible tube alone. By means of this separation, the pressure applied in the upstream chamber has little effect on the pressure in the downstream chamber which is vented to the outside.

We chose this two-chamber design to reduce the undesirable effects on the flow of the downstream rigid support. A set of preliminary experiments were conducted with this same system but without the two-chamber test section. The flow was observed to be highly oscillatory and largely governed by the downstream parameters and the nature of the point of attachment between the rigid and collapsing tubes. As this means of support is highly non-physiologic, we sought another configuration which minimized the influence of this artifact. The introduction of a pressurizing sleeve removed the attachment point from the pressurized zone and, although it did not eliminate the effect of reflections from the rigid tube, the effect on flow inside the collapsing portion of the tube was minimized.

There are, however, two possible drawbacks with this method of pressure application. The plastic sleeve, due to its own structural integrity, cannot apply a perfectly uniform pressure around the circumference of the vessel. In regions where the plastic makes sharp bends in order to follow the contour of the tube, the plastic might actually depart from the tube as shown in the sketch.

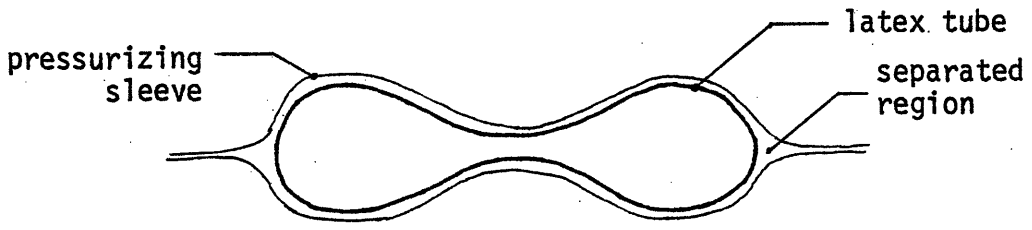

In these experiments the resulting non-uniformities in the circumferential pressure distribution are kept small by using a very flexible, thin-walled plastic sleeve.

The second artifact occurs at the two ends of the pressurized zone. With the application of pressure the plastic sleeve itself will collapse onto the penrose tube except at the ends where it connects to a rigid support. The contour of the plastic will be determined primarily by its diameter and the amount of slack in the sleeve. This contour will, in general, not follow exactly the contour of the tube, again leading to a region of non-uniform compression, this time in the longitudinal direction as well as circumferential. Presumably, keeping the length of this region to a minimum reduces the effect it exerts on the overall flow.

It should be noted that although the method we employed for reducing end effects is not perfect, no method was found which could eliminate these effects completely. Ours was a compromise of sorts, but one which apparently worked considering the agreement between theoretical and experimental results presented in the next chapter.

Description of the Flow Experiments

The value of each parameter in the experiment was selected so as to reflect the general characteristics of the physiologic system to be modeled. Since exact scaling was not possible, the choices were somewhat arbitrary but fell within the expected physiologic range.

The complete experimental sequence is presented in Table 3. [The

reference experiment (number 1 in the table) is the test to which all others were compared.] In the column directly below the test number are listed the parameters of the test. In each case, one parameter was varied (the value underlined in each column) and its effect on the measured variables observed. For the most part the parameters labeled on the left correspond to our previous notation. Several parameters have not been mentioned previously. S refers to the time required for the pressure to reach $1 - \frac{1}{e}$ of its maximum value, $p_{e_{max}}$. The initial external pressures in the two chambers are labeled p_{e_1} and p_{e_2} for the upstream and downstream chambers, respectively.

Measurements and Instrumentation. In each experiment flow rate and pressure just downstream of the test section were measured. In addition, transmural pressure was recorded at seven positions along the collapsing portion of the tube except in those tests with non-zero initial flow rate.

Flow rates were measured using a Carolina Medical Instruments E-M Flowmeter. Sodium chloride was added to the flow solution to produce the required ionic content. Calibrations were performed and the instrument was found to be linear over the entire range of measurements.

Pressure measurements were made with a C.J. Enterprises Differential Pressure Transducer with a 5 psi range. In order to obtain measurements of transmural pressure, a catheter (No. 18 stainless steel hypodermic needle, 49 cm in length) was inserted from the upstream end. Internal pressure was measured at the tip of the catheter; external

pressure via a tap in the side of the test chamber.

The open end of the catheter was pointed in the downstream direction. Because of flow separation at the base of the needle, errors were anticipated of the order of ρu^2 . The actual error can be estimated by comparison to experiments measuring base pressure[56] and are approximately $0.17\rho u^2$ for the worst possible case.

Additional error is associated with the limited time response of the catheter-transducer system. The resistance and inductance of the catheter combined with the compliance of the transducer comprise an R-L-C circuit which can be analyzed accordingly. Based on computed values for R, L, and C , we can estimate the characteristics of the system which were:

- damping coefficient $\xi = 0.57$;
- settling time (time for the signal to come to within 2% of an applied step in pressure) = 0.11 sec;
- maximum overshoot in response to a step function = 0.11 .

Our observations of the response to a near step function confirmed these predictions. Clearly, this response characteristic <u>is</u> a limiting factor in making high frequency pressure measurements. Our objective, however, was merely to observe the collapse process as a function of distance, and the achieved accuracy was sufficient for that purpose. The absence of high frequency components from the recordings do not, however, preclude their existence, the cut-off frequency being approximately 10 Hz.

As the tube collapses around the catheter another source of error arises. In the adjacent sketch we see a cross-sectional view of the

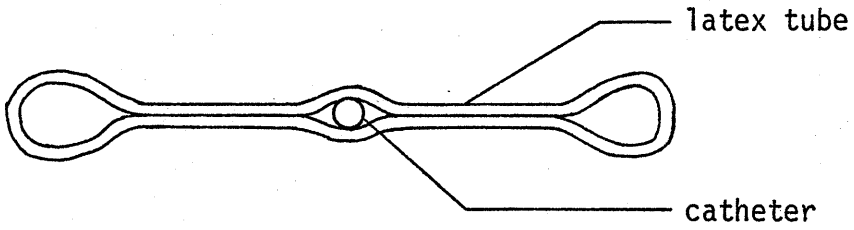

catheter-tube configuration in the collapsed state. It is obvious that the pressure at the catheter tip is not necessarily the pressure in the two sidelobes of the collapsed tube. Because of the two small channels immediately adjacent to the catheter and running parallel to it the measured pressure may correspond to a point somewhere upstream of the catheter tip. These errors will become more pronounced as the tube collapses but will not affect the results prior to collapse.

Also, when the tube collapses around the catheter as shown, flow will be disturbed to a greater and greater extent as the catheter is inserted further into the tube. The influence of the catheter was clearly visible when the catheter tip was moved to different radial positions at the same longitudinal location. As expected, the pre-collapse pressure profile was unaffected but the falling portion of the pressure trace (signifying tube collapse) differed quite significantly.

As a final remark concerning the instrumentation for the experiment, a Honeywell Visicorder was used for recording all pressure and flow traces. The response time of this recorder was not a factor limiting our results.

The Collapsible Tube. The collapsible tube used in these tests was a penrose drainage tube from Davol Inc., made of latex rubber with

a ½ inch diameter. Because of the process by which the tube is made, the wall thickness varies nearly linearly from one end to another. The range for this tube was between 0.280 and 0.365 mm. For all but the final test (Experiment 21) the tube was positioned with the thin-walled end pointing upstream. The characteristics of the tube are given in Table 7.

Experimental Results. The test numbers refer to the listing in Table 3 of all experiments. The results of these tests are presented in the following format:

(1) A complete set of flow and pressure traces for Expt. 1 (Fig. 9).

(2) Exit flow rate for each of the experiments (Figs. 10-13).

(3) Quantitative comparison of characteristic parameters (Table 4).

The three plots in Fig. 9 show the applied external pressure, six transmural pressure recordings, and the volume flow rate at the exit of the test section, each plotted against time. The five lower curves in the center plot are pressure measurements made at ξ = 0.06, 0.15, 0.24, 0.33, and 0.42 . The upper curve in the same graph is the transmural pressure as measured just downstream of the test section.

The plots of exit flow in Figs. 10-13 contain both the experimental result (dashed line) and the predictions of the theory (solid line) which will be discussed in Chapter X. The tabulated results of item (3) above are provided as a means of going beyond mere graphical comparisons and of putting the comparisons on a quantitative basis. A number of characteristic quantities have been identified on the flow and pressure traces in Fig. 9. These are (referring to the numbers in the figure and in the

table where applicable);

I. maximum flow rate;

II. time of maximum flow rate;

III. emptying time--defined as the time at which the flow rate first goes to zero;

IV. time between the first flow maxima and first flow minima;

V. ratio between the first two flow maxima;

VI. collapse time--defined as the time at which the pressure trace first deviates from the plateau region near zero transmural pressure.

Each quantity is presented in the table in the form of a ratio between the values of the parameter in each particular test and the value of the same parameter in Test 1. For item VI above the single number represents the average of five ratios computed for each of the five pressure traces inside the collapsing portion of the tube. Included in Table 4 are the comparisons for the flow simulations as well. These will be referred to again in the following chapter.

From these experiments alone, however, much can be said concerning the nature of unsteady flow from a collapsible tube. The collection of transmural pressure recordings and visual observations support the intuitive concept that the collapse proceeds in the upstream direction, starting at the downstream end of the pressurized zone. The early stages of collapse occur very rapidly. Within a second of the onset of pressure, the tube is highly collapsed at the downstream end. This necked down region impedes the emptying of the remainder of the tube due to the

resulting high viscous flow resistance. This zone of collapse can be seen to propagate upstream more and more slowly as the tube empties. Eventually, the tube reaches a new equilibrium configuration, the pressurized zone being more or less uniformly collapsed depending on the amplitude of the external pressure and the magnitude of the steady flow rate. (See Chapter X for a more complete physical description.)

Analysis of Flow Oscillations. One primary oscillation frequency is evident in the recordings of downstream flow rate. We can explain this mechanism by analogy to a nearly equivalent electrical circuit consisting of two capacitors, a resistor, and an inductor.

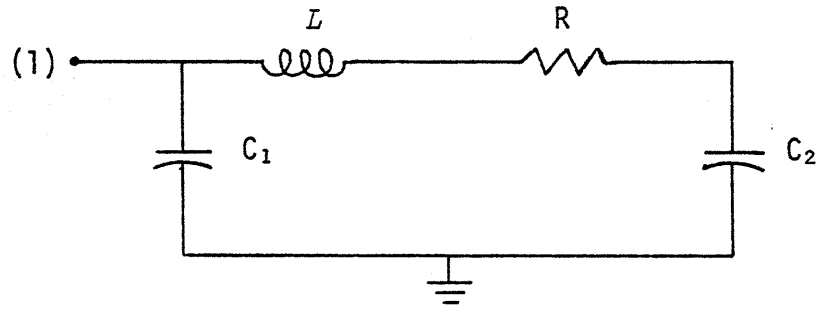

The circuit is initially excited by an impulse event at (1) which is created in our real system by the initial collapse of the tube. This charges C_1 and sets up a flow through L and R into C_2. The response of the system as a whole is a damped oscillation such as is seen in the recordings of flow rate at the exit. The oscillation frequency is determined, in the analog model, by the equation

$$\omega_n = \left(\frac{1}{LC_1} + \frac{1}{LC_2}\right)^{\frac{1}{2}} . \qquad (77)$$

We can see that if one capacitance is much smaller than the other (say, $C_1 << C_2$), then

$$\omega_n \cong \left(\frac{1}{LC_1}\right)^{\frac{1}{2}} \quad . \tag{78}$$

In the flow experiment, C_1 is represented by the section of flexible tubing downstream of the necked down zone. Most of the volume excursion can be seen to take place in the region extending approximately 2 cm downstream from the point of maximum constriction. This capacitance, although difficult to estimate, is likely to be much smaller than the downstream capacitance in the experimental model. A rough estimate of the smaller capacitance can be made, based on the length of the partially collapsed zone ℓ, the cross-sectional area difference $A_2 - A_1$, and the pressure required to collapse the vessel $\Delta p_{collapse}$ (see diagram). For the following estimates,

$$\ell = 2 \text{ cm}$$

$$A_2 - A_1 \simeq 1 \text{ cm}^2$$

$$\Delta p_{collapse} \simeq 1000 \text{ dynes/cm}^2 ,$$

$$C_1 = \frac{\Delta V}{\Delta p} = 10^{-3} \frac{\text{cm}^3}{\text{dynes/cm}^2} \quad .$$

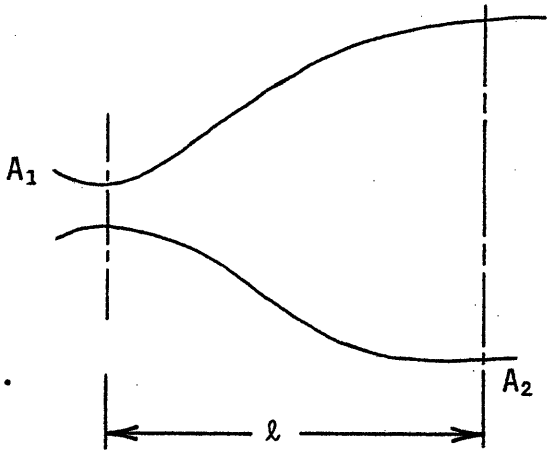

This value is approximately an order of magnitude below that of the downstream capacitance even if we neglect the presence of the discharge reservoir which would act essentially as a ground (infinite capacitance). The frequency of oscillations based on this value for C_1 and for L (= $\rho L/A$)

of $22/0.317 = 69.4$ gm/cm^4 gives us

$$f_n \equiv \frac{\omega_n}{2\pi} \cong 0.6 \text{ Hz} \quad ,$$

which is in excellent agreement with the observed frequency (~ .8 Hz) considering the simplicity of the model.

Another mode of oscillation which is not evident in most flow traces but which was observed in the pressure recordings made at the flow meter can be attributed to wave propagation back-and-forth in the downstream section of the collapsible tubing. Waves excited by the impulsive flow acceleration can be reflected at any point in the system where the impedance changes abruptly. Abrupt changes can be found at the downstream point of attachment to the rigid tube, and at the point of sudden change in area. The frequency of the oscillations associated with the mechanism is determined by the length of the wave-carrying segment and the mean wave speed. Strong nonlinearities in wave speed within the range of transmural pressures occurring in this section of tubing, give rise to quite a wide range of possible frequencies for this mode of oscillation, as evidenced by the following calculation:

$$L = 25 \text{ cm}$$

$$C = 60\text{-}700 \text{ cm/sec}$$

$$f_n = \frac{C}{2L} = 1.20 \rightarrow 14 \text{ Hz} \quad .$$

Again, agreement is good between these estimates and the range of observed frequencies.

Our ability to analyze wave processes is somewhat limited in the experiments due to the lack of high resolution information concerning the pressures and flows at points inside the tube. In this respect, the numerical simulations proved to be indispensible. In the next chapter we discuss these wave phenomena again in light of the more detailed information available through the numerical methods of analysis.

The results of the entire range of experiments were surprisingly similar in many respects. Of particular interest is the apparent decoupling between the processes inside the collapsing part of the vessel (see, in particular, those parameters which measure collapse times and emptying time) and the components determining the downstream boundary condition. The question arises of whether or not this apparent decoupling can be attributed to a critical ($u = c$) or supercritical ($u \geq c$) condition at the throat or region of minimum area. Again, this question can be better analyzed with the aid of the computer results and will be taken up in the next chapter.

The most significant effects on the measured variables can be attributed to changes in the fluid viscosity and in the rise-time and maximum value of the external pressure. Also significant in terms of the total emptying time was the introduction of non-zero initial flow rates. We would expect these changes to affect the entire flow system regardless of the situation at the necked down region. The effect of viscosity changes are related to the findings of Appendix B. There we see that, if the flow is viscous dominated, the emptying time should vary inversely with the square of the viscosity. The experiments do

not exhibit this trend, although there is a strong effect due to the change in viscosity, and we conclude that flow, at least during an important initial phase, is not dominated by viscous forces. (In fact, if an initial period of inertial-dominated flow did not exist, the flow rates for small times would approach infinity.) Although not dominated by viscous effects, the flow from the collapsing vessel is certain to be influenced by them, particularly in the latter stages of collapse. This result merely tells us that neither viscous nor inertial effects can be neglected in a valid final analysis.

An important observation is that, although peak flow rate increases (to a decreasing extent) for both increases in $p_{e_{max}}$, and decreases in rise time, the time it takes to drain the tube of fluid appears to be a constant in these tests. We are led to believe that some flow limiting mechanism is present which establishes an upper limit on the flow during all or a significant part of the emptying process. One mechanism has been postulated[57,58] which, in essence, states that flow velocity in horizontal tubes cannot exceed wave velocity. These arguments are generally based on the assumptions of frictionless, steady flow and their applicability in these highly unsteady flow situations may be disputed. This question will be addressed further in Chapter X.

For our purpose, it is sufficient to recognize that a limit does apparently exist, and that simple modifications in the external pressure pulse are limited in their effect on drainage time. Also, our observations indicate that flow limitation occurs at the necked down region and that, if we hope to significantly reduce the time required to empty the

tube, we should look to other means of pressurization which eliminate this choking condition. Such methods will be investigated in Chapter XII.

Additional interpretations of the experimental results are given in the next chapter in the context of the numerical simulations.

CHAPTER X:

NUMERICAL SIMULATION OF FLOW EXPERIMENTS

In this chapter we examine the results of the flow experiment simulations and make direct comparisons between the experiment and the predictions of the theory. The simulations were felt to be necessary for several reasons. First, as noted earlier, they allowed us to make a direct comparison between the predictions of the simulation and a real situation--a situation which was a greatly simplified version but which possessed many of the same qualities of the system eventually modeled. This comparison helped us to determine the extent to which we could trust the results of the subsequent simulations which could not be modeled conveniently by experiment.

The simulations aided also in determining how and to what extent each parameter change affected the overall process. This could not be accomplished solely by experimentation because of the lack of detailed information that could be obtained by direct measurement. Applying the results of both the experiment and theory to future simulations, we could predict which of the many parameters would have a strong influence (and therefore should be selected very carefully) and which would have little or no influence on the results.

Finally, through the simulations we were able to look inside the collapsible tube in a way not possible experimentally. Specifically, we could investigate the region of the tube near the throat and come to a better understanding of the mechanisms of, for example, the

phenomenon of flow limitation in a collapsible tube.

Description of the Theoretical Model

The numerical methods have been described in detail in Chapters V and VI. The input parameters include the characteristics of the hydraulic circuit, pressure cycle, and compliant tubing. The circuit and pressure cycle are described completely by the parameters found in Table 3, where the notation is as defined earlier.

The spatial distribution of external pressure was approximated by two quadratic curves, symmetric about the half pressure point. The width of this variable pressure region (which we call the "pressure ramp") was an important and somewhat troublesome parameter. If made too wide, the numerically predicted oscillations were found to be of a much lower frequency than those observed experimentally.† If too short, the computational procedure was adversely affected giving rise to large errors in the region where external pressure varied most rapidly. Thus, it was necessary to perform some simulations using the wide pressure ramp (those which were prone to instabilities because of the violent nature of the results). These are denoted by an "A" in the simulation number. All others employ the narrow ramp which had a total length of approximately 5 cm, half the length of the wide ramp.

---

†See pp. 118-120 for an explanation of this phenomenon.

All the experiments were performed using the same penrose tube. The tube law used in the calculations was one which had been determined experimentally using similar tubes and is plotted in Figs. 7 and 8. In Appendix D, the methods and results of the tube law experiments are discussed in detail. The experimental method required a complete pressure-volume curve for two segments of different length from the same tube. The curves were subtracted from one another to eliminate end effects and analyzed, taking into account the non-uniformity of the wall thickness.

The spatially varying characteristics of the vessel were determined by measuring the wall thickness as a function of distance using a micrometer. The measurement of wall thickness using this method could be in error by as much as 5% which corresponds to as much as a 16% error in K_p. (This does not include the errors in the tube law itself.) A technique is currently being developed that will enable us to measure the local tube law in tubes of up to 100 cm in length to better precision than was possible using the earlier methods. Unfortunately, this new technique was not available at the time these experiments were conducted.

Sources of Error

Errors which affect the numerical results come from a variety of sources. Two of these have already been mentioned: errors in the universal tube law and the way in which tube stiffness varies spatially.

We have also noted that the nature of the pressure ramp (both its shape and width) affect the solution. Since we can only estimate the true nature of the pressure distribution along the plastic pressurizing sleeve, this will contribute some errors as well. In addition, the model used for the various types of flow resistance will cause errors which are most noticeable in situations where the flow is oscillatory. The governing equations themselves, in that they are a one-dimensional approximation to the real flow, may cause inaccuracies particularly when the flow is highly convergent or divergent and hence more nearly two-dimensional.

Another source of error is the numerical solution itself. Errors in a solution procedure as complex as this are difficult to estimate directly. We can, however, discover the magnitude of one source of error--the discretization error--in an indirect way. To do this, we first realize that all discretization (or truncation) errors are proportional to the grid spacing and can be investigated by keeping the ratio between $\Delta\tau$ and $\Delta\xi$ constant, but making the mesh finer. The order of the approximation involved would determine to what power of $\Delta\xi$ or $\Delta\tau$ this error varies. The crudest approximations used in our calculations were of first-order in the interpolation procedures, for example. Therefore, we would expect the errors to vary as $\Delta\xi^2$ or $\Delta\tau^2$ and the solution, by this reasoning, should converge to the correct result as $\Delta\xi$ and $\Delta\tau$ approach zero.

We performed three computations of the same flow simulation with the mesh spacing being cut in half each time. This corresponded to, in terms of $\Delta\xi$, a spacing of $\Delta\xi = 0.02$, 0.01, and 0.005, or 51, 101, and

201 spatial increments for the three runs. The result in terms of flow rate at the exit is superimposed in Fig. 14.† Clearly, in proceeding from 51 to 201 points, the solution appears to converge quite well. The 51 point solution seems inadequate, however, and we therefore have used a 101 point spatial grid for all the computations presented here.

Comparisons Between the Experimental and Theoretical Results

We have plotted the volume flow rate (at the first rigid tube downstream of the test section) measured experimentally and as predicted by the theory in Figs. 10-13. This format allows a direct visual comparison between the measured and predicted behavior of the one measured parameter which best characterizes flow in the entire collapsible tube.

Qualitative Description of the Results. The theoretical curves exhibit two distinct modes of oscillation. The low frequency disturbance corresponds essentially to the sloshing of fluid between two capacitors separated by the resistive and inductive elements. As shown in Chapter IX, the frequency of this oscillation mode depends primarily on the smaller of the two capacitors--in this case, the compliance of the region of the tube at the pressure ramp. The distinct difference between simulations using the small versus the large (denoted by an "A") pressure ramp can be attributed to a change in this compliance which

---

†Because of a considerable increase in cost, the 201 point computation was only carried out for the first part of the cycle.

coincides with a change in the width of the pressure ramp. The high frequency oscillations evident in the theoretical curves but absent in the experiment represent waves which are being reflected between the point of attachment of the downstream rigid tube to the penrose tube and the edge of the pressurized zone in the penrose tube (a point at which the impedance changes abruptly and which is thus a source of reflection). The frequencies associated with oscillations of this type have been estimated in Chapter IX and agree well (in order of magnitude) with the observed oscillations. The fact that these oscillations are clearly visible on the theoretical but not the experimental curve can be attributed to a combination of several factors. First, as is evident in Fig. 14, decreasing the size of the computational grid has the effect of minimizing these oscillations. This indicates that their presence can be partly attributed to numerical errors. The errors probably arise in the region where large changes take place over a relatively small distance (in the immediate neighborhood of the pressure ramp).

Real waves do exist, however, and can be seen in pressure measurements made in the rigid duct just downstream of $\xi = 1$. In the experiments, the waves damp out very rapidly whereas the theory predicts that they persist through much of the cycle. One reason for their persistence is that the flow resistance forms used in the computation are not capable of accurately predicting the viscous damping of relatively high frequency waves. Thus, once started, the waves are likely to continue much longer in the theoretical prediction than in the experiment. Tube viscoelasticity

may also be an important factor. In reality, any waves of relatively high frequency will be increasingly affected by the viscoelasticity of the tube wall. Our model does not include viscoelasticity, and therefore would not predict the additional damping due to this effect.

For the purpose of the following discussion we can define three relatively distinct phases of emptying as characterized by the plot of volume flow rate versus time:

(1) the initial transient peak;

(2) the period of relatively constant flow rate;

(3) viscous emptying.

The most consistent difference between the experimental and theoretical curves occurs during phase two, that of nearly constant flow rate. We can see that the mean flow rate predicted by the theory is distinctly higher than that observed by experiment. In agreement with the observation of higher flow rates, the time for the flow rate to go to zero is less for the simulation than the experiment. There are several possible explanations for this discrepancy. Later in this chapter we present an argument, one result of which is that the mean flow rate during phase two depends directly upon the local wave speed as characterized by c_0. If we fail to accurately predict the stiffness of our tube, the resulting error in c_0 could account for the observed differences. Other factors which may influence the results during phase two are the

approximate flow resistance functions[†] and the shape and extent of the pressure ramp.

A More Quantitative Approach to the Comparison of Theory and Experiment. The results of the simulations are compared directly to the corresponding experiment in the two ways discussed in the previous chapter. As discussed earlier, Figs. 10-13 provide a direct visual comparison between the experimental (dashed) and theoretical (solid) curves of volume flow rate at the exit of the test section. In Table 4 the quantitative comparisons of the type described earlier are presented for both the experiments and the simulations. In each case, we have tabulated the values of the ratio between a particular variable of experiment (or simulation) "n" and the value of the same variable of experiment (or simulation) "1." The ratios for the experiment and simulation of the same test are listed beside each other. We chose this form rather than a direct comparison for each test between the theory and the corresponding experiment for the following reason. Our main concern is in the prediction of trends in actual flow situations, trends which might otherwise be overshadowed by the intrinsic differences between the theoretical and experimental models. A direct

---

[†]Flow at the throat is very nearly turbulent in most simulations. A significant error could result by failing to accurately predict the Reynolds number at which turbulence will occur. In addition, even in laminar flow the boundary layer narrows in a converging section of the tube, resulting in larger actual shear stresses than those predicted by the simulation.

comparison is provided, however, for Test 1. The values found in the first row in the table constitute ratios comprised of experimental and theoretical results for the same test. The Roman numerals in the table refer to the parameters identified in the previous chapter.

The results expressed in this manner can be viewed in two ways. First, if the parameter varied in any particular test has no influence on the flow, then all ratios will be exactly equal to one. The greater the influence, the greater the departure from one. Secondly, the relative success of each simulation can be determined by direct comparison of the two sets of ratios labeled "experiment" and "theory."

Discussion of Results. In general, the agreement was good particularly for those tests in which the pressure cycle was varied. The agreement in those simulations in which parameters of the downstream hydraulic circuit were varied is somewhat less satisfying, particularly in Expt. 14, where the downstream pressure has been increased. This result could have been influenced by the errors, for positive transmural pressures, in using a universal dimensionless pressure-area law. The characteristics of the tube change when going from negative to positive transmural pressure, a change which is accompanied by a change in the normalizing parameter used to reduce all the data onto a single curve. Thus, in attempting to use one universal curve for the entire range of transmural presusres, the region of positive transmural pressure deviates from the true curve. In other words, stiff tubes will be too stiff and compliant tubes

will be too compliant, the dividing line being at a K_p of approximately 200 dynes/cm^2 . We justify this type of a normalization on the basis that our interest is primarily in the collapsed tube and that, in most calculations, the tube rarely extends very far into the positive pressure regime. This experiment, however, is an exception and could have been influenced by this anomaly of the P-α law. We should add that the apparent errors found in Expt. 14 tend to bring the results of the simulation closer to the experimental results. That is, if we compare, not the ratios formed by Simulation 14 and Simulation 1 against the ratios formed by Expt. 14 and Expt. 1, but rather the results of Expt. 14 and Simulation 14 directly, the agreement improves.

Changing the viscosity of the fluid by a factor of five also strongly influenced the results--an effect which was reflected in the numerical solution. It is significant to note, though, that the changes which took place during the early part of the cycle were much less dramatic than those at later times. This leads us to assume that the early stages are largely dominated by inertial effects--a concept that will come up again in later discussion.

It should be noted that, in general, variations in downstream parameters had little effect on the results considering the large variations from reference conditions they represent. This observation coincides with the possibility of critical or supercritical flow velocities ($u \geq c$) at the throat of the collapsing tube which would prevent the flow from being accelerated beyond the critical point.

In only one experiment were the tube properties changed in any way.

This was accomplished in Expt. 21 by reversing the tube so that the thin-walled section pointed downstream. Although the tube wall varied considerably in thickness from one end to the other (giving rise to a variation of c_0 from 69.9 to 103 cm/sec), both the experimental and theoretical results changed surprisingly little. This is the result we would expect if the flow had been largely determined by the tube properties in the region surrounding the point of minimum area, since reversing the tube produced the least change around $\xi = 0.5$. This is an additional piece of evidence which helps to substantiate our claims made later, that "choking" does occur and is primarily determined by the tube properties at the throat.

Simulations in Which A_0 and c_0 Were Varied

We simulated several additional situations for which no corresponding experiment was conducted. The purpose of these was to investigate the effect of changes in c_0 and A_0 independently. The equivalent experiments could not be conducted because we lack the stringent control over wall thickness and tube radius that would be necessary to construct two tubes which, for example, had exactly the same c_0 but differing areas. In this series of calculations, A_0 and c_0 were given specified values (independent of ξ) as indicated below:

Simulation 59: $A_0 = 1.06$ cm , $c_0 = 60 \frac{\text{cm}}{\text{sec}}$, $p_{e_{max}} = 2.6 \times 10^4 \frac{\text{dynes}}{\text{cm}^2}$

Simulation 60: $A_0 = 2.0$ cm , $c_0 = 60 \frac{\text{cm}}{\text{sec}}$, $p_{e_{max}} = 2.6 \times 10^4 \frac{\text{dynes}}{\text{cm}^2}$

Simulation 63: $A_0 = 1.06$ cm , $c_0 = 150 \frac{\text{cm}}{\text{sec}}$, $p_{e_{max}} = 1.65 \times 10^5 \frac{\text{dynes}}{\text{cm}^2}$

The applied pressure in Simulation 63 was increased so that the dimensionless group, $(1/\rho c_0^2)(\partial p_e/\partial \xi)$, was kept constant. All other parameters corresponded to those of Expt. 1.

The results of these simulated conditions are presented in Figs. 15 to 18. For each simulation the normalized variables are plotted in the following sequence:

(1) Transmural pressure versus time at four different locations within the pressurized region (Fig. 15).

(2) Volume flow rate versus time at the same four locations (Fig. 16).

(3) The ratio between flow velocity and wave speed (U/C) at the same four locations (Fig. 17).

(4) Cross-sectional area versus distance at six equally spaced times between $t = 0$ and the final time (Fig. 18).

We can draw several very useful conclusions from these results. First, in comparing the graphs of Simulations 59 and 60 we notice that a change in A_0 has virtually no effect on the solution in terms of normalized variables, at least in the collapsing portion of the tube. The flow rate just downstream of the pressurized zone, however, is strongly influenced due probably to the lack of appropriate scaling in the downstream boundary condition. The results are nearly identical over most of the cycle, differing only slightly in the period of viscous emptying at the very end. The analysis found in Chapter VII can be used as a guide in understanding this observation. Looking at the dimensionless groups on page 84 we find that A_0 appears only in the boundary condition parameters and the group which represents the ratio

between viscous and inertial forces, and as such has the form of a Reynolds number, $\rho c_0 A_0 / C_f \mu L$. The fact that much of the solution is independent of the Reynolds number suggests that most of the process is governed primarily by inertial effects, at least within the pressurized region. We know, however, that viscous effects must be significant in a narrow region close to the minimum in cross-sectional area in order to maintain such a large pressure drop across the region. Granted, the inertial effects and head-loss term contribute to the pressure drop but are not likely to constitute the entire effect. We can estimate, from the numerical solution, the relative magnitude of the inertial and viscous terms and, in doing so, find them to be comparable at the throat.

We seem to have come upon a contradiction. One one hand, we observe that the solution is independent of the term involving viscous stresses. On the other, we can show that viscous and inertial effects are comparable in at least one region of the tube. These two statements can be reconciled if we can demonstrate that the presence of viscous effects at the throat do not influence the solution upstream. During that time for which $u > c$ in any region between the throat and some point upstream, the two solutions are effectively uncoupled. Hence, if the following criteria are satisfied, then the solution upstream will not exhibit the effect of viscous stresses:

(1) viscous effects were not yet significant at the time flow velocities became supercritical;

(2) at no time since first going supercritical has the flow become entirely subcritical;

(3) viscous effects are insignificant upstream of the supercritical region.

Although sustained supercritical flow is not observed at any of the points plotted in Fig. 17, the detailed solution results indicate that the flow was, indeed, supercritical until a normalized time of approximately $\tau \cong 4$ in Simulation 59 and until $\tau \cong 3$ in Simulation 60.

It is interesting to note that during an initial period, the flow transiently becomes supercritical. It then quickly returns to a condition of $u \cong c$ which constitutes an apparent upper bound for the quasi-steady period immediately following.

By contrast, when we compare the results of Simulations 59 and 63 we find subtle differences both inside and outside of the pressurized region. These differences are evident both at the end of the cycle (as in the previous comparison) and during the early phases of collapse. Since, in comparing the results of Simulations 59 and 60 we found that the flow inside the collapsing portion of the tube was largely independent of $\rho c_0 A_0/C_f \mu L$ and since p_{max} was adjusted to maintain proper scaling of $(\rho c_0^2)\partial p_e/\partial \xi$, then the observed influence must be attributable to boundary effects. The flow trace at $\xi = 0.65$ does indicate the presence of a strong reflection reaching the edge of the pressurized zone just prior to choking. The nature of this reflected wave which is determined largely by the boundary conditions prevents the flow rates even in the collapsing region from reaching the same

maximum values. However, after choking occurs, the normalized results show strong similarities, reflecting the fact again that the flow is isolated from the downstream boundary conditions. And in spite of the dissimilarities during the initial phase, the emptying time is virtually unaffected.

In dimensional terms since flow rate is normalized by the product A_0c_0 , actual flow rates scale as A_0c_0 . This implies that, for example, doubling either A_0 or c_0 causes flow rates to approximately double, at least in regions that are relatively uninfluenced by boundary conditions. Additionally, since time is normalized by L/c_0 , dimensional emptying time is independent of A_0 and varies inversely with c_0 --the stiffer tube will empty more rapidly. Again, this result could be deduced from arguments based on volume flow rate alone.

An Approximate Theoretical Analysis Using a More Physical Approach

The results discussed above provide the framework for the following analysis. Our objective is, given certain very general characteristics of the tube and the mode of pressurization, to determine a semi-quantitative description of the flow process. To do this we begin with the basic principles governing collapse and the associated fluid dynamics, and attempt to extract order of magnitude estimates for such parameters as the maximum flow rate, Q_{peak} ; the magnitude of the flow rate during the second, quasi-steady phase, Q_{max_2} ; and the time required to empty the vessel, t_{empty} .

We would like to be able to predict, using a relatively simple model, the salient features of the collapse process. For this purpose we consider the different phases of flow individually making an appropriate set of approximations in each case; first the initial transient phase.

Phase One: The Initial Transient Phase. Our main objective in the following analysis is to estimate the peak flow rate occurring during the initial phase of collapse.

The tube can be divided into two parts: an upstream region which is compressed by a time-varying but spatially uniform external pressure; and a downstream region over which the external pressure is constant. For this discussion we assume that (1) the pressure changes abruptly (over a distance comparable to the tube diameter) and (2) the boundaries are distant enough so that we can ignore the effect of reflections. Initially, the fluid is everywhere at rest.

As the external pressure along the upstream portion of the tube increases, the tube begins to collapse at the boundary between the two regions. The time varying area at this point will be referred to as the "throat" area, A_T , and it is assumed that the area is a minimum at or very near this point during the entire initial phase.

We can think of the time dependent external pressure as being comprised of a series of infinitesimal step-changes of magnitude Δp_e . For each increment in external pressure, the internal pressure increases by some small amount, Δp_i . The relationship between Δp_i and Δp_e

depends upon the extent of vessel collapse locally. Instantaneously, Δp_i will equal Δp_e, but the consequent collapse will cause Δp_i to decrease with time following a single pressure increment.

Using small amplitude approximations we can derive an expression for the change in velocity as the compression wave propagates downstream into the undisturbed fluid. Using the equations of mass and momentum conservation across the compression wave we find that the velocity increment, Δu, can be written as

$$\Delta u = \frac{\Delta p_i}{\rho c_0} \quad , \tag{79}$$

where c_0 is the initial wave speed. Summing over a series of pressure increments, we can obtain an expression for $Q(t)$:

$$Q(t) = \sum \frac{A_0 \Delta p_i}{\rho c_0} \quad . \tag{80}$$

This summation can be expressed in integral form for a smoothly varying p_i and integrated to obtain:

$$Q(t) = \frac{A_0}{\rho c_0} \left[p_i(t) - p_i(0) \right] \quad . \tag{81}$$

The implicit assumption in writing Eq. (81) is that A_0 and c_0 are both constant. In reality, the compression waves entering the downstream region act to further inflate the tube causing A_0 and c_0 to increase. However, the increases in A_0 will be relatively small for an already circular tube and the changes in c_0, although more

significant, will not change the general character of the results.

Coincident with the increase in flow rate downstream, the tube begins to collapse in the upstream pressurized region. Rarefaction waves propagating in the upstream direction act to accelerate the flow and deflate the vessel. The region influenced by these waves has a length $c_0 t$, and contains initially a volume $c_0 t A_0$. As a consequence the volume expelled from the upstream portion, $V(t)$, cannot exceed $c_0 t A_0$. We might estimate the actual expelled volume as follows:

$$V(t) = K_1 c_0 t (A_0 - A_T) \tag{82}$$

where A_T is the throat area and K_1 is a shape factor which must be less than one. A second expression for $Q(t)$ can be obtained by differentiating Eq. (82) with respect to time:

$$Q(t) = K_1 c_0 \left(A_0 - A_T - t \frac{dA_T}{dt} \right) . \tag{83}$$

At the time of maximum flow rate, $dQ/dt = 0$. This condition gives the following expressions upon differentiation of Eqs. (81) and (83), which are valid at the instant of maximum flow:

$$\left.\begin{aligned} \frac{dp_i}{dt} &= 0 \qquad (84a) \\ 2\frac{dA_T}{dt} + t_p \frac{d^2 A_T}{dt^2} &= 0 \qquad (84b) \end{aligned}\right\} \quad \text{at} \quad t = t_p$$

Here t_p denotes the time at which peak flow occurs.

Physically, Eq. (84a) implies that some mechanism must be present to cause the internal pressure to decrease, thus decelerating the flow. This mechanism is provided by vessel collapse to a state at which the rising external pressure is offset by the increasing ability of the tube to resist collapse. To complete the analysis, then, we need to consider the tube law at the throat.

Assuming that the tube is in the similarity range when the flow maximum occurs we can use the following tube law:

$$p_e - p_i = K_p \left(\frac{A_T}{A_0}\right)^{-3/2} \quad . \tag{85}$$

Differentiating this expression and setting $dp_i/dt = 0$, gives, upon one differentiation,

$$\frac{dA_T}{dt} = -\frac{2}{3} \frac{A_T^{5/2}}{K_p A_0^{3/2}} \frac{dp_e}{dt} \quad , \tag{86a}$$

and, differentiating again,

$$\frac{d^2A_T}{dt^2} = \frac{10}{9} A_T^4 \left(\frac{dp_e/dt}{K_p A_0^{3/2}}\right)^2 \quad . \tag{86b}$$

Substituting Eq. (86a) and (86b) into (84b) we get an expression for t_p :

$$t_p = \frac{6}{5} \frac{K_p}{dp_e/dt} \left(\frac{A_0}{A_T}\right)^{3/2} \quad . \tag{87}$$

Whereupon, evaluating Eq. (83) for the maximum flow rate, Q_p , we find

$$Q_p = K_1 c_0 A_0 \left(1 - \frac{1}{5}\frac{A_T}{A_0}\right)$$

or

$$Q_p \cong K_1 c_0 A_0 \quad \text{for} \quad \frac{A_T}{A_0} \ll 1 \quad . \tag{88}$$

This suggests that the peak flow rate is independent of the type of pressurization except in that it may affect K_1 or, to a lesser extent, A_T. It depends primarily on the product $c_0 A_0$ for the initial state of the vessel.

Equation (88) agrees quite well with our previous observations. Peak flow rate is relatively unaffected by any of the changes imposed in our tests.

Phase Two: A Period of Quasi-Steady Emptying. All the experiments exhibit a period of relatively constant flow rate following the initial transient peak, with the exception of the decaying flow oscillations in the region downstream of the collapsing zone. During this second phase, we might consider the flow to be quasi-steady and make the appropriate approximations.

The local stagnation pressure for steady, horizontal flow is

$$P \equiv p + \tfrac{1}{2}\rho u^2 \quad . \tag{89}$$

We can replace u by Q/A and solve Eq. (89) for the flow rate:

$$Q = A\sqrt{\frac{2}{\rho}(P - p)} = A\sqrt{\frac{2}{\rho}\left[(P - p_e) - (p - p_e)\right]} \quad . \tag{90}$$

At a particular instant during the emptying process we might consider the flow locally to have a fixed value of $P - p_e$. Actually, P will be a decreasing function of distance in the flow direction due to frictional losses, but a value of P can still be identified with any location. The flow rate, then, will be a function only of $(p - p_e)$ since A is related to $p - p_e$ by way of the tube law. Since $A \to 0$ as $p-p_e \to -\infty$ and since $u \to 0$ as $(p-p_e) \to (P-p_e)$, we might expect Q to have a maximum with respect to $p-p_e$. To determine this maximum we differentiate Eq. (90) with respect to $p-p_e$ and set the result equal to zero:

$$\frac{dQ}{d(p-p_e)} = u\frac{dA}{dp} + A\frac{1}{2}\frac{2}{\rho}\left[(P-p_e) - (p-p_e)\right]^{-\frac{1}{2}}\left(-\frac{2}{\rho}\right) = 0 \ . \quad (91)$$

Whereupon, substituting the expression for c , we obtain

$$\frac{A}{\rho u}\left(\frac{u^2}{c^2} - 1\right) = 0$$

or

$$\frac{u^2}{c^2} = 1 \ . \quad (92)$$

This implies that for fixed values of $P-p_e$ in steady flow situations, the maximum flow rate is achieved when $u = c$, constituting a means of flow limitation or "choking" in the terminology of compressible fluid flow. The maximum flow rate, then, in steady or quasi-steady flows is limited by the minimum value of cA along the tube. Since, in general, cA decreases with A , flow limitation or "choking" will

occur at the point of minimum area.

In the range of similarity the product cA for a particular tube is a very weak function of transmural pressure. Using the similarity tube law,

$$A = A_0 \left(\frac{p_e - p}{K_p} \right)^{-2/3} \tag{93}$$

and the expression for wave speed,

$$c^2 = \frac{A}{\rho} \frac{d(p - p_e)}{dA} , \tag{94}$$

we can show that

$$Q_{max_2} = Ac = A_0 \left(\frac{3}{2\rho} K_p \right)^{1/2} \left(- \frac{p - p_e}{K_p} \right)^{-1/6} , \tag{95}$$

where Q_{max_2} denotes the maximum flow rate during the second phase of flow. Thus, for wide ranges of external pressure, the maximum flow rate during phase two of the emptying process is likely to be approximately constant if the assumption of quasi-steady flow is valid.

Expressed in normalized form, Eq. (95) becomes

$$\frac{Q_{max_2}}{A_0 c_0} = \alpha C = \left(\frac{3}{2} \beta \right)^{1/2} (-P)^{-1/6} , \tag{96}$$

which demonstrates the direct dependence on $A_0 c_0$ of the maximum flow rate during steady flow. Therefore, as in the case of the initial transient peak, the maximum flow rate during later stages of emptying depends primarily upon the tube characteristics expressed in terms of the

product A_0c_0 .

Phase Three: Viscous Drainage. As the extent of the collapsed region increases, eventually viscous effects will become an important factor. The flow rate will become unchoked and depart noticeably from the nearly constant plateau region. This period of viscous emptying we refer to as phase three.

In our experiments phase three seemed to occur only at the very end of the flow cycle and had little effect on the overall results. The points at which viscous effects first become important would, of course, be a function of the total tube length and the fluid viscosity. On this basis in veins, as in the laboratory experiments, phase three is likely to have a very limited influence. If other systems are considered where viscous effects are a dominant influence, the results of Appendix B could be used to predict the behavior of the tube.

The time required to empty the vessel or to reach a new steady state would depend on these three phases in combination. However, as noted, phases one and two govern, to a large extent, the behavior of our tests. Based on the results that both the initial flow maximum and the maximum allowable flow rate during phase two are proportional to A_0c_0 , we would expect the emptying time to vary according to the expression

$$t_{empty} \propto \frac{\text{total volume expelled}}{A_0c_0} \quad . \qquad (97)$$

Since the expelled volume is somewhat less than the initial volume, this

can also be written as

$$t_{empty} \cong K_3 \frac{L}{c_0} \quad , \tag{98}$$

where L is the length of the pressurized region. Consequently, the emptying time should be independent of all parameters except the tube properties and the expelled volume.

Evaluation of the Approximate Expressions. We can now compare the results obtained by experiment or simulation to the predictions of this more approximate analysis. If confirmed it would provide a useful means of predicting the relative qualitative behavior of different systems to different types of pressure cycles without requiring a complete theoretical simulation. The results of our approximate descriptions are summarized below:

$$\begin{aligned} \cdot \quad Q_p &\cong K_1 c_0 A_0 \\ \cdot \quad Q_{max_2} &\cong K_2 c_0 A_0 \\ \cdot \quad t_{empty} &\cong K_3 \, L/c_0 \end{aligned} \tag{99}$$

In normalized form, these become

$$\begin{aligned} \cdot \quad Q_p &\cong K_1 \\ \cdot \quad Q_{max_2} &\cong K_2 \\ \cdot \quad \tau_{empty} &\cong K_3 \end{aligned} \tag{100}$$

Expressing these relations in dimensionless form points up the rather amazing prediction that, at least qualitatively, all the results

should be the same regardless of tube size or stiffness and independent of other system parameters.

This was indeed observed to a large degree in the experiments with the exception of Expt. 19, in which the viscosity of the fluid was increased. This we would explain on the basis of an extended phase three demonstrating the presence of significant viscous effects.

The most severe test comes in trying to predict the results of Simulations 59, 60, and 63. Here, too however, we find strong confirmation of our predictions. In normalized form all the results exhibit very much the same behavior, the similarities being particularly striking between Simulations 59 and 60.

All these conclusions, however, are based on one particular type of pressurization--uniform external pressure. In the next several chapters, we consider the venous system of the leg and explore two alternate modes of compression with distinctly different results.

CHAPTER XI:

A MODEL OF THE VENOUS NETWORK

The anatomical information required by the numerical simulation of induced venous flows primarily pertains to the geometry and structural properties of the system of vessels and their environment. In this chapter, we will discuss the nature and origin of that information which has been used in the flow simulations. In many instances, quantitative data was not available in the literature. Whenever possible, we sought to obtain more precise physiologic data on our own. In other cases, we used a basic understanding of the principles involved to create a realistic, if not precise, model.

The Geometry of the Venous System and Normal Flow Conditions

The section of the venous tree which was explicitly included in our model extended from the deep veins of the lower calf, through the muscular veins of the upper calf, and into the popliteal, femoral, and iliac veins.

As noted earlier, the complicated inter-relation of the deep veins of the calf vary according to a wide range of common configurations.[59] Our intent was not to create an exact replica of this system but only to produce an estimate of the number of vessels, their cross-sectional area, and the approximate flow rate at each location in the leg. The model itself restricts us to systems of uniformly branching vessels so the non-symmetry inherent in individual systems could not be reproduced.

Our information concerning vessel geometry and size came from two sources; the literature and a venographic study of our own. The basic system is described in several texts[59,60] although some discrepancies are found with respect to the detailed configuration. The main vessels, starting with the iliac vein and heading distally, are listed below:

- Iliac
- Femoral
- Popliteal
- Peroneal, posterior tibial, anterior tibial (one or two each)
- Numerous muscular veins.

Figure 19 shows schematically how these vessels are arranged. The diagram includes only those vessels directly included in the model, i.e., only the deep veins are shown. The extent of muscular vascularization depends largely on the state of development of the calf muscles. The muscular veins join the main tributaries (peroneal and anterior and posterior tibial veins) at arbitrary locations and may, in fact, communicate with these vessels at more than one point, forming a sort of by-pass through which blood can pass into the muscular regions. This arrangement lends itself to the efficient operation of the muscle pump described in Chapter III.

The literature sources of geometrical information noted earlier made little mention of the relative size of the individual vessels and provided almost no quantitative information. Our data on vessel dimensions came from a study we conducted on a small sample of normal venograms obtained from the MGH Radiology Department. Because of the

density of vessels in the upper calf and the two-dimensionality of the venograms, the resolution in this region was very restricted. Additionally, due to the nature of the dye injection and the presence of valves, many of the vessels probably were not filled and therefore were not visible on the x-ray. However, the diameters of those vessels in the thigh and the major vessels in the calf were readily obtainable, making the appropriate adjustment for the scale of the x-ray.

Because it was felt that the total blood volume at locations in the calf were underestimated by the venographic method (due to partial filling and overlapping), plethysmographic studies were reviewed to gain more precise measurements of total venous volume. Since most of these results were stated in terms of mℓ of blood per 100 mℓ of tissue for the entire calf, we can only estimate the distribution of blood within the vessels. Based on a number of independent studies,[61,62] a value of approximately 3.5 mℓ/100 mℓ was chosen as an average venous blood volume in normal supine posture. A certain fraction of this volume would, of course, occupy the superficial veins and would not be visible in the venograms. However, deep venous blood volume as estimated from the venograms still fell short of that which would be predicted on the basis of estimates from the literature with superficial blood volume subtracted out. For our model, then, we chose to use the distribution determined from the venograms, but boosted the curve to a level which gave better agreement with the total volume estimates. Likewise, the number of vessels (equivalent to C_f in the model) at a particular level in the calf obtained from the venograms was adjusted to reflect the information from

all sources including the literature and the results of the venogram study. The summarized results expressed as total cross-sectional area A_0 and number of primary vessels C_f as a function of location are found in Table 5, along with the distribution of c_0, in the form used for the computer simulation of venous blood flow.

Outside the region explicitly included in our model lie those parts of the circulation which are included within one of the two boundary conditions. Far upstream, a mean arterial pressure of approximately 100 mm Hg drives blood through the capillary bed. Based on measurements made by Roberts,[63] the mean flow rate through the popliteal vein was estimated at 180 mℓ/min. The arterial pressure and resting flow rate allow us to compute the capillary resistance which is estimated at approximately 4.12×10^4 gm/cm^4-sec . Since, in our model, all vessels which drain through the popliteal vein are part of our system, no additional influx of blood from tributaries is allowed. Downstream, however, in the femoral and iliac veins, tributaries which are not part of our system increase the resting flow rate from ~ 180 mℓ/min at the knee to ~ 450 mℓ/min at the groin. Because the location and relative size of these tributaries vary and because they exert only an indirect effect on the flow inside the deep calf veins, we have modeled this influx of blood by a constant tributary flow per unit length of 0.108 mℓ/sec/cm .

At the downstream end of our system, the iliac vein connects with its counterpart from the other leg to form the abdominal vena cava, which eventually drains into the atrium of the right heart. We have modeled this portion of the circulatory system as two rigid vessels

separated by a capacitance tank. Together, they represent the inductance, resistance, and capacitance of the vessels leading back to the heart. Based on vessel dimensions given by Burton[64] and a pressure-volume curve for the vena cava,[64] the lengths and areas of the rigid vessels were selected upstream and downstream of the capacitance tank (L_1 = 20 cm, A_1 = 1.5 cm^2 , L_2 = 5 cm, A_2 = 1.5 cm^2). The value used for the capacitance of these vessels was 0.011 $m\ell/(dyne/cm^2)$. The discharge pressure was given a value of 10 cm H_2O (this value may seem high, but it is significant only in terms of the state of filling it creates at the level of the calf).

The assumption of symmetry is perhaps the weakest of the several assumptions made in arriving at our model. One could certainly argue that the system really consists of two quite different parallel systems. One, which we will call the "direct system," consists of the anterior and posterior tibial veins and the peroneal veins which pass nearly straight through the calf from the ankle to the junction with the popliteal vein. The other system (the "indirect system") is comprised of vessels which empty into one of the vessels of the direct system and which follow a much more tortuous path through the calf muscles. The indirect system is more compliant than the first and connects at its upstream end with either capillaries perfusing calf muscle, superficial veins via the system of laterial or interconnecting vessels, or a more distal point in one of the vessels of the direct system. In normal resting conditions, the indirect system sees little of the normal blood flow originating at the foot or lower calf. In exercise, however, the

indirect system becomes the pumping chamber for the calf muscle pump described in Chapter III and receives a considerable fraction of the blood reaching the leg. Clearly, some compromises must be made in modeling the real system by one which contains only uniform branching.

Weaknesses of the Model. The errors associated with the uniform branching model can be divided into two parts. First, those attributable to the fact that some pathways are much shorter than others (e.g., one pathway entering the indirect system might, in a very short distance, terminate in a capillary bed while another, in the direct system, might extend to the foot). Second, those errors associated with asymmetry in the compliance or area of the two tributaries.

Consider the effect of different pathway length. Although some pathways end in a relatively short distance, because of the close proximity of the large veins to the muscular tissue, the length of the smaller veins is very small and hence the volume is likely to be small as compared to that of the large sinuses. The effect is analogous to the branching pattern of an evergreen which has a large main trunk with relatively short, much smaller branches leading from it. The behavior of this kind of system would not differ significantly from a system having the same total volume, but consisting of only one vessel (the trunk). This has been our approach, essentially; include only the large vessels explicitly in the model taking into account the volume of the smaller vessels by increasing the size of the large vessels accordingly. With this reasoning, the length differences become less significant

since most of the larger vessels extend beyond the large muscle mass at the top of the calf. One must be careful, however, in how the length variable is interpreted. Distance is measured along the vessel axis and, since the vessels of theindirect system are quite tortuous as compared to the other vessels, the same value of x (or ξ) may correspond to different positions along a straight line connecting the knee and ankle.

This representation raises one more question, this one concerning the point in the system at which blood enters from the capillaries. If the "evergreen analogy" is used, then the influx of capillary blood should be distributed along the system, while in fact the model allows inflow only at $\xi = 0$, the upstream end. Although basically a poor assumption, we can justify our model by looking ahead. The results of the flow simulations (see Chapter XII) indicate that the induced flows are many times greater than the initial flow rate and are therefore relatively unaffected by this small error in locating the fluid inflow.

The errors associated with differences in vessel area and compliance are somewhat more difficult to rationalize. These structural differences will result in different rates of emptying of the two systems. Although we cannot incorporate the asymmetry into our model, we can predict how this asymmetry will affect relatively emptying rates by simulating two systems differing in either stiffness or area. The results of these tests have been discussed in Chapter X.

Structural Properties of the Veins

The second category of needed information centers around the structural properties of the vein. More precisely, a "tube law" in the same sense as was used in earlier discussion is required. The computer program does, in fact, allow for variations in the "stiffness" of the vessels with location, but requires that each vessel satisfy the same "normalized" tube law.

In Chapter VIII, we provided a theoretical basis for formulating a tube law for a particular vessel based only on its dimensions, environment, and wall structural properties. Because of the sparse literature concerning the characteristics of collapsed veins *in vivo*, we must rely largely on our theoretical background. The information that is available--which primarily concerns vessels in the distended range--has been used as a guideline and as a means of checking the validity of our model.

Literature Survey. We will look first at the existing literature. This information has been obtained from a variety of sources, most of the papers falling into one of the following categories:

(1) direct *in vivo* determination of vein tube law;

(2) experiments on excised veins;

(3) plethysmography;

(4) radiographic methods;

(5) wave speed measurements.

Of these methods, the results from studies classified under item (1)

above would be most useful to us. Unfortunately, only one investigation[65] provided reliable *in vivo* results, those pertaining to a canine jugular vein having quite a different environment from a deep calf vein. The results, however, do extend into the range of partial collapse and provide a foundation for our estimated vein tube law.

The results of the experiments conducted using excised vein segments show that the vein, as one might expect, behaves in a manner very similar to the penrose tubing,[66†] in this type of preparation. And if we compare the results of these studies to the results of Alexander mentioned above, we find considerable discrepancy, more than could be attributed to differences in the vessel wall itself. The conclusion is that the vein behaves quite differently in its natural environment immersed in muscular tissue. We would expect the greatest deviation from the *in vitro* results for those volume changes which cause the greatest distortion of the vessel (i.e., for the collapsing region) (see the analysis in Chapter VIII of the effect of surrounding tissue). For either large positive or large negative distending pressures, however, the vein should respond in much the same way as it would in an isolated preparation and for these limiting cases, these results are useful.

Radiographic techniques have great potential for obtaining precise compliance curves for individual vein segments when used in conjunction with simultaneous catheter pressure measurement. Unfortunately, though, experiments of this type have not yet been performed.

---

†See Appendix D for the results of our experiments using penrose drainage tubing.

Measurement of wave speed, since it can be directly related to the slope of the pressure-area curve by Eq. (3), would provide an indirect means of predicting the vein tube law. Some studies have been conducted in which wave speed was measured at different distending pressures in the canine abdominal vena cava.[67] These results are useful at least for the purpose of comparing the order of magnitude of predicted wave speeds with the experimental measurements. But, because of the differences in vessel characteristics between the vena cava and the deep veins of the leg, the comparison should not be pressed to provide any further information.

Constructing a Tube Law for the Veins

The Range of Positive Transmural Pressures. Most of the data of use in determining the pressure-area law for veins has been obtained indirectly by one of the many plethysmographic techniques. However, due to the wide variety of methods used and the intrinsic difficulty in establishing precise reference pressures and volumes, the published results are not consistent. Each technique introduces its own artifacts, the effect of which are rarely even acknowledged. These studies do, however, provide our greatest insight into the true *in vivo* behavior of the leg veins. Therefore, in the following discussion we will consider a representative sample of plethysmographic data.

In this sample four different techniques were used to vary the transmural venous pressure. They were:

(1) changing the subject's orientation on a tilt table;[68]

(2) occluding the veins emptying the calf with a range of occlusion pressures;[69]

(3) varying the pressure in the plethysmograph;[70]

(4) forcing all the blood (both arterial and venous) out of the calf and allowing it to refill to a predetermined transmural pressure.[62]

The volume changes were measured by either a water or air plethysmograph enclosing some portion of the calf or by integrating the volume flow rate trace during pressurization to the desired value. Most investitators give only volume changes while two (Litter *et al.*,[62] Wilkins *et al.*[70]) provide information on the absolute venous volume at some reference pressure. To compare the various sets of data, it was sometimes necessary to make a reasonable estimate of a reference volume, usually at the venous pressure and volume corresponding to the supine subject, with no external pressure.

In none of these studies was the internal venous pressure measured. Therefore we can only estimate it knowing the position of the subject and whether or not an occlusion cuff was used. In those studies in which transmural pressure is increased by use of a proximal pressure cuff it was assumed that the venous pressure was equal to the occluding pressure. The results from a variety of studies have been analyzed, providing, where necessary, reasonable values for the parameters not given. There is good agreement among these studies for large positive transmural pressures. At low pressures, however, where we would expect collapse

to begin, either the data ends or there is a considerable amount of variability.

Small Positive and Negative Transmural Pressures. There is good reason to be suspect of these low pressure results. First, when the patient is supine, there can be as much as a 10 cm H_2O hydrostatic pressure difference between the vessels in the upper and lower parts of the leg. Therefore, the actual transmural pressure is smeared between these two limits for any particular external pressure. Thus, at low pressures, the apparent collapse will occur much more gradually in these experiments as compared to tests in which a single vein is analyzed.

A second source of error in these results is related to the constant influx of arterial blood through the capillaries which, in steady state, flows through the entire venous system. As a result, internal pressure gradients are present which become more and more accentuated as the vessels collapse. Finally, since all of these methods measure changes in limb volume rather than local cross-sectional area, significant errors are introduced due to the effective averaging over long segments of vessels which may have spatially varying internal pressures.

In conclusion, it seemed reasonable to discard most of the low pressure data of these plethysmographic studies and in its place use a curve with a shape similar to that obtained by Alexander. This combination of results provides us with a tube law which extends into the partially collapsed state but we can go no further with data from the literature.

The effect of the surrounding muscular tissue was discussed in

Chapter VIII. We concluded from a very approximate argument that the vessel collapse should occur over a range of pressures no less than about 10 cm H_2O. This estimate, in fact, agrees quite well with the partial results obtained from Alexander's data. Our approach at this point, then, is to extend the tube law to small negative pressures at roughly the same slope as determined by our previous estimate until the vessel is collapsed and wall bending moments become significant.

The lower portion of the tube law is the most difficult to obtain. We expect, as mentioned earlier, that the surrounding tissue again becomes less significant and the pressure-area law is therefore determined primarily by the characteristics of the isolated vein. Our theoretical results show that these characteristics are governed by the dimensional parameter $K_p = E_b(t/R)^3/12(1-\nu^2)$, where E_b is the Young's modulus for bending.

A logical approach, then, would be to compute this portion of the tube law based on experimental measurements of E_b and the dimensions of the vessel. Here too, however, we encounter problems. First, all measurements of E have been obtained with the wall in tension, not bending. At low transmural pressures, the collagen fibers exist in a loosely woven network and consequently do not affect the observed tension modulus. This same vessel, when subjected to bending stresses, might appear much stiffer. The reasoning behind this statement can be illustrated using the following example. The two sheets of paper shown below, although differing greatly in their <u>apparent</u> tension modulus, will exhibit the same resistance to bending. Therefore, the existence

of even a small amount of collagen fiber (due to its high Young's modulus) can have a strong influence on the bending stiffness of the vessel regardless of its orientation within the wall. Even with detailed information concerning the microscopic wall structure, a calculation of E_b would be extremely difficult, however. All that we can say is that the wall is likely to have a higher bending modulus than tension modulus at least at very low degrees of vessel elongation.

Values for the tension modulus at low transmural pressures are in the range of 10^6 dynes/cm^2 .[71] The range of values for the individual constituents of the wall are as follows:[64]

- smooth muscle: $6 \times 10^4 - 1 \times 10^5$ dynes/cm^2
- elastic fibers: 3×10^6 dynes/cm^2
- collagenous fibers: 1×10^4 dynes/cm^2

Each constituent is found in roughly equal quantity in a typical vein.[72] We would expect, then, based on the reasoning given above, that the bending modulus for veins would be somewhat greater than 10^6 dynes/cm^2.

In addition to E_b , we require the values of h/R for the various vessels for computing K_p . Here, we find considerable variability in the literature among the different veins, values for h/R ranging from 0.018 to 0.035 according to one source[71] and 0.2 for mid-sized veins according to another.[64] Because K_p depends on h/R to the third power, this range of values gives rise to a dramatic variation in K_p

If we compute the two extremes, we find that $0.19 < K_p < 8.9 \times 10^3$ dynes/cm^2.

We expect that at the lower values, the surrounding tissue would again exert a dominant effect. As a reasonable approximation based on observations of veins and on some of the results on excised veins,[66] we have chosen the mean value of K_p for the veins modeled in our study to be 133 dynes/cm^2 . This is somewhat more compliant than the penrose tubes used in the laboratory experiments.

Piecing this information together, we obtained the pressure-area curve shown in Fig. 20. We chose, in this case, to define A_0 at a transmural pressure not equal to zero because it appears that veins are already partially collapsed at that pressure. For comparison with previous results, it was desirable to have $\alpha = 1$ correspond to a nearly circular vessel.

Clearly, there is potential for considerable error in the tube law obtained in this manner. What is needed are direct *in vivo* measurements of compliance using either radiographic methods or carefully conducted strain gage plethysmography. These will be discussed in Chapter XIV, where recommendations are made for additional research.

The Distribution of External Pressure

Another factor which enters into the physiologic model is the distribution of pressure at the level of the veins in the leg. Clinically, pressures are applied to the external surface of the leg by means of an inflatible boot or cuff. The muscular tissue would tend to smear out

the step change in external pressure at the edge of the cuff. Intuitively, one might anticipate that the length of this smearing effect would correspond roughly with the diameter of the leg.

Direct measurements of interstitial pressures beneath the edge of a pressure cuff at different depths and at different positions relative to the edge of the cuff have, in fact, been made.[73] The results indicated very little pressure variation with depth and confirmed our intuitive prediction that pressure variations occur over a distance comparable to the limb diameter, approximately 5 cm in the arm. Pressures beneath the cuff, outside of the range of end effects, were 100% of the applied pressure. These experimental results are reflected directly in the form of the pressure distribution used in our experiments and plotted in the upper center graph in each of the figures describing the results of the venous flow simulations.

Comments on Other Physiologic Features

Additional comments should be made concerning other features of the real physiologic system which are not directly portrayed in our model. These include:

- the venous valves;
- smooth muscle tone;
- the effect of previous venous disease.

Venous Valves. The valves have been included in the model, at least to the extent that backflow is not permitted. They would also presumably

have an effect on flow resistance since the cross-sectional area of the vessel may vary somewhat locally. Also, the flow along the valve leaflets could separate and cause somewhat greater losses than those predicted in the model. In our opinion, these effects would be minimal and the overall picture of vessel collapse would not change noticeably even if they were included in some way.

Smooth Muscle Tone. The state of contraction of smooth muscle could cause significant shifts in the tube law under varying conditions. However, it is known that the deep veins contain relatively little smooth muscle; consequently, the influence of an adrenergic response would be less significant in these vessels. Additionally, since our estimate of vessel characteristics already is subject to considerable error, we feel that the relatively small corrections dictated by changes in muscular tone would be unwarranted.

Previous Venous Disease. The primary effects of previous venous disease would be the valve incompetency and varicosities often associated with the post-phlebotic syndrome. In terms of the model, this condition would permit the possibility of backflow (extremely rare in the simulations) and would tend to increase total venous volume while increasing compliance. These effects would influence the flow in the same manner as increases in A_0 and c_0 did in the results discussed in Chapter X.

In summary, although our model can be justified on the basis of our theoretical concepts, much additional physiologic testing is in order to confirm and refine the assumptions made here.

CHAPTER XII:

SIMULATING VENOUS HEMODYNAMICS FOR THE PURPOSE OF UNDERSTANDING AND OPTIMIZING THE TECHNIQUE OF EPC

The Method for Evaluating Different Pressure Cycles

In Chapter III we stated some criteria for the prevention of DVT which were based on current knowledge of the interaction between the fluid dynamics of the blood flow and the process of thrombus formation. These criteria were:

- high flow pulsatility;
- increased volume flow rate;
- increased flow velocities;
- increased shear stresses;
- clearance of valve sinuses.
- mechanical stressing of the vessel walls;
- complete periodic emptying of the vessels.

For the purpose of making comparisons between the various means of external compression, we need to convert these criteria into an objective evaluation scheme. We have chosen to consider the following variables of the solution:

(1) Volume flow rate, Q, at four locations inside the calf.

(2) Flow velocity, u, at the same four locations.

(3) A measure of the shear stress, u/R, at the same four locations.

(4) Time required to reach a new steady state.

(5) Whether or not the vessels collapse at locations inside the calf.

(6) Does backflow tend to occur at any time during the cycle?

Items (1)-(3) have a clear relationship to the criteria listed above. We have chosen to consider Q, u, and u/R only at locations inside the calf because this is the region in which thrombi are most likely to originate. The four locations indicated represent points equally spaced between $\xi = 0.1$ and $\xi = 0.4$ in the model, the last point being nearly at the level of the knee, close to the edge of the pressurizing cuff.

The time required to reach steady state (4) refers to the time it takes until the vessels have emptied about as much as they are going to. We would like this time kept to a minimum for the following reasons. Shortened periods of compression may permit an increase in cycle frequency and hence, more frequent flow enhancement. Secondly, since during compression we may be slightly impeding blood flow from the arteries, a reduction in compression time would help to maintain normal mean flow rates.

The basis for criterion (5) is not obvious. We reason that, if the vessels do collapse along the entire length of the system, then it is less likely that pockets of relatively stagnant blood might persist. Also, if the claim that arm compression can help to prevent leg DVT is substantiated, we might postulate that vessel wall contact may help in the release of some anti-thrombotic cell constituent.

Item (6) above concerns the mixing in the sinuses behind venous valves. If a tendency for backflow is introduced at some time during

the cycle, the valves will close. The repeated opening and closing of the valves should help to promite mixing in and around the valve sinuses. What effect, if any, induced backflow in the collapsed vessel would have is unclear, however, and although this criterion has been included, it and number (5) should be viewed with some skepticism. This matter will come up again in a later discussion in which we consider the value of employing some kind of pressure pulse which would have the effect of trying to reverse the flow direction periodically. For the present we will consider only the compression phase of the pressure cycle.

The detailed results of the venous flow simulations are presented in the form of six graphs, each providing some additional information concerning the flow at different locations in the system. For each simulation, we plot the following variables:

(1) the maximum applied pressure, $p_{max}(t)$, versus time, t ;

(2) the ratio of local applied pressure to maximum applied pressure, $p(x,t)/p_{max}(t)$, plotted as a function of normalized distance, x/L ;

(3) normalized cross-sectional area plotted against x/L at six successive times;

(4) a measure of the shear stress (flow velocity u dividied by a characteristic vessel radius R) plotted versus time at four equally spaced positions beneath the pressurizing cuff in the calf;

(5) the flow velocity u plotted against time at the same four locations;

(6) volume flow rate, Q , plotted against time at the same four locations.

In addition to the information readily attained from one of these two methods of comparison, we have also tried to define trends which may be exhibited by the results. To do this, we have selected the same variables (Q, u, u/R at four calf locations) and have plotted the maximum value of each as a function of the varied parameter (e.g., rise time, or maximum pressure). This approach quickly points out the general effect a change in maximum pressure, for example, might have on peak flow rate. It also gives us an idea of how much additional enhancement might be achieved by changing a particular parameter beyond the range of the simulations.

Classification of Venous Flow Simulations

The venous flow simulations fall into four general categories. Each is described below.

A. Current Mode of Pressurization. The current pressure cycle and the method of pressure application were discussed in Chapter III. Basically, the cycle consists of a very slow pressure rise, the shape of the pressure-time curve (S-shaped) being determined primarily by the filling characteristics of the large plastic boots. With the fastest cycles, maximum pressure of 30-50 mm Hg is reached in 3-5 seconds and held there for approximately 5-10 seconds, then released.

B. Uniform Pressure Application. This compression technique is very similar to the method described in (A) but with one major exception. The pressure rise is now assumed to be linear in time until reaching the maximum value, then held constant for the remainder of the cycle. The pressure is assumed uniform along the calf, falling off at the knee at the edge of the cuff. This change was made so that we could systematically investigate the effects of the rate of pressurization and the maximum applied pressure without these effects being influenced by the shape of the pressure curve. Two series of tests were conducted using this method. In one, the rise time was varied while the maximum pressure was kept constant. In the other, the rise time was held constant while the maximum pressure was varied.

C. Linear Pressure Application. In these tests, the time course of pressure remained the same as in (B), rising linearly to a maximum pressure which was held until the end of the cycle. The pressure distribution, however, was modified. In view of the rather dramatic results obtained using a pressure distribution which varied quadratically (see Appendix A) we decided to try some form of a non-uniform spatial distribution of pressure. As the simplest case we chose to simulate a pressure which fell in a linear fashion between a maximum value at the ankle to zero at the knee. In the series of tests using this mode of pressurization, both the maximum applied pressure and the rate of pressurization were varied and their effects examined.

D. Wave-Like Pressure Application. Here, the external pressure might rise to a maximum value linearly as in (B) and (C) or be applied instantaneously. This time, though, the pressure distribution is a function of time. The front of pressure moves in a wave-like motion beginning at the ankle and proceeding toward the knee. When the wave reaches the knee it stops and remains there for the duration of the cycle. This method of pressurization effectively "milks" the blood from the vessels as the pressure wave advances. In a series consisting of four simulations, the effect of pressure wave velocity was investigated.

Discussion of Results

The main features of the results obtained using the physiologic model were much the same as in the latex tube tests. This was in spite of a significant change in the tube law, the distributed stiffness of the vessels, and the addition of a varying friction parameter, C_f . The non-linearities in the vein tube law were less severe due to the influence of surrounding tissue. This, and probably the increase in fluid viscosity, accounted for the improved stability in these simulations over the previous computations.

Current Pressure Cycle. The results of the current pressure cycle are shown in Fig. 21. Qualitatively, the collapse process occurs in much the same way as described before. Collapse occurs first at the downstream edge of the pressurized region although, in accord with the

comments made above, the changes associated with collapse are much less abrupt. By the time a narrow throat is well established at the knee, much of the tube has already emptied and what little additional emptying that occurs takes place very slowly. Because of a significant influx of fluid from the arterial side, the new steady-state configuration that we see at the end of the 5-second pressurization cycle is one in which much of the system is still partially filled. The region of severe collapse that we see at the edge of the pressure cuff is the source of a large pressure drop due to viscous effects. This pressure gradient is large enough with the normal resting flow rate that pressures within the vessels beneath the cuff maintain an internal pressure high enough to resist collapse even for pressures of up to 70 mm Hg as we shall see in a later discussion.

The fact that the vessels collapse to an extremely small cross-sectional area at only one, relatively narrow location helps to explain the results shown in the bottom three graphs of the figure. Flow rate, as one would expect, falls off gradually but significantly proceeding from the knee toward the ankle. Velocity and shear rate, however, both drop precipitously when we move just a short distance upstream of the narrow throat. The fall is even more severe if we consider the maximum values of u and u/R found in Table 6 at the point of minimum throat area ($x/L = 0.44$), which was not plotted. This shows that while shear rates and velocities are extremely high at the knee along most of the system the departure from normal is negligible by comparison. These observations provide an excellent example to demonstrate why it is

necessary to get more information than merely a measure of the volume flow rate in the femoral vein when evaluating different pressure cycles.

Uniform Pressure Application--The Effect of Rise Time. In the next series of tests we investigated the effect of rise time using a linear increase in pressure to a maximum of 30 mm Hg in times of 1/3 sec (Fig. 22), 1 sec (Fig. 23), 1.6 sec (Fig. 24), 3 sec (Fig. 25), and 5 sec (Fig. 26). In each case, collapse of the system occurred in much the same way as with the current pressure cycle. In general, decreasing the rise time caused Q, u, and u/R each to increase as indicated on the graphs in Fig. 27 of Q_{max}, u_{max}, and $(u/R)_{max}$ plotted against rise time. The one exception to this rule can be seen in the bottom two plots between rise time of 1/3 and 1 second when it appears that u_{max} and $(u/R)_{max}$ as measured at $x/L = 0.44$ peak at a rise time of approximately 1 second.

These results are in general agreement with the measurements of Roberts *et al.*[63] of femoral vein flow rate during different compression rates. His experiments covered a range of from 0.89 to 9.4 mm Hg/sec which overlaps with the two slowest cycles used in our tests. We can compare Roberts' findings with the increase in flow pulsatility predicted by our results assuming that his measurements were made at some point in the thigh, say $x/L = 0.71$. The comparisons are shown below in terms of percent increase in flow pulsatility ($100 \times Q_{max}/Q_{mean}$):

	Rate of Compression (mm Hg/sec)	Increase in Flow Pulsatility
Roberts *et al.*[63]	6	550%
	10	650%
Simulation	6	520%
	10	740%

The agreement is surprisingly good considering the variability we would expect between different patients.

Roberts indicated that flows could not be altered significantly with further changes in rise time, a conclusion which seems unjustified in view of our results which show pulsatility in the femoral vein increases to a value of approximately 1300% before leveling off for compression rates greater than approximately 30 mm Hg/sec. Thus, we can conclude from these results that the optimal compression rate for uniform compression would be approximately 30 mm Hg/sec and the further decreases in rise time provide little or no additional prophylactic value.

Uniform Pressure Application--The Effect of Maximum Pressure. The sequence of tests corresponding to Figs. 23 and 28 - 30 comprise our study of the effect of maximum applied pressure. We somewhat arbitrarily chose to maintain a constant rise time of 1 second while varying the maximum pressure attained during this period from 20 to 70 mm Hg. As a result, the rate of compression (in mm Hg/sec) varies from test to test.

Figure 31 illustrates how Q_{max} , u_{max} , and $(u/R)_{max}$ vary with changes in external pressure. As shown in these plots, increasing the

maximum pressure beyond 30 mm Hg even as high as 70 mm Hg does not significantly alter any of the variables except for $(u/R)_{max}$ at the point of maximum constriction. This is a direct result of the higher applied pressure causing a smaller throat area. The important factor demonstrated here is that the applied pressure be sufficient to assure collapse of the veins. Pressures much higher than this, while providing marginal improvement, cause the patient considerably greater discomfort.

One interesting feature of normal resting venous blood flow can be seen in these graphs. That is how extremely small normal physiologic flow velocities and shear rates are in these vessels. (It is not surprising that thrombin clots most frequently arise in deep veins.) These shear rates are so low ($\sim$ 10 sec^{-1}) as to raise a question concerning the validity of our assumption that the blood behaves as a Newtonian fluid. We can justify the assumption, however, on the basis that viscous effects only play a significant role in regions where the tube is highly collapsed and consequently where shear rates are several orders of magnitude higher. In the rest of the tube inertial effects are the primary determining influence.

Linear Pressure Application. In the next series of simulations we investigated what we called the linear pressure application. The results of these tests are shown in Figs. 32 to 34. Several distinctions can be immediately seen between these results and the induced flows with uniform external compression.

We mentioned earlier that we were motivated to try this mode of

pressurization based on the encouraging results of the investigation of uniform vessel collapse (see Appendix A). As anticipated the collapse occurred first at the upstream end of the system ($x/L = 0$) and propagated in the downstream direction. Thus the narrow throat at the knee which was an important factor in the previous tests never formed. In the absence of this necked down region, the collapse is seen to be more complete and to take place over a considerably shorter time than before.

An additional benefit of this pressurization mode is that the peak values of Q, u, and u/R are much more evenly distributed (see Table 6). The peak values for u and u/R are nearly constant along the entire system whereas in the previous tests, the magnitude of these peak values varied over one to two orders of magnitude, the maximum value occurring over a very small distance right at the knee.

The three figures represent results of tests in which first the rise time and then the maximum pressure were varied. The decrease in rise time from 1 to 1/3 second keeping the maximum pressure constant caused moderate increases in each variable from 20% to 37%. Again, we conclude that a rise time of 1 second is probably sufficient. As a practical matter the small improvements that might be gained by reducing the rise time any further are probably not warranted in view of the increasing difficulty in attaining shorter rise times.

Similar results were found when the maximum pressure was raised from 30 to 50 mm Hg while the rise time was kept at 1/3 sec. With this modification the improvements ranged from 41% and 42% in Q_{max} and u_{max} to 72% in $(u/R)_{max}$. The case with which this higher pressure could be

implemented clinically depends on the actual design of the pressurizing cuff and the pressure cycling device. It seems, though, in view of current methods, that increasing the maximum pressure to 50 mm Hg would require only minor modifications. Weighing the cost in terms of design practicality against the improved flow conditions we feel that the increase in pressure would be warranted.

Wave-Like Pressure Application. The final modification we made in the mode of calf compression took the form of a wave-like pressure application. For each of the tests in this sequence, the maximum pressure was held constant with time at 30 mm Hg while the wave swept from the ankle toward the knee. In the results presented in Figs. 35 to 38 , the one parameter investigated was the speed of propagation of this wave of pressure. The tests correspond to speeds of 10, 20, 30, and 50 cm/sec. It should be noted that in the region of spatially varying pressure at the front of the wave (between $x = x_w$ and $x = x_w - L_R$ where x_w is the position of the leading edge of the wave and L_R is the width of the variable pressure region), pressure was described by the relation

$$p_e(x,t) = p_{e_{max}}(t) \left\{ 1 + \sin\left[\frac{\pi}{2} + \frac{\pi}{L_R} (x - x_w + L_R) \right] \right\}$$

where L_R was 0.15 in dimensionless form. We should also mention that the region behind the wave front remained pressurized for the duration of the pressure application.

As in the case of linear pressurization, the maximum value of each of the variables plotted (Q, u, u/R) were much more uniform over the entire system than in the case of uniform compression and showed a general upward trend for increasing wave speed (see Table 6). Once again, the reason can be traced to the absence of a narrow throat at the knee. The point of collapse in these tests generally follows the motion of the wave front although at the higher speeds there was some indication of the pressure wave overtaking the region of collapse. The limiting case (which we did not approach in our tests) would be that of an instantaneous uniform pressure application as in the first sequence of tests but with the rise time approaching zero. This extreme situation would revert back to one in which a throat is formed at the knee as before. There is, then, a limit on how fast the wave of pressure should progress. Intuitively, we might expect the limiting process to occur when the pressure wave propagation speed is roughly equal to or greater than the speed of wave propagation in the vessels. This would be at approximately 60-200 cm/sec according to our tube law, depending on the initial degree of vessel inflation.

The curves of flow rate, velocity, and shear rate in Figs. 35 to 38 exhibit considerable oscillations. Since the peak spacing varies but the total number of oscillations that occur in any particular trace remains roughly the same from one simulation to the next, we anticipate that the unsteadiness is introduced as a result of numerical errors and is not due, for example, to real wave reflections. The errors probably arise in the region of rapidly varying cross-sectional area where

truncation errors will be largest.

Our tests culminated at a speed of 50 cm/sec due to difficulties in the numerical solution at higher speeds. The problem can be attributed to the extremely high flow rates, and consequently high fluid inertia in the downstream rigid ducts in the model. The flow begins to decelerate rapidly when the pressure wave reaches its final position. This rapid deceleration induces large negative transmural pressures at the point where the compliant tube and rigid tube meet. The tests which did run to completion provide us with an ample picture of how the variables behave within the range of practical application. With a propagation speed of 30 cm/sec, the pressure wave reaches the knee in a little more than a second. If the wave is created by some sort of a segmented pressure cuff, it would be increasingly difficult to produce wave motion in times shorter than this.

We must realize too that the flows and velocities induced by a wave moving at 30 cm/sec are already extremely high. Before we attempt further increases, the physiologic effect of volume flow rates perhaps 20 or more times as large as resting flow should be determined.

Comparing the last two modes of pressure application, we find strong similarities. We can compare, for example, the linear pressure application of 50 mm Hg with a rise time of 1/3 sec to the wave pressure with a propagation speed of 30 cm/sec. The mean value of the peak flow rates are within 1% of each other; the mean value of u_{max} is 12% greater in the linear pressure application; and the mean value of $(u/R)_{max}$ is 63% greater with the wave of compression. The choice between the two cycles

would have to be made on the basis of practicality in terms of actual implementation in a clinically viable design.

The Effect of Approximations Made in the Development of the Model

Before reaching conclusions concerning what we would recommend as an optimal pressure cycle, three possible deficiencies in the model should be examined in view of how they might influence the results--in particular those results using one of the two newly proposed means of pressurization. Specifically, how would (1) unsymmetric branching; (2) different tube law; and (3) the effect of vessels running in a direction not parallel to the axis of the leg affect the predictions made here?

(1) Unsymmetric branching. In situations in which the vessels collapse at the upstream end first and the collapse region propagates in the downstream direction, the effect of unsymmetric branching should be minimal. The driving force in these cases is a gradient in external pressure applied to the outer surface of the leg, which is unaffected by the local properties of the vessels beneath. Therefore the vessels must collapse in the manner described above and the possibility of leaving a region of stagnant blood in a particular vessel due to unsymmetry is remote.

(2) A different tube law. Much of the same arguments stated above apply here as well. Regardless of the detailed shape of the tube law collapse should occur in the expected way. If, however, the tube law is found to be such that the wave speed in the vessels is actually lower than what we have predicted, the speed of the wave of pressure would

have to be adjusted so as not to exceed this value. If, on the other hand, the tube law varied drastically from one position to another in the same vessel it is conceivable that the linear pressure application could leave pockets of stagnant blood. This can be thought of in the following way. If the vessel is found to be progressively more compliant proceeding in the downstream direction, although the external pressure at downstream points is less, it may be sufficient to cause collapse whereas the higher pressures upstream might not collapse the stiffer part of the vessel. The result would be a situation similar to that observed in the case of uniform pressurization. It is, however, highly unlikely that vessel properties would change so abruptly so as to cause this phenomenon.

(3) The effect of vessels running in a direction not parallel to the axis of the leg. In all previous analyses, it has been implicitly assumed that distance inside the vessels corresponded to distance outside the leg with a one-to-one correspondence. Obviously, the veins follow a more tortuous path and at certain locations their axis may be nearly at right angles to the leg axis.

For cases of linear variation of external pressure, the direct effect of this anomaly would be to decrease the pressure gradient locally--the greater the departure of the vessel from the leg axis, the smaller the pressure gradient. If the departure is severe enough to cause a pressure distribution which is less steep than the quadratic distribution then the vessel will collapse first at the proximal end of the segment. (This comes as a result of the analysis of Appendix A. There we find that

uniform collapse occurs for a quadratic pressure distribution. Hence, a linear distribution such as was used in the simulations causes collapse upstream first and a distribution more shallow than the quadratic one would, by analogy, cause collapse downstream first.) This is hardly a dire consequence, though, since it simply brings us back to a case more like the uniform compression but with the throat being much less severe.

The same sort of event could occur in the case of wave-like compression and again, although it creates a less than optimal condition, the effect is likely to be relatively small.

Additional Considerations for Cycle Optimization

Our comparisons until now have focused exclusively on the first three criteria stated at the beginning of this chapter. These are probably the most important flow criteria so our prior neglect of items (4)-(6) can be justified. We should, however, consider the two proposed modified methods and evaluate them on the basis of our complete list of criteria including items (4)-(6).

In both methods, the emptying time has been greatly reduced, occurring in a period from 1 to 2 seconds in each case. This is in sharp contrast to the current method which approaches a steady state very slowly once the throat has formed.

Both new methods, again in contrast to the current technique, cause the vessels to collapse at all points in the system, thus satisfying criterion (5).

In none of the simulations, however, did we induce the tendency for

backflow which would have the benefit of closing the venous valves, thus promoting mixing of the blood in the sinuses. We could, however, easily close all the valves simply by either reversing the direction of motion of the pressure wave or reversing the external pressure gradient. This could be incorporated into any procedure if it was felt that this were an important criterion.

Analysis of the Complete Pressure Cycle

Assuming now that we adopt either the wave-like or the linear pressure application we still must address the question of the relative lengths of the different portions of the cycle: How long should the pressure be applied? How long should the rest period be?

We have actually already answered the first question. The pressure should be maintained just long enough to reach a new steady state which, with either of these methods, is close to two seconds, depending on the maximum pressure, the rate of pressurization and, in the case of wave-like compression, the wave propagation speed.

The remainder of the cycle, then, is the time required for refilling. If the pressure is simply released and the filling allowed to take place naturally, studies have shown[74] that a rest period of approximately 45 seconds is needed to return the vessels to their original state.

This time might be reduced nominally by applying an occlusion cuff to the thigh filled to a pressure of 20 or 30 mm Hg during the refilling phase. This would prevent the escape of any blood from the deep veins

until they are completely filled. This could also be used as a means of "charging" the deep veins with some additional blood volume which could be useful if some dependent parts of the circulation resist filling under normal venous pressures. The actual time required for refilling, though, with a fixed inflow of less than 3 mℓ/sec from the arterial side, requires a minimum of 25-30 seconds and there is no way to reduce this portion of the cycle any further.

It would be extremely useful in determining the entire pressure cycle if we could estimate, even roughly, the behavior of inflow during the entire process. To do this, we can divide the cycle into two phases; one for filling and one for emptying of the calf veins. In absence of any compression at all, we can define a mean volume flow rate

$$Q_m = R(p_A - p_V) \quad , \tag{101}$$

where R is the resitance of the capillary bed, p_A is arterial pressure, and p_V the mean venous pressure at the calf. During most of the period of external compression, the vessels are likely to be partially collapsed and thus at a transmural pressure of about zero. The pressure inside the veins is, then, roughly the same as the external pressure, p_e . If we assume R to be constant and recognize that p_A will not be affected by compressions of less than about 100 mm Hg, we can write an expression for the flow rate into the veins during compression,

$$Q_c = R(p_A - p_e) \quad . \tag{102}$$

This, of course, would be somewhat less than Q_m . During the portion of the cycle required for refilling (if we adjust our cycle appropriately) the veins will again have a transmural pressure of about zero, thus an internal pressure of zero as well (since $p_e = 0$ during the refilling process). Hence we can express the arterio-venous flow rate during refilling as

$$Q_R = R\, p_A \quad . \tag{103}$$

Accordingly, if the compression portion of the cycle has a period of t_c and the refill portion, t_R , the mean volume flow rate through the capillaries during the entire cycle is

$$Q_{m_c} = \frac{Q_c t_c + Q_R t_R}{t_c + t_R} \quad . \tag{104}$$

We can compare the mean flow rates more conveniently in the form of a ratio:

$$\frac{Q_{m_c}}{Q_m} = \frac{Q_c t_c + Q_R t_R}{(t_c + t_R) Q_m} \quad . \tag{105}$$

Replacing Q_c, Q_R, and Q_m with the previous expressions we obtain

$$\frac{Q_{m_c}}{Q_m} = \frac{1}{p_A - p_V} \left[p_A - p_e \left(\frac{t_c}{t_c + t_R} \right) \right] \quad . \tag{106}$$

Finally, if we assume that $t_c << t_r$ (the filling process occurs

much more slowly than emptying), then we can rewrite this expression in approximate form as

$$\frac{Q_{m_c}}{Q_m} \cong \frac{1 - \frac{p_e}{p_A}\frac{t_c}{t_R}}{1 - \frac{p_V}{p_A}} \quad . \tag{107}$$

Hence, if $(p_e t_c)/p_V t_R < 1$, the mean flow rate during intermittent compression is greater than that in the resting state. This equation has some particularly interesting implications. First, we find that the current cycle (with $t_c \cong 10$ sec, $t_R \cong 45$ sec and $p_e = 45$ mm Hg) has no tendency to increase the mean volume flow rate which agrees with previous measurements[63] using similar cycles which demonstrate that Q_{m_c} is equal to or slightly below Q_m. Another conclusion is that the effect of a change in posture from supine to erect (with an accompanying increase in p_e so as to assure vessel collapse) is to cause an increase in mean flow rate. And, clearly, a decrease in t_c/t_R will have the same effect. We can compare this approximation to the findings of Allwood[16] mentioned earlier. In his experiments a net increase in mean flow of 60% was measured for a sitting individual with a compression cycle consisting of 1 sec of compression to 110 mm Hg and 4 seconds of refilling. Assuming that in this posture $p_A \cong 170$ mm Hg and $p_V \cong 80$ mm Hg, our equation predicts an increase of 58%.

We also find, using this equation, that for our proposed alternate methods of either a linear pressure application or wave-like compression, only slight enhancement of mean flow rates is obtained. For the following

values:

p_e =	50 mm Hg	30 mm Hg
t_c =	2 sec	2 sec
t_R =	40 sec	40 sec
p_A =	100 mm Hg	100 mm Hg
p_V =	10 mm Hg	10 mm Hg
$\frac{Q_{m_c}}{Q_m}$ =	1.08	1.09

True, the analysis is a crude approximation at best, but serves to illustrate the influence changes in the various parameters will have on the overall process.

Conclusions

Based on our findings which have been discussed in some detail in this chapter, we can gather all our pertinent observations and come to some conclusions concerning our concept of the optimal compression cycle.

First, some of the more important observations:

- The current method of spatially uniform compression along the calf causes a necked down region at the edge of the pressure cuff which severely impedes further emptying of the vessels located distal to the point of collapse.

- Using the method of uniform compression, the effectiveness of the method generally increases with decreasing rise times.

- The effectiveness also improves as the applied pressure is increased, but only marginally for pressures greater than 30 mm Hg.

- The upstream constriction can be eliminated by either of the two newly proposed methods: linear or wave-like pressure application.

- With either method, flow rates, flow velocities, and shear rates at points inside the calf can be increased significantly above what is attainable with uniform compression.

- Both new methods provide collapse of the entire deep venous system.

- The time required to empty the system can be reduced to approximately 1-2 seconds using these methods.

- In the linear mode of compression, the method is made more effective either by increasing the maximum applied pressure or by reducing rise time.

- For wave-like compression, both Q_{max} and u_{max} increase with increasing pressure wave propagation velocities.

- Filling time might be reduced by applying an occlusion cuff at the thigh during the refilling phase of the cycle.

- The mean flow rate through the calf might actually be increased if $\frac{p_e}{p_V}\frac{t_c}{t_R} < 1$.

In view of these findings, it appears that either the method of linear pressure application or wave-like compression has considerable potential. The two methods are very nearly equal in terms of protection from DVT according to our criteria and offer the possibility of considerable improvements over the current method. Additional studies are of course necessary before either method is tried clinically and these steps will be discussed in the next chapter.

The choice between these two methods should be made on the basis of design considerations of the compression cuff and pressure source. If the linear method is selected, our predictions indicate that a maximum pressure of approximately 50 mm Hg should be used with as rapid a rise time as can be obtained by reasonable methods but certainly less than 1 sec. If the second method is employed, the speed of the pressure wave should be about 30 cm/sec. In both cases, the compression portion of the cycle should last about two seconds, the refilling phase 30-45 sec.

This completes the present analysis. What remains is to refine and test these predictions. In the next chapter we will discuss the future directions for this and related investigations.

CHAPTER XIII:

RECOMMENDATIONS FOR FUTURE RESEARCH

In this chapter we consider ways in which the results of the present investigation could be either extended or refined, so that we come closer to achieving those goals set forth in Chapter II. In addition, we will explore two new fields of research in which our present knowledge could be put to other purposes.

Possible Refinements in the Present Model

The Physiologic Model. We can first look at the results obtained thus far and ask, how might they be improved? It was noted previously that the accuracy of the physiologic model was compromised due to the scarcity of detailed, quantitative information concerning the structural properties and geometry of the relevant vessels. Specifically, errors in the flow simulations can most likely be attributed to the rather broad assumptions made in formulating a tube law for the veins and in predicting the variations in A_0 and c_0 along the system. Although corrections in these parameters would probably not reverse or even significantly alter the trends we observed, they would provide some additional confidence in the results which, when dealing with a problem of clinical significance, can be very important.

Three methods can be suggested for a further investigation of venous anatomy and vein characteristics:

(1) the construction of venous casts;

(2) venography;

(3) plethysmography.

Venous casts, although requiring a certain amount of skill to construct, provide an excellent three-dimensional picture of the complex venous network. They can also provide some information concerning the state of the collapsed vessels if the casting material is allowed to harden while an external pressure is applied to the limb. Care must be taken, however, in comparing collapse characteristics of a vessel in an amputated limb to those of living tissue.

Either venography or plethysmography can be used as a means of deriving a pressure-area law for veins. Ideally, a single vein could be observed venographically while an increasing external pressure is being applied. Simultaneously, the internal pressure might be measured by means of a catheter inserted to the level of the venographic observation. Similar information could be obtained for all the vessels at a particular cross-section of the calf by means of plethysmography with graded external pressures. If internal pressures are <u>not</u> directly measured, however, the results must be interpreted very carefully because of the varying degree of flow resistance (and hence changes in pressure gradient) due to flow, at points downstream of the volume measurement.

Another area of considerable uncertainty was the criteria used in the optimization procedure. Obviously, the problem of determining the precise fluid dynamic influence on the onset of thrombosis is one of enormous difficulty. We recognize the problem, but feel that it is

highly improbable that our efforts would lead to a significant contribution in this field.

Improvements in the Numerical Procedure. A shortcoming of the numerical procedures was encountered as we pushed toward larger and larger volume flow rates, as in the case shown in Fig. 38. When the flow began to decelerate, the tube started to pinch off at $\xi = 1$, eventually causing the solution to break down. The reason the tube area drops so catastrophically at the downstream end has to do with the fact that, in order to decelerate flow in the first downstream rigid duct, the pressure at $\xi = 1$ must be less than the pressure in the capacitance element. For high rates of deceleration, large pressure gradients are necessary, eventually causing the tube to collapse. In terms of the present study, sufficient information was obtained prior to the failure of the solution so it was not deemed necessary to revamp the computational procedure. If, however, we decide that even higher flow rates are desirable, we may have to consider a different form for the boundary condition that either eliminates this non-physiologic event or enables the numerical solution to cope with it.

The Development of New Experimental Models. One purpose of the hydraulic experiments was to provide evidence of the validity of the theoretical model with respect to variations in the different parameters. The range of experiments was sufficiently diverse to thoroughly investigate the effect of parameters of the boundary conditions and of the

spatially uniform pressure application. Lacking, however, were experiments in which the effect of tube properties and of either non-uniform or wave-like pressure applications were considered. For the sake of completeness, we should at least weigh the value of these tests against the difficulties that would be encountered in their implementation. We obviously cannot evaluate every detail of the theoretical model--if we could there would be no need for the theoretical calculations at all. But, perhaps, in view of the dramatic differences predicted by the theory in some instances, some additional experiments may be warranted.

Immediate Objectives in the Study of DVT Prophylaxis

Physiologic Studies. We want to consider now the direction that new research should take so as to extend the usefulness or applicability of the present work. Clearly, the next, most important step would be the clinical confirmation of the findings in Chapter XII concerning the optimal pressure cycle. An apparatus will have to be designed and constructed which allows us to pressurize the calf with either a linearly varying or wave-like compression. The performance of the device can then be tested by various methods either on patients or volunteers. Three testing procedures are available:

- venography;
- plethysmography;
- direct measurement of flow rates and/or pressures during either venography or surgery.

Venography has the potential to provide us with a more complete picture of vein emptying than either of these other methods. Typically, at the end of a normal venogram, the radio-opaque dye could be ejected by a pressurizing cuff that had been fitted to the leg at the beginning of the testing procedure. Cine viewing would provide us with information concerning the collapse of all vessels which were originally filled with dye. Flow rates could be estimated by taking the time derivative of volume changes upstream of any particular point. There are disadvantages to this method, however. First, we can never be sure that all deep vessels are filled with dye initially, particularly the large muscular veins which are of considerable interest. Secondly, we can obtain at most two two-dimensional cine recordings and are limited accordingly in constructing a three-dimensional representation of vessel collapse. The problem is compounded even further if only one view can be obtained. Finally, the flow process is likely to be altered by high concentrations of a dye which has a significantly greater density than the blood itself. This is particularly true in the inertia-dominated initial phases.

Plethysmographic techniques have the vast advantage of being totally non-invasive and can be conducted in our laboratory on normal, healthy volunteers. Using mercury strain gages positioned along the subject's calf beneath a pressurizing cuff, we obtain a direct, continuous output representing the local changes in cross-sectional area as a function of time. Again, we can estimate volume flow rates based on the accumulative volume change (area change integrated over distance) upstream of any point.

These first two procedures provide us with similar information, area changes as a function of time. The shortcomings of these methods could be compensated for by direct measurement of flow rate, velocities, or pressure at different locations within the collapsing network or just downstream of it. This could be accomplished, at least partially, in two ways. During surgery, it is at times possible to place an electromagnetic flow probe around the femoral vein. Recordings of flows during calf compression would be a valuable addition to the above results. During catheterization of the lower extremity, it may be possible to thread a pressure or velocity sensing catheter retrograde in the femoral vein, to a level just below the knee, beneath the edge of the pressure cuff. Again, recordings made by this means during compression provide another independent piece of information.

Although none of the methods provide a complete picture by themselves, each compliments the other in such a way that when we piece all the information together, we should have a reasonably good idea of how actual venous flows relate to our predictions.

Design of a New Compression Cuff and Pressure Source. If we hope to test some of the different pressure cycles suggested in the previous chapter we cannot overlook the need for the pressure cuff and pressurizing apparatus. The current boot is extremely large and requires a minimum of 3-5 seconds to inflate. The cycles we have proposed require rise times on the order of a fraction of a second. In addition we have special needs in terms of either a spatially linear or wave-like pressure

application.

One of our first steps, then, must be the design and construction of a compression sleeve and the accompanying pressurizing apparatus. Some criteria for the design include that it be segmented to allow for spatial gradations in pressure, that it require a very small volume for complete inflation, and that it be comfortable and not cumbersome for the patient. In addition, we feel that it should cover only the calf, not the entire lower leg and that it be adjustable so as to accommodate all or least a large segment of the population.

Clinical Trials of a Potentially More Effective Method. The final step, following clinical confirmation of the theoretical results, would be a trial comparison between the postulated optimal pressure cycle and one of the more successful alternative procedures; low dose heparin, for example. The value of this study would then have been fully realized. Only by way of numerical simulations could we have made a logical study of the various alternative pressure cycles. Clinical trials of all, or even some, of the methods examined theoretically would have taken years to complete. In addition, the ethics of such a plan would be highly questionable.

The discussion so far has been directed toward the more immediate objectives: those which relate directly to the study of EPC. The following comments which are made with a much broader perspective consider other applications of the theory of collapsible tube flow.

New Fields of Research

Two other research topics follow closely along the lines of the present study. With our present understanding of unsteady flow in collapsible tubes and the capabilities and interests of the individuals in the Fluid Mechanics Laboratory, a favorable situation exists for branching out into either of the following research areas.

External Cardiac Assist (ECA). A method of cardiac assist using external compression of the lower extremities has been suggested and tried on a very limited basis.[75] The idea was similar to that used in the intra-aortic balloon pump--increase aortic pressure during diastole and reduce it during systole, thereby reducing afterload (and thus the strain on a damaged heart) and enhancing coronary circulation. Rather than displacing volume in the aorta, such as with the balloon pump, it was suggested that the pressure surrounding the legs be cycled in such a way that blood be pushed into the aorta during diastole and drained from it during systole, effectively accomplishing the same purpose.

The previous trials have not been well accepted and the results were not particularly convincing. The concept, however, is attractive and deserves additional consideration before being discarded.

In principle, the process of "squeezing" the blood from the legs into the aorta is much the same as squeezing blood from the veins. The vessel network has different characteristics; the initial pressure is much higher, and the flow is initially in the opposite direction; but none of these differences require the development of a completely

different model.

A study of ECA would necessarily be a large-scale, multi-faceted investigation requiring cooperation between several research groups. It would, though, be a task well worth the considerable efforts required.

A Model of the Airways of the Lung. The lung airways constitute another system of potentially collapsible vessels. Under conditions of normal respiration, the external pressure surrounding the airways, and the alveoli at which they terminate, varies in a cyclic fashion causing air to be transferred into and out of the lung. In extreme cases, the external pressure can be raised to levels which are sufficient to collapse the airways. This occurs in certain diseased states such as asthma, where due to the increased flow resistance in small airways much greater muscular effort--hence much greater external pressures--are necessary to satisfy the oxygen needs of the body. Collapse can also occur in forced expiration or coughing in which high external pressures are needed to produce the correspondingly large flow rates and flow velocities.

A model similar to ours could be applied in either instance as a means of gaining a better understanding of the important phenomena. In asthma, one belief is that the sounds one hears are the sounds produced by airway oscillations and are often described by analogy to the "Bronx cheer." The vibrational frequency of the sound and whether or not the sounds occur could contain useful diagnostic information concerning the airways directly involved in the oscillations and the surrounding tissue.

Respiratory physiologists generally agree that airway collapse

accounts for flow limitation observed in curves of flow rate during a cough or a forced expiration maneuver. The characteristics of this maximum flow curve and the transients produced by forced expiration are currently being considered for their diagnostic value.

In both cases just described we have a phenomenon of unsteady flow in a collapsible tube. In each, an understanding of the fluid dynamic mechanisms involved would greatly contribute to the current attempts to determine their diagnostic potential. Modeling respiratory flows is not an easy task, however, and would require a somewhat different model than that which was used to simulate induced venous flows. Inertial effects of the vessel wall are likely to be important as are the effects of viscoelasticity at the higher frequencies and wave propagation speeds encountered in the lung. Our basic understanding of flows of this general type would, however, give us a solid background from which we could formulate a new model that could be applied to a variety of simulations of respiratory flows.

RDK:cp

REFERENCES

1. Wessler, S., "Anticoagulant therapy," JAMA, 228(6), 757-761 (1974).

2. Gurewich, from a panel discussion at the American Heart Assoc. Mtg., 1975. Emergency Medicine, Nov. 1976.

3. Clagett and Salzman, "Prevention of venous thromboembolism in surgical patients," N.E. J. Med. 290(2), 93-95 (1974).

4. Lewis, C.E., Mueller, C., Edwards, W.S., "Venous stasis on the operating table." Am. J. Surg. 124, 780-784 (1972).

5. Horton, D.A., unpublished data.

6. Cockett, F.B., "Pathology and treatment of venous ulcers of the leg," Br. J. Surg. 43, 260 (1955).

7. Beecher, H.K., Field, M.E., Krogh, A., "The effect of walking on the venous pressure in the ankle," Scand. Arch. F. Physiol. 73, 133 (1936).

8. Conrad, M.C., Functional Anatomy of the Circulation to the Extremities, Yearbook Medical Pub., Chicago, 1971.

9. Rabinov, K. and Paulin, S., "Roentgen diagnosis of venous thrombosis in the leg," Arch. Surg. 104, 134 (1972).

10. Cotton, L.T. and Clark, C., "Anatomical localization of venous thrombosis," Ann. Rev. Coll. Surg. 36, 214, 224 (1965).

11. Arnoldi, C.C., Greitz, T., Linderholm, H., "Variations in cross-sectional area and pressure in the veins of the normal human leg during rhythmic muscular exercise," Acta Chir. Scand. 132, 507-522 (1966).

12. Duomarco and Rimini, in Cardiovascular Functions (A.A. Luisada, ed.), McGraw Hill, New York, 1962, p. 167-173.

13. Ludbrook, J., "Functional aspects of the veins of the leg," Am. Heart J. 64, 796 (1962).

14. Ludbrook, J., "The musculovenous pumps of the human lower limb," Am Heart J., 71, 635 (1966).

15. Ludbrook, J., Aspects of Venous Function in the Lower Limbs, Charles C. Thomas, Springfield, Ill., 1966.

16. Allwood, M.J., "The effect of an increased local pressure gradient on blood flow in the foot," Clin. Sci. 16, 231 (1957).

17. Nicolaides, A.N., Kakkar, V.V., Field, F.S., Fish, P., "Venous stasis and deep vein thrombosis," Brit. J. Surg. 59(9), 713-717 (1972).

18. Virchow, R.L.K., Thrombose and Embolie, Frankfurt, Germany, 1856.

19. Sevitt, S., Burns: Pathology and Therapeutic Applications, Ch. 19, Butterworths, London, 1957.

20. Hume, M., Sevitt, S., Thomas, D.P., Venous Thrombosis and Pulmonary Embolism, Harvard University Press, Cambridge, Mass. 1970.

21. Gallus, A.S., in Venous Thromboembolism: Prevention and Treatment (J.L. Madden and M. Hume, eds.), Appleton, Century, Crofts, New York, 1976.

22. Sevitt, S., "Venous thromboembolism," Proc. Roy. Soc. Med. 68(4), 261 (1975).

23. Kakkar, V.V., in Prophylactic Therapy of Deep Vein Thrombosis and Pulmonary Embolism (J. Fratantoni and S. Wesseler, eds.), DHEW Publ. No. (NIH) 76-866.

24. Scottish Study. "A multi-unit controlled trial: Heparin versus dextran in the prevention of deep-vein thrombosis," Lancet 2, 118-120 (1974).

25. Harris, W.H., Salzman, E.W., Athanasoulis, C., Waltman, A.C., Baum, S., DeSanctis, R.W., "Comparison of warfarin, low molecular weight dextran, aspirin, and subcutaneous heparin in prevention of venous thromboembolism following total hip replacement," J. Bone and Joint Surg. 50A, 1552-1562 (1974).

26. Rosenberg, I.L., Evans, M., Pollock, A.V., "Prophylaxis of post-operative leg vein thrombosis by low-dose subcutaneous heparin or preoperative calf muscle stimulation: a controlled clinical trial," Brit. Med. J., 1, 649-651 (1975).

27. Vroonhaven, T.J., Van Zijil, J., Miller, H., "Low-dose heparin vs. oral anticoagulants in prevention of postoperative DVT," Lancet, 1, 376-377 (1974).

28. Gallus, A.S., Hirsh, J., Tuttle, R.J., Treibilcock, R., O'Brien, S.E., Carroll, J.J., Minden, J.H., Hudecki, S.M., "Small subcutaneous doses of heparin in prevention of venous thrombosis," N.E. J. Med. 288, 545-551 (1973).

29. Nicolaides, A.N., Desai, S., Douglas, J.N., Fourides, G., Dupon, P.A., Lewis, J.D., Dodsworth, H., Luck, R.J., Jamieson, C.W., "Small doses of subcutaneous sodium heparin in preventing deep venous thrombosis after major surgery," Lancet, 2, 840-893 (1972).

30. Lee, B.Y., Trainor, F.S., Kavner, D., Madden, J.L., Dratz, H.M., Ejercito, E.M., "Noninvasive prevention of thrombosis of deep veins of the thigh using intermittent pneumatic compression," Surg. Gyn. and Obst. 142, 705-714 (1976).

31. Hills, N.H., Pflug, J.J., Jeyasingh, K., Boardman, L., Calnan, J.S., "Prevention of deep vein thrombosis by intermittent pneumatic compression of the calf," Brit. Med. J. 1, 131-135 (1972).

32. Roberts, V.C., Cotton, L.T., "Prevention of poast-operative deep vein thrombosis in patients with malignant disease," Brit. Med. J. 1, 358-360 (1974).

33. Clark, W.B., MacGregor, A.B., Prescott, R.J., Ruckley, C.V., "Pneumatic compression of the calf and post-operative deep vein thrombosis, Lancet, 2, 5-7 (1974).

34. Browse, N.L. and Negus, D., "Prevention of post-operative leg vein thrombosis by electrical muscle stimulation: an evaluation with ^{125}iodine-labelled fibrinogen," Brit. Med. J. 3, 615-618 (1970).

35. Rosenberg, I.L., Pollack, A.V., "A comparison of mechanical and chemical methods of prevention of post-operative venous thrombosis," Brit. J. Surg. 61, 924 (1974).

36. Rosengarten, D.S., Laird, J., Jeyasingh, K., Marfin, P., "The failure of compression stockings (Tubigrip) to prevent deep venous thrombosis after operation," Brit. J. Surg. 57, 296-299 (1970).

37. Turpie, A.G.G., in Venous Thromboembolism: Prevention and Treatment (J.L. Madden and M. Hume, eds.), Appleton, Century, Crofts, New York, 1976.

38. Arnoldi, C.C., "Elastic compression in the prevention of venous thrombosis," VASA, 5(2) (1976).

39. Knight, M.T.N. and Dawson, R., "Reduction of the incidence of deep vein thrombosis (DVT) in the legs by intermittent compression of the arms," Brit. J. Surg. 63, 668 (1976).

40. Flaherty, J.E., Keller, J.B., Rubinow, S.I., "Post buckling behavior of elastic tubes and rings with opposite sides in contact," SIAM J. J. Appl. Math., 23(4), 446-455 (1972).

41. Milne-Thompson, L.M., Theoretical Hydrodynamics, Macmillan, New York, 1950.

42. Schlichting, H., Boundary-Layer Theory, McGraw-Hill, New York, 1960.

43. Hartree, D.R., "Some practical methods of using characteristics in the calculation of non-steady compressible flows," Los Alamost Report LA-HU-1 (1952).

44. Von Neumann, J. and Richtmyer, R.D., "A method for the numerical calculation of hydrodynamic shocks," J. Appl. Phys. 21, 232-237 (1950).

45. Lax, P.D., "Weak solutions of nonlinear hyperbolic equations and their numerical computation," Comm. Pure Appl. Math. 7, 157-193 (1954).

46. Richtmyer, R.D. and Morton, K.W., Difference Methods for Initial Value Problems, 2nd ed., Wiley-Interscience, New York, 1967.

47. McDonald, D.A., Blood Flow in Arteries, Williams and Wilkins Co., Baltimore, 1974.

48. Strandness, D.E. and Sumner, D.S., Hemodynamics for Surgeons, Grune and Stratton, New York, 1975.

49. Tadjbakhsh, I. and Odeh, F., "Equilibrium states of elastic rings," J. Math. Ann. and Appl. 18, 59-74 (1967).

50. Kresch, E. and Noordergraaf, "A cross-sectional shape of collapsible tubes," Biophys. J., 12, 274-294 (1972).

51. Timoshenko, S., Strength of Materials, D. Van Nostrand Co., New York, 1950.

52. Gow, B.S. and Taylor, H.G., "Measurement of viscoelastic properties of arteries in the living dog," Circ. Res. 23, 111-122 (1968).

53. Bergel, D.H., "The dynamic elastic properties of the arterial wall," J. Physiol. 156, 458-469 (1961).

54. von Gierke, H.E., Oestreicher, H.L., Franke, E.K., Parrack, H.O., von Wittern, W.W., "Physics of vibrations in living tissues," J. Appl. Physiol. 4, 886-900 (1952).

55. Kivity, Y. and Collins, R., "Nonlinear wave propagation in viscoelastic tubes: application to aortic rupture," J. Biomech. 7(1), 67-76 (1974).

56. Hoerner, S.F., Fluid-Dynamic Drag, published by the author, 1965.

57. Griffiths, D.J., "Hydrodynamics of male micturition: I. Theory of steady flow through elastic-walled tubes," Med. & Biol. Engrg., 9, 581-588 (1971).

58. Dawson, S.V. and Elliot, E.A., "Expiratory flow limitation at wave speed," Fed. Proc. 33(3), 324 (1974).

59. Dodd, H. and Cockett, F.B., The Pathology and Surgery of the Veins of the Lower Limb, E.S. Livingstone Ltd., Edingurgh, 1956.

60. Conrad, M.C., Functional Anatomy of the Circulation to the Extremities, Yearbook Medical Pub.,1971.

61. Coles, D.R., Kidd, B.S.L., Moffat, W., "Distensibility of blood vessels of the human calf determined by local application of subatmospheric pressures," J. Appl. Physiol. 10, 461 (1957).

62. Litter, J. and Wood, J.E., "The volume and distribution of blood in the human leg measured *in vivo*: I. The effects of graded external pressure," J. Clin. Invest. 33, 798 (1954).

63. Roberts, V.C., Sabri, S., Beeley, A.H., Cotton, L.T., "The effect of intermittently applied external pressure on the hemodynamics of the lower limb in man," Brit. J. Surg. 59(3), 223-226 (1972).

64. Burton, A.C., Physiology and Biophysics of the Circulation, Yearbook Medical Publ., Chicago, 1972.

65. Alexander, R.S., in The Handbook of Physiology-Circulation II, Ch. 31, American Physiological Society, Washingtion, 1962, 1075-1098.

66. Reddy, R.V., Noordergraaf, A., and Moreno, A.H., "In vitro changes of shapes of veins under pressure," 23rd ACEMB, 1970, p. 15.

67. Anliker, M., Wells, M.K. and Ogden, E., "The transmission characteristics of large and small pressure waves in the abdominal vena cava," IEEE Trans. Bio-Medical Engrg, BME-16(4), 262-273 (1969).

68. Ludbrook, J. and Loughlin, J., "Regulation of volume in postarteriolar vessels of the lower limb," Amer. Heart J., 67, 493 (1964).

69. Kidd, B.S.L., Lyons, S.M., "The distensibility of the blood vessels of the human calf determined by graded venous congestion," J. Physiol. 140, 122-128 (1958).

70. Wilkins, R.W., Mixter, G., Stanton, J.R., Litter, J., "Elastic Stockings in the prevention of pulmonary embolism: a preliminary report," N.E. J. Med. 246, 360-364 (1952).

71. Attinger, E.O., "Wall properties of veins," IEEE Trans. on Bio-Medical Engineering, BME-16(4), 253-261 (1969).

72. Burton, A.C., "Relation of structure to function of the tissues of the wall of blood vessels," Physiol. Rev. 34, 619 (1944).

73. Thomson, A.E. and Doupe, J., "Ascultatory measurement of arterial blood pressures," Canad. J. Res. 27(E), 72-80 (1949)

74. Raines, J.K., and Harris, W.H., "Design of an intermittent mechanical compression system for the reduction of deep venous thrombosis," Proc. 9th Ann. Mtg. of AAME, 1974.

75. Soroff, H.S., Giron, F., Ruiz, U., Birtwell, W.C., Hirsch, L.J., Deterling, R.A., "Physiologic support of heart action," N.E. J. Med. 280, 693-704 (1969).

TABLE 1. Risk Factors for Venous Thrombosis[a]

General surgery, particularly:

- major abdominal
- thoracic
- gynecologic
- retropubic prostatectomy
- neurosurgery

Orthopedic surgery

- hip fracture
- elective hip replacement
- knee surgery
- tibial fracture

Increasing age

Malignancy

Prior history of venous thrombosis

Bed rest

Varicose veins

Obesity

Pregnancy

Use of oral contraceptives

Recent travel

Stroke

Myocardial infarct

Congestive heart failure

Leg trauma

Blood group

(a) See Ref. 21 for a complete discussion of these risk factors and for specific references.

TABLE 2. Clinical Evaluation of Prophylactic Methods Against Deep Vein Thrombosis

I. CHEMICAL METHODS

Type of Therapy	Patient Group	% DVT	
		Control	Treated
Heparin[23]	General surgery	24.6	7.7
Heparin[24]	General surgery	37	12
Heparin[25]	Total hip replacement	--(a)	73
Heparin[26]	Elective surgery	41	15
Heparin[27]	General surgery	--(a)	2
Heparin[28]	Surgery in malignant disease	40	7
Heparin[29]	Elective surgery	16	4
Dextran[24]	General surgery	37	25
Dextran[25]	Total hip replacement	--(a)	20-25
Warfarin[25]	Total hip replacement	--(a)	20-25
Aspirin[25]	Total hip replacement	--(a)	35
Acenocoumarol[27]	General surgery	--(a)	18

II. PHYSICAL METHODS

Type of Therapy	Patient Group	% DVT	
		Control	Treated
External pneumatic compression[30]	General surgery	--	0
External pneumatic compression[31]	Non-malignant disease	40	15
External pneumatic compression[31]	Malignant disease	50	50
External pneumatic compression[37]	Neurosurgery	19	1.5
External pneumatic compression[32]	General surgery	26	6.4
External pneumatic compression[32]	Malignant disease	32	4.5
External pneumatic compression[33]	General surgery	20	0
Electrical muscle stimulation[34]	General surgery	21	8.2
Electrical muscle stimulation[35]	Non-malignant disease	35	10
Electrical muscle stimulation[35]	Malignant disease	56	55
Compression stockings[36]	Elective surgery	32	32

(a) No control group.

TABLE 3. Summary of Flow Experiments[a]

Parameter	Experiment Number									
	1	2	3	4	5	6	7	8	9	10
$p_{e_{max}}$ (cm H_2O)	27	10	17.5	62	30	30	28	28	29	28
S (sec)	0.25	0.42	0.30	0.30	0.07	0.15	0.65	0.78	0.25	0.25
Q_i (mℓ/sec)	0	0	0	0	0	0	0	0	0	0
$p_B-p_{e_1}$ (cm H_2O)	3.1	3.05	3.0	3.0	3.0	3.1	3.1	3.1	4.75	4.6
$p_B-p_{e_2}$ (cm H_2O)	3.2	3.15	3.0	3.0	3.0	3.1	3.1	3.1	4.75	4.6
C_V (cm^5/dyne)	0.011	0.011	0.011	0.011	0.011	0.011	0.011	0.011	0.002	0.082
L_1 (cm)	22	22	22	22	22	22	22	22	22	22
A_1 (cm^2)	0.317	0.317	0.317	0.317	0.317	0.317	0.317	0.317	0.317	0.317
L_2 (cm)	22	22	22	22	22	22	22	22	22	22
A_2 (cm^2)	1.26	1.26	1.26	1.26	1.26	1.26	1.26	1.26	1.26	1.26
ρ (gm/cm^3)	1.00	1.00	1.00	1.00	1.00	1.00	1.00	1.00	1.00	1.00
μ (gm/cm-sec)	0.01	0.01	0.01	0.01	0.01	0.01	0.01	0.01	0.01	0.01

Parameter	11	12	13	14	15	16	17	18	19	20	21[b]
$p_{e_{max}}$ (cm H_2O)	28	28	28	28	28	27	27	28	28	82	31
S (sec)	0.25	0.25	0.25	0.25	0.25	0.25	0.25	0.25	0.25	0.32	0.25
Q_i (mℓ/sec)	0	0	0	0	0	1.2	2.8	11.5	0	0	0
$p_B-p_{e_1}$ (cm H_2O)	2.9	3.0	3.1	8.8	0.45	3.0	2.9	3.0	3.4	3.0	3.0
$p_B-p_{e_2}$ (cm H_2O)	2.9	3.0	3.1	8.8	0.50	3.0	2.9	3.0	3.4	3.0	3.1
C_V (cm^5/dyne)	0.011	0.011	0.011	0.011	0.011	0.011	0.011	0.011	0.011	0.011	0.011
L_1 (cm)	41.2	9.0	22	22	22	22	22	22	22	22	22
A_1 (cm^2)	0.317	0.317	0.317	0.317	0.317	0.317	0.317	0.317	0.317	0.317	0.317
L_2 (cm)	22	22	17.2 13.0	22	22	22	22	22	22	22	22
A_2 (cm^2)	1.26	1.26	0.317 1.26	1.26	1.26	1.26	1.26	1.26	1.26	1.26	1.26
ρ (gm/cm^3)	1.00	1.00	1.00	1.00	1.00	1.00	1.00	1.00	1.14	1.00	1.00
μ (gm/cm-sec)	0.01	0.01	0.01	0.01	0.01	0.01	0.01	0.01	0.055	0.01	0.01

(a) The parameter varied in each test is underlined.

(b) Tube reversed.

TABLE 4. Tabulated Comparison of Experimental and Theoretical Results

Test #	Parameter (as defined in text, see p. 117)											
	(I)		(II)		(III)		(IV)		(V)		(VI)	
	Expt.	Theory	Expt.	Theory	Expt.	Theory	Expt.	Theory	Expt.	Theory	Expt.	Theory
1[a]	1.13		0.76		0.80		1.03		0.86		1.51	
1A[a]	1.13		0.85		0.80		1.47		0.94		1.13	
2	0.49	0.60	2.12	2.22	1.13	1.18	1.25	1.07	0.77	0.69	1.72	1.20
2A	0.49	0.62	2.12	2.30	1.13	1.08	1.25		0.77		1.72	1.42
3	0.80	0.76	1.36	1.33	1.04	1.03	1.00	1.07	0.89	0.91	1.10	1.10
4A	1.47	1.44	0.61	0.80	0.99	0.91	1.18	0.80	1.21	1.38	0.94	0.85
5	1.33	1.17	0.53	0.67	0.99	0.95	1.16	1.07	1.25	1.13	0.91	0.91
5A	1.33	1.22	0.53	0.60	0.99	0.89	1.16	1.10	1.25	1.40	0.91	0.84
6	1.22	1.10	0.78	0.78	0.96	0.95	1.06	1.07	1.09	1.10	0.95	0.95
8	0.85	0.76	1.53	1.56	1.08	1.06	0.97	1.0	0.85	0.87	1.28	1.12
9	1.0	0.98	1.02	1.11	1.01	0.98	0.77	0.71	0.96	0.98	0.98	1.04
10	1.07	0.95	1.00	1.00	1.01	0.97	0.90	0.79	1.01	0.95	1.02	1.05
11	0.89	0.86	1.20	1.22	1.11	1.06	1.16	1.36	1.02	0.89	1.04	1.02
12	1.16	1.11	0.80	0.78	1.04	0.95	0.85	0.71	1.05	1.07	1.09	0.97
13	1.05	1.00	0.98	1.00	1.08	1.00	0.99	0.93	1.00	1.00	1.10	1.00
14	0.96	0.90	1.17	1.22	1.08	1.06	0.62	0.93	0.80	0.97	1.15	0.84
15	0.97	0.89	0.80	0.88	1.08	1.06	1.51	--[b]	1.44	--[b]	0.94	0.78
17	1.02	1.02	0.98	0.96	1.57	1.30	0.99	0.96	0.97	0.98	--[c]	0.99
18	1.13	1.06	1.02	1.00	0.48[d]	1.00	0.96	1.29[d]	0.79	0.98	--[c]	--
19	0.77	0.84	1.02	1.11	--[e]	--[e]	0.88	0.86	1.44	1.23	1.62	0.99
21	1.13	1.05	1.00	0.96	0.92	0.97	1.04	1.07	1.02	1.01	1.05	0.98

(a) Ratios are direct comparisons of theory and experiment.

(b) Second flow maximum cannot be determined.

(c) Transmural pressures not measured.

(d) These values were very difficult to determine from data.

(e) Emptying time could not be clearly identified but is much greater than in Test 1 for both experiment and theory.

TABLE 5. Values of A_0, c_0, and C_f used in the venous flow simulations

ξ	A_0	c_0	C_f
0.0	1.4000	251.6000	8.0267
0.01	1.4000	244.0000	7.9433
0.02	1.4000	239.0000	7.8867
0.03	1.4000	234.0000	7.8333
0.04	1.4000	229.0000	7.7767
0.05	1.4000	224.0000	7.7233
0.06	1.4000	219.0000	7.6667
0.07	1.4000	214.3333	7.6133
0.08	1.4000	210.3333	7.5567
0.09	1.4000	207.3333	7.5000
0.10	1.4000	205.6660	7.4433
0.11	1.4000	205.0000	7.3867
0.12	1.4000	205.0000	7.3333
0.13	1.4000	205.0000	7.2767
0.14	1.4000	205.0000	7.2233
0.15	1.4110	205.0000	7.1667
0.16	1.4333	204.6666	7.1133
0.17	1.4667	204.0000	7.0567
0.18	1.5000	202.6667	7.1033
0.19	1.5333	200.3333	7.2500
0.20	1.5667	196.6667	7.5000
0.21	1.6000	191.6667	7.7500
0.22	1.6333	186.0000	7.9167
0.23	1.6667	180.0000	8.0000
0.24	1.7000	174.0000	8.0000
0.25	1.7333	168.0000	8.0000
0.26	1.7667	162.0000	8.0000
0.27	1.8000	156.3333	8.0000
0.28	1.8333	151.3333	8.0000
0.29	1.8667	147.3333	8.0000
0.30	1.8890	144.3333	8.0000
0.31	1.9000	142.0000	8.0000
0.32	1.9000	140.6667	7.8533
0.33	1.9000	140.6668	7.5633
0.34	1.8900	142.6667	7.1267
0.35	1.8600	146.6668	6.6900
0.36	1.8000	152.6667	6.2500
0.37	1.7200	159.6667	5.8133
0.38	1.6300	166.6668	5.3767
0.39	1.5400	173.0002	4.9400
0.40	1.4500	179.0000	4.5000
0.41	1.3567	185.0001	4.0633
0.42	1.2633	190.6668	3.6267
0.43	1.1700	195.6667	3.1900
0.44	1.0800	199.6667	2.7500
0.45	0.9900	202.6667	2.3133
0.46	0.9000	204.3334	1.8767
0.47	0.8200	205.0000	1.4400
0.48	0.7613	205.0000	1.1467
0.49	0.7343	205.0000	1.0000
0.50	0.7287	205.0000	1.0000
0.51	0.7333	205.0000	1.0000
0.52	0.7377	205.0000	1.0000
0.53	0.7423	205.0000	1.0000
0.54	0.7467	205.0000	1.0000
0.55	0.7510	205.0000	1.0000
0.56	0.7553	205.0000	1.0000
0.57	0.7597	205.0000	1.0000
0.58	0.7643	205.0000	1.0000
0.59	0.7687	205.0000	1.0000
0.60	0.7730	205.0000	1.0000
0.61	0.7773	205.0000	1.0000
0.62	0.7817	205.0000	1.0000
0.63	0.7863	205.0000	1.0000
0.64	0.7907	205.0000	1.0000
0.65	0.7953	205.0000	1.0000
0.66	0.7997	205.0000	1.0000
0.67	0.8040	205.0000	1.0000
0.68	0.8083	205.0000	1.0000
0.69	0.8127	205.0000	1.0000
0.70	0.8173	205.0000	1.0000
0.71	0.8217	205.0000	1.0000
0.72	0.8263	205.0000	1.0000
0.73	0.8307	205.0000	1.0000
0.74	0.8350	205.0000	1.0000
0.75	0.8393	205.0000	1.0000
0.76	0.8437	205.0000	1.0000
0.77	0.8483	205.0000	1.0000
0.78	0.8527	205.0000	1.0000
0.79	0.8573	205.0000	1.0000
0.80	0.8617	205.0000	1.0000
0.81	0.8660	205.0000	1.0000
0.82	0.8703	205.0000	1.0000
0.83	0.8747	205.0000	1.0000
0.84	0.8793	205.0000	1.0000
0.85	0.8837	205.0000	1.0000
0.86	0.8880	205.0000	1.0000
0.87	0.8923	205.0000	1.0000
0.88	0.8967	205.0000	1.0000
0.89	0.9013	205.0000	1.0000
0.90	0.9057	205.0000	1.0000
0.91	0.9103	205.0000	1.0000
0.92	0.9147	205.0000	1.0000
0.93	0.9190	205.0000	1.0000
0.94	0.9233	205.0000	1.0000
0.95	0.9277	205.0000	1.0000
0.96	0.9323	205.0000	1.0000
0.97	0.9367	205.0000	1.0000
0.98	0.9413	205.0000	1.0000
0.99	0.9460	205.0000	1.0000
0.100	0.9500	205.0000	1.0000

TABLE 6. Summary of Tube Information[a]

Tube	Range of Wall Thickness (cm)	Length (cm)	Weight (gm)	$\frac{\text{weight}}{\text{unit length}}$	K_p (expt'l) (dynes/cm^2)	K_p (calc) (dynes/cm^2)	A_0 (cm^2)	A_0 from positive pressure data	Density (gm/cm^3)
5L	0.0308 to 0.0359	28.8	3.98	0.138	205	287	1.073	1.137	1.07
5S	0.0211 to 0.0308	54.1	6.01	0.111					1.11
8L	0.0298 to 0.0318	25.0	3.30	0.132	192	226	1.052	1.145	1.11
8S	0.0238 to 0.0289	57.3	6.59	0.115					1.13
9L	0.0207 to 0.0251	49.9	2.45	0.0984	95	93	0.881	1.110	1.12
9S	0.0244 to 0.0308	57.5	7.08	0.123					1.16
Tube used in flow expt's	0.0285 to 0.0366	57.8	7.59	0.131		268			1.05

In all cases, tube circumference = 3.85 cm

TABLE 7. Maximum values of Q, u, and u/R at five calf locations for each venous simulation

Type of Cycle	Rise Time (sec)	P_{max} (mm Hg)	Parameter	ξ=0.10	ξ=0.20	ξ=0.30	ξ=0.40	ξ=0.44
Current pressure cycle	5	30	Q_{max}	6.2	11.5	20.2	31.1	51.3
			u_{max}	5.6	9.8	13.1	33.8	105.8
			$(u/R)_{max}$	26.9	44.5	55.0	202.5	957.8
Uniform pressure cycle	1/3	30	Q_{max}	10.9	21.9	38.3	54.0	85.7
			u_{max}	8.2	15.9	21.7	47.0	147.8
			$(u/R)_{max}$	36.1	67.6	83.7	206.3	1088
	1	30	Q_{max}	7.6	13.7	23.7	42.4	55.1
			u_{max}	6.4	11.3	14.3	46.8	141.5
			$(u/R)_{max}$	30.1	50.0	56.6	257.4	1344
	1.6	30	Q_{max}	7.5	13.6	22.7	37.8	46.3
			u_{max}	6.6	11.2	13.6	42.8	113.7
			$(u/R)_{max}$	30.5	49.2	54.1	257.6	1264
	3	30	Q_{max}	6.7	11.4	18.2	28.9	33.9
			u_{max}	5.6	9.0	10.8	36.2	67.3
			$(u/R)_{max}$	25.9	39.4	45.3	253.7	730.2
	5	30	Q_{max}	5.6	9.0	14.0	21.5	24.2
			u_{max}	5.0	7.5	8.8	30.9	39.8
			$(u/R)_{max}$	23.4	33.5	40.8	242.9	479.1
	1	20	Q_{max}	7.0	13.4	23.4	35.8	57.0
			u_{max}	6.3	11.4	14.9	35.9	111.6
			$(u/R)_{max}$	29.7	51.0	61.4	179.6	847.2
	1	50	Q_{max}	7.8	15.8	28.5	43.9	64.4
			u_{max}	6.7	12.7	17.2	40.3	146.3
			$(u/R)_{max}$	30.9	55.8	68.9	235.0	1490
	1	70	Q_{max}	9.4	18.5	33.3	50.7	81.0
			u_{max}	7.2	14.1	19.2	44.4	163.8
			$(u/R)_{max}$	32.9	61.1	75.7	260.2	1865

(continued)

TABLE 7. (continued)

Type of Cycle	Rise Time (sec)	P_{max} (mm Hg)	Parameter	ξ=0.10	ξ=0.20	ξ=0.30	ξ=0.40	ξ=0.44
Linear pressure application	1	30	Q_{max}	18.0	28.9	42.2	49.5	50.5
			u_{max}	18.0	25.4	23.1	28.7	38.8
			$(u/R)_{max}$	121.2	138.9	125.6	87.7	109.3
	1/3	30	Q_{max}	32.3	49.4	47.0	58.4	60.6
			u_{max}	32.9	36.3	25.7	34.1	47.3
			$(u/R)_{max}$	175.2	149.9	129.1	118.0	136.0
	1/3	50	Q_{max}	43.2	68.6	81.6	83.8	86.9
			u_{max}	47.2	52.1	38.1	46.7	63.9
			$(u/R)_{max}$	271.5	256.0	207.7	246.3	219.3
	Wave Speed (cm/sec)							
Wave-like pressure application	10	30	Q_{max}	19.2	22.1	32.8	34.7	33.9
			u_{max}	32.1	21.9	17.4	23.1	26.0
			$(u/R)_{max}$	582.8	461.8	420.5	497.2	249.5
	20	30	Q_{max}	31.5	41.1	59.1	54.6	53.1
			u_{max}	27.8	25.4	27.2	33.0	40.2
			$(u/R)_{max}$	508.3	371.2	332.4	518.4	281.0
	30	30	Q_{max}	48.7	51.8	95.5	90.9	88.3
			u_{max}	31.1	31.3	43.6	51.7	61.5
			$(u/R)_{max}$	484.8	371.2	286.4	458.3	374.0
	50	30	Q_{max}	83.9	85.2	134.7	158.4	
			u_{max}	56.9	51.9	60.8	95.6	
			$(u/R)_{max}$	536.2	452.2	963.2	303.4	

LIST OF FIGURES

Fig. 1 The hydraulic model used in the experiments.

Fig. 2 The test section of the hydraulic model illustrating the separation of the two chambers.

Fig. 3 Schematic representation of an applied pressure cycle and the corresponding volume flow rate exiting from the collapsing tube.

Fig. 4 Stages of vessel collapse with uniform external compression shown schematically for a typical vein in the lower leg.

Fig. 5 The physiologic model: total cross-sectional area, A_0 , wave speed, c_0 (both at normal physiologic pressures), and a friction factor, C_f , plotted against distance between the ankle and the thigh.

Fig. 6 Various types of pressure cycles.

Fig. 7 Log-log plot of normalized transmural pressure, P, versus normalized cross-sectional area, α . The points represent experimental results for three different tubes; the solid line is the theoretical prediction.

Fig. 8 Linear plot of normalized transmural pressure, P, versus normalized cross-sectional area, α . The points represent three sets of experimental results; the solid line is the theoretical prediction.

Fig. 9 Complete set of results for Experiment 1. Top: applied external pressure. Center: transmural pressure at ξ = 0.06, 0.15, 0.24, 0.33, 0.42 and at the exit (proceeding from the bottom trace up). Bottom: volume flow rate at the exit of the test section. The Roman numerals correspond to the different quantities defined on p. 117 of the text.

Fig. 10 A comparison of volume flow rates at the exit of the test section between experiment (dashed lines) and theory (solid lines). Tests 1, 1A, 2, 2A, 3 and 4A.

Fig. 11 A comparison of volume flow rates at the exit of the test section between experiment (dashed lines) and theory (solid lines). Tests 5,5A, 6, 8, 9, and 10.

Fig. 12 A comparison of volume flow rates at the exit of the test section between experiment (dashed lines) and theory (solid lines). Tests 11, 12, 13, 14, 15, and 17.

Fig. 13 A comparison of volume flow rates at the exit of the test section between experiment (dashed lines) and theory (solid lines). Tests 18, 19, and 21.

Fig. 14 Volume flow rate at the exit of the test section as computed for three different grid spacings: 51 points ($\Delta\xi = 0.02$), 101 points ($\Delta\xi = 0.01$), and 201 points ($\Delta\xi = 0.005$).

Fig. 15 Results of Simulations 59, 60, and 63. Normalized transmural pressure, P, plotted against normalized time, τ , at four different locations inside the collapsing portion of the vessel: $\xi = 0.09$, 0.19, 0.29, and 0.39 (from top to bottom).

Fig. 16 Results of Simulations 59, 60, and 63. Normalized volume flow rate, Q, plotted against normalized time, τ, at five different locations inside the collapsing portion of the vessel: $\xi = 0.09$, 0.19, 0.29, 0.39, and 0.64 (from bottom to top).

Fig. 17 Results of Simulations 59, 60, and 63. U/C plotted against normalized time, τ, at four different locations inside the collapsing portion of the vessel: $\xi = 0.09$, 0.19, 0.29, and 0.39 (from bottom to top).

Fig. 18 Results of Simulations 59, 60, and 63. Normalized cross-sectional area, α, plotted against normalized distance, x/L, at six different times, $\tau = 0.0$, $\tau_{max}/10$, $\tau_{max}/5$, $2\tau_{max}/5$, $3\tau_{max}/5$, and τ_{max} . (from top to bottom).

Fig. 19 Schematic representation of the deep veins of the leg.

Fig. 20 The tube law used in the venous flow simulations.

Fig. 21 Venous flow simulation. The currently used clinical pressure cycle. From the upper left, proceeding counterclock-wise: (1) maximum applied pressure vs. time; (2) volume flow rate at $\xi = 0.1$, 0.2, 0.3, 0.4 vs. time; (3) flow velocity at same four locations vs. time; (4) shear rate at the same four locations vs. time; (5) normalized cross-sectional area vs. distance at six times, $t = 0$, $t = t_{max}/10$, $t = t_{max}/5$, $t = 2t_{max}/5$, $t = 3t_{max}/5$, $t = t_{max}$; (6) Distribution of external pressure.

Fig. 22 Venous flow simulation. Uniform pressure application; p_{max} = 30 mm Hg; rise time = 1/3 sec. Same six graphs as described for Fig. 21.

Fig. 23 Venous flow simulation. Uniform pressure application; p_{max} = 30 mm Hg; rise time = 1 sec. Same six graphs as described in caption for Fig. 21.

Fig. 24 Venous flow simulation. Uniform pressure application; p_{max} = 30 mm Hg; rise time = 1.6 sec. Same six graphs as described in caption for Fig. 21.

Fig. 25 Venous flow simulation. Uniform pressure application; p_{max} = 30 mm Hg; rise time = 3 sec. Same six graphs as described in caption for Fig. 21.

Fig. 26 Venous flow simulation. Uniform pressure application; p_{max} = 30 mm Hg; rise time = 5 sec. Same six graphs as described in caption for Fig. 21.

Fig. 27 Q_{max}, u_{max}, and $(u/R)_{max}$ plotted as a function of rise time for the simulations of Figs. 22-26.

Fig. 28 Venous flow simulation. Uniform pressure application; p_{max} = 20 mm Hg; rise time = 1 sec. Same six graphs as described in caption for Fig. 21.

Fig. 29 Venous flow simulation. Uniform pressure application; p_{max} = 50 mm Hg; rise time = 1 sec. Same six graphs as described in caption for Fig. 21.

Fig. 30 Venous flow simulation. Uniform pressure application; p_{max} = 70 mm Hg; rise time = 1 sec. Same six graphs as described in caption for Fig. 21.

Fig. 31 Q_{max}, u_{max}, and $(u/R)_{max}$ plotted as a function of maximum applied pressure for the simulations of Figs. 23 and 28-30.

Fig. 32 Venous flow simulation. Linear pressure application; p_{max} = 30 mm Hg, rise time = 1 sec. Same six graphs as described in cpation for Fig. 21.

Fig. 33 Venous flow simulation. Linear pressure application; p_{max} = 30 mm Hg, rise time = 1/3 sec. Same six graphs as described in caption for Fig. 21.

Fig. 34 Venous flow simulation. Linear pressure application; p_{max} = 50 mm Hg, rise time = 1/3 sec. Same six graphs as described in caption for Fig. 21.

Fig. 35 Venous flow simulation. Wave-like pressure application; p_{max} = 30 mm Hg; wave propagation speed = 10 cm/sec. Same six graphs as described in caption for Fig. 21. The pressure distribution is shown at three consecutive times.

Fig. 36 Venous flow simulation. Wave-like pressure application; p_{max} = 30 mm Hg; wave propagation speed = 20 cm/sec. Same six graphs as described in caption for Fig. 21. The pressure distribution is shown at three consecutive times.

Fig. 37 Venous flow simulation. Wave-like pressure application; p_{max} = 30 mm Hg; wave propagation speed = 30 cm/sec. Same six graphs as described in caption for Fig. 21. The pressure distribution is shown at three consecutive times.

Fig. 38 Venous flow simulation. Wave-like pressure application; p_{max} = 30 mm Hg; wave propagation speed = 50 cm/sec. Same six graphs as described in caption for Fig. 21. The pressure distribution is shown at three consecutive times.

Fig. 39 Schematic of uniformly collapsing tube system.

Fig. 40 Simulation results for uniform vessel collapse. Collapse time, t_c^*, maximum required pressure (p_{max} in dynes/cm^2) and maximum volume flow rate (Q_{max} in mℓ/sec), each plotted as a function of b, where $p(x) = p_{max} - bx^2$.

Fig. 41 Tube law measuring apparatus.

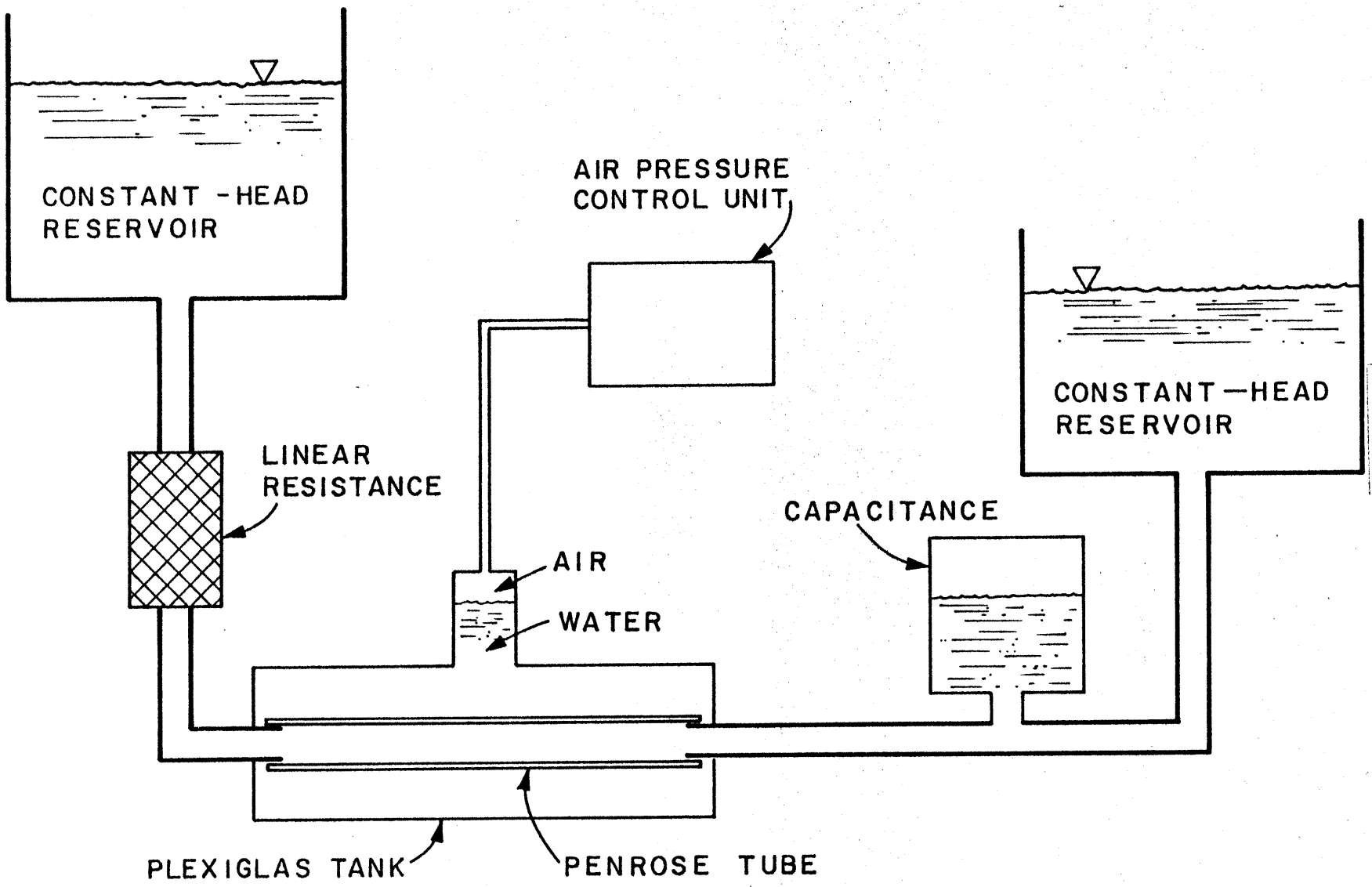
CONSTANT -HEAD
RESERVOIR
AIR PRESSURE
CONTROL UNIT
CONSTANT —HEAD
RESERVOIR
LINEAR
RESISTANCE
CAPACITANCE
AIR
WATER
PLEXIGLAS TANK
PENROSE TUBE

FIG. 1

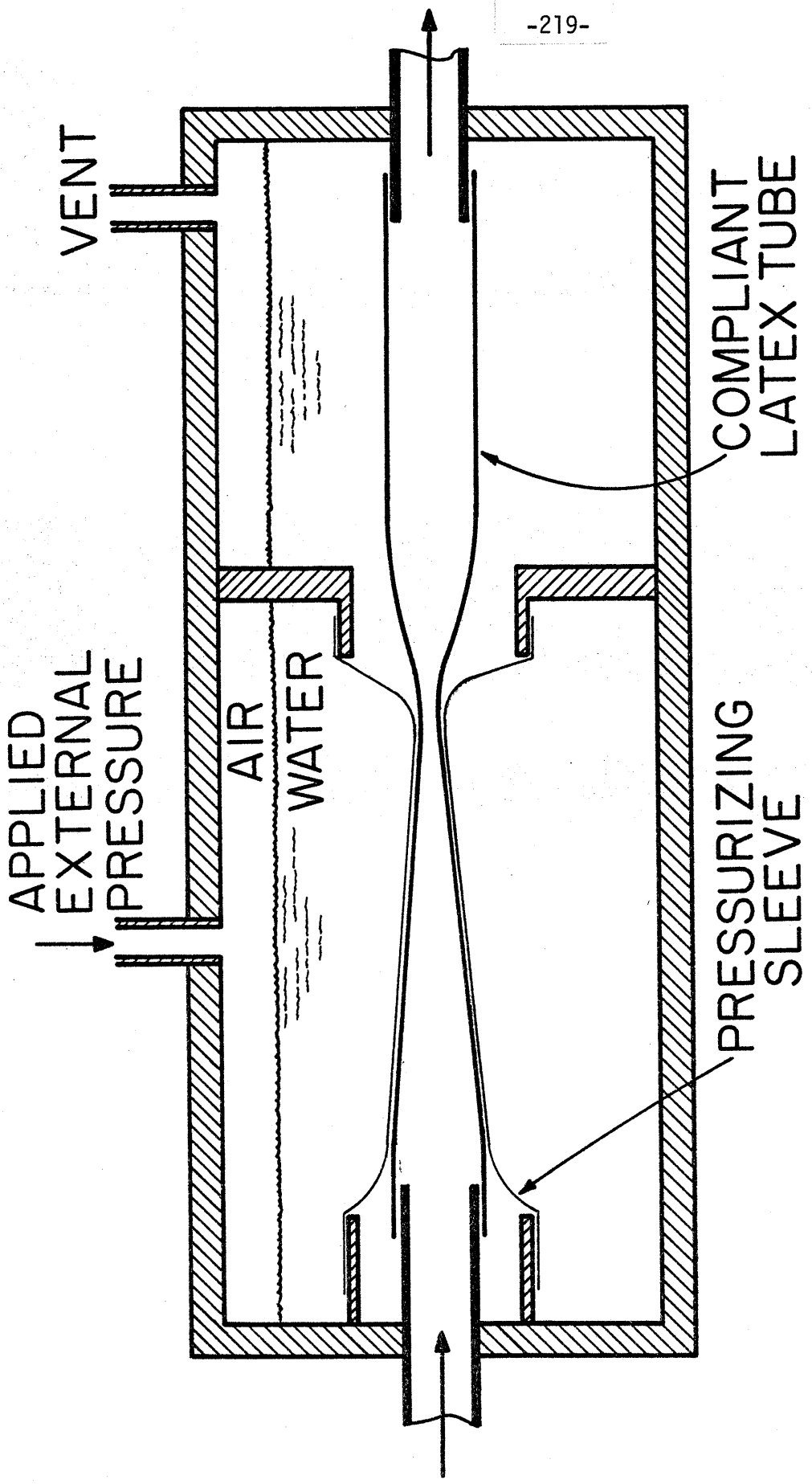
VENT
APPLIED EXTERNAL PRESSURE
AIR
WATER
COMPLIANT LATEX TUBE
PRESSURIZING SLEEVE

FIG. 2

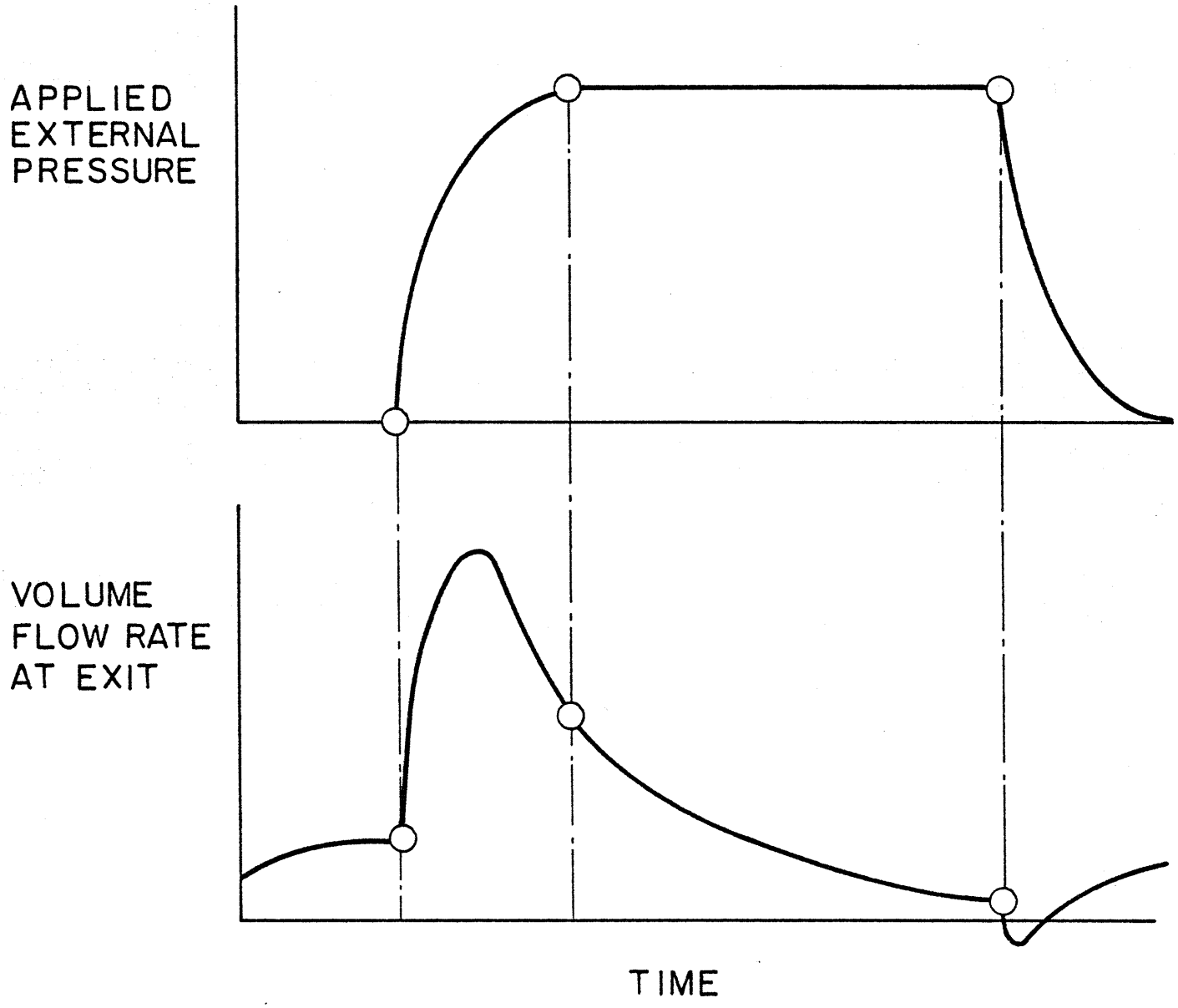

FIG. 3

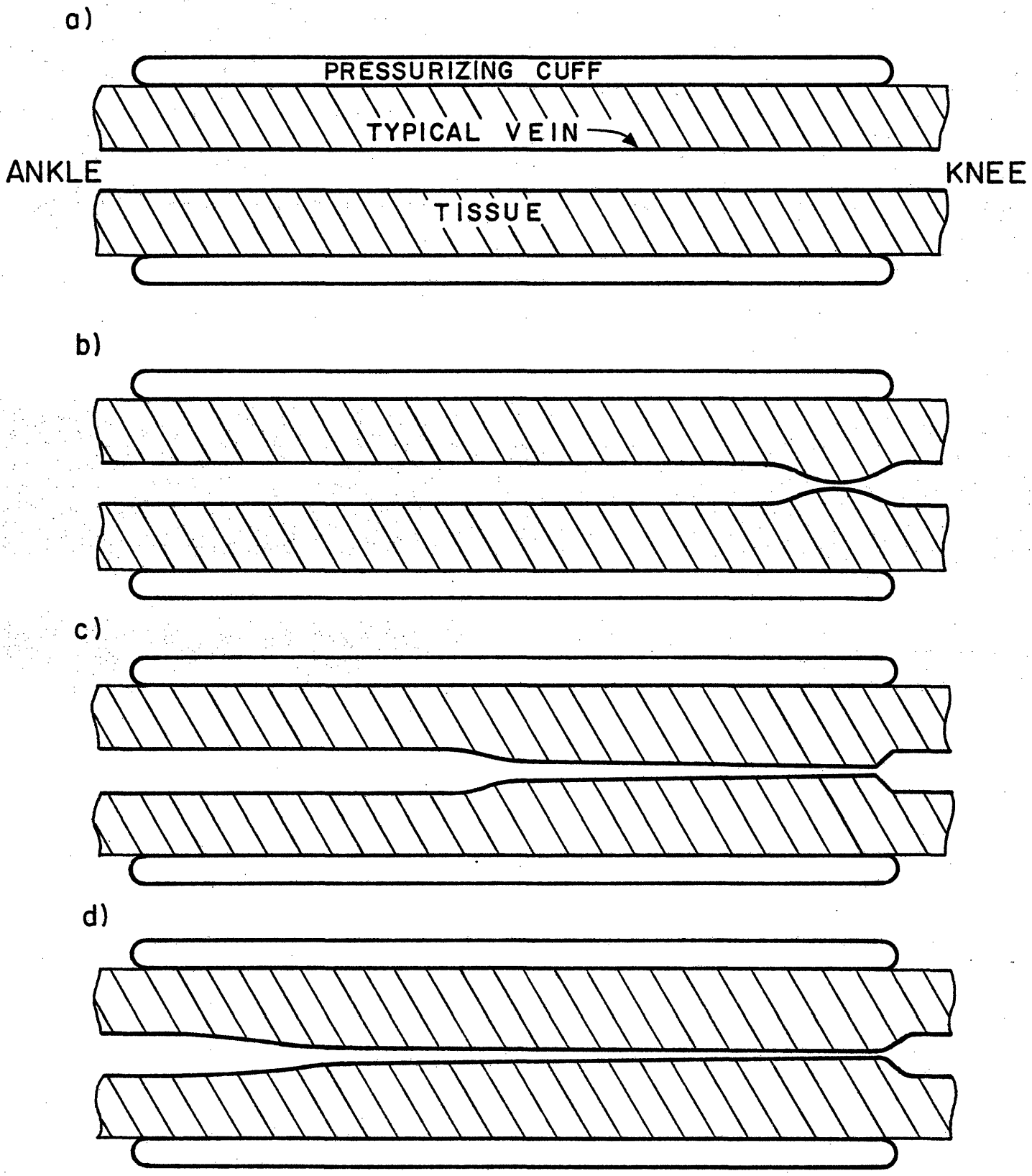

FIG. 4

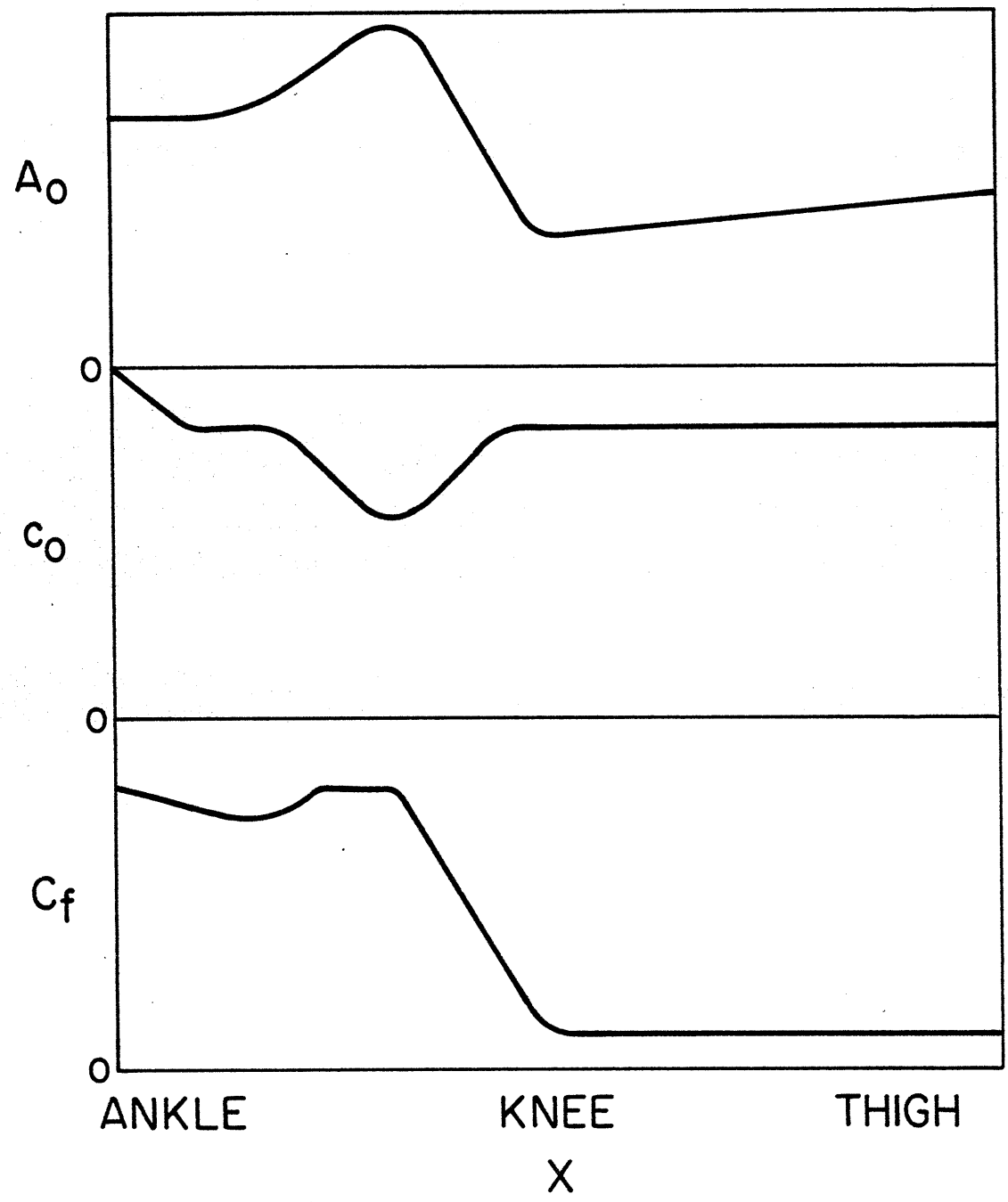

FIG. 5

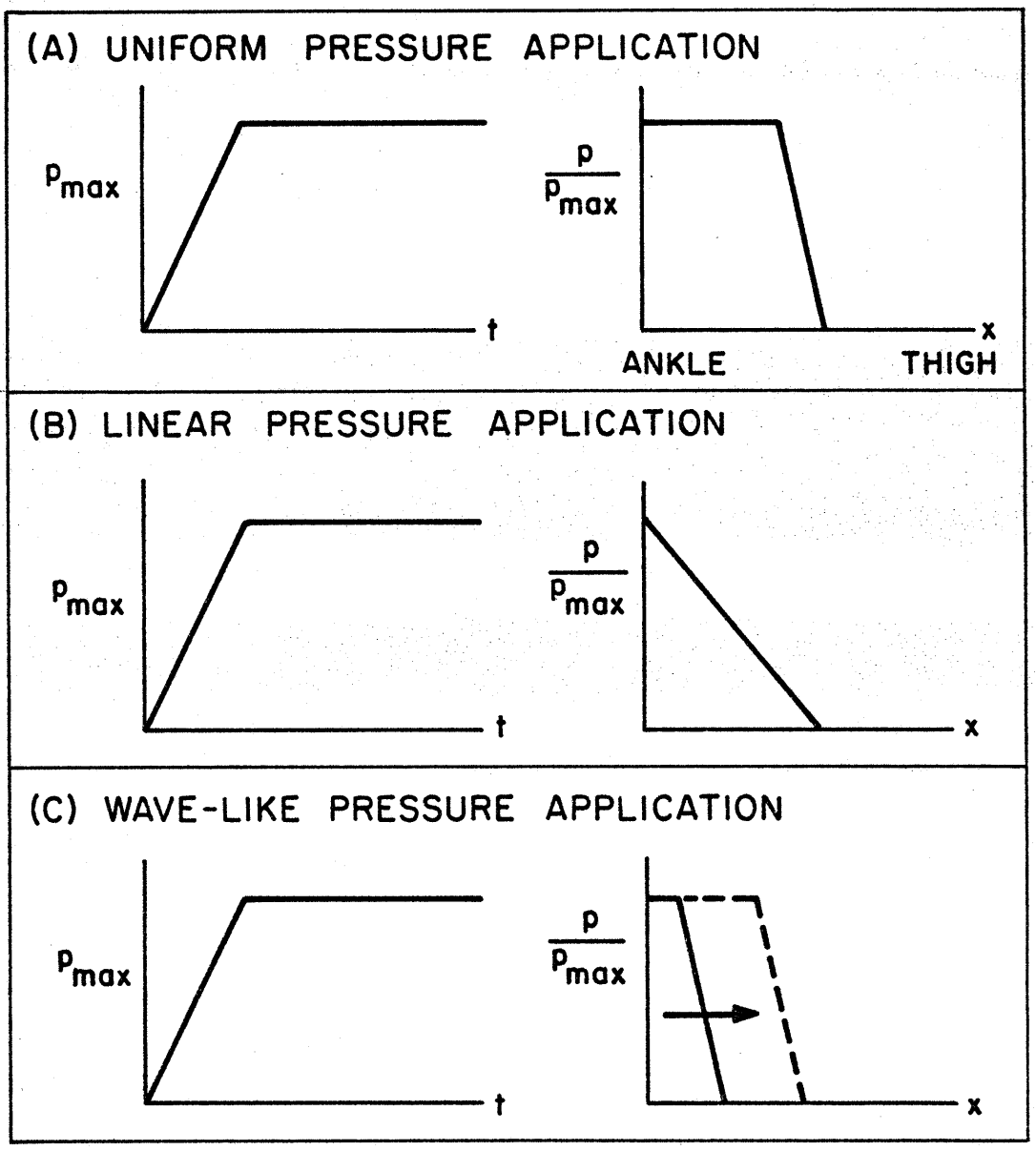
(A) UNIFORM PRESSURE APPLICATION
p_{max}
t
$\frac{p}{p_{max}}$
x
ANKLE
THIGH
(B) LINEAR PRESSURE APPLICATION
p_{max}
t
$\frac{p}{p_{max}}$
x
(C) WAVE-LIKE PRESSURE APPLICATION
p_{max}
t
$\frac{p}{p_{max}}$
x

FIG. 6

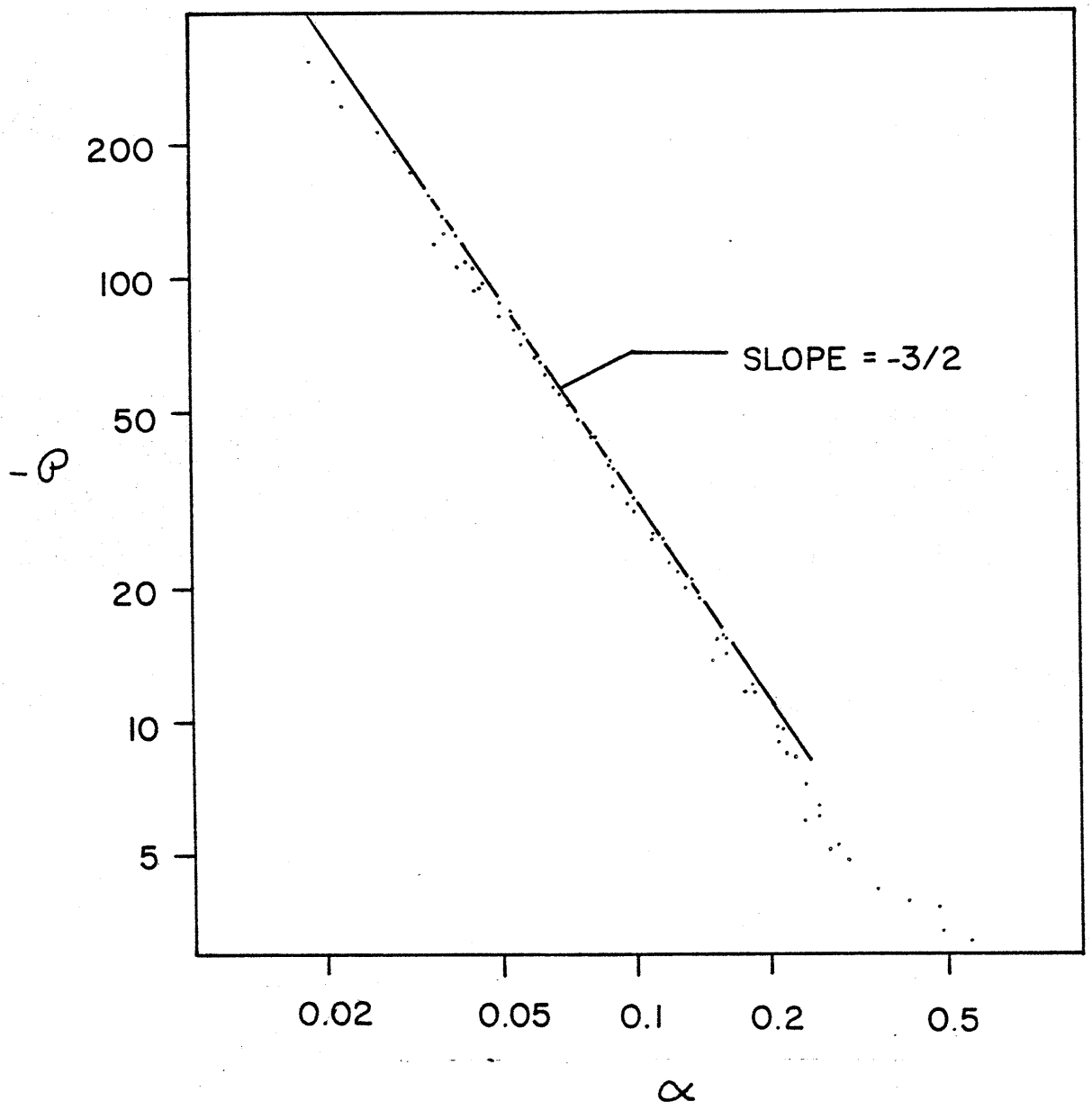

FIG. 7

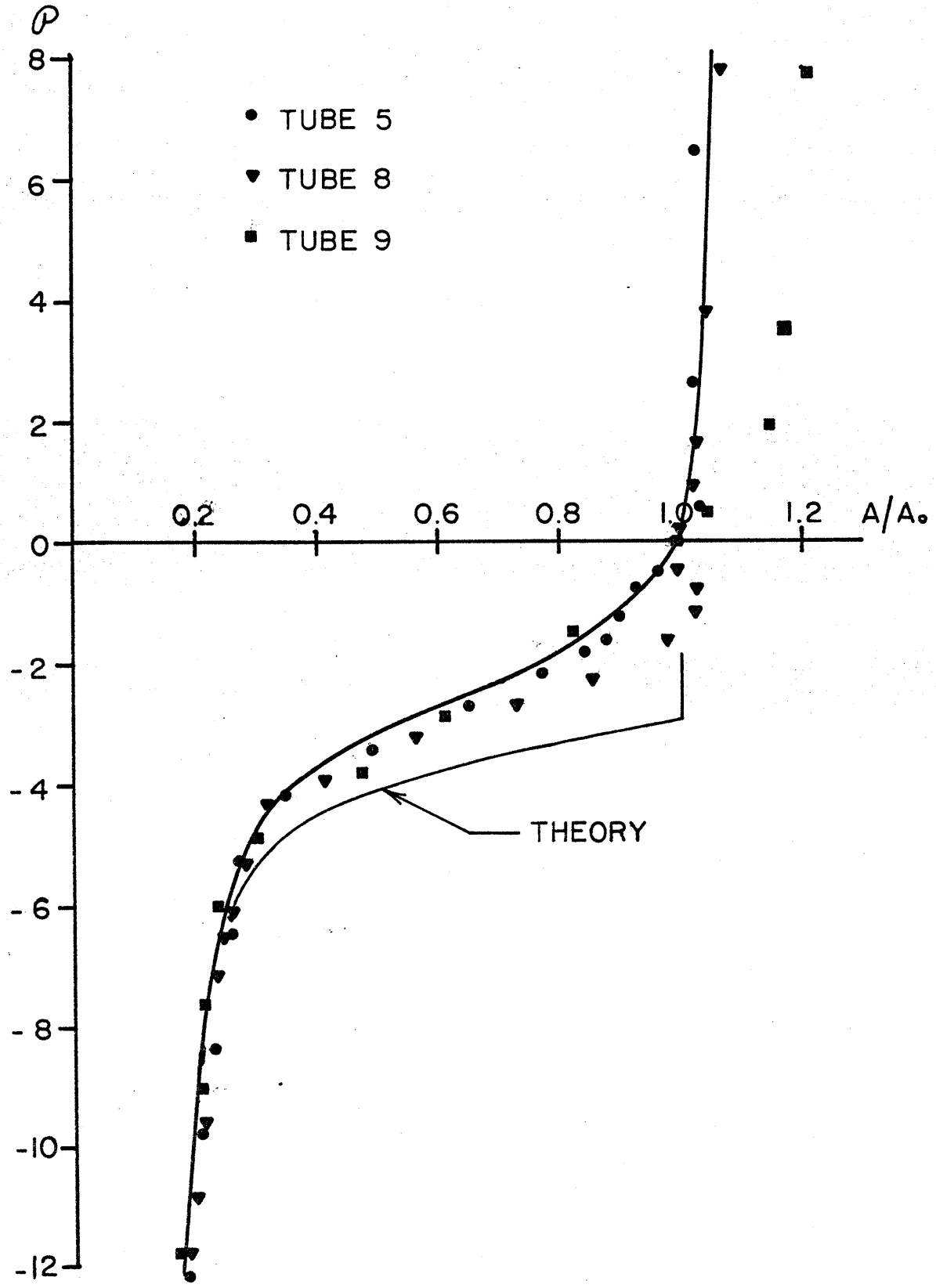

FIG. 8

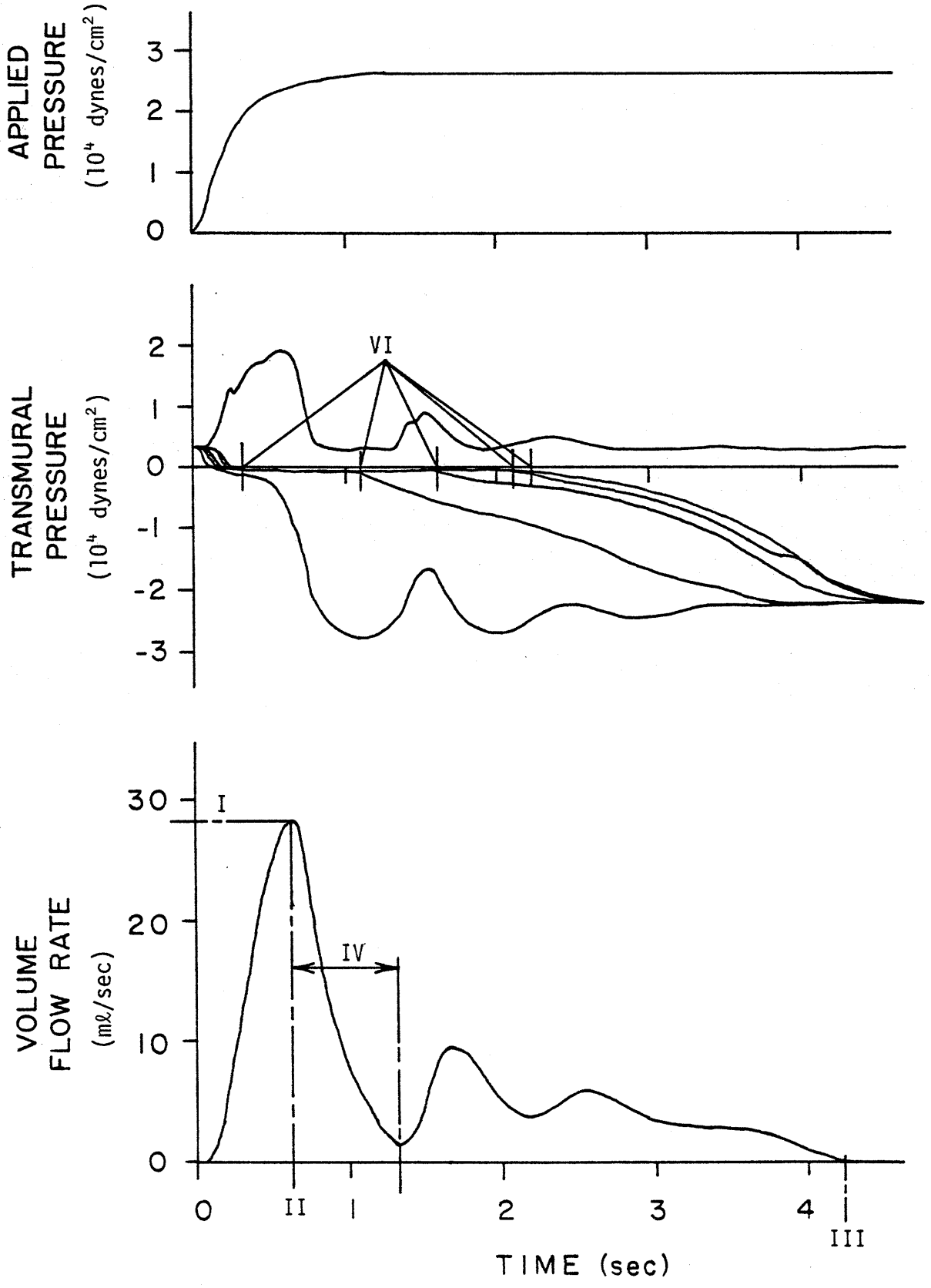
APPLIED PRESSURE
(10^4 dynes/cm^2)
3
2
1
0
TRANSMURAL PRESSURE
(10^4 dynes/cm^2)
2
1
0
-1
-2
-3
VI
VOLUME FLOW RATE
(mℓ/sec)
30
20
10
0
I
IV
0
II
I
2
3
4
III
TIME (sec)

FIG. 9

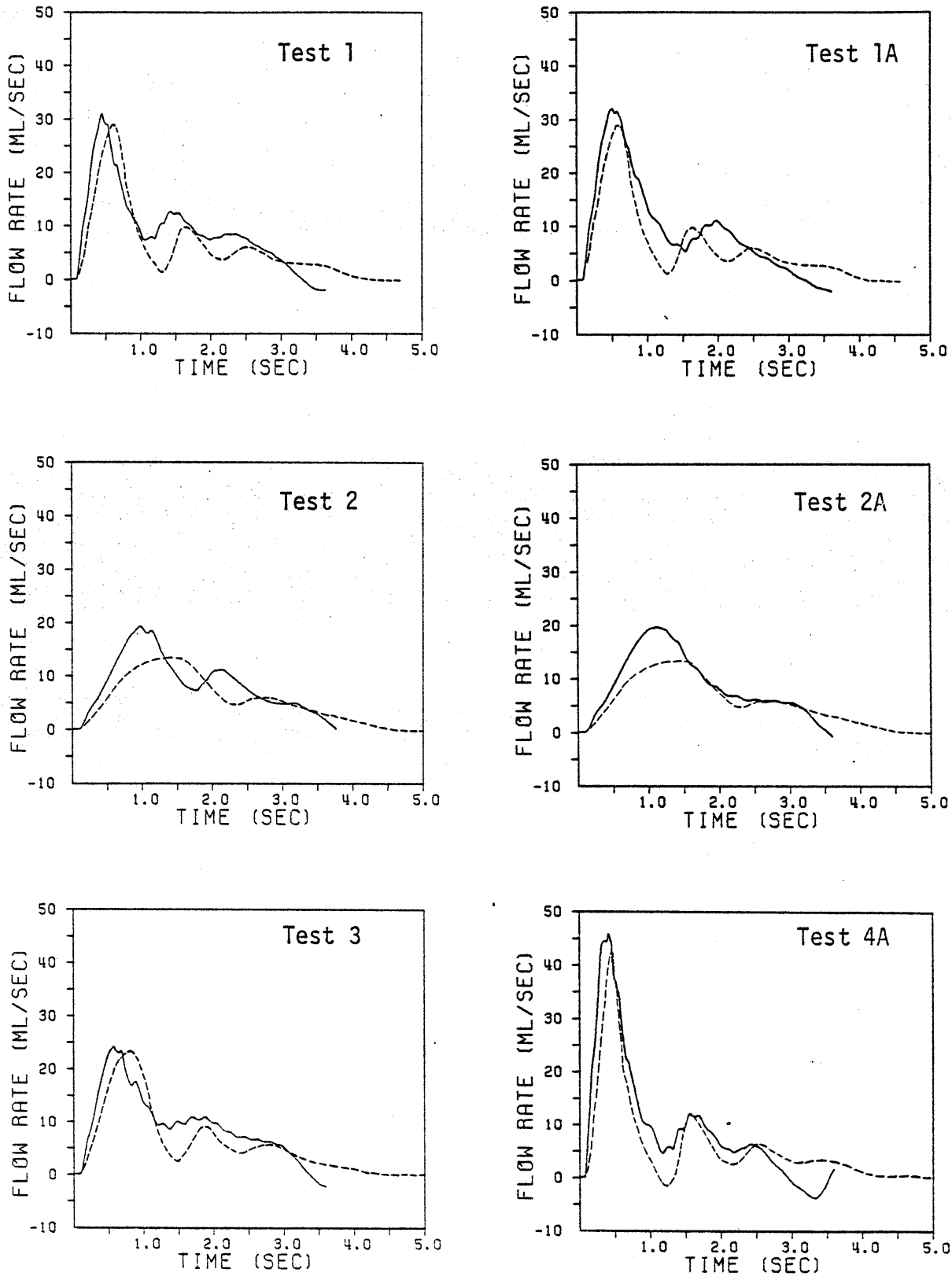
Test 1
Test 1A
Test 2
Test 2A
Test 3
Test 4A
FLOW RATE (ML/SEC)
TIME (SEC)
50
40
30
20
10
0
-10
1.0
2.0
3.0
4.0
5.0

FIG. 10

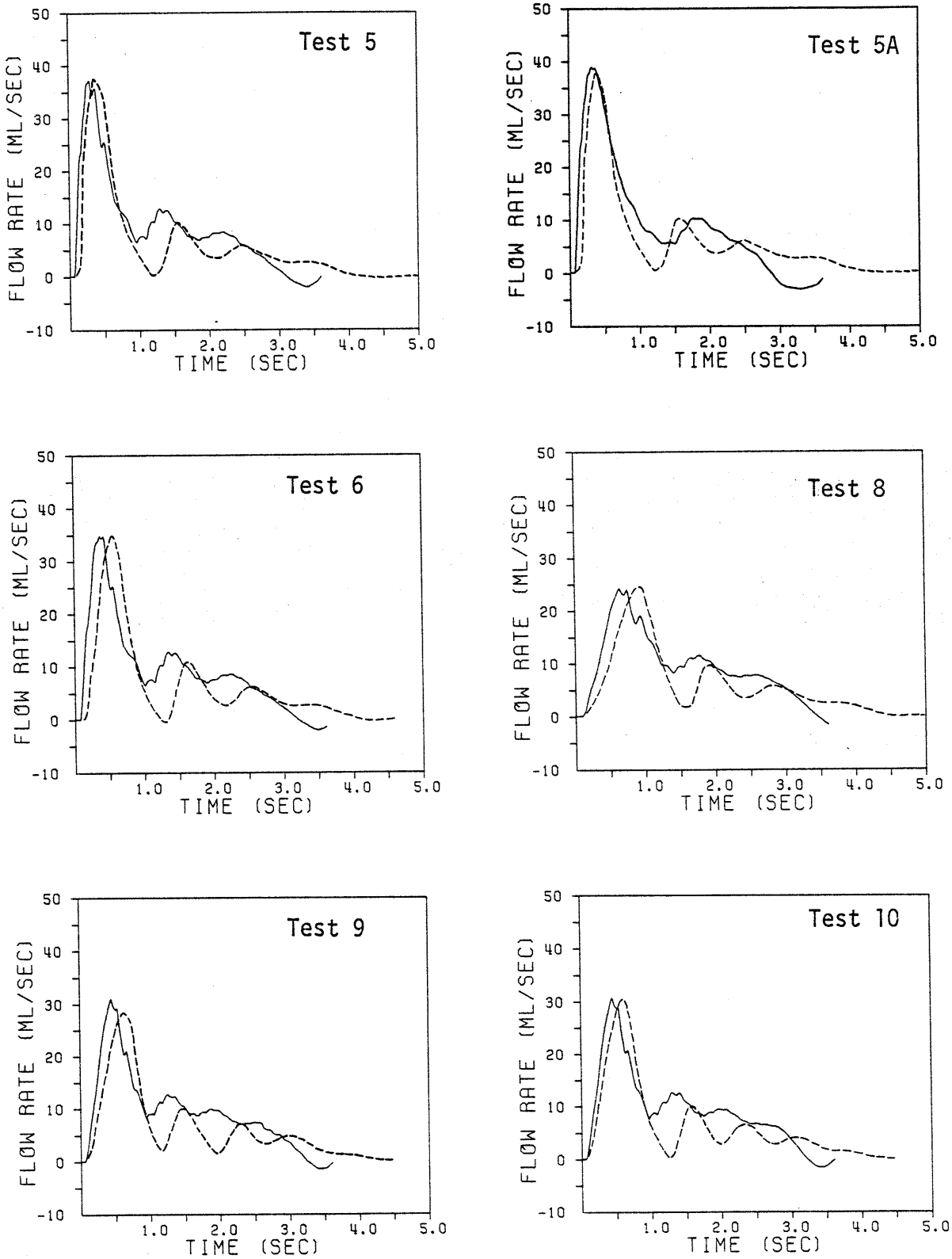
Test 5
Test 5A
Test 6
Test 8
Test 9
Test 10
FLOW RATE (ML/SEC)
TIME (SEC)
50
40
30
20
10
0
-10
1.0
2.0
3.0
4.0
5.0

FIG. 11

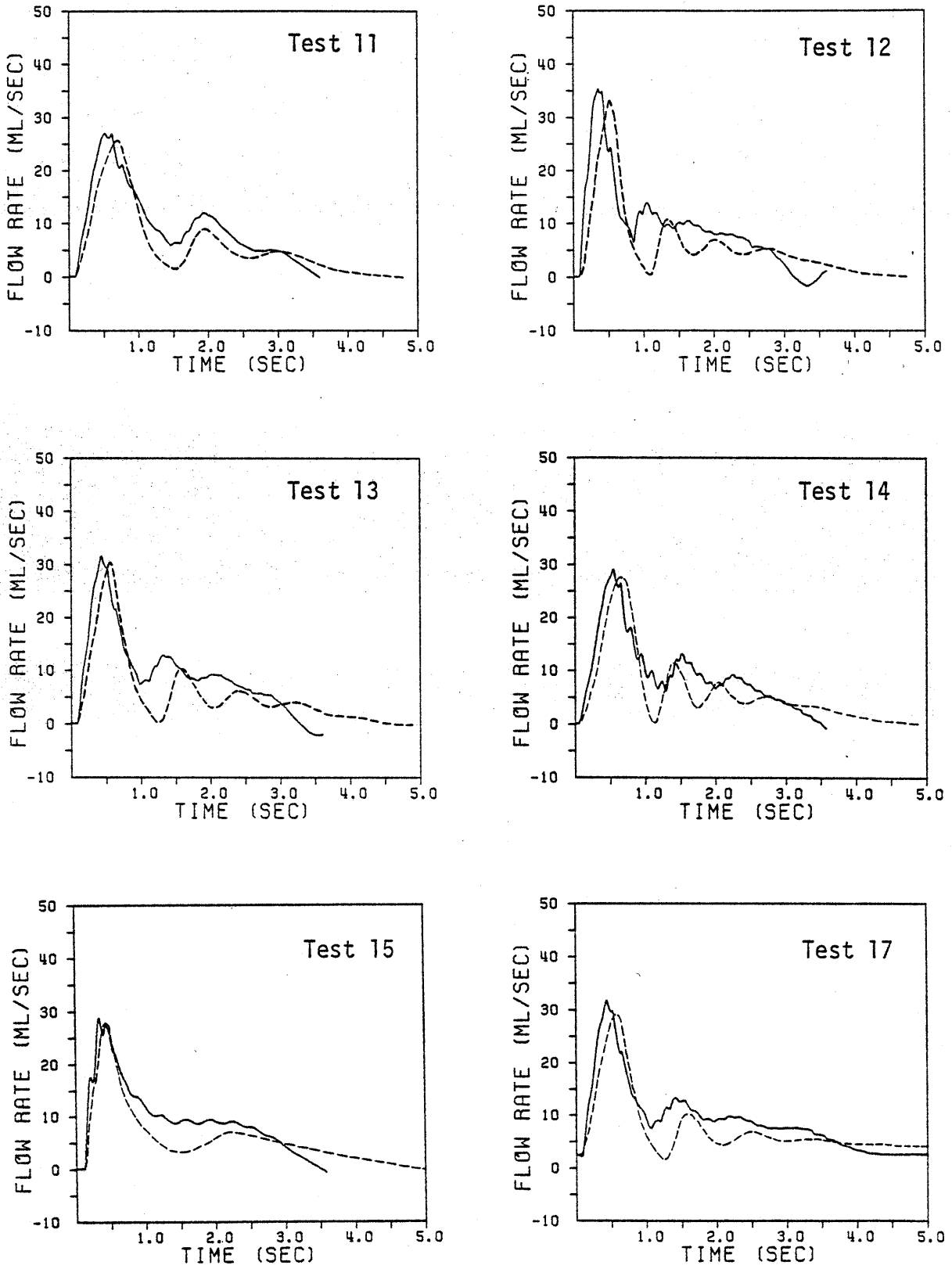
Test 11
Test 12
Test 13
Test 14
Test 15
Test 17
FLOW RATE (ML/SEC)
TIME (SEC)
50
40
30
20
10
0
-10
1.0
2.0
3.0
4.0
5.0

FIG. 12

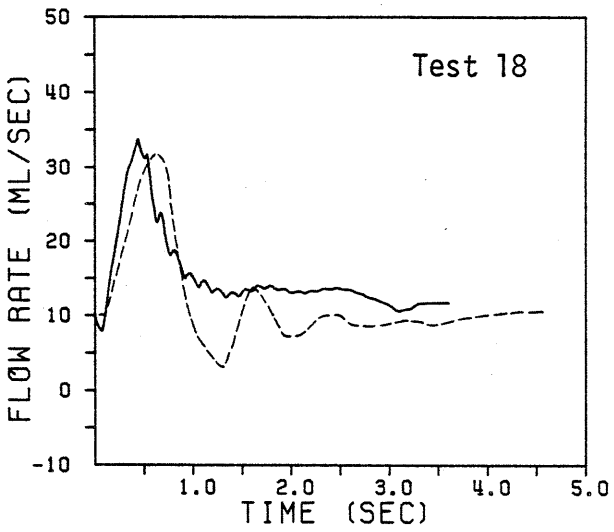
Test 18
FLOW RATE (ML/SEC)
50
40
30
20
10
0
-10
1.0
2.0
3.0
4.0
5.0
TIME (SEC)

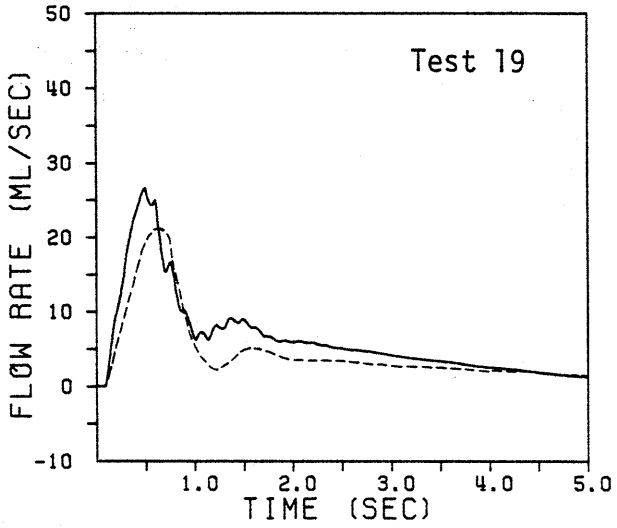
Test 19
FLOW RATE (ML/SEC)
50
40
30
20
10
0
-10
1.0
2.0
3.0
4.0
5.0
TIME (SEC)

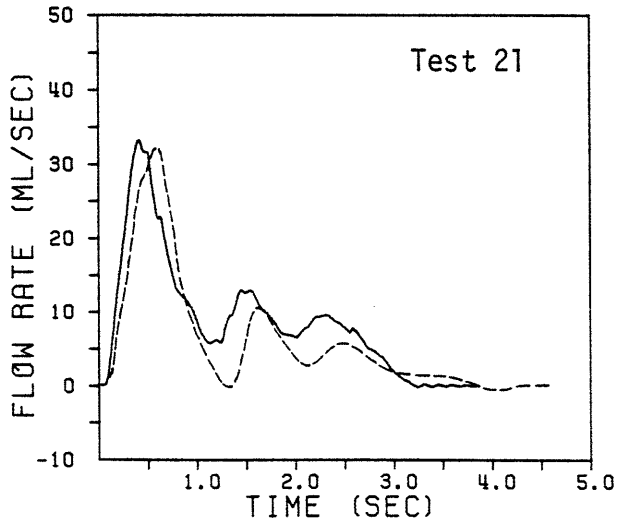
Test 21
FLOW RATE (ML/SEC)
50
40
30
20
10
0
-10
1.0
2.0
3.0
4.0
5.0
TIME (SEC)

FIG. 13

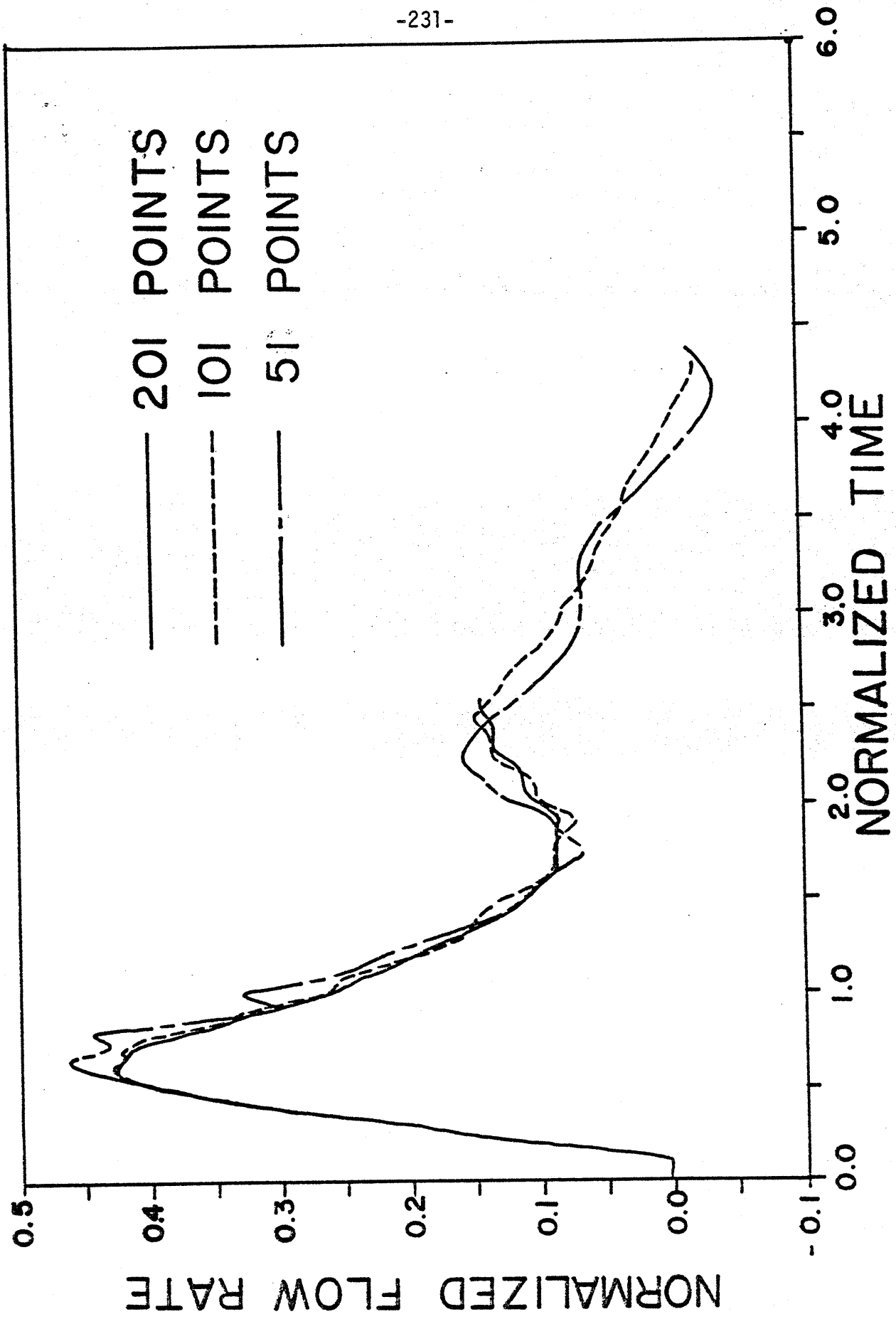
201 POINTS
101 POINTS
51 POINTS
NORMALIZED FLOW RATE
NORMALIZED TIME
0.5
0.4
0.3
0.2
0.1
0.0
-0.1
0.0
1.0
2.0
3.0
4.0
5.0
6.0

FIG. 14

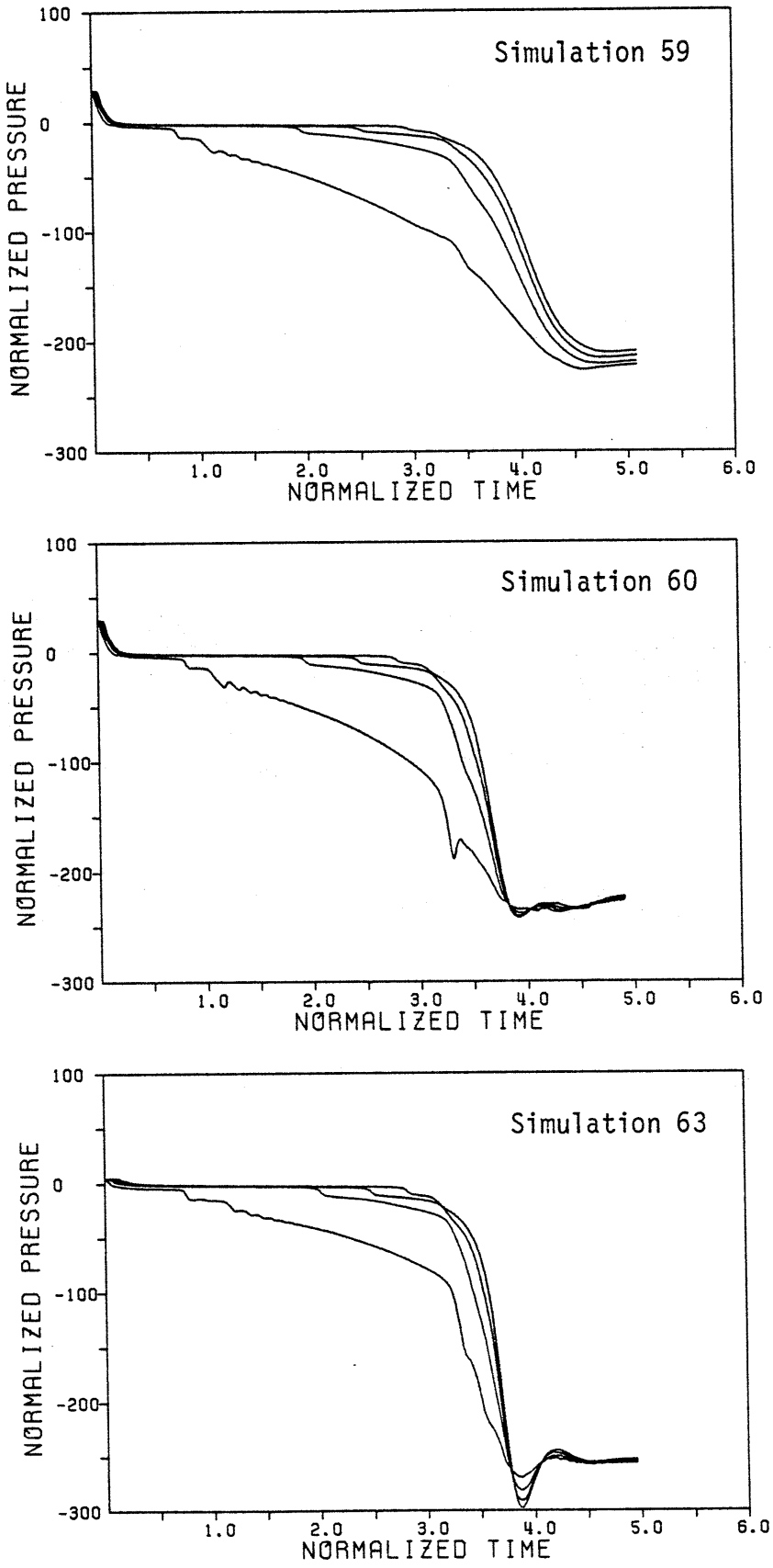
Simulation 59
NORMALIZED PRESSURE
100
0
-100
-200
-300
1.0
2.0
3.0
4.0
5.0
6.0
NORMALIZED TIME
Simulation 60
NORMALIZED PRESSURE
100
0
-100
-200
-300
1.0
2.0
3.0
4.0
5.0
6.0
NORMALIZED TIME
Simulation 63
NORMALIZED PRESSURE
100
0
-100
-200
-300
1.0
2.0
3.0
4.0
5.0
6.0
NORMALIZED TIME

FIG. 15

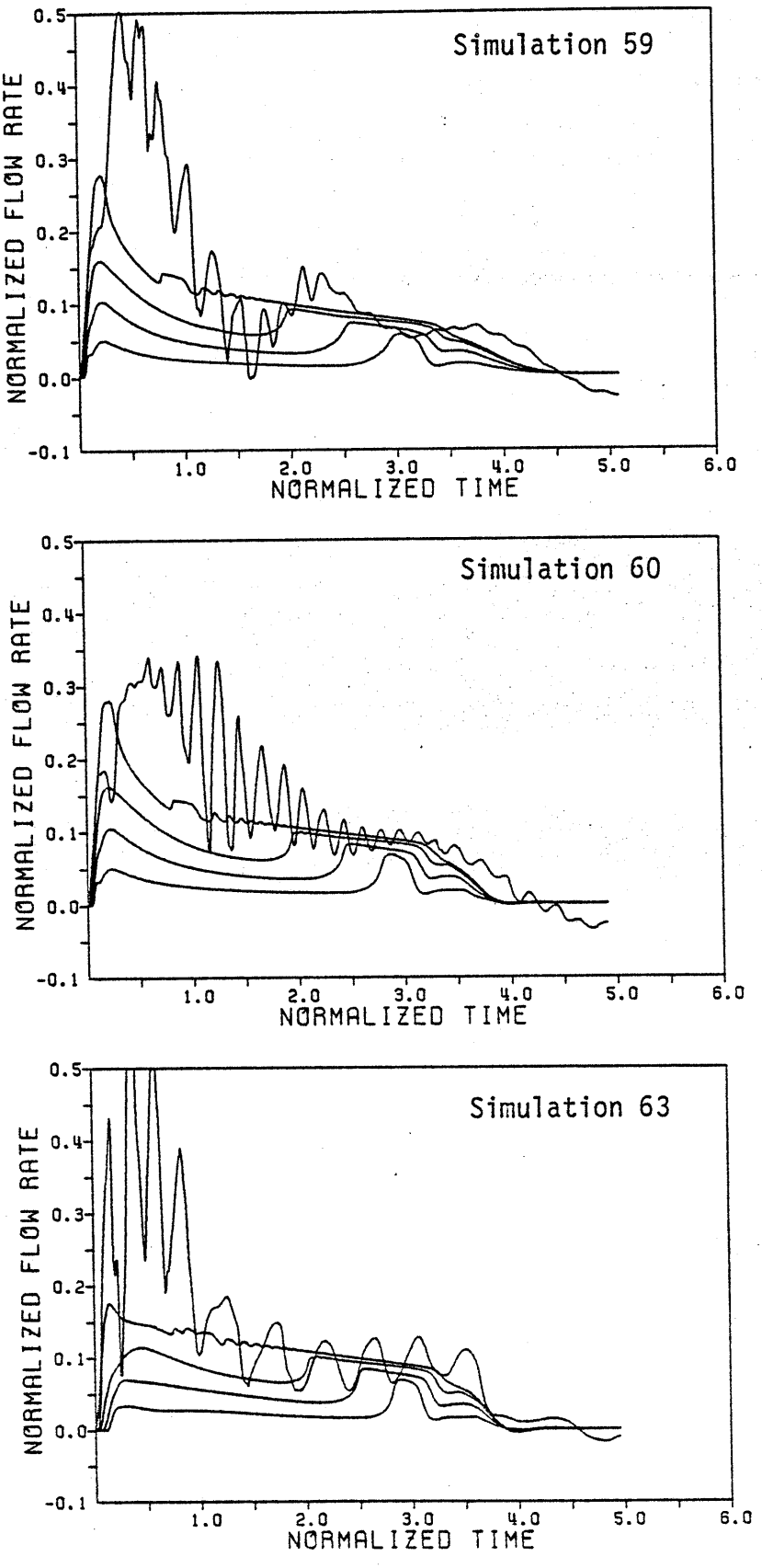
Simulation 59
NORMALIZED FLOW RATE
NORMALIZED TIME
0.5
0.4
0.3
0.2
0.1
0.0
-0.1
1.0
2.0
3.0
4.0
5.0
6.0
Simulation 60
NORMALIZED FLOW RATE
NORMALIZED TIME
Simulation 63
NORMALIZED FLOW RATE
NORMALIZED TIME

FIG. 16

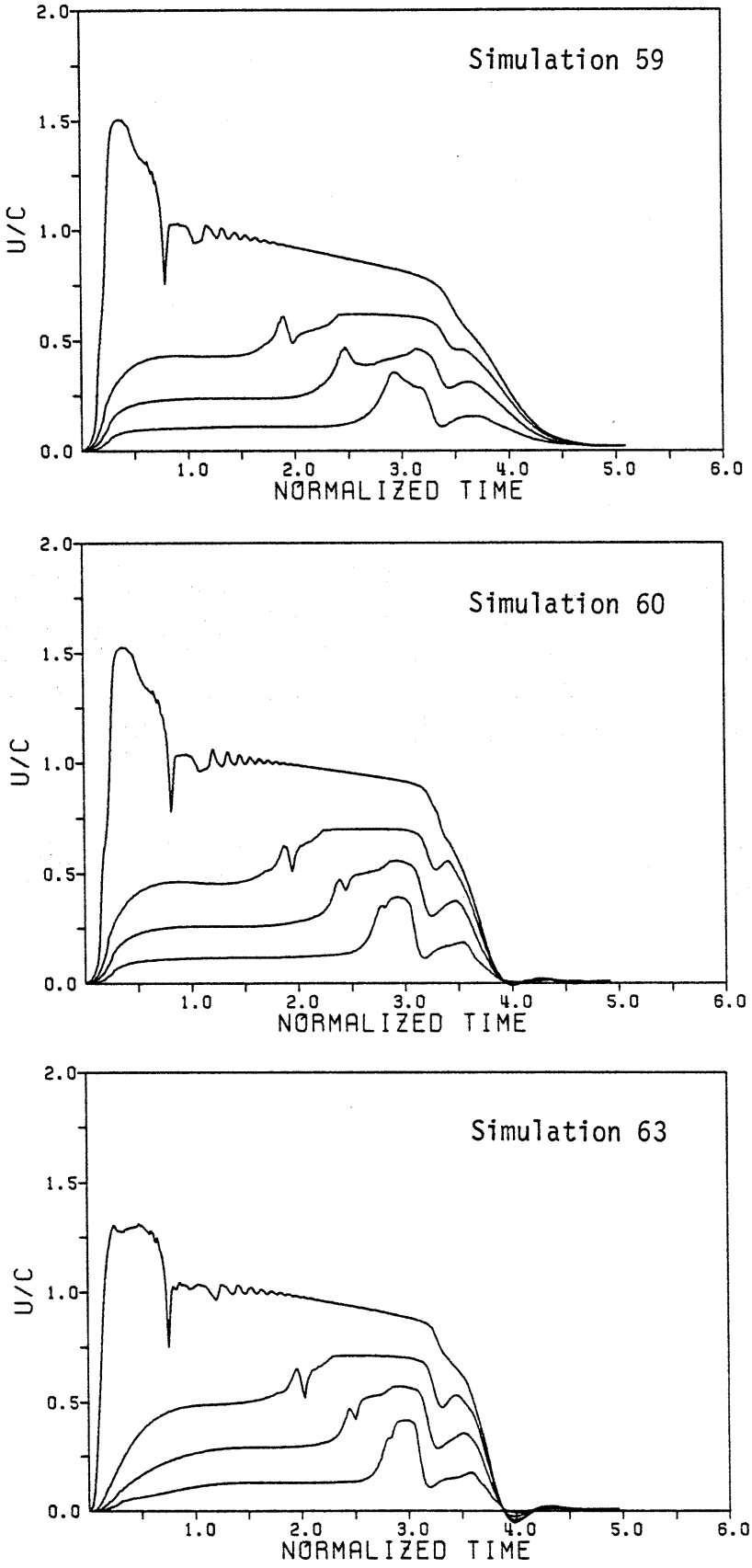
Simulation 59
U/C
NORMALIZED TIME
Simulation 60
U/C
NORMALIZED TIME
Simulation 63
U/C
NORMALIZED TIME

FIG. 17

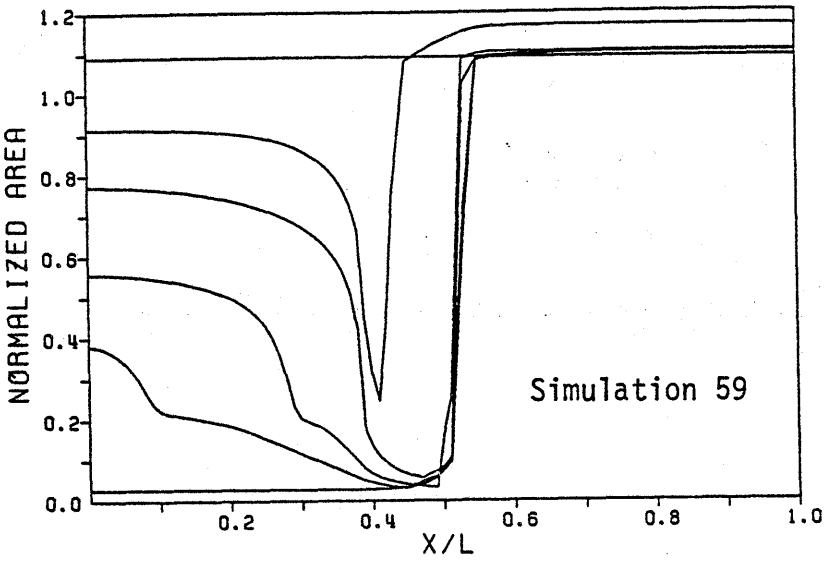
NORMALIZED AREA
1.2
1.0
0.8
0.6
0.4
0.2
0.0
0.2
0.4
0.6
0.8
1.0
X/L
Simulation 59

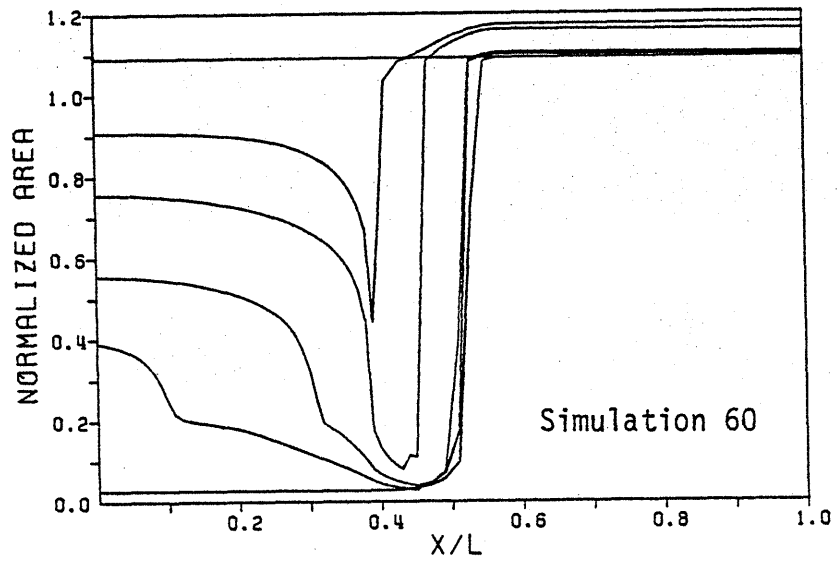
NORMALIZED AREA
1.2
1.0
0.8
0.6
0.4
0.2
0.0
0.2
0.4
0.6
0.8
1.0
X/L
Simulation 60

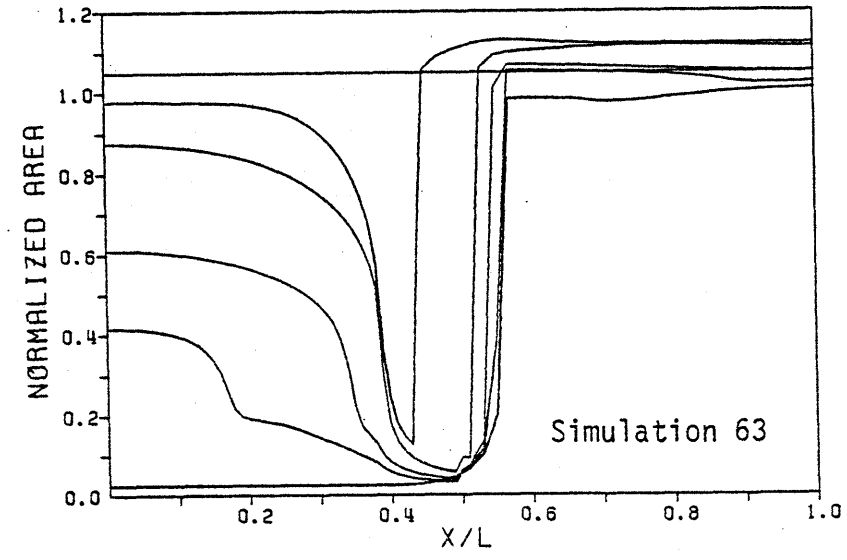
NORMALIZED AREA
1.2
1.0
0.8
0.6
0.4
0.2
0.0
0.2
0.4
0.6
0.8
1.0
X/L
Simulation 63

FIG. 18

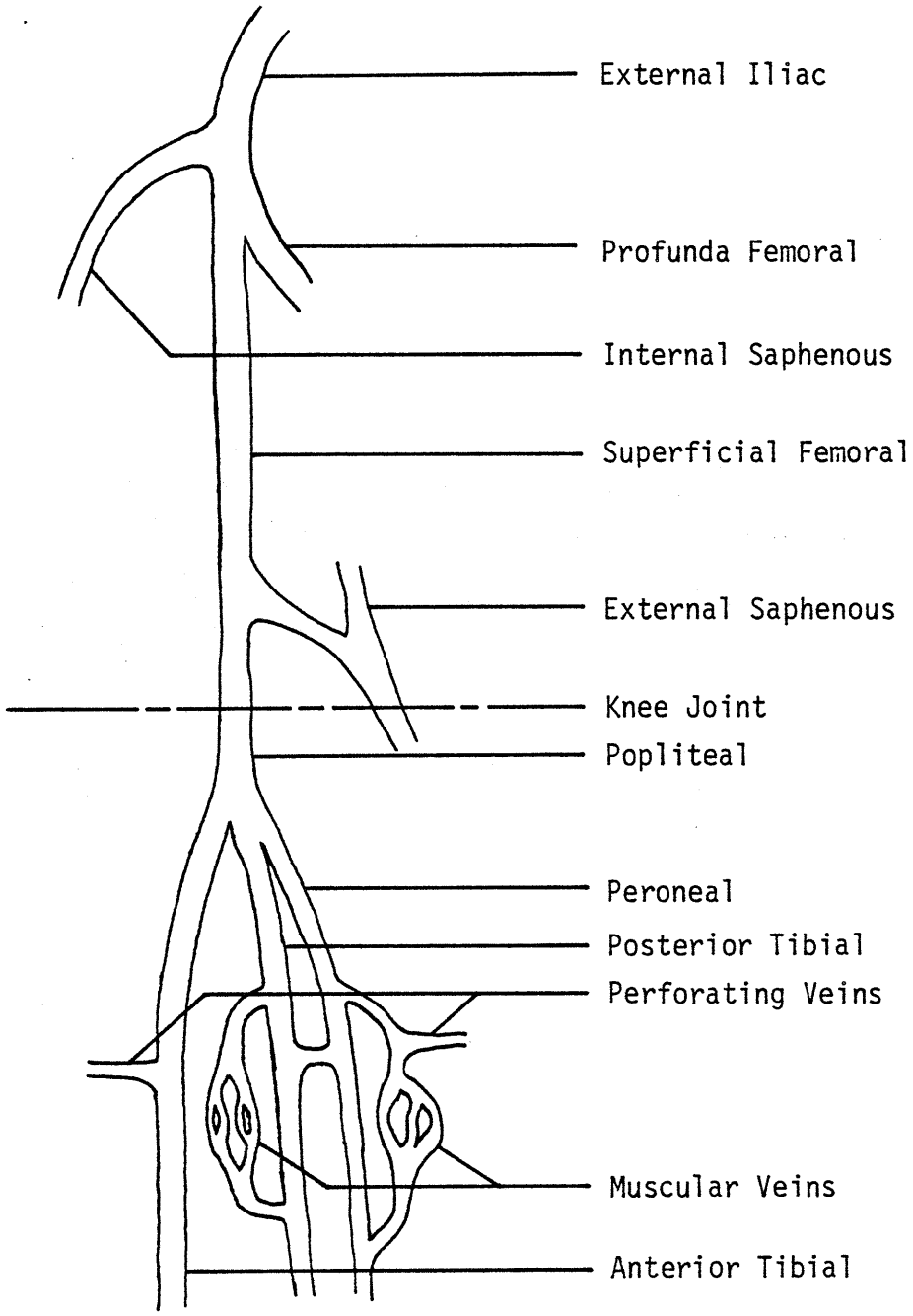
External Iliac
Profunda Femoral
Internal Saphenous
Superficial Femoral
External Saphenous
Knee Joint
Popliteal
Peroneal
Posterior Tibial
Perforating Veins
Muscular Veins
Anterior Tibial

FIG. 19

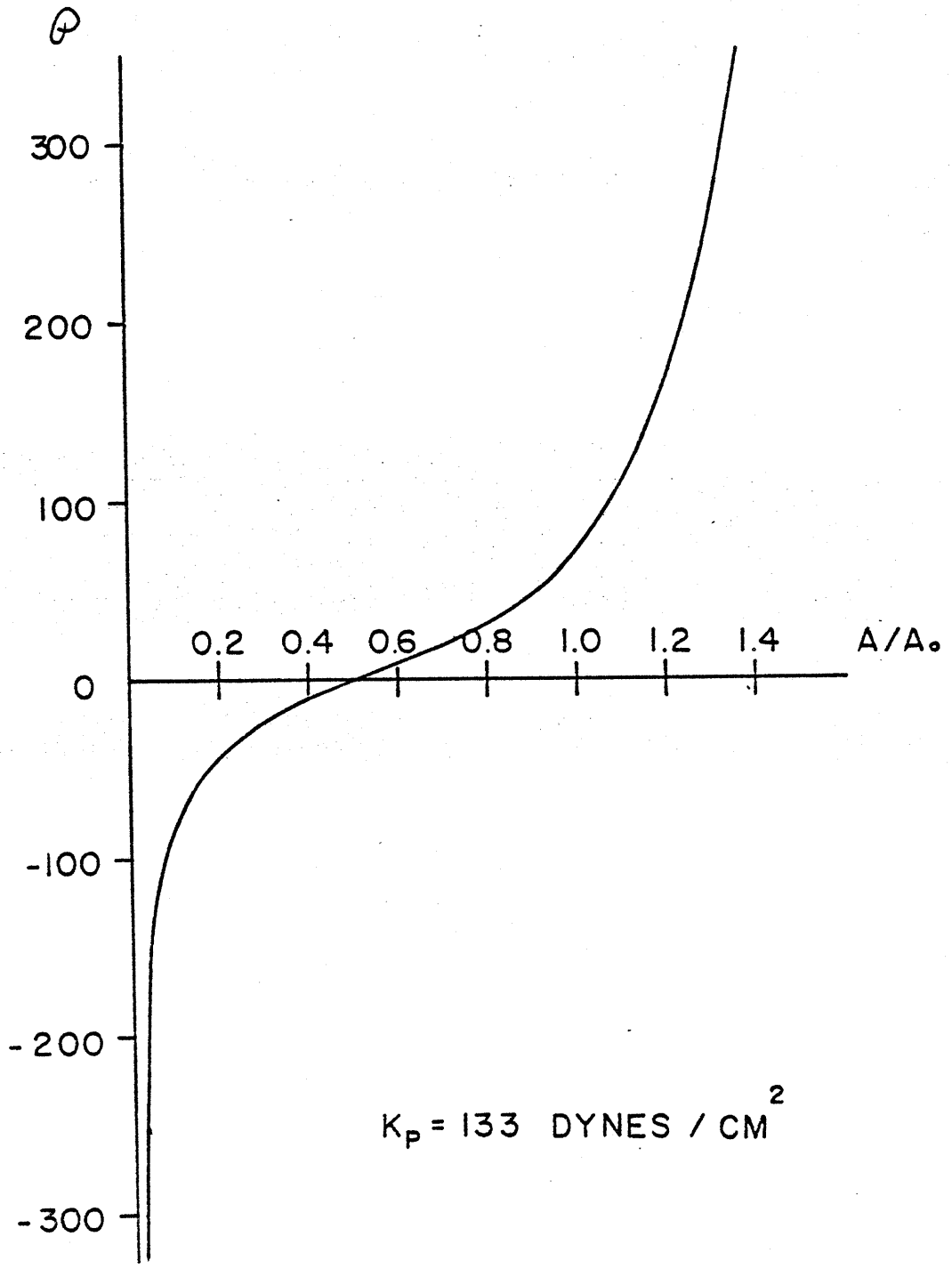
P
300
200
100
0
-100
-200
-300
0.2
0.4
0.6
0.8
1.0
1.2
1.4
A/A₀
K_p = 133 DYNES / CM^2

FIG. 20

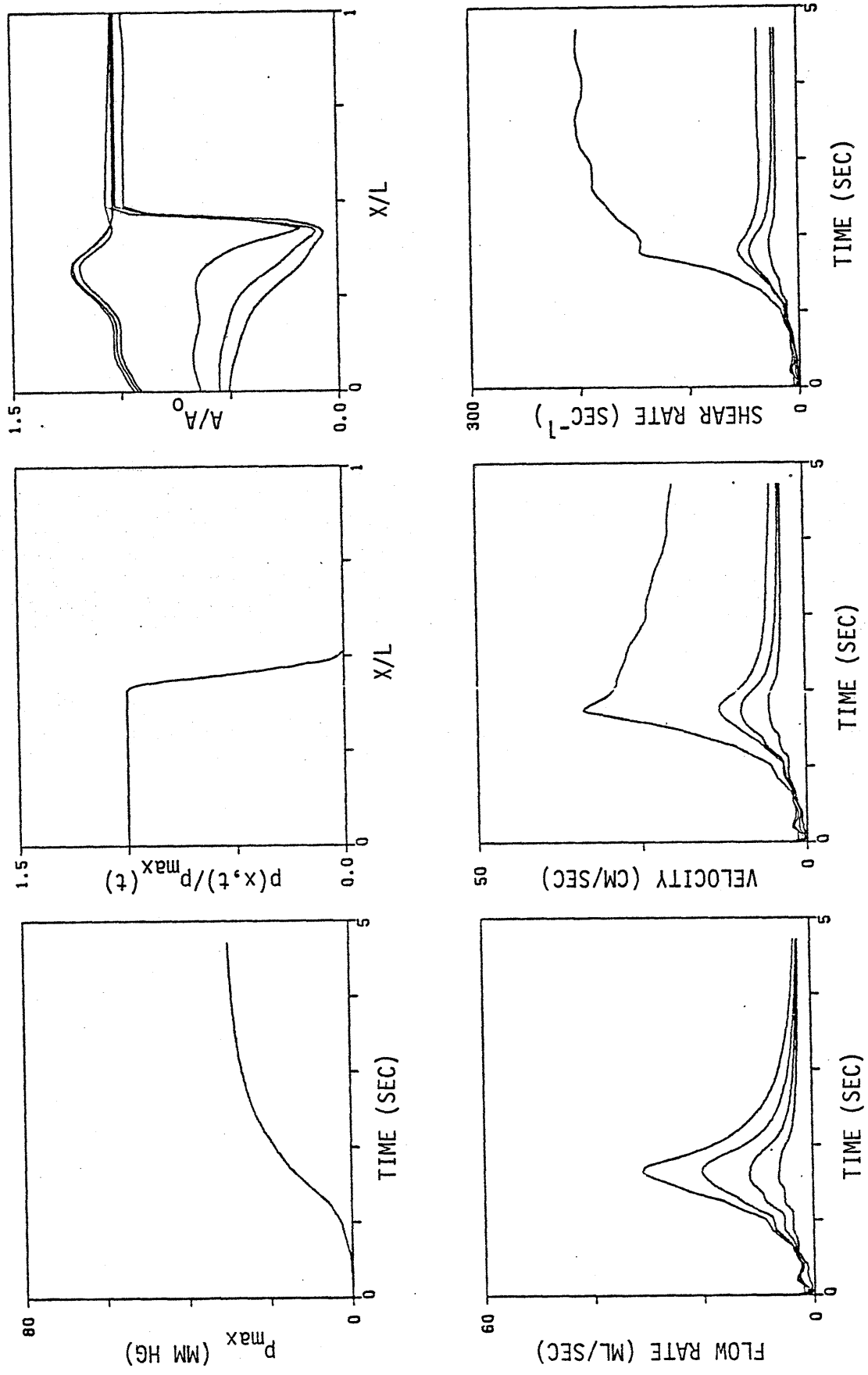
FLOW RATE (ML/SEC)
VELOCITY (CM/SEC)
SHEAR RATE (SEC^{-1})
P_{max} (MM HG)
$p(x,t)/p_{max}(t)$
A/A_o
TIME (SEC)
X/L

FIG. 21

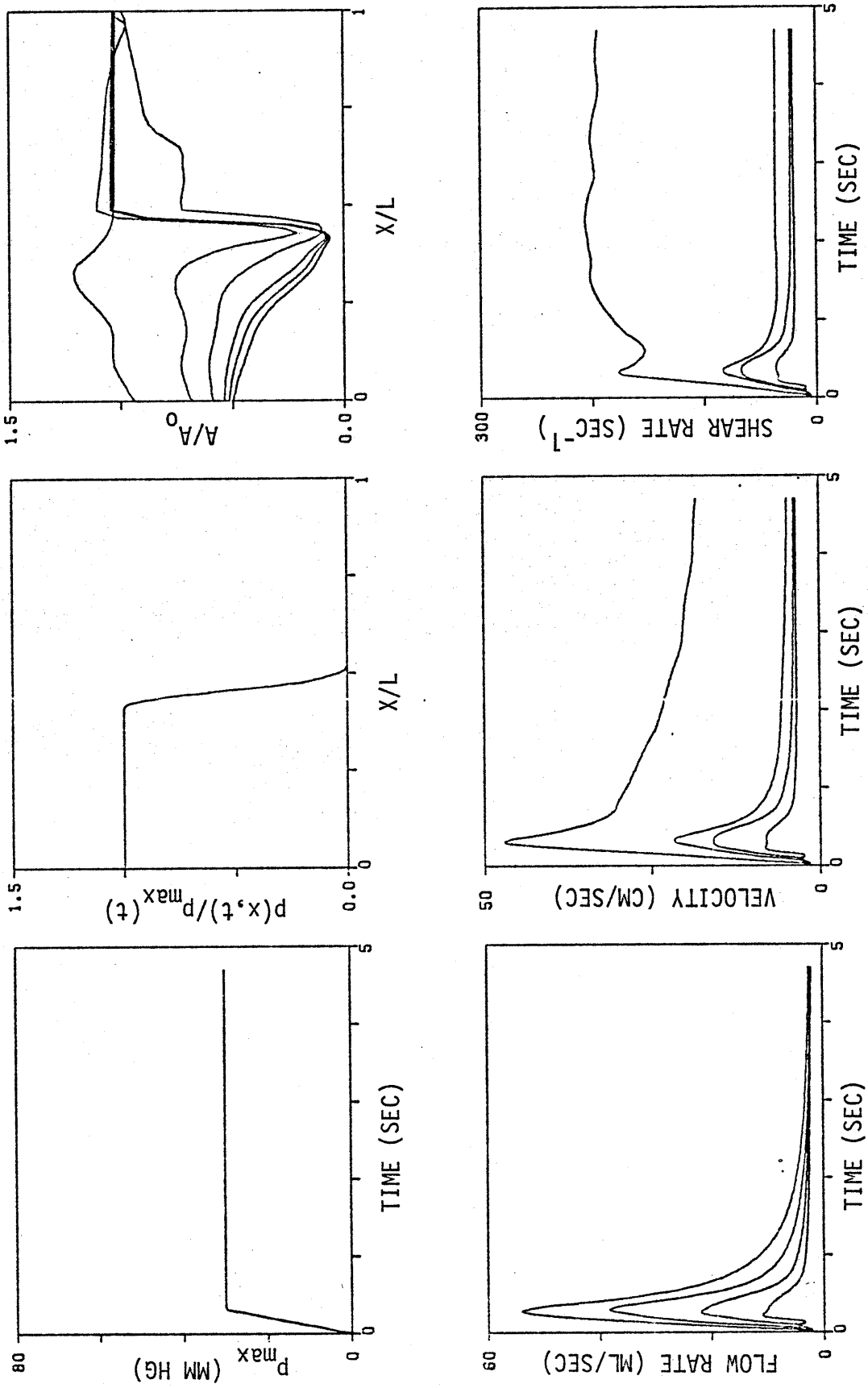
FLOW RATE (ML/SEC)
VELOCITY (CM/SEC)
SHEAR RATE (SEC^{-1})
P_{max} (MM HG)
$p(x,t)/p_{max}(t)$
A/A_o
TIME (SEC)
X/L

FIG. 22

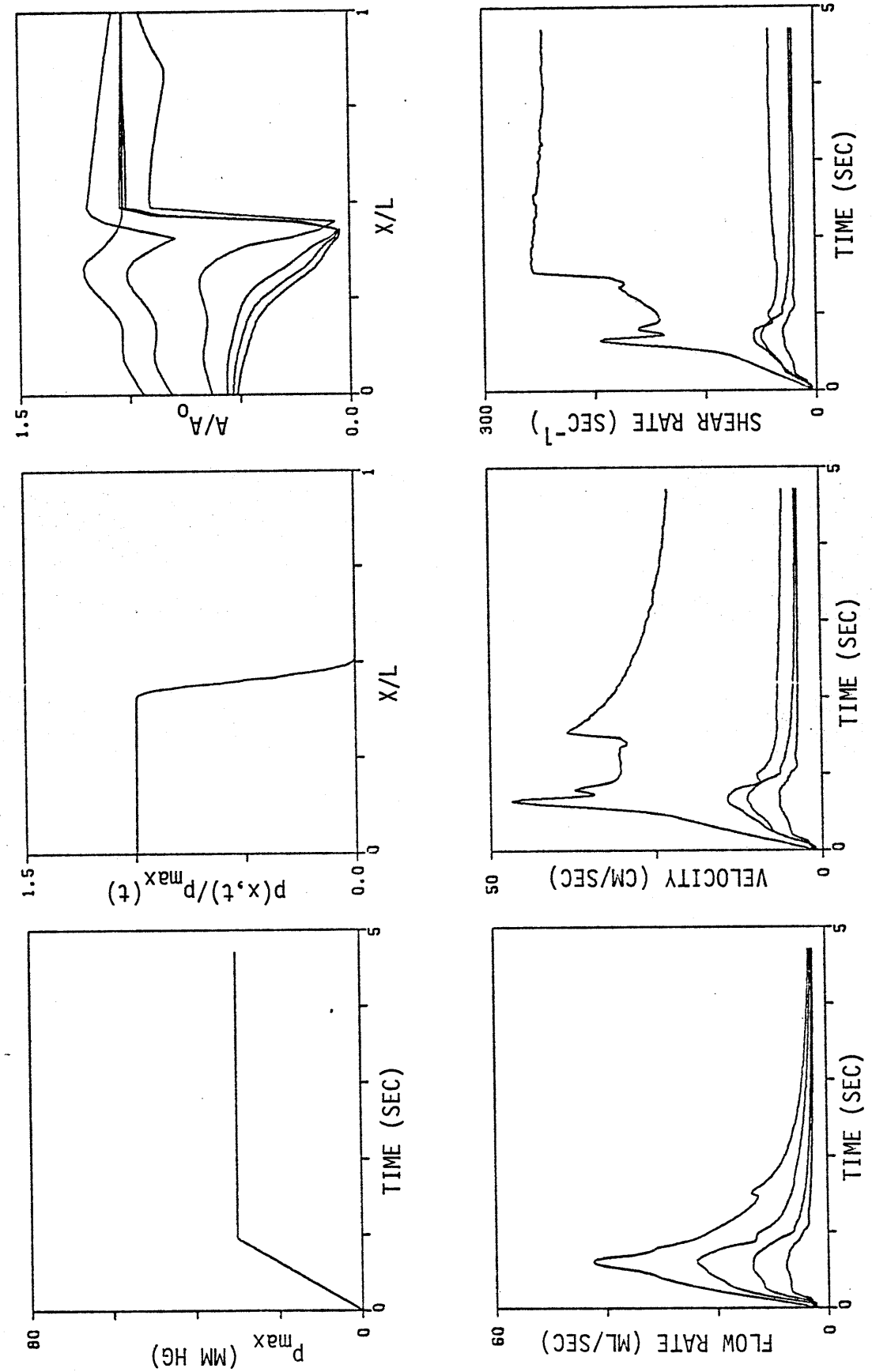
FLOW RATE (ML/SEC)
VELOCITY (CM/SEC)
SHEAR RATE (SEC^{-1})
P_{max} (MM HG)
$p(x,t)/p_{max}(t)$
A/A_o
TIME (SEC)
X/L

FIG. 23

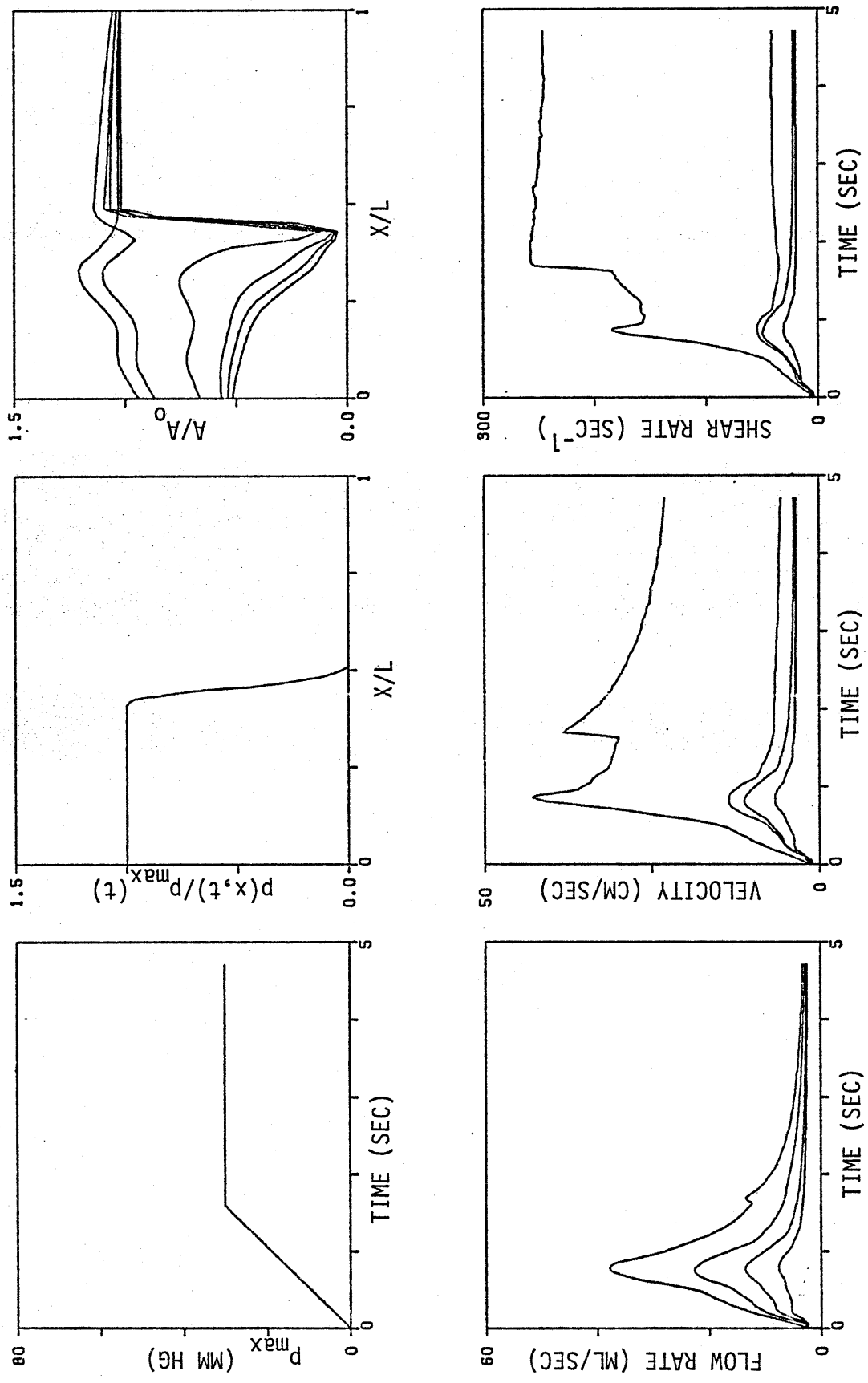
FLOW RATE (ML/SEC)
TIME (SEC)
VELOCITY (CM/SEC)
TIME (SEC)
SHEAR RATE (SEC^{-1})
TIME (SEC)
p_{max} (MM HG)
TIME (SEC)
$p(x,t)/p_{max}(t)$
X/L
A/A_o
X/L

FIG. 24

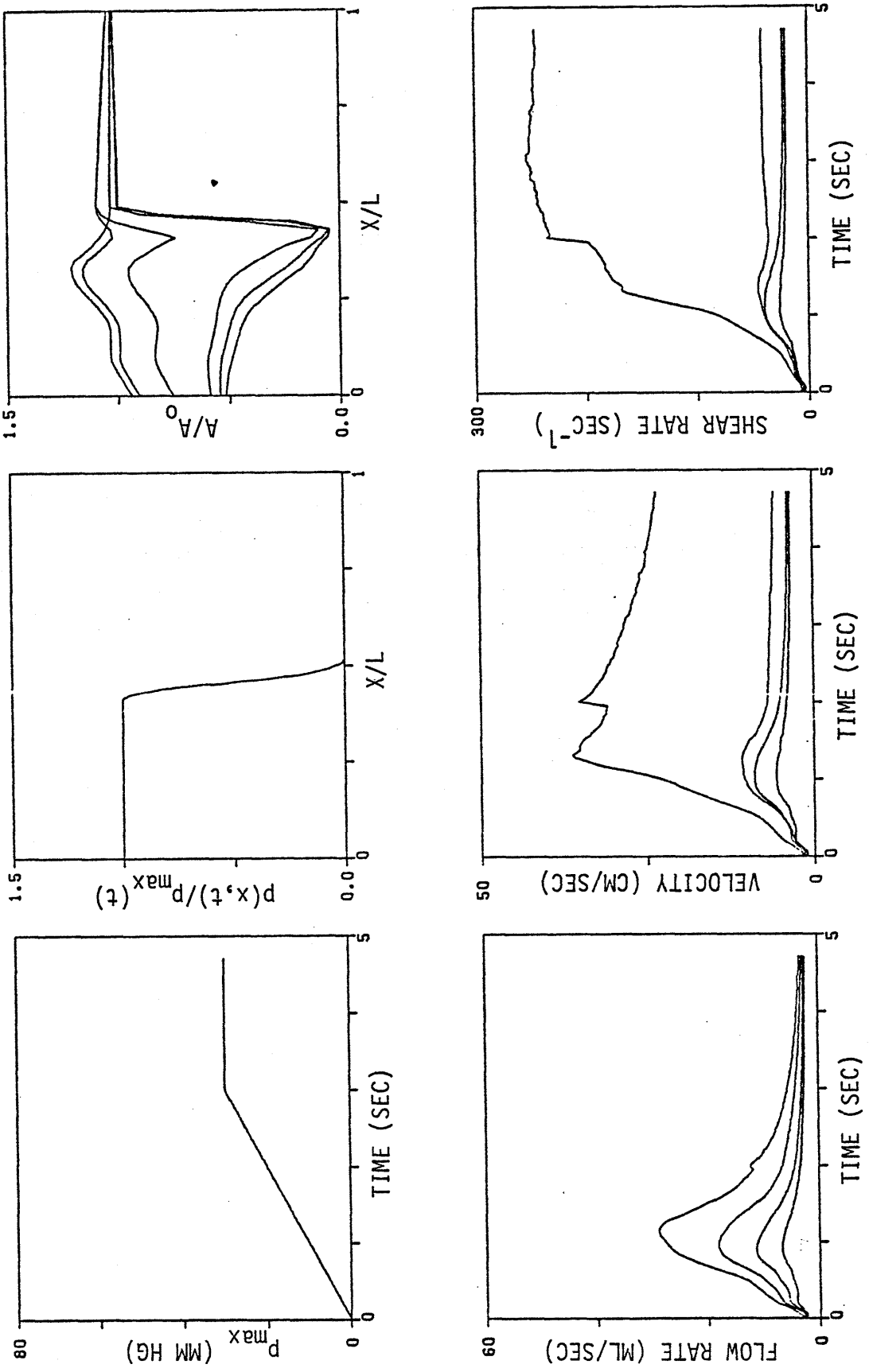
A/A$_o$
X/L
SHEAR RATE (SEC^{-1})
TIME (SEC)
p(x,t)/p$_{max}$(t)
X/L
VELOCITY (CM/SEC)
TIME (SEC)
p$_{max}$ (MM HG)
TIME (SEC)
FLOW RATE (ML/SEC)
TIME (SEC)

FIG. 25

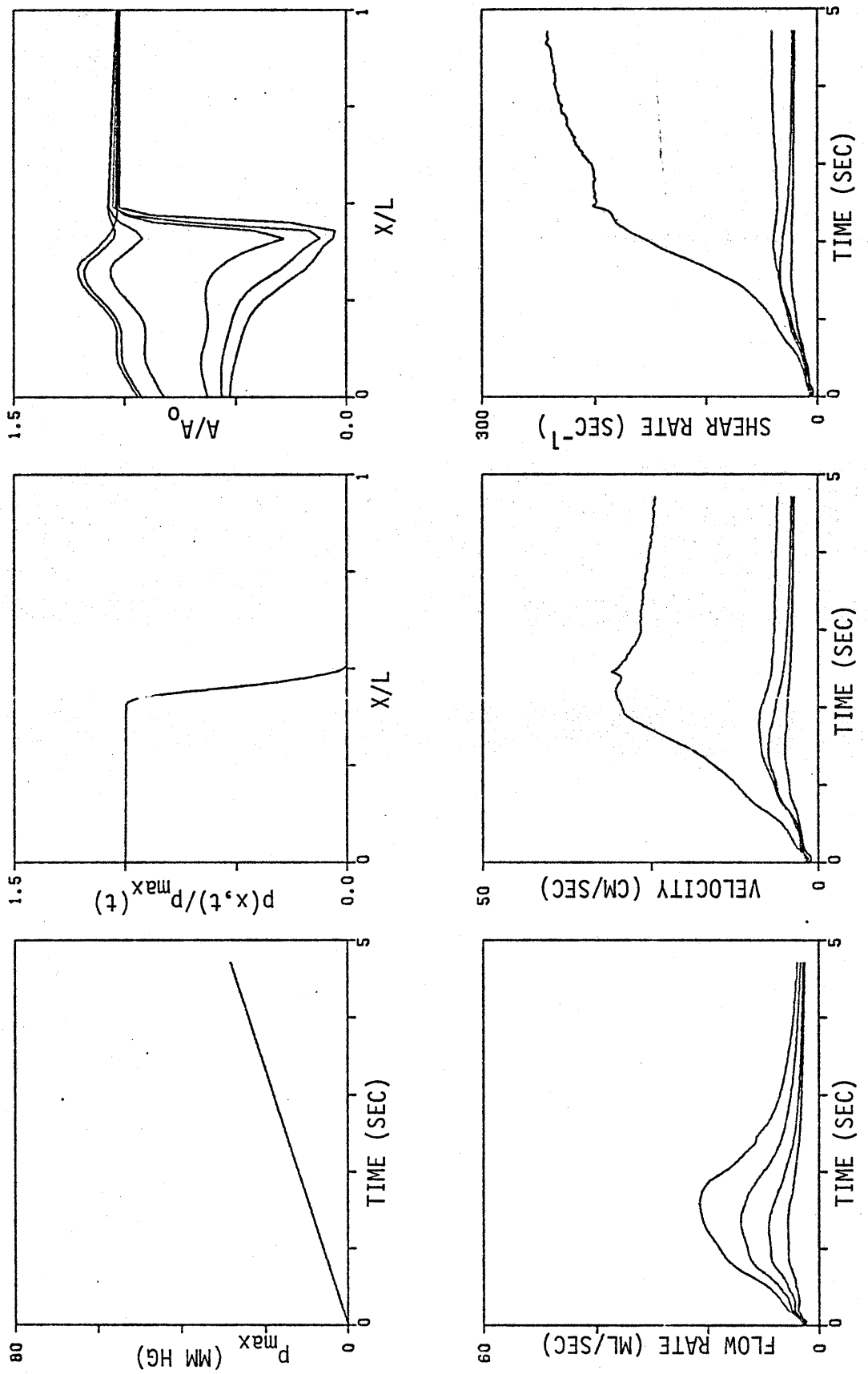
FLOW RATE (ML/SEC)
VELOCITY (CM/SEC)
SHEAR RATE (SEC^{-1})
P_{max} (MM HG)
$p(x,t)/p_{max}(t)$
A/A_o
TIME (SEC)
X/L

FIG. 26

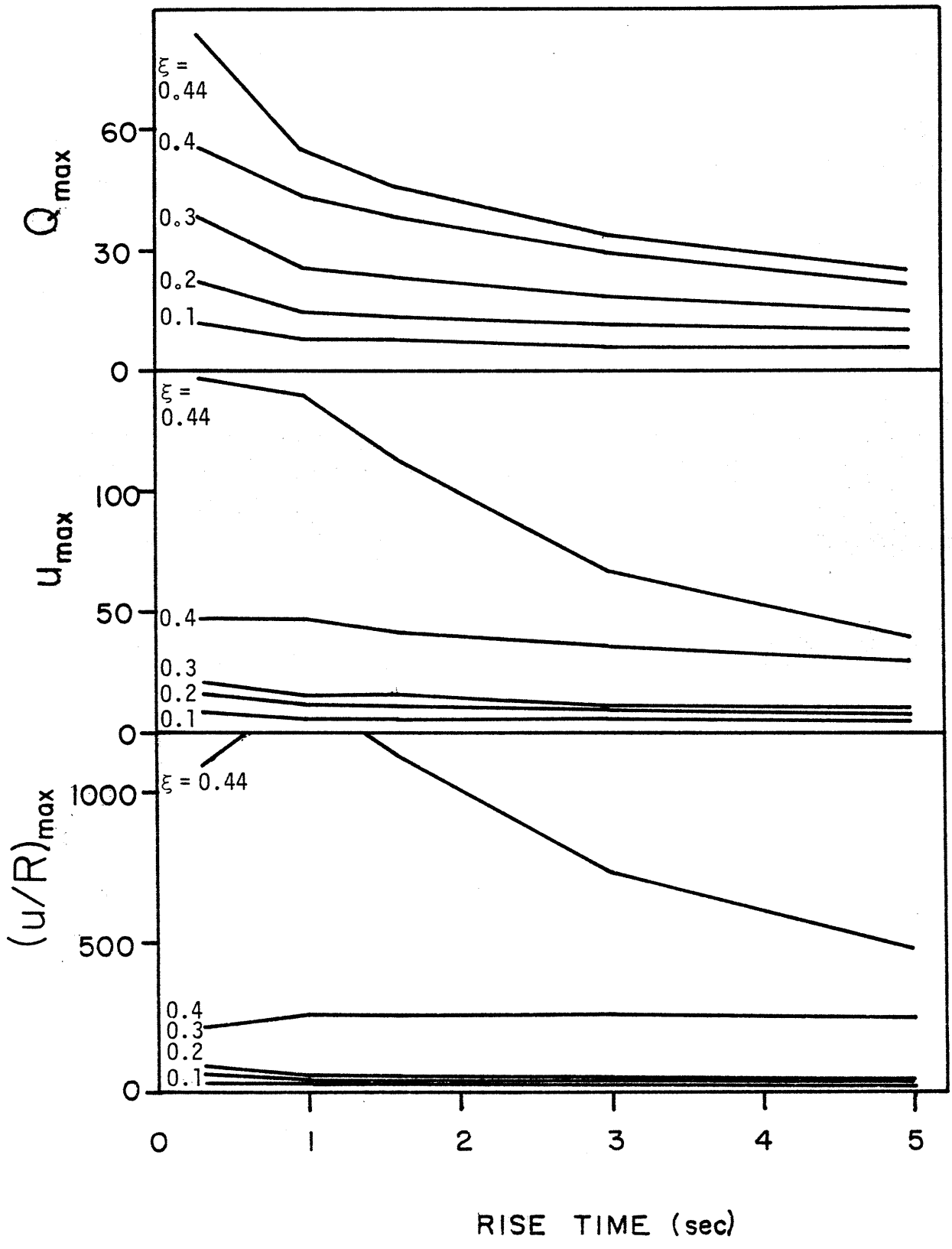
Q_{max}
60
30
0
ξ = 0.44
0.4
0.3
0.2
0.1
U_{max}
100
50
0
ξ = 0.44
0.4
0.3
0.2
0.1
$(U/R)_{max}$
1000
500
0
ξ = 0.44
0.4
0.3
0.2
0.1
0
1
2
3
4
5
RISE TIME (sec)

FIG. 27

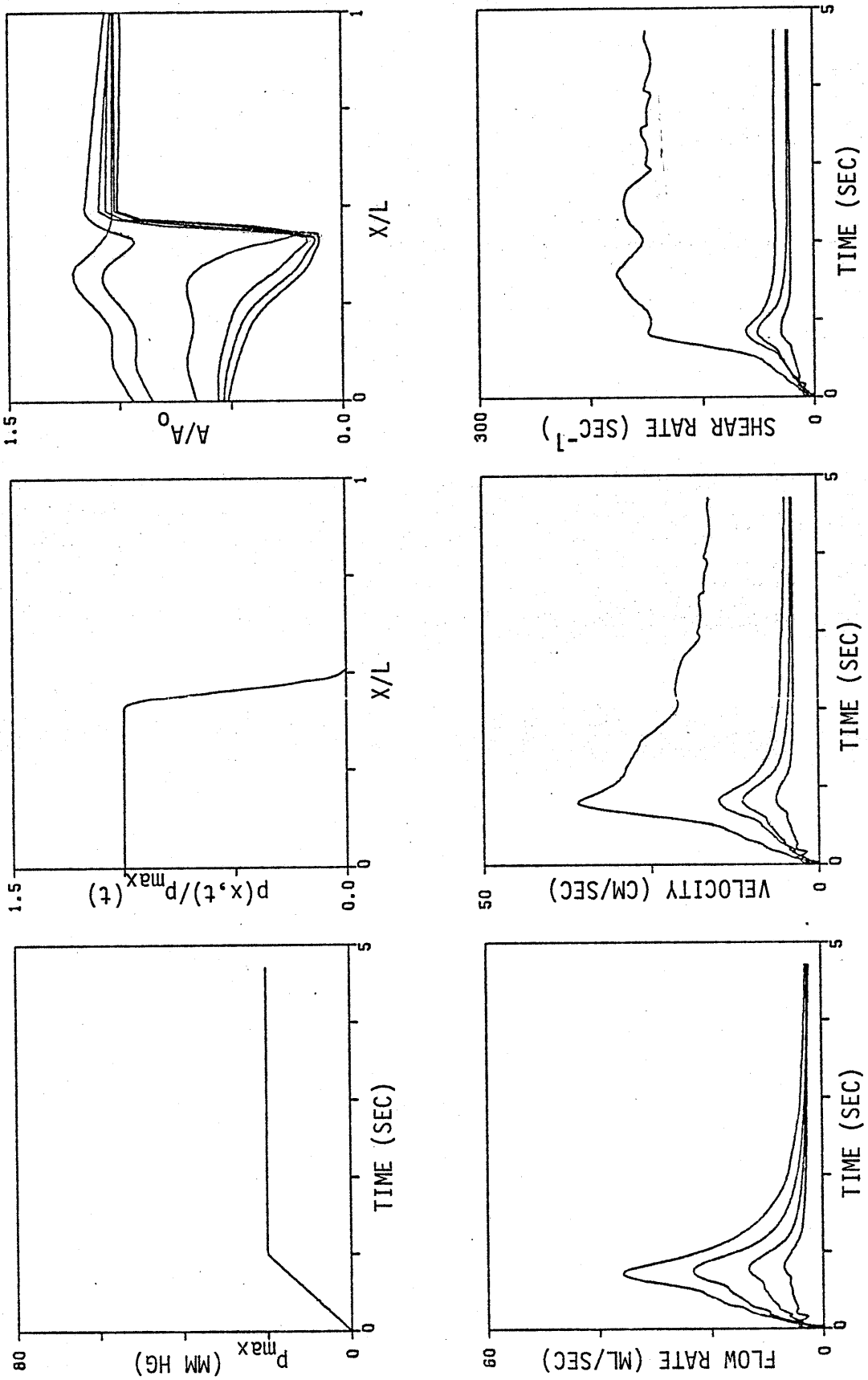
FLOW RATE (ML/SEC)
VELOCITY (CM/SEC)
SHEAR RATE (SEC^{-1})
p_{max} (MM HG)
$p(x,t)/p_{max}(t)$
A/A_o
TIME (SEC)
X/L

FIG. 28

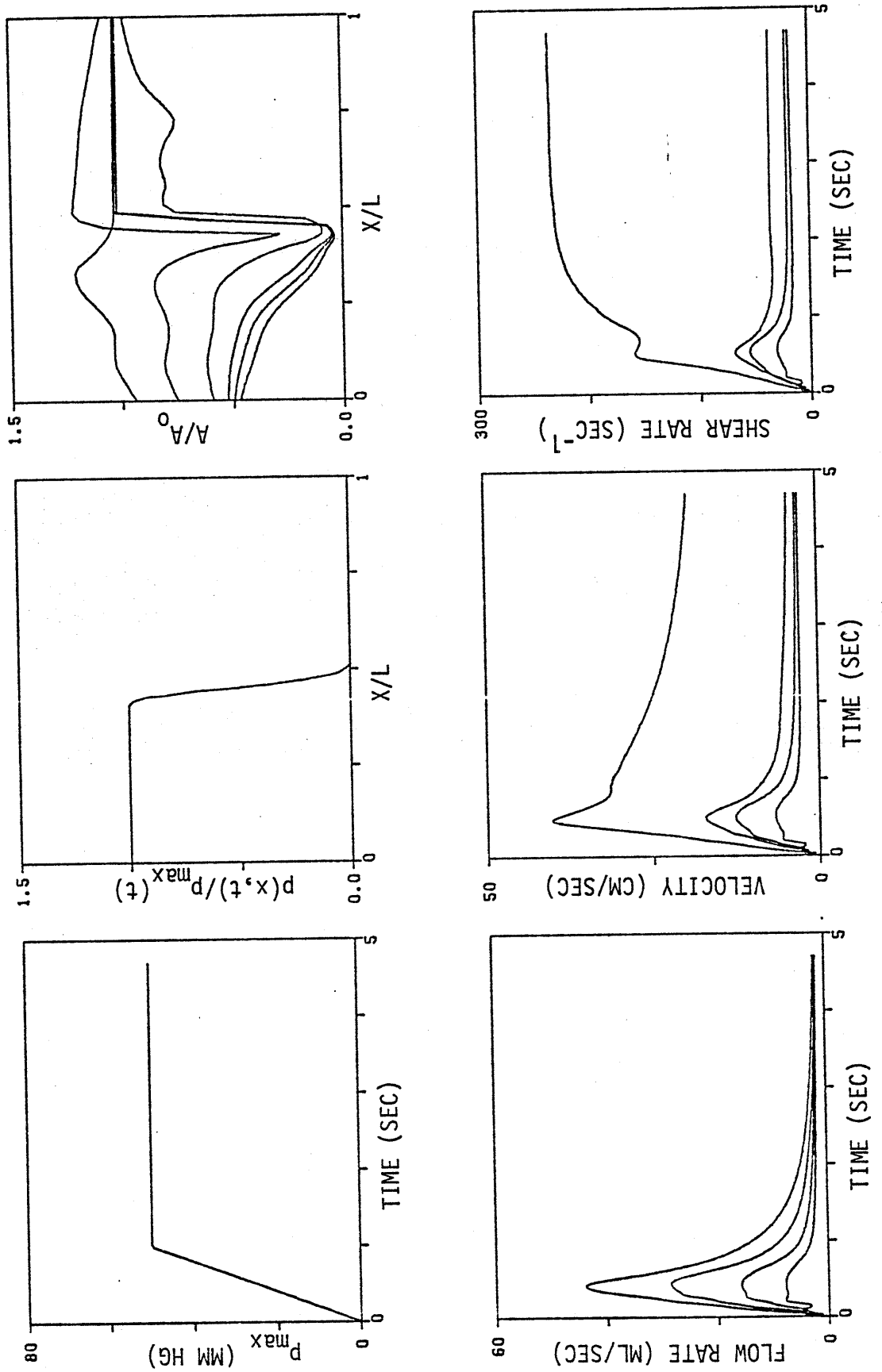
A/A$_o$
X/L
SHEAR RATE (SEC^{-1})
TIME (SEC)
p(x,t)/p$_{max}$(t)
X/L
VELOCITY (CM/SEC)
TIME (SEC)
p$_{max}$ (MM HG)
TIME (SEC)
FLOW RATE (ML/SEC)
TIME (SEC)

FIG. 29

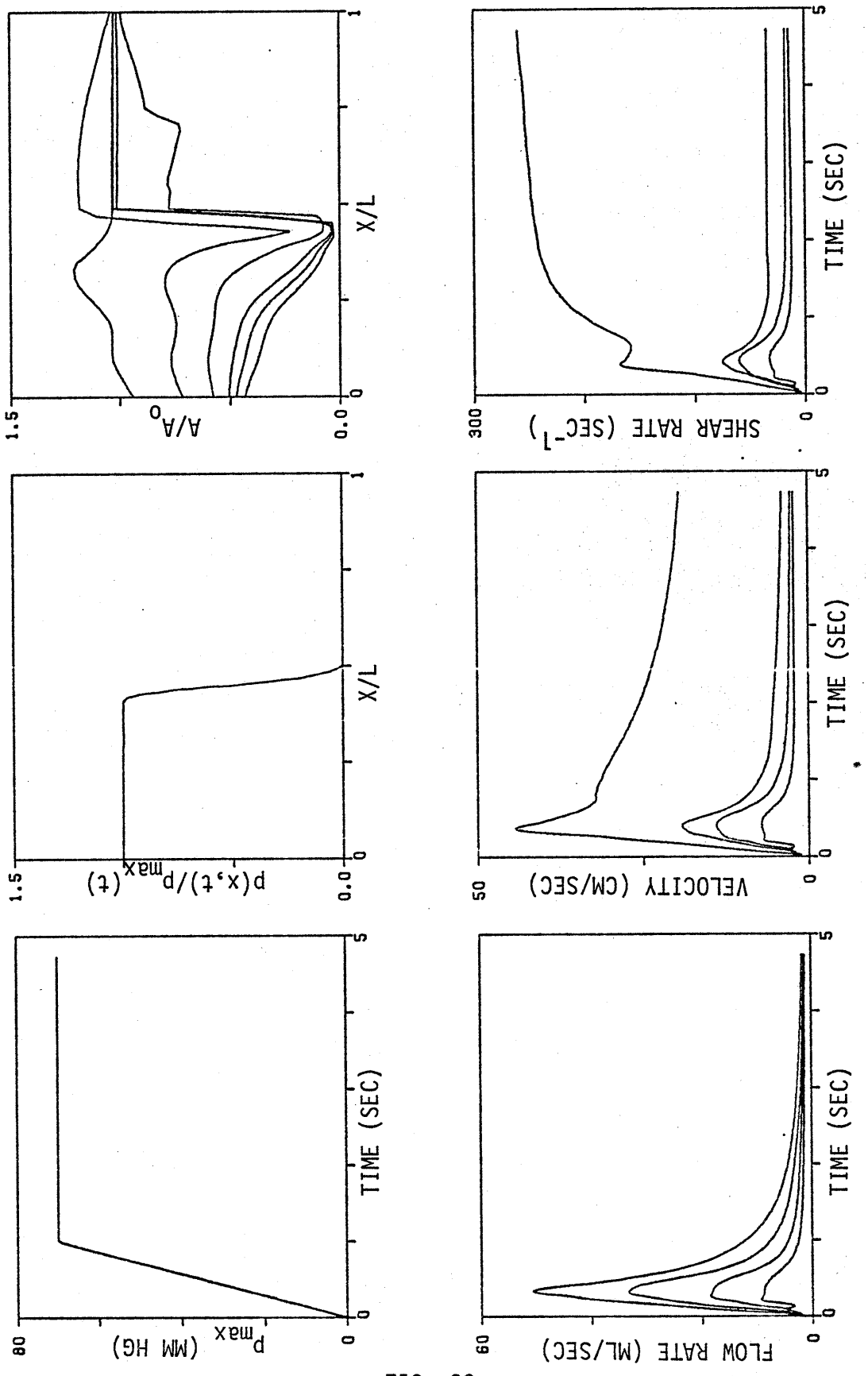
FLOW RATE (ML/SEC)
60
0
5
TIME (SEC)
VELOCITY (CM/SEC)
50
0
5
TIME (SEC)
SHEAR RATE (SEC^{-1})
300
0
5
TIME (SEC)
P_{max} (MM HG)
80
0
5
TIME (SEC)
$p(x,t)/p_{max}(t)$
1.5
0.0
1
0
X/L
A/A_o
1.5
0.0
1
0
X/L

FIG. 30

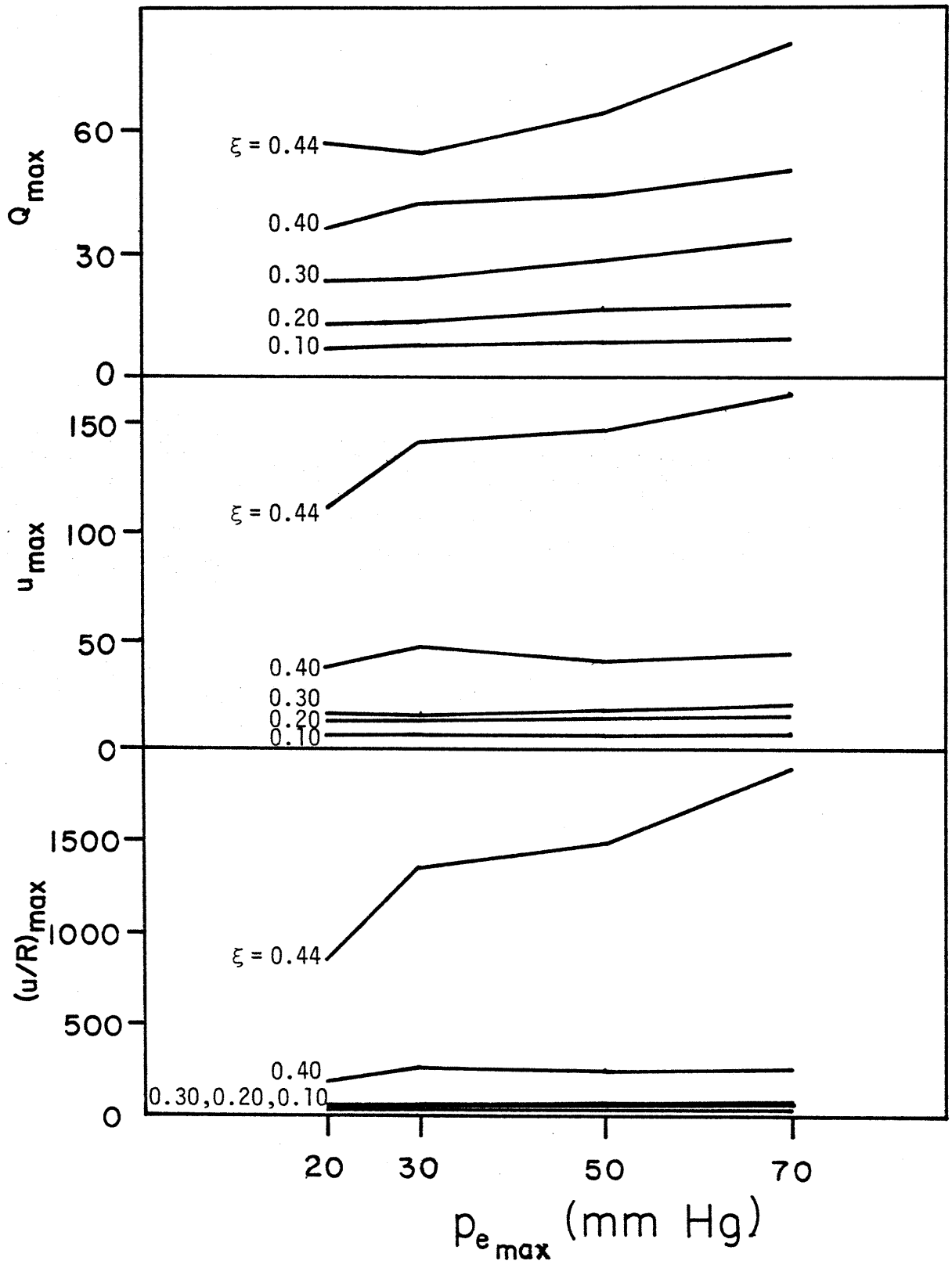
Q_{max}
60
30
0
ξ = 0.44
0.40
0.30
0.20
0.10
u_{max}
150
100
50
0
ξ = 0.44
0.40
0.30
0.20
0.10
$(u/R)_{max}$
1500
1000
500
0
ξ = 0.44
0.40
0.30,0.20,0.10
20
30
50
70
$p_{e\,max}$ (mm Hg)

FIG. 31

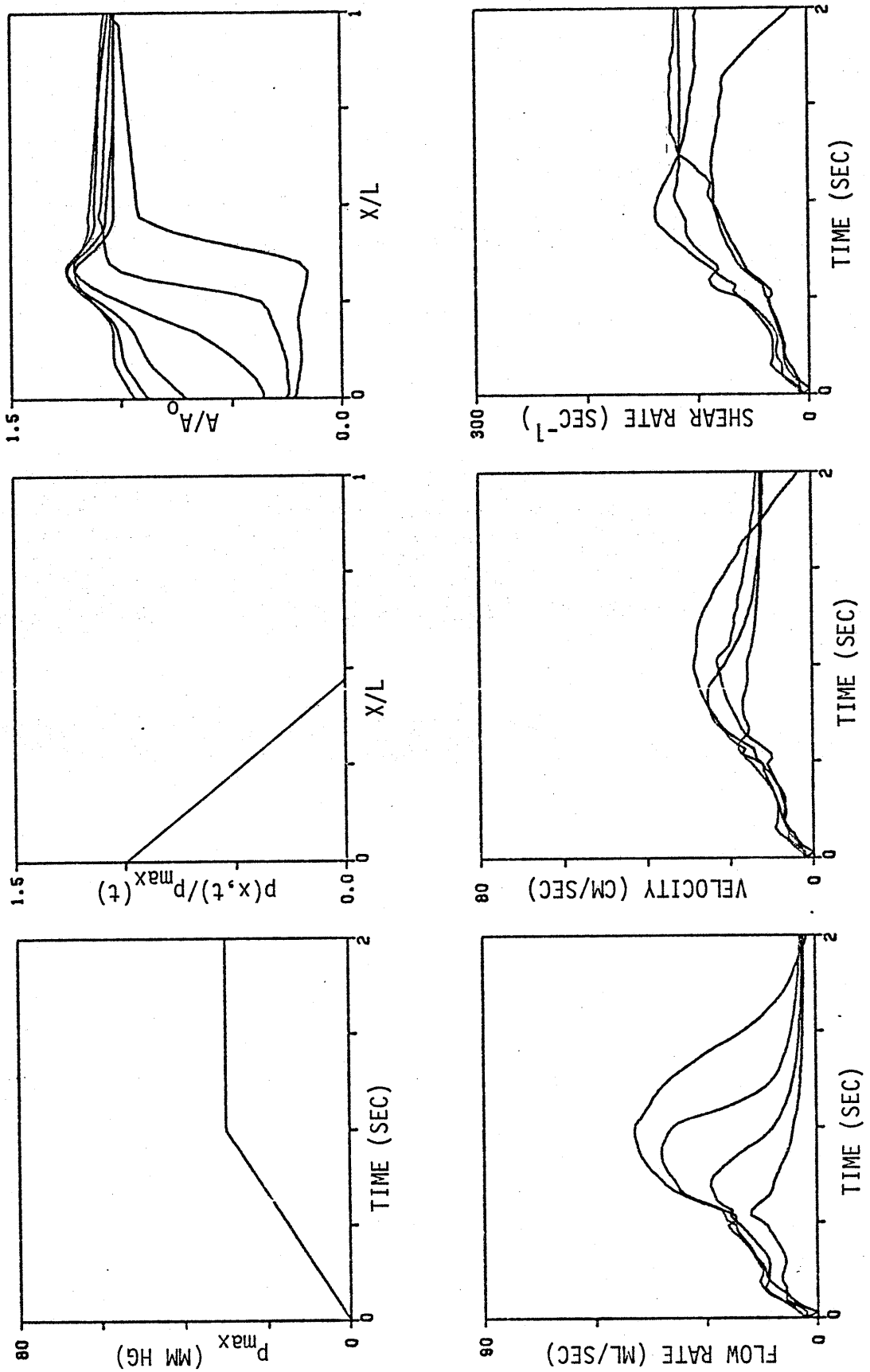
FLOW RATE (ML/SEC)
VELOCITY (CM/SEC)
SHEAR RATE (SEC^{-1})
p_{max} (MM HG)
$p(x,t)/p_{max}(t)$
A/A_o
TIME (SEC)
X/L

FIG. 32

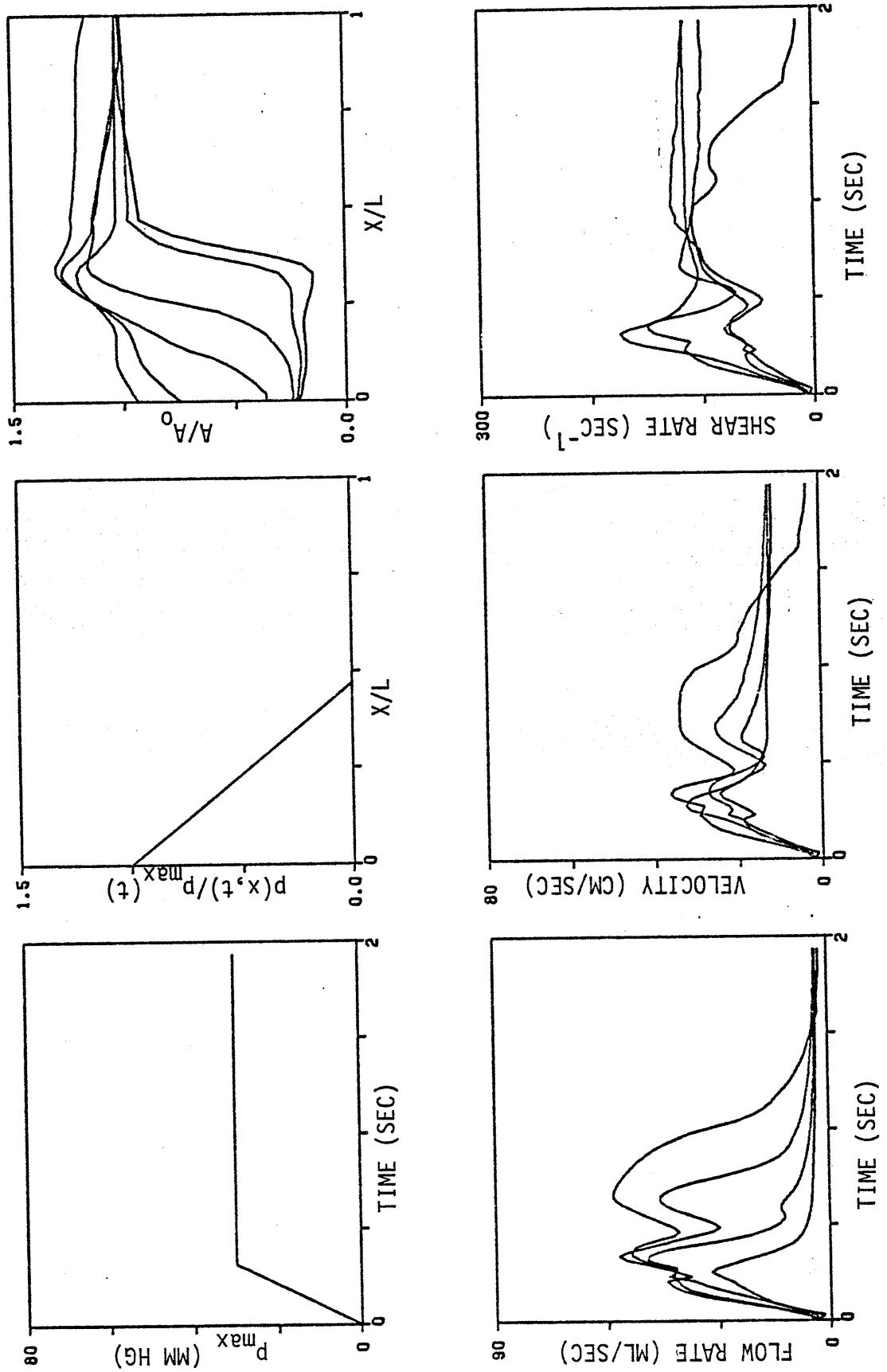
A/A$_o$
X/L
SHEAR RATE (SEC^{-1})
TIME (SEC)
p(x,t)/p$_{max}$(t)
X/L
VELOCITY (CM/SEC)
TIME (SEC)
p$_{max}$ (MM HG)
TIME (SEC)
FLOW RATE (ML/SEC)
TIME (SEC)

FIG. 33

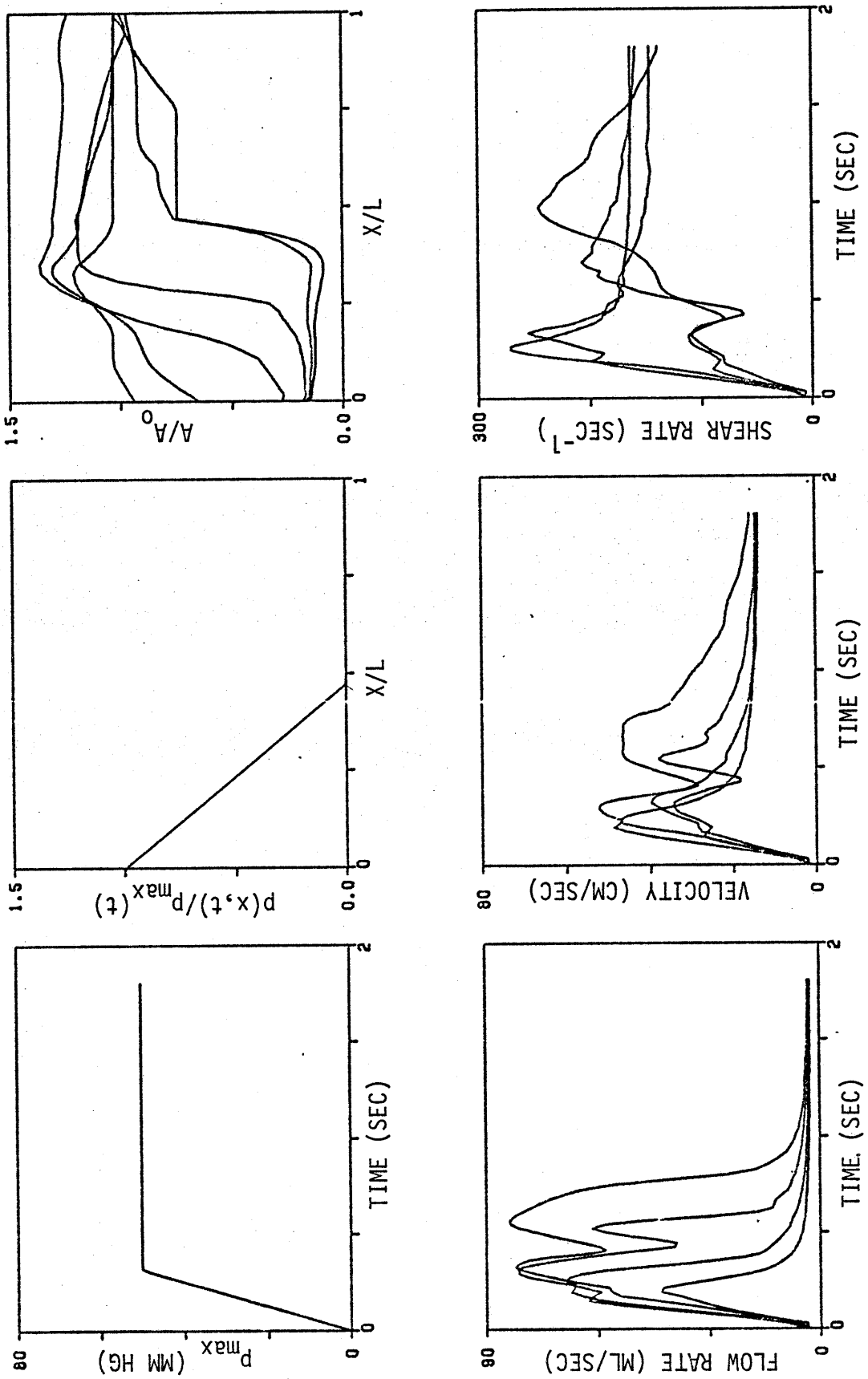
A/A$_o$
X/L
SHEAR RATE (SEC^{-1})
TIME (SEC)
p(x,t)/p$_{max}$(t)
X/L
VELOCITY (CM/SEC)
TIME (SEC)
p$_{max}$ (MM HG)
TIME (SEC)
FLOW RATE (ML/SEC)
TIME (SEC)

FIG. 34

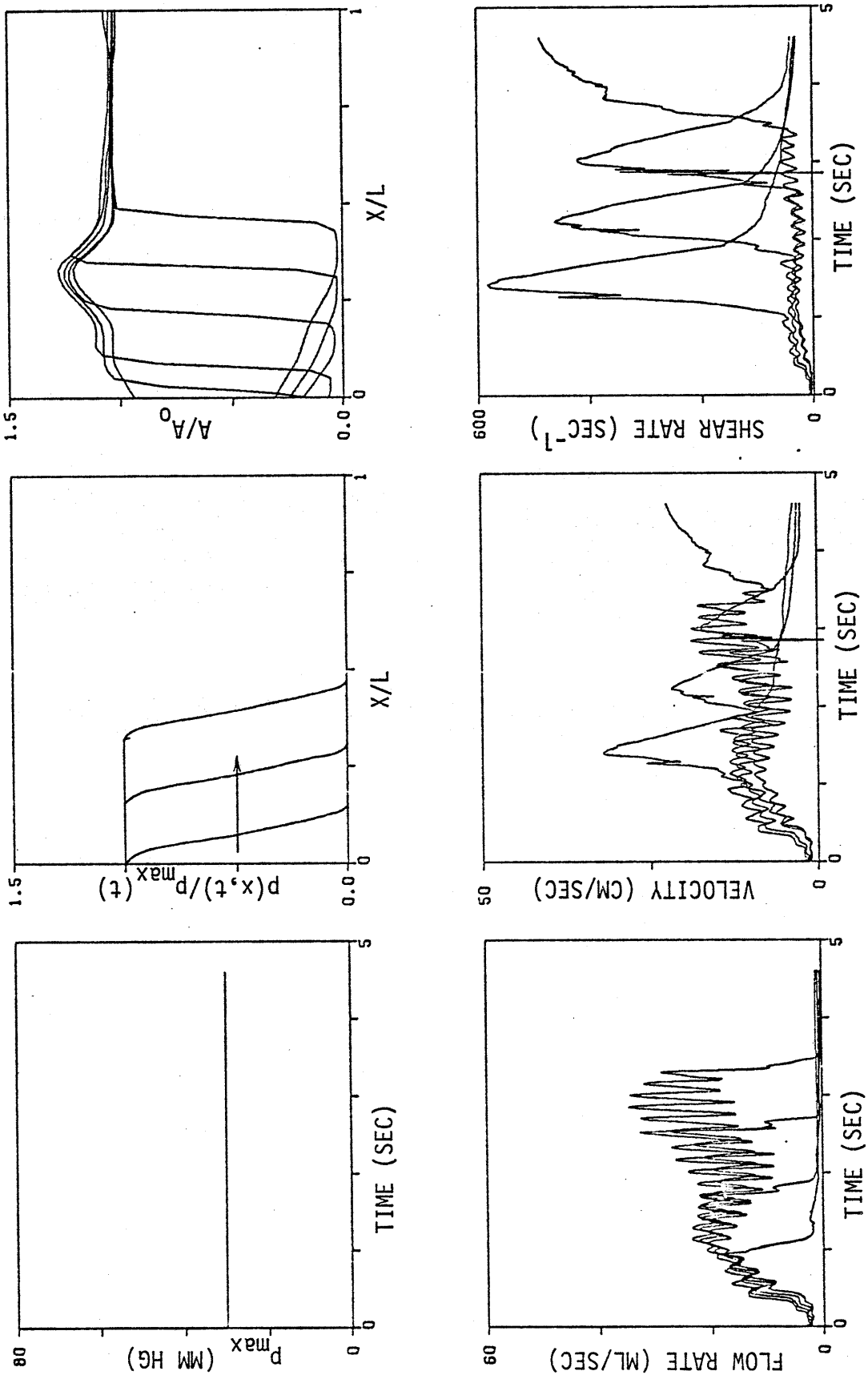
FLOW RATE (ML/SEC)
60
0
5
TIME (SEC)
VELOCITY (CM/SEC)
50
0
5
TIME (SEC)
SHEAR RATE (SEC^{-1})
600
0
5
TIME (SEC)
p_{max} (MM HG)
80
0
5
TIME (SEC)
$p(x,t)/p_{max}(t)$
1.5
0.0
0
X/L
1
A/A_o
1.5
0.0
0
X/L
1

FIG. 35

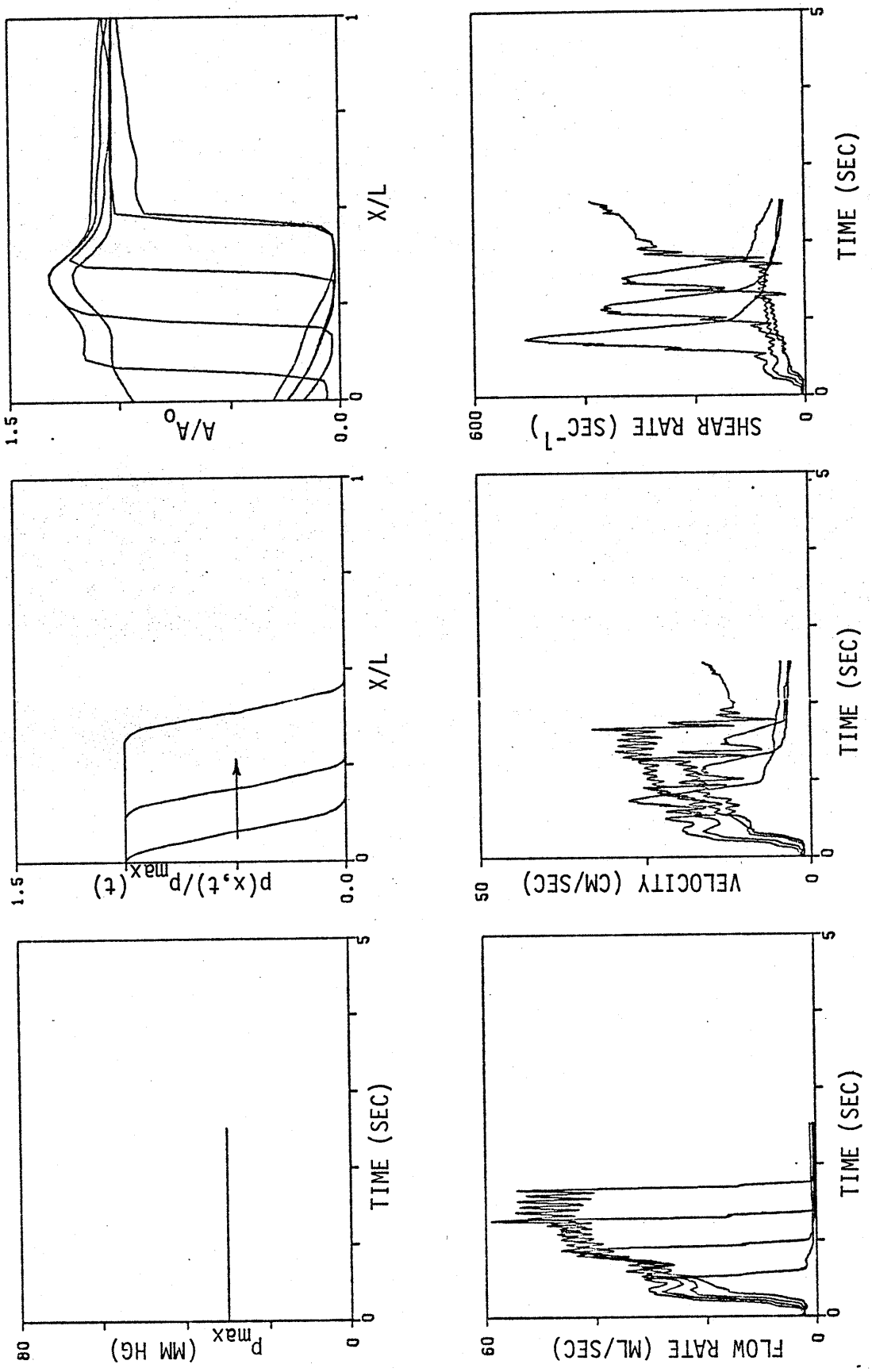
A/A$_o$
X/L
SHEAR RATE (SEC^{-1})
TIME (SEC)
p(x,t)/p$_{max}$(t)
X/L
VELOCITY (CM/SEC)
TIME (SEC)
p$_{max}$ (MM HG)
TIME (SEC)
FLOW RATE (ML/SEC)
TIME (SEC)

FIG. 36

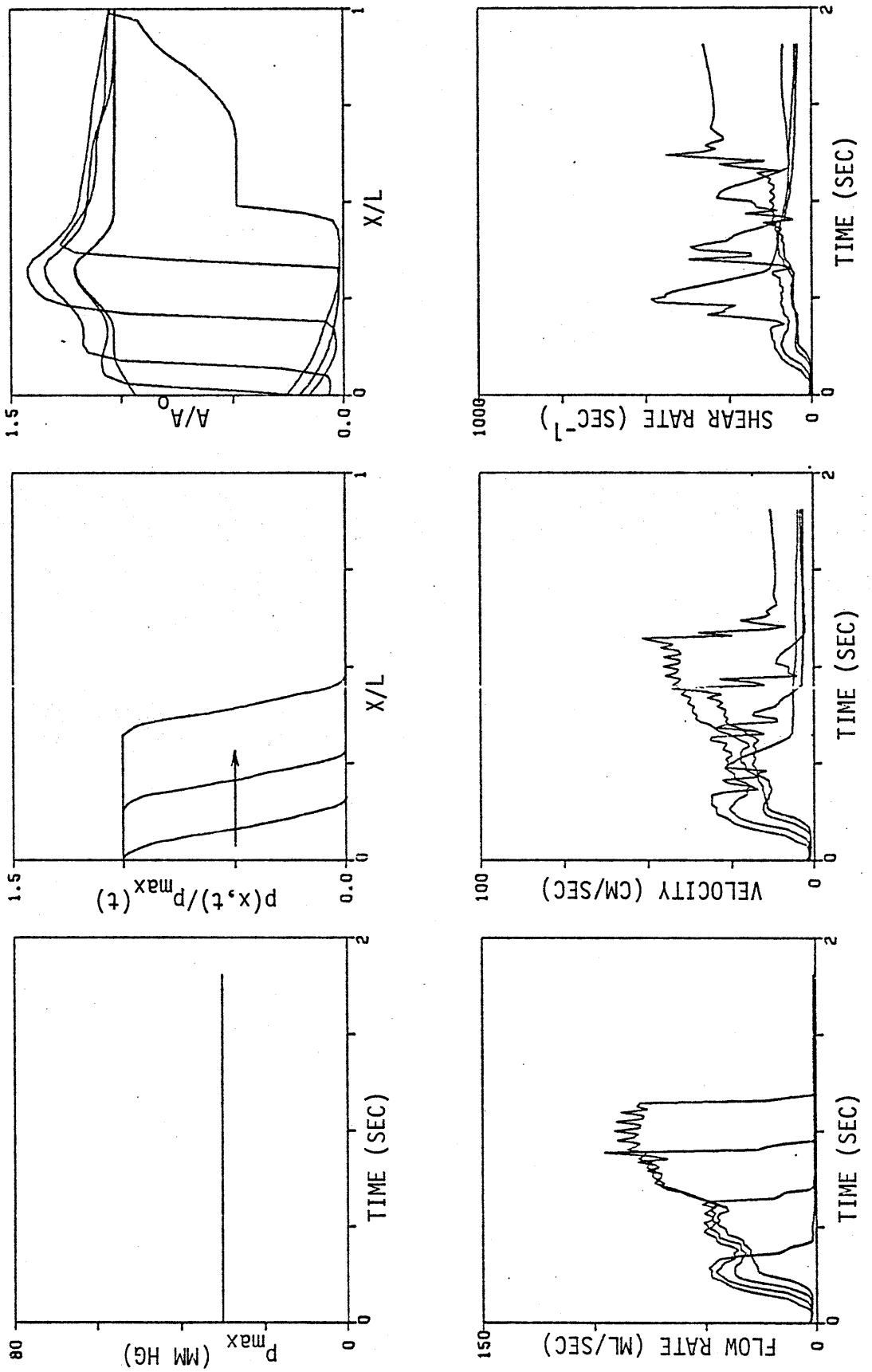
A/A0
X/L
SHEAR RATE (SEC-1)
TIME (SEC)
p(x,t)/pmax(t)
X/L
VELOCITY (CM/SEC)
TIME (SEC)
pmax (MM HG)
TIME (SEC)
FLOW RATE (ML/SEC)
TIME (SEC)

FIG. 37

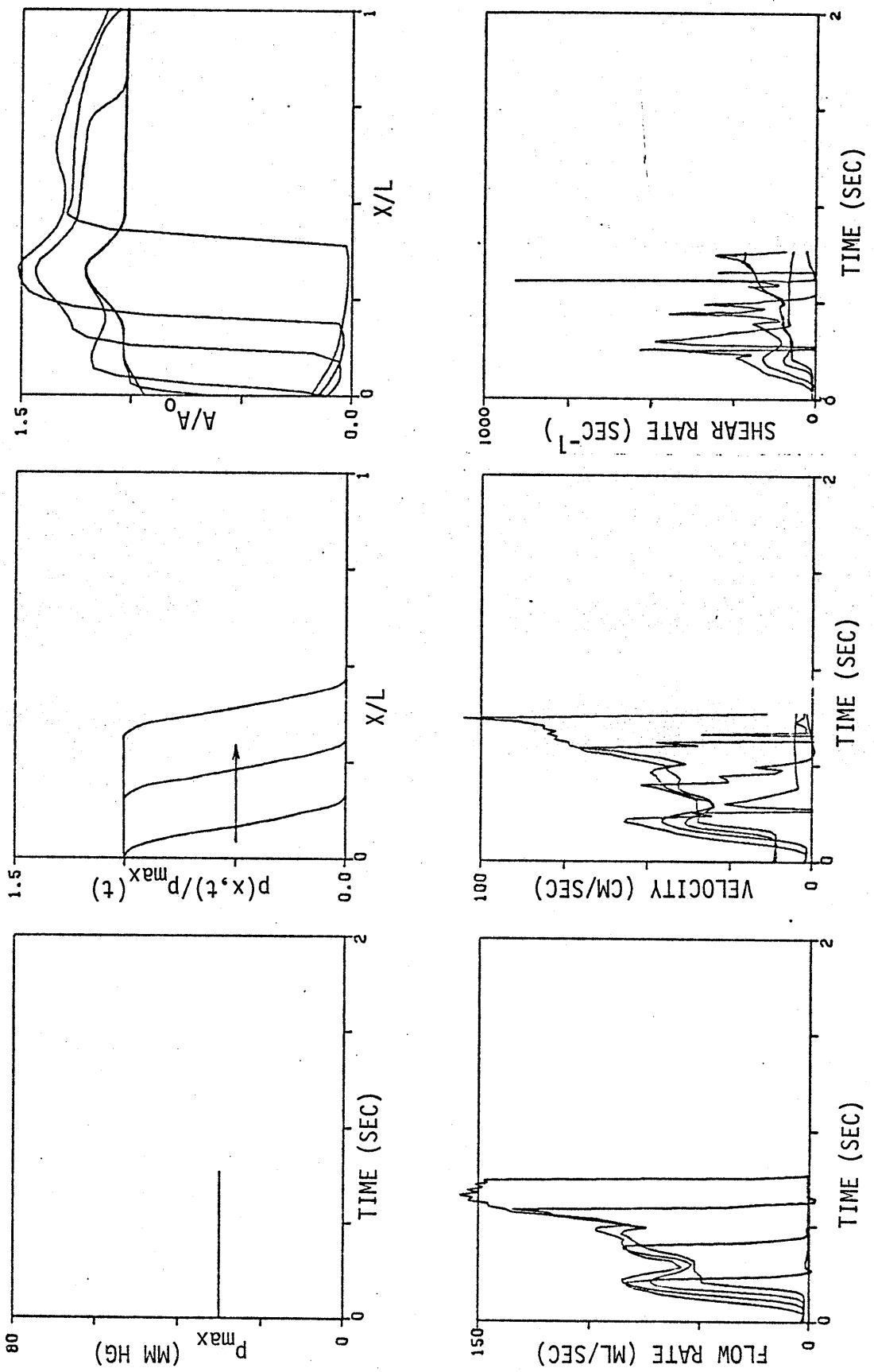
A/A$_o$
X/L
SHEAR RATE (SEC^{-1})
TIME (SEC)
p(x,t)/p$_{max}$(t)
X/L
VELOCITY (CM/SEC)
TIME (SEC)
p$_{max}$ (MM HG)
TIME (SEC)
FLOW RATE (ML/SEC)
TIME (SEC)

FIG. 38

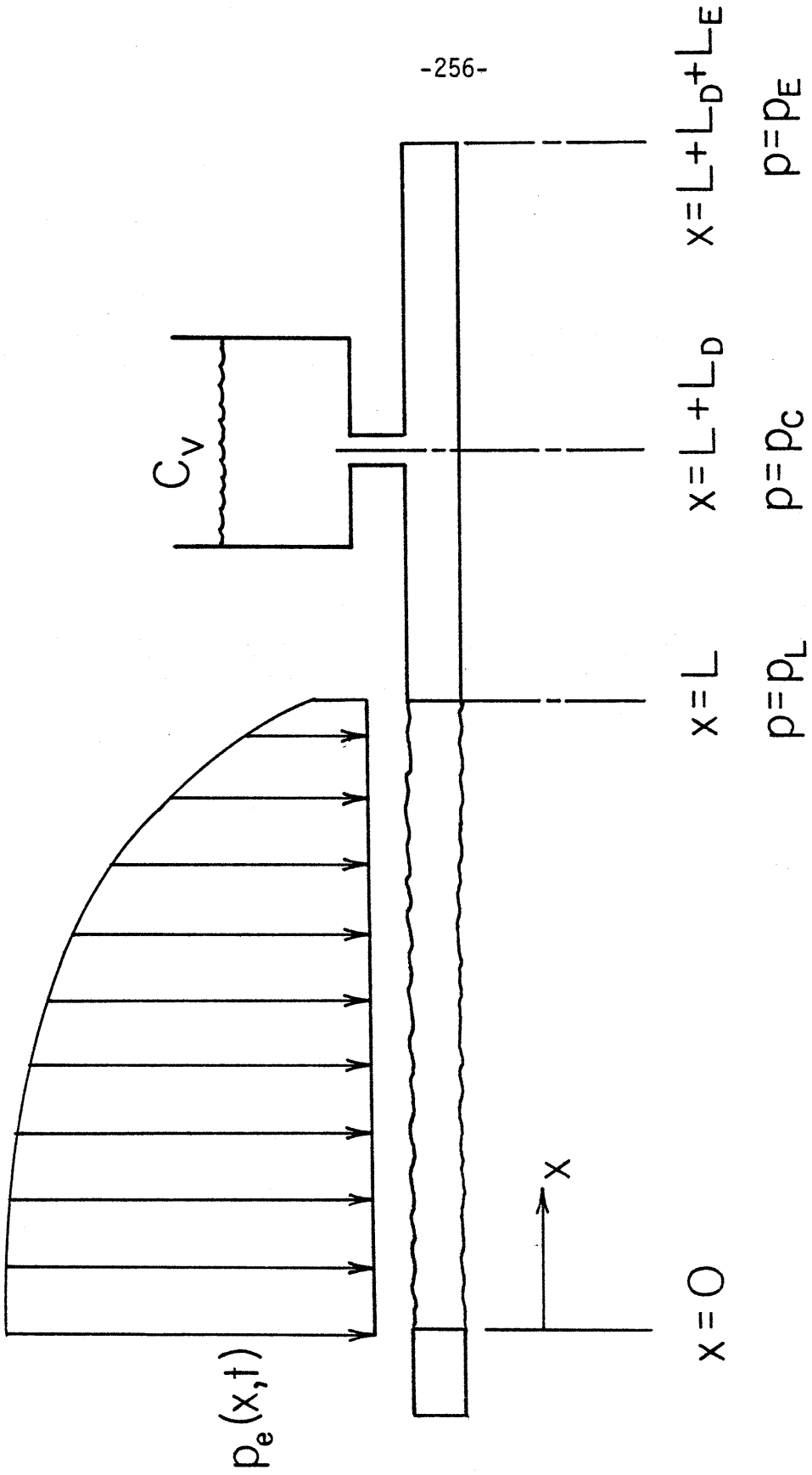

FIG. 39

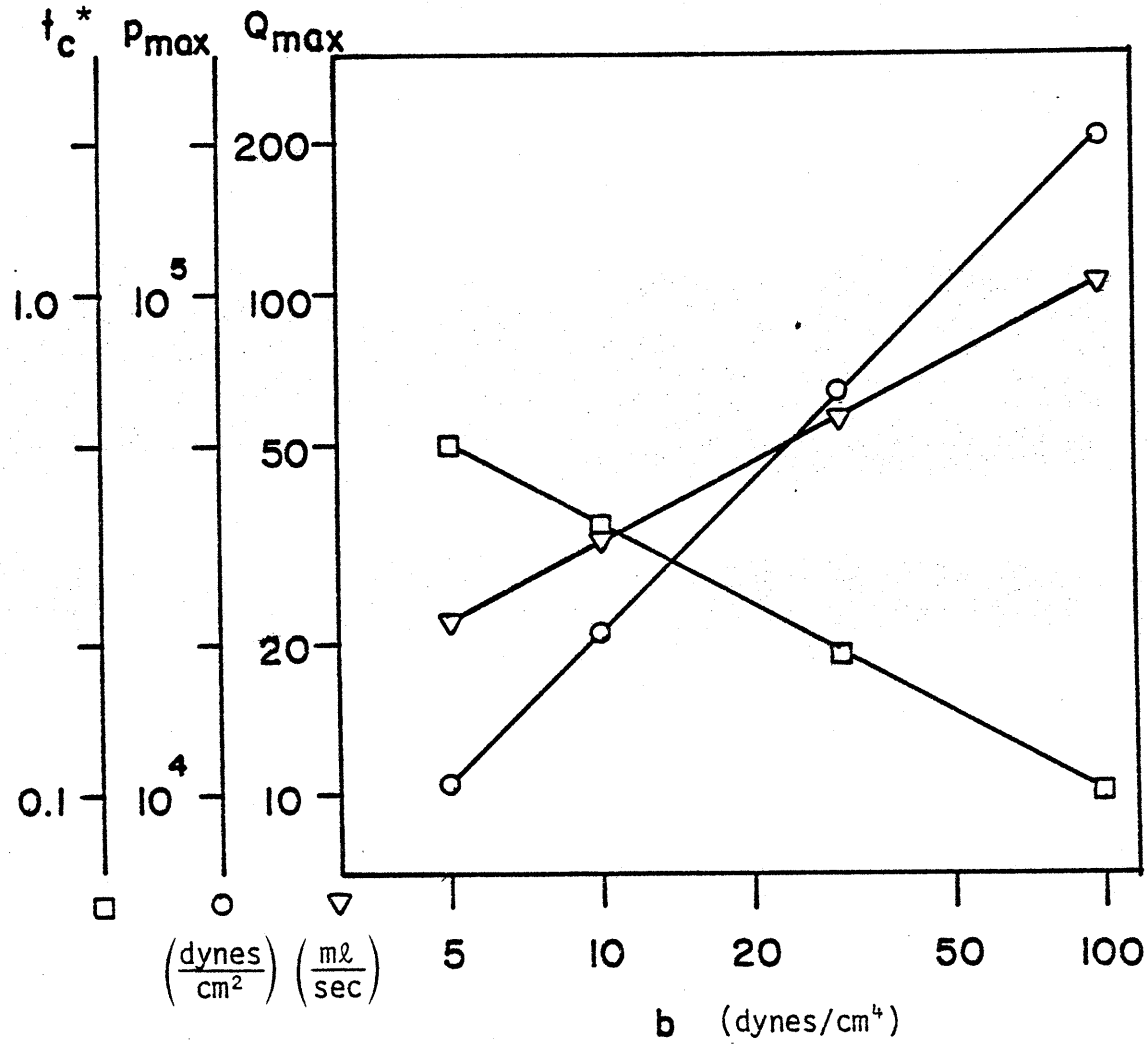
t_c^*
P_{max}
Q_{max}
200
100
50
20
10
1.0
0.1
10^5
10^4
□
○
▽
$\left(\frac{dynes}{cm^2}\right)$
$\left(\frac{ml}{sec}\right)$
5
10
20
50
100
b (dynes/cm⁴)

FIG. 40

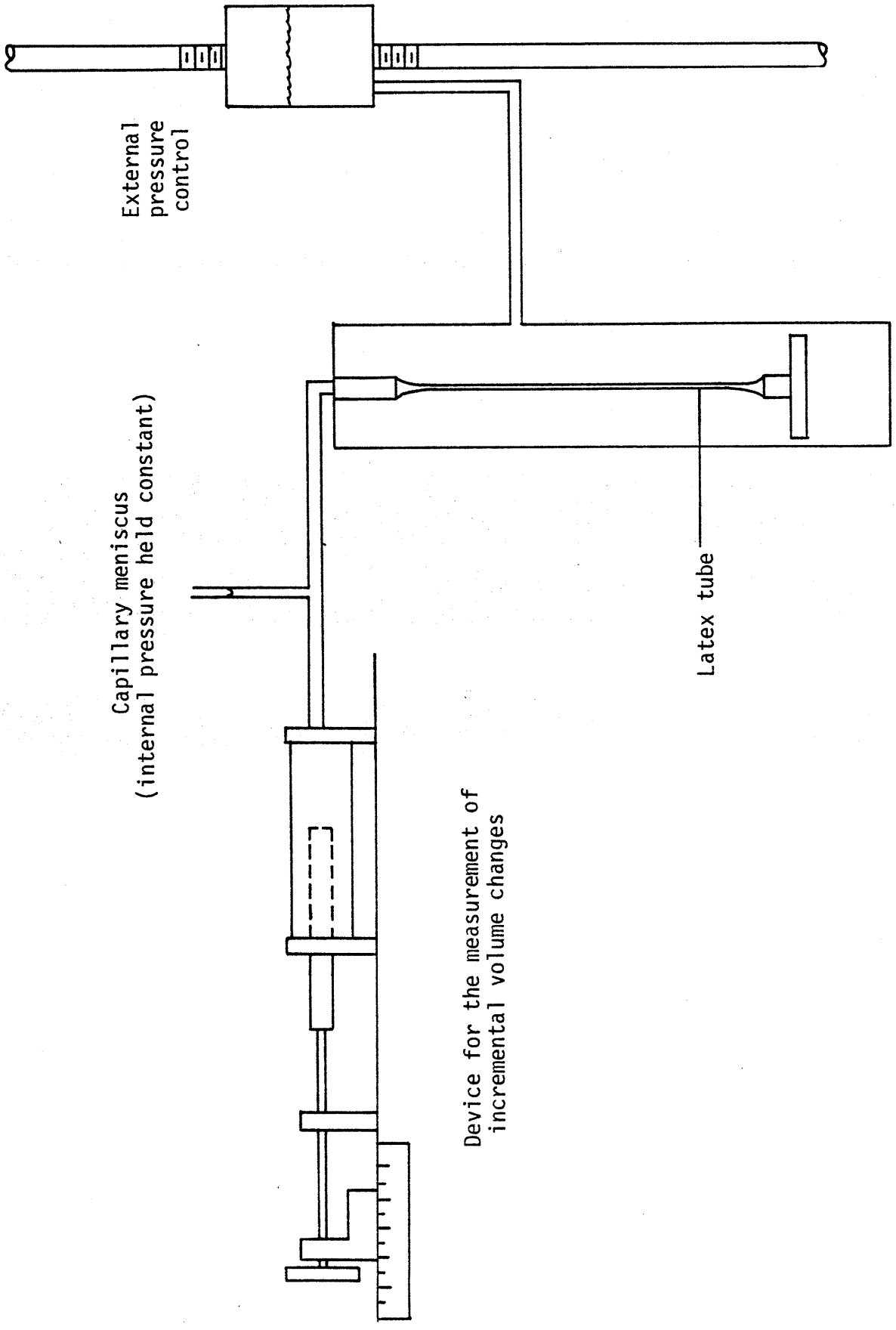
External pressure control
Capillary meniscus (internal pressure held constant)
Latex tube
Device for the measurement of incremental volume changes

FIG. 41

APPENDIX A:
UNIFORM COLLAPSE OF A SINGLE VESSEL

In one instance the equations derived for flow through a collapsible tube reduce to a set of nonlinear ordinary differential equations. The purpose of this appendix is to explore this special case and to consider the insights it might provide into more complicated situations.

Description of the Model

The system to be analyzed is shown in Fig. 39. It consists of a uniform collapsible tube blocked at $x = 0$ and connected at $x = L$ to a pair of rigid ducts of length L_D and L_E separated by a capacitance tank. The pressure at the end of the second duct is held constant. The values of L, L_E, L_D, and the capacitance, C_V, are chosen so as to create a lumped parameter model of what a single vein in the calf might "see" in terms of proximal inertance and capacitance. With this model, no attempt is made to simulate the complexities of the point of attachment between the collapsible and rigid tubes. The internal pressure, p, is assumed to be constant across the attachment point and the tube law is assumed to be unaffected by this physical constraint.

The Governing Equations

This analysis is motivated by the presumed existence of a spatially-varying external pressure which will cause the tube to collapse uniformly,

i.e., independently of x. We assume that $\partial A/\partial x = 0$ and write the governing flow equations as

$$A \frac{\partial u}{\partial x} + \frac{dA}{dt} = 0 \qquad \text{(A-1)}$$

$$\rho \frac{\partial u}{\partial t} + \rho u \frac{\partial u}{\partial x} + \frac{\partial p_e}{\partial x} + \frac{P\tau_w}{A} = 0 \quad . \qquad \text{(A-2)}$$

The uniform tube assumption implies that if $\partial A/\partial x = 0$ then $\partial(p-p_e)/\partial x$ is equal to zero as well. Imposing the condition that $u_{x=0} = 0$ we can integrate Eq. (A-1) to give

$$u = -\frac{x}{A}\frac{dA}{dt} \quad . \qquad \text{(A-3)}$$

Introducing the following normalized variables,

$$\xi \equiv \frac{x}{L} \quad ; \qquad \alpha \equiv \frac{A}{A_0} \quad ;$$
$$U \equiv \frac{u\tau}{\xi L} \quad ; \qquad t = t^*\tau \qquad \text{(A-4)}$$

yields the following form for (A-3):

$$U = -\frac{1}{\alpha}\frac{d\alpha}{dt^*} \quad . \qquad \text{(A-5)}$$

Substitution into (A-2) with some rearrangement results in the expression

$$\xi \frac{dU}{dt^*} + \xi U^2 + \frac{\tau^2}{\rho L^2}\frac{\partial p_e}{\partial \xi} + \frac{\tau^2}{\rho L}\frac{P\tau_w}{\alpha A_0} = 0 \quad . \qquad \text{(A-6)}$$

Of those expressions previously derived for the flow resistance, we will choose to use the one representing fully developed flow in a collapsed tube. Although the collapse takes place very rapidly, it can be shown that shear stresses become important only during the later stages when the tube is essentially collapsed and when the flow is more nearly fully developed. Replacing the quantity $P\tau_w/\alpha A_0$ in (A-6) by the appropriate expression we can rewrite the momentum equation as

$$\frac{1}{\rho}\left(\frac{A_0}{70\mu L}\right)^2 \frac{\partial p_e}{\partial \xi} = -\xi\left(\frac{dU}{dt^*} + U^2 + \frac{U}{\alpha}\right) \quad , \qquad \text{(A-7)}$$

where we have defined τ in the following manner so as to simplify the resulting expression:

$$\tau \equiv \frac{A_0}{70\nu} \quad . \qquad \text{(A-8)}$$

By examining Eq. (A-7) we see that the necessary condition for the assumed uniform tube collapse is that the external pressure take on the general form, expressed as

$$p_e = a - bL^2\xi^2 \quad , \qquad \text{(A-9)}$$

where a and b can both be functions of t^*. Assuming the applied external pressure is of the expressed form we can reduce Eq. (A-7) to an ordinary differential equation,

$$\frac{dU}{dt^*} = \gamma - U^2 - \frac{U}{\alpha} \qquad \text{(A-10)}$$

where

$$\gamma \equiv \frac{2b}{\rho}\left(\frac{A_0}{70\nu}\right)^2 \quad .$$

Between Eqs. (A-5) and (A-10) we can determine each variable at any time, t^* , given one initial condition which we state as

$$\alpha_{t^*=0} = 1 \qquad \text{and} \qquad U_{\xi=0} = 0 \qquad . \tag{A-11}$$

To solve for the applied pressure at $\xi = 0$, we must take into account the downstream boundary condition.

Assuming that frictional effects can be neglected in the discharge ducts, the momentum equations for the two lengths of rigid tubing (L_D and L_E) can be written:

$$\frac{du_D}{dt} = \frac{1}{L_D\rho}\left(p_{\xi=1} - p_c\right) \tag{A-12}$$

$$\frac{du_E}{dt} = \frac{1}{L_E\rho}\left(p_c - p_E\right) \tag{A-13}$$

where the pressures and lengths are defined in Fig. 39. The pressure in the capacitance tank is governed by the expression:

$$\frac{dp_c}{dt} = \frac{1}{C_V}\left(A_D u_D - A_E u_E\right) \quad . \tag{A-14}$$

Here, $C_V = dV_c/dp_c$ and A_D and A_E are the cross-sectional areas of the two discharge vessels.

Differentiating (A-14) and replacing u_E using Eq. (A-13), we obtain

$$\frac{d}{dt}\left(\frac{dp_c}{dt}\right) = \frac{1}{C_V}\left[A_D \frac{du_D}{dt} - \frac{A_E}{L_E \rho}(p_c - p_E)\right] . \qquad \text{(A-15)}$$

We can write Eq. (A-15) in normalized form, recognizing that

$$u_D = \frac{\alpha U}{A_D} 70\nu L$$

and

$$p_L = K_p P_{\xi=1} + \alpha - bL^2 .$$

The result of this normalization is

$$\frac{d}{dt^*}\frac{dp_c}{dt^*} = \frac{A_0 L}{C_V}\left[\alpha\left(\gamma - 2U^2 - \frac{U}{\alpha}\right)\right] - \left(\frac{A_0}{70\nu}\right)^2 \frac{A_E}{\rho L_E C_V}(p_c - p_E). \qquad \text{(A-16)}$$

Using the approximation for the tube law,

$$P = -\alpha^{-3/2} + \alpha^{10} ,$$

we can solve for the magnitude of the external pressure as a function of time:

$$\alpha = p_c + \frac{LL_D\rho}{A_0 A_D}(70\nu)^2\left[\alpha\left(\gamma - 2U^2 - \frac{U}{\alpha}\right)\right] + K_p(\alpha^{-3/2} - \alpha^{10}) + bL^2 . \qquad \text{(A-17)}$$

Discussion of Results

Equations (A-5), (A-10), (A-16), and (A-17) completely define the given system and can be solved by a standard Runge-Kutta technique.

The results of the numerical solution are illustrated in Fig. 40. The maximum flow rate, Q_{max} , the maximum applied pressure, p_{max} , and the time required for collapse, t_c^* (for α to reach 0.26) are plotted against b . The units of Q_{max} are mℓ/sec, p_{max} is expressed in dynes/cm^2 , and t_c^* is dimensionless.

A number of cases have been simulated in which b was varied between the limits of 5 and 100 dynes/cm^4 . As indicated by the maximum pressures required to maintain uniform collapse, this range covers all pressures that might reasonably be used for EPC. The flow rate and maximum applied pressure both increase with increasing b , while the collapse time decreases.

It appears from these results that the only limitation exists in how rapidly one can apply these increasingly large pressures. It should be noted, however, that the emptying rate presumes an extremely rapid pressure application, one which would be difficult to attain in a real situation. This restriction combined with the parabolic pressure distribution and lack of constraint at the downstream end make this technique difficult, if not impossible, to explore experimentally. The usefulness of this result lies essentially in the concept of using some sort of a spatially varying external pressure so as to prevent the flow limitation associated with a uniform pressure application. Clearly, there exists a great potential with such a scheme to significantly reduce the emptying time of the vessels, thereby inducing larger flow rates and shear stresses throughout.

A more practical method might be to apply a linearly varying

external pressure. This would produce a collapse which proceeds from the upstream end and would eliminate the downstream collapse observed in situations of uniform compression. This concept is explored further in the text of Chapter XII.

APPENDIX B:

A SIMILARITY SOLUTION FOR VISCOUS DOMINATED FLOW

Under certain circumstances, the equations governing unsteady collapsible tube flow can be simplified considerably. In such limiting cases, the flow can by analyzed much more simply and, as was the case in Appendix A, the results can help us to better understand the entire flow process. In this appendix we consider the case of viscous dominated quasi-steady flow.

Description of the Model

The model is similar to that used in the previous discussion except that the collapsible tube extends from $x = 0$ to ∞. When pressure is first applied fluid empties at the point where there exists a pressure gradient--at $x = 0$--and proceeds in the negative x-direction.

Theoretical Description

The equations governing the flow are those of conservation of momentum:

$$\frac{\partial u}{\partial t} + u \frac{\partial u}{\partial x} + \frac{1}{\rho} \frac{\partial p}{\partial x} + \nu g(A) \frac{u}{A} = 0 \quad , \qquad \text{(B-1)}$$

(where g is a weak function of A); continuity:

$$\frac{\partial A}{\partial t} + \frac{\partial Q}{\partial x} = 0 \quad ; \qquad \text{(B-2)}$$

and the tube law:

$$\frac{p - p_e}{K_p} = P(\alpha) \quad . \tag{B-3}$$

The assumptions we make for this analysis are:

(1) The tube is infinitely long, uniform, and is pressurized beginning at $t = 0$ by a constant pressure, p_e .

(2) At some stage in the process, the flow becomes quasi-steady, i.e.,

$$\frac{\partial u}{\partial t} \ll \nu g(A) \frac{u}{A} \ ,$$

and the convective acceleration term is small compared with the viscous stresss term:

$$u \frac{\partial u}{\partial x} \ll \nu g(A) \frac{u}{A} \quad .$$

(3) Reynolds number based on tube diameter is small (and t is sufficiently large) so that we can assume that the flow is laminar and fully developed.

(4) For large x , $A \to A_0$ and $p \to p_e$.

(5) The outlet pressure is constant, maintaining a constant cross-sectional area at $x = 0$ (note that Q will be in the direction of negative x).

As a result of (2) and (3), the momentum equation can be reduced to the following form:

$$\frac{\partial p}{\partial x} = -\mu g(A) \frac{Q}{A^2} \quad . \tag{B-4}$$

Using the tube law we can eliminate pressure by introducing the wave speed, c . Differentiating (B-3) and substituting $c^2 = K_p \frac{\alpha}{\rho} \frac{dP}{d\alpha}$, where $\alpha = A/A_0$, we obtain

$$\frac{\partial p}{\partial x} = - \frac{\rho c^2}{\alpha} \frac{\partial \alpha}{\partial x} \quad , \tag{B-5}$$

which can be substituted directly into Eq. (B-4) to give

$$Q = - \frac{\rho c^2 A_0{}^2 \alpha}{\mu g(\alpha)} \frac{\partial \alpha}{\partial x} \quad . \tag{B-6}$$

Combining this with (B-2) produces a nonlinear partial differential equation which has the form of the diffusion equation,

$$\frac{\partial \alpha}{\partial t} - \frac{\partial}{\partial x}\left[J(\alpha) \frac{\partial \alpha}{\partial x} \right] = 0 \tag{B-7}$$

where

$$J(\alpha) = \frac{\rho A_0}{\mu} \frac{c^2 \alpha}{g(\alpha)} \quad .$$

Solution of Eq. (B-7) requires two boundary conditions and an initial condition. The boundary conditions are

$$\begin{aligned} \alpha(0,t) &= \alpha_{exit} \\ \alpha(\infty,t) &= 1 \quad . \end{aligned} \tag{B-8}$$

Ideally, we could stipulate the initial condition that $\alpha = 1$ for all $x > 0$ at $t = 0$. Realistically, however, the unsteady terms are likely to be dominant or at least significant at small times. Therefore, it would be more appropriate to begin the analysis at some later, time, t_0 ,

when the previously stated assumptions are valid. This condition can be stated as

$$\alpha(x,t_0) = \hat{\alpha}(x) \quad . \tag{B-9}$$

The nature of Eq. (B-7) leads us to expect that a similarity variable exists of the form

$$\xi \equiv \frac{x}{\sqrt{t}} \quad . \tag{B-10}$$

Although we can express the conditions (B-8) in terms of ξ, Eq. (B-9) does not, in general, admit to this kind of variable transformation. To the extent that (B-9) resembles the solution to Eqs. (B-7) and (B-8) with the initial condition $\alpha(x,0) = 1$, at some time t_1 [i.e., $\hat{\alpha}(x) = \alpha(x,t_1)$], the following remarks are valid.

We introduce the similarity variable ξ into the governing equations with the assumption that $\alpha = \alpha(\xi)$ only. After some manipulation, we obtain the following ordinary differential equation in ξ :

$$\frac{d}{d\xi}\left[J(\alpha)\frac{d\alpha}{d\xi}\right] + \frac{\xi}{2}\frac{d\alpha}{d\xi} = 0 \quad , \tag{B-11a}$$

along with the transformed boundary conditions,

$$\begin{aligned} &\text{at } \xi = 0 : \quad \alpha = \alpha_{exit} \\ &\text{at } \xi = \infty ; \quad \alpha = 1 \quad . \end{aligned} \tag{B-11b}$$

Discussion of the Similarity Formulation

We can draw several conclusions based on the existence of a similarity variable without actually solving Eq. (B-11a).

The exit flow rate [Q(0,t)] can be computed from the expression

$$Q(0,t) = \frac{d}{dt}(\text{tube volume}) = \frac{d}{dt}\int_0^\infty -(A_0 - A)\,dx$$

$$= \frac{d}{dt}\left[A_0\sqrt{t}\int_0^\infty -(1-\alpha)\,d\xi\right]. \qquad \text{(B-12)}$$

Since $\alpha = \alpha(\xi)$, then

$$Q(0,t) = \frac{d}{dt}(\text{constant} \cdot \sqrt{t}) = -\frac{\text{constant}}{\sqrt{t}} \quad . \qquad \text{(B-13)}$$

Based on our previous discussion with respect to the early stages of collapse during which the similarity solution is not valid, we replace t in Eq. (B-13) by $t-t_1$. To make a direct comparison between these predictions and actual observations, we could rewrite (B-13) in the following manner:

$$t = t_1 + \frac{K}{Q(0,t)^2} \quad . \qquad \text{(B-14)}$$

The form of Eq. (B-14) suggests that if we plot experimental results for $1/Q(0,t)^2$ versus time, we would expect to see the features shown in the following figure.

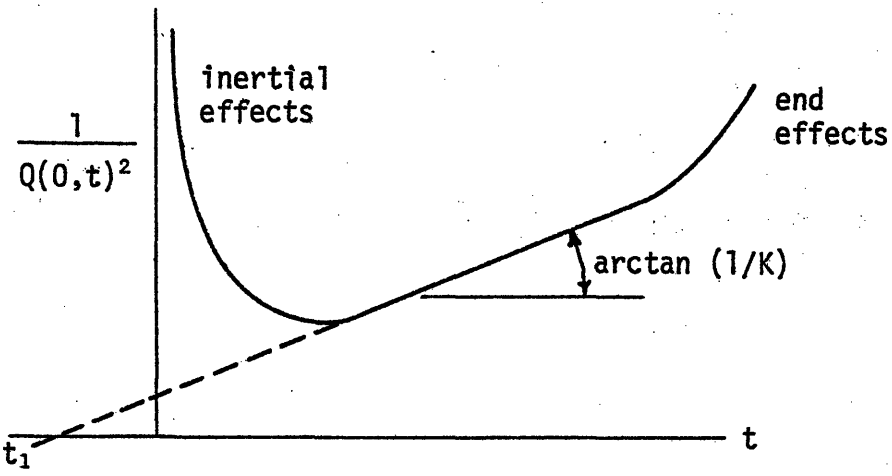

The initial phase shown in the diagram is dominated by inertial effects and since $Q(0,t)_{t\to 0} \to 0$, then $[1/Q(0,t)^2]_{t\to 0} \to \infty$. In a tube of finite length, the flow rate must approach zero [i.e., $1/Q(0,t)^2 \to \infty$] as the end effects become significant. In between these regions on the graph, if all the conditions mentioned above are satisfied, the curve should be a straight line with a slope of $1/K$ and an x-intercept of t_1 .

Similarly, we could estimate the time necessary to displace a certain volume of fluid, say V_E , by integrating the volume flow rate over time:

$$V_E = \int Q\, dt = \text{constant } \sqrt{t} \quad .$$

The time required for equal volume displacements, since the constant in the above expression varies inversely with μ , should vary as the square of the viscosity.

We attempted to correlate these estimates with our experimental or theoretical results but with little success. Our experiments, for the

most part, were primarily inertia-dominated or at least strongly influenced by inertial effects during most of the cycle. A possible exception could be made in the case of Expt. 19 in which the viscosity was increased by a factor of five. Clearly, in the later stages of this experiment, viscosity plays an important role, but again the results of that experiment could not be entirely explained by these predictions.

APPENDIX C:

COMPUTER PROGRAM FOR NUMERICAL CALCULATIONS

```
C                                                                       MOCS0001
C     ****************************************************************  MOCS0002
C                                                                       MOCS0003
C     THEORETICAL SOLUTION OF FLOW THROUGH A NETWORK OF                 MOCS0004
C     COLLAPSIBLE TUBES USING A COMBINATION OF THE METHODS OF           MOCS0005
C     CHARACTERISTICS AND FINITE DIFFERENCES                            MOCS0006
C                                                                       MOCS0007
C     ****************************************************************  MOCS0008
C                                                                       MOCS0009
      DIMENSION U1(101), U2(101), A1(101), A2(101), P1(101), P2(101),   MOCS0010
     2          C1(101), C2(101), X(101), DPX(101), Q(101), Q1(101),    MOCS0011
     3          PEX(101), PSI(101), AO(101), CO(101), CF(101), DPTX(101)MOCS0012
     4          , DADX(101), DCDX(101), DELC(101), QL(101), AUX(10),    MOCS0013
     5          REALT(50), PET(50)                                      MOCS0014
      COMMON A(25),BETA                                                 MOCS0015
      COMMON/CINT/P(25), C(25)                                          MOCS0016
      COMMON/CHEAR/RHO, T, DT, XL, QI, CO1, NQ                          MOCS0017
C                                                                       MOCS0018
C     FUNCTION STATEMENTS                                               MOCS0019
C                                                                       MOCS0020
C     INTERPOLATION                                                     MOCS0021
C                                                                       MOCS0022
      YINT(XO,X1,Y1,Y2) = Y1 + (X1-XO)/DX*(Y2 - Y1)                     MOCS0023
C                                                                       MOCS0024
C     LOCATE POINT WHERE CHARACTERISTIC CURVE INTERSECTS T=CONSTANT     MOCS0025
C                                                                       MOCS0026
      XRT1(XS,DTK,U2K,C2K,DELCK) = XS - DTK/2.*(U2K + URT + DELCK*C2K    MOCS0027
     2   + DELCR*CRT)                                                   MOCS0028
      XLT1(XS,DTK,U2K,C2K,DELCK) = XS - DTK/2.*(U2K + ULT - DELCK*C2K    MOCS0029
     2   - DELCL*CLT)                                                   MOCS0030
C                                                                       MOCS0031
C                                                                       MOCS0032
C     INPUT PARAMETERS                                                  MOCS0033
C                                                                       MOCS0034
C                                                                       MOCS0035
C     IF PROGRAM IS TO BE STARTED  AT T = 0 THEN NSTRT = 0              MOCS0036
```

```
C                                                                       MOCS0037
      READ (5,100) NSTRT                                                MOCS0038
  100 FORMAT (I5)                                                       MOCS0039
C                                                                       MOCS0040
C        N = NUMBER OF SPATIAL INCREMENTS                               MOCS0041
C        NN = NUMBER OF POINTS IN P-A TABLE                             MOCS0042
C        NNM = SIMULATION NUMBER                                        MOCS0043
C        KX = NUMBER OF TIME INCREMENTS                                 MOCS0044
C        KSTP = FURTHEST POINT DOWNSTREAM FOR MOC CALCULATION           MOCS0045
C        NPO = NUMBER OF POINTS IN PE-T TABLE                           MOCS0046
C                                                                       MOCS0047
      READ (5,101) N, NN, NNM, KX, KSTP, NPO                            MOCS0048
  101 FORMAT (6I5)                                                      MOCS0049
      READ (5,102) (X(K),PEX(K),AO(K),CO(K),CF(K),QL(K), K=1,N)         MOCS0050
  102 FORMAT (6F10.4)                                                   MOCS0051
      READ (5,103) RHO, XL, XKP, ZA, ZB, PA, PB, DT, CV, S,             MOCS0052
     2   PM, XMU, AA, AB, XLA, XLB, TSTP, HLS, WS, PEXC, DTM            MOCS0053
  103 FORMAT (E15.5)                                                    MOCS0054
      READ (5,104) (A(K),P(K),C(K), K=1,NN)                             MOCS0055
  104 FORMAT (3F10.5)                                                   MOCS0056
C                                                                       MOCS0057
C        COMPUTE OFTEN USED QUANTITIES                                  MOCS0058
C                                                                       MOCS0059
      MN = N-1                                                          MOCS0060
      MMN = MN - 1                                                      MOCS0061
      MEND = MMN - 1                                                    MOCS0062
      LL = 10                                                           MOCS0063
      NO = 0                                                            MOCS0064
      PI = 3.14159                                                      MOCS0065
      BETA = XKP/RHO/CO(1)**2                                           MOCS0066
      R1 = 8.*PI*XMU*XLA/AA**2                                          MOCS0067
      R2 = 8.*PI*XMU*XLB/AB**2                                          MOCS0068
      XPSI = 0.0                                                        MOCS0069
      RA = ZA*XMU                                                       MOCS0070
      EL1 = RHO*XLA/AA                                                  MOCS0071
      EL2 = RHO*XLB/AB*AO(1)*CO(1)**2/XL                                MOCS0072
```

```
      ZB = (R1 + R2)/XMU                                                        MOCS0073
      XC = CO(1)*AO(1)*ZA*XMU/XKP                                               MOCS0074
      CO1 = CO(1)                                                               MOCS0075
      DX = X(2) - X(1)                                                          MOCS0076
      XT = 0.                                                                   MOCS0077
      DO 1 K=2,MN                                                               MOCS0078
      CF(K) = CF(K)*XMU                                                         MOCS0079
      DADX(K) = (AO(K+1) - AO(K-1))/DX/2./AO(K)                                 MOCS0080
      DCDX(K) = (CO(K+1) - CO(K-1))*BETA/DX/2./CO(1)**2*CO(K)                   MOCS0081
    1 DELC(K) = CO(K)/CO(1)                                                     MOCS0082
      DADX(N) = (AO(N) - AO(N-1))/DX/AO(N)                                      MOCS0083
      DADX(1) = (AO(2) - AO(1))/DX/AO(1)                                        MOCS0084
      DCDX(N) = BETA*(CO(N) - CO(N-1))/DX/CO(1)**2*CO(N)                        MOCS0085
      DCDX(1) = BETA*(CO(2) - CO(1))/DX/CO(1)                                   MOCS0086
      CF(N) = CF(N)*XMU                                                         MOCS0087
      CF(1) = CF(1)*XMU                                                         MOCS0088
      DELC(N) = CO(N)/CO(1)                                                     MOCS0089
      DELC(1) = 1.0                                                             MOCS0090
C                                                                               MOCS0091
CC       INITIAL CONDITIONS - INERTIAL TERMS OMITTED                            MOCS0092
C                                                                               MOCS0093
      T = 0.0                                                                   MOCS0094
      PE = PM                                                                   MOCS0095
      DO 8 K=1,N                                                                MOCS0096
    8 PEX(K) = 0.0                                                              MOCS0097
      KN = 0                                                                    MOCS0098
      KNN = 1                                                                   MOCS0099
      TCHKM = DT                                                                MOCS0100
      TCHK = DT                                                                 MOCS0101
      KFD = 0                                                                   MOCS0102
      IF (NSTRT.EQ.1) GO TO 14                                                  MOCS0103
      VM = 0.                                                                   MOCS0104
      Q(1) = 0.0                                                                MOCS0105
      DO 2 K=2,N                                                                MOCS0106
    2 Q(K) = Q(K-1) + (QL(K) + QL(K-1))/2.*DX*XL                                MOCS0107
      QI = (PA - PB - Q(N)*(R1 + R2) - 8.*PI*XMU*XL*Q(N)/2./AO(1)**2)/          MOCS0108
```

```
     2    (RA + R1 + R2 + 8.*PI*XMU*XL/AO(1)**2)                          MOCS0109
          P2(N) = (PB + (R1 + R2)*(OI + Q(N)))/RHO/CO(N)**2/BETA          MOCS0110
          DO 3 K=1,N                                                      MOCS0111
     3    Q(K) = (QI + Q(K))/AO(1)/CO(1)                                  MOCS0112
          PC1 = PB + R2*Q(N)*AO(1)*CO(1)                                  MOCS0113
          CALL ZINT(2,A2(N),P2(N))                                        MOCS0114
          CALL ZINT(3,A2(N),C2(N))                                        MOCS0115
          U2(N) = Q(N)/A2(N)*AO(1)/AO(N)                                  MOCS0116
          THETA = 0.                                                      MOCS0117
          XD = 16.*PI*CO(1)*AO(1)*XL/RHO                                  MOCS0118
          PSI(N) = CF(N)/(CO(N)*AO(N)*C2(N))**2*Q(N)*XD +                 MOCS0119
     2    4.*P2(N)*(A2(N)/C2(N)/DELC(N))**2*DCDX(N)                       MOCS0120
C                                                                         MOCS0121
C         INTEGRATION OF INITIAL CONDITIONS USING SIMPSONS RULE           MOCS0122
C                                                                         MOCS0123
          DO 5 LX=1,MN                                                    MOCS0124
          K = N - LX                                                      MOCS0125
          PSI(K) = CF(K)/(CO(K)*AO(K)*C2(K+1))**2*Q(K)*XD +               MOCS0126
     2    4.*P2(K+1)*(A2(K+1)/C2(K+1)/DELC(K))**2*DCDX(K)                 MOCS0127
          IF ((K/2)*2.NE.K) GO TO 4                                       MOCS0128
          C2(K) = C2(K+1)                                                 MOCS0129
          P2(K) = P2(K+1)                                                 MOCS0130
          A2(K) = A2(K+1)                                                 MOCS0131
          GO TO 5                                                         MOCS0132
     4    THETA = THETA - DX/3.*(PSI(K+2) + 4.*PSI(K+1) + PSI(K))         MOCS0133
          A2(K) = (A2(N)**2 - THETA)**.5                                  MOCS0134
          CALL ZINT (3,A2(K),C2(K))                                       MOCS0135
          CALL ZINT (1,A2(K),P2(K))                                       MOCS0136
     5    CONTINUE                                                        MOCS0137
          DO 6 K=2,MN,2                                                   MOCS0138
          A2(K) = (A2(K+1) + A2(K-1))/2.                                  MOCS0139
          CALL ZINT (1,A2(K),P2(K))                                       MOCS0140
     6    CALL ZINT (3,A2(K),C2(K))                                       MOCS0141
          DO 7 K=1,N                                                      MOCS0142
     7    U2(K) = Q(K)/A2(K)*AO(1)/AO(K)                                  MOCS0143
          QI = QI/AO(1)/CO(1)                                             MOCS0144
```

```
      QB = Q(N)                                                          MOCS0145
      QB1 = QB                                                           MOCS0146
      QB2 = QB                                                           MOCS0147
      GO TO 9                                                            MOCS0148
C                                                                        MOCS0149
C        STARTING PROGRAM AT T.GT.0                                      MOCS0150
C                                                                        MOCS0151
 14   READ (5,103) VM, QB, T                                             MOCS0152
      READ (5,250) A2, Q                                                 MOCS0153
      DO 15 K=1,N                                                        MOCS0154
      U2(K) = Q(K)/A2(K)*AO(1)/AO(K)                                     MOCS0155
      CALL ZINT (1,A2(K),P2(K))                                          MOCS0156
 15   CALL ZINT (3,A2(K),C2(K))                                          MOCS0157
      QB1 = QB                                                           MOCS0158
      QB2 = QB                                                           MOCS0159
      QSTRT = 0.0                                                        MOCS0160
      DO 16 K=1,N                                                        MOCS0161
 16   QSTRT = QSTRT + (QL(K) + QL(K-1))/2.*DX*XL                         MOCS0162
      QI = (PA - PB - QSTRT*(R1 + R2) - 8.*PI*XMU*XL*QSTRT/2./AO(1)**2)/ MOCS0163
     2   (RA + R1 + R2 + 8.*PI*XMU*XL/AO(1)**2)                          MOCS0164
      QI = QI + QSTRT                                                    MOCS0165
      PC1 = PB + R2*QI                                                   MOCS0166
      QI = QI/AO(1)/CO(1)                                                MOCS0167
      NQ = 1                                                             MOCS0168
 9    CONTINUE                                                           MOCS0169
C                                                                        MOCS0170
C        PRINT SIMULATION PARAMETERS                                     MOCS0171
C                                                                        MOCS0172
      WRITE (6,151) NNM                                                  MOCS0173
 151  FORMAT(10X,'SOLUTION FOR FLOW THROUGH A NETWORK OF COLLAPSIBLE'/10 MOCS0174
     2X,'TUBES USING A COMBINATION OF THE METHODS'/10X,'OF CHARACTERISTI MOCS0175
     3CS AND FINITE DIFFERENCES'///15X,'SIMULATION NUMBER',I3//10X,'PHYS MOCS0176
     4ICAL CONSTANTS USED IN THIS COMPUTATION:'//)                       MOCS0177
      WRITE (6,152) XL, XKP, CO1,BETA, PM, PA, PB, CV, ZA, ZB, S, XT,    MOCS0178
     2   AA, AB, XLA, XLB                                                MOCS0179
 152  FORMAT (10X,' XL   = ',E10.3,' XKP  = ',E10.3,' CO1  = ',E10.3,    MOCS0180
```

```
     2             ' BETA = ',E10.3/10X,                                          MOCS0181
     3             ' PM   = ',E10.3,' PA   = ',E10.3,' PB   = ',E10.3,            MOCS0182
     4             ' CV   = ',E10.3/10X,                                          MOCS0183
     5             ' ZA   = ',E10.3,' ZB   = ',E10.3,' S    = ',E10.3,           MOCS0184
     6             ' XT   = ',E10.3/10X,                                          MOCS0185
     7             ' AA   = ',E10.3,' AB   = ',E10.3,' XLA  = ',E10.3,           MOCS0186
     8             ' XLB  = ',E10.3///15X,                                        MOCS0187
     9             ' PARAMETERS WHICH MAY VARY WITH X;'//)                        MOCS0188
      WRITE (6,153) (X(K),PEX(K),AO(K),CO(K),CF(K), K=1,N)                        MOCS0189
 153  FORMAT (10X,' X = ',E10.3,'  PEX = ',F10.3,'  AO = ',E10.3,                 MOCS0190
     2   ' CO = ',F10.3,'  CF = ',E10.3)                                          MOCS0191
      WRITE (6,154)                                                               MOCS0192
 154  FORMAT (//10X,'PRINTED FORMAT:'/10X,                                        MOCS0193
     2   '1) AREA AT EVERY OTHER POINT BETWEEN 3 AND 37'/10X,                     MOCS0194
     3   '2) FLOW RATE AT EVERY OTHER POINT BETWEEN 3 AND 37'/10X,                MOCS0195
     4   '3) AREA AT EVERY FIFTH POINT BETWEEN 16 AND 101'/10X,                   MOCS0196
     5   '4) FLOW RATE AT EVERY FIFTH POINT BETWEEN 16 AND 101'//12X,             MOCS0197
     6   'ALL VARIABLES ARE STORED IN DISK MEMORY IN AN UNFORMATED',              MOCS0198
     7   ' MODE'/'1')                                                             MOCS0199
C                                                                                 MOCS0200
C        PROCEED TO SOLVE FOR TIMES GREATER THAN ZERO                             MOCS0201
C                                                                                 MOCS0202
      DO 70 KKK=1,KX                                                              MOCS0203
      LL = LL+1                                                                   MOCS0204
C                                                                                 MOCS0205
C        DATA OUTPUT (TO BOTH LINE PRINTER AND DISK)                              MOCS0206
C                                                                                 MOCS0207
      IF (LL.LT.10) GO TO 10                                                      MOCS0208
      WRITE  (6,155) T, PE, Q(N), QB, VM, A2(N)                                   MOCS0209
 155  FORMAT (5X,'TIME = ',F10.3,'  PE = ',E10.3,'  Q(EXIT) = ',E10.3,'           MOCS0210
     2  QB = ',E10.3,'  VM = ',E10.3,'  A2(N) = ',E10.3)                         MOCS0211
      WRITE (6,156) (A2(K), K=3,37,2)                                             MOCS0212
      WRITE (6,156) (Q(K), K=3,37,2)                                              MOCS0213
      WRITE (6,156) (A2(K), K=16,101,5)                                           MOCS0214
      WRITE (6,157) (Q(K), K=16,101,5)                                            MOCS0215
 156  FORMAT (1X,18F7.3)                                                          MOCS0216
```

```
 157  FORMAT (1X,18F7.3/)                                                    MOCS0217
      WRITE (1) T, PE, Q(N), OB, VM                                          MOCS0218
      WRITE (1) A2,Q,P2,C2                                                   MOCS0219
      IF (T.GE.TSTP) GO TO 80                                                MOCS0220
      LL = 0                                                                 MOCS0221
C                                                                            MOCS0222
C        ADJUSTMENTS IN DT                                                   MOCS0223
C                                                                            MOCS0224
  10  DT1 = DT                                                               MOCS0225
      DT = TCHKM                                                             MOCS0226
      IF (DT.GT.DTM) DT = DTM                                                MOCS0227
      T = T + DT                                                             MOCS0228
      TCHKM = 1.                                                             MOCS0229
      KN = 0                                                                 MOCS0230
      KNN = 0                                                                MOCS0231
      QN = Q(N)                                                              MOCS0232
      IF (T.GE.REALT(NPO-1)) GO TO 12                                        MOCS0233
      CALL IVP (REALT,0,PET,NPO,T,3,-1.0,PET1,AUX,IER1)                      MOCS0234
      PE = PM*PET1                                                           MOCS0235
      GO TO 13                                                               MOCS0236
  12  PE = PM                                                                MOCS0237
  13  CONTINUE                                                               MOCS0238
C                                                                            MOCS0239
C        *****ALTERNATE FORM USED FOR WAVE-LIKE COMPRESSIONS************     MOCS0240
C                                                                            MOCS0241
      XW = WS*T/CO(1)                                                        MOCS0242
      PEU = 0.0                                                              MOCS0243
      IF (XW.GT.0.50) GO TO 13                                               MOCS0244
      DO 12 KW=1,N                                                           MOCS0245
      IF (X(KW).LT.XW) PEX(KW) = PI/PEXC*COS(PI/2. + PI/PEXC*(X(KW) -        MOCS0246
     2   XW + PEXC))                                                         MOCS0247
  12  IF (X(KW).LT.(XW - PEXC)) PEX(KW) = 0.0                                MOCS0248
  13  CONTINUE                                                               MOCS0249
C                                                                            MOCS0250
C        ************************************************************        MOCS0251
C                                                                            MOCS0252
```

```
      DO 11 K=1,N                                                       MOCS0253
      Q1(K) = Q(K)                                                      MOCS0254
      A1(K) = A2(K)                                                     MOCS0255
      U1(K) = U2(K)                                                     MOCS0256
      C1(K) = C2(K)                                                     MOCS0257
      P1(K) = P2(K)                                                     MOCS0258
      DPX(K) = PEX(K)*PE/RHO/CO(1)**2                                   MOCS0259
      PEU = PEU - DX*PEX(K)                                             MOCS0260
   11 CONTINUE                                                          MOCS0261
      PEU = PEU*PM                                                      MOCS0262
C                                                                       MOCS0263
C        DOWNSTREAM BOUNDARY CONDITIONS (X=L)                           MOCS0264
C                                                                       MOCS0265
      UA = Q(N)/AA*AO(1)                                                MOCS0266
      UB = QB2/AB*AO(1)                                                 MOCS0267
      CRT = C1(N)                                                       MOCS0268
      URT = U1(N)                                                       MOCS0269
      DELCR = DELC(N)                                                   MOCS0270
      X2 = AO(1)*CO(1)/RHO/CO(N)**2/BETA*(R1 + CO(1)*EL1/XL/DT +        MOCS0271
     2   1./(2.*CV*CO(1)/XL/DT + 1./R2))                                MOCS0272
      X3 = EL1*AO(1)/XL/DT/RHO/BETA*Q1(N)*CO(1)**2/CO(N)**2             MOCS0273
     2   - HLS*(UA/DELC(N))**2/BETA                                     MOCS0274
      DO 20 K=1,3                                                       MOCS0275
      X1 = 1./RHO/CO(N)**2/BETA*(PB + XPSI + 1./(1. + XL*DT/2./R2/CV/   MOCS0276
     2   CO(1))*(PC1 - PB - XPSI + AO(1)*XL/CV*(VM + DT/2.*(Q1(N) -     MOCS0277
     3   QB))))                                                         MOCS0278
      XRT = XRT1(X(N), DT, U2(N), C2(N), DELC(N))                       MOCS0279
      QRT = YINT(X(N-1),XRT,Q1(N-1),Q1(N))                              MOCS0280
      ART = YINT(X(N-1),XRT,A1(N-1),A1(N))                              MOCS0281
      CFR = YINT(X(N-1),XRT,CF(N-1),CF(N))                              MOCS0282
      AOR = YINT(X(N-1),XRT,AO(N-1),AO(N))                              MOCS0283
      DPXR = YINT(X(N-1),XRT,DPX(N-1),DPX(N))                           MOCS0284
      DELCR = YINT(X(N-1),XRT,DELC(N-1),DELC(N))                        MOCS0285
      DCDXR = YINT(X(N-1),XRT,DCDX(N-1),DCDX(N))                        MOCS0286
      DADXR = YINT(X(N-1),XRT,DADX(N-1),DADX(N))                        MOCS0287
      CALL ZINT(1,ART,PRT)                                              MOCS0288
```

```
      CALL ZINT(3,ART,CRT)                                                    MOCS0289
      URT = QRT/ART*AO(1)/AOR                                                 MOCS0290
      HR = DPXR + 2.*PRT*DCDXR                                                MOCS0291
      H2 = DPX(N) + 2.*P2(N)*DCDX(N)                                          MOCS0292
      GR = ART*URT*DADXR                                                      MOCS0293
      G2 = A2(N)*U2(N)*DADX(N)                                                MOCS0294
      CALL SHEAR (ART,URT,CFR,FR,AOR)                                         MOCS0295
      CALL SHEAR (A2(N),U2(N),CF(N),F2,AO(N))                                 MOCS0296
      XLAM = BETA*(A2(N)/C2(N)**2*AO(N)/AO(1)*(U2(N) - DELC(N)*C2(N)) +       MOCS0297
     2   ART/CRT**2*AOR/AO(1)*(URT - DELCR*CRT))                              MOCS0298
      XGAM = DT/2.*(AO(N)/AO(1)*(A2(N)*(F2 + H2) + DELC(N)*C2(N)*G2)          MOCS0299
     2   + AOR/AO(1)*(ART*(FR + HR) + DELCR*CRT*GR)) - .5*(Q(N) + QRT)        MOCS0300
     3   *ALOG(AO(N)/AOR)                                                     MOCS0301
      P2(N) = (X1 + X2*(QRT - XLAM/2.*PRT - XGAM) - X3)/(1. - X2*XLAM         MOCS0302
     2   /2.)                                                                 MOCS0303
      IF (ABS(P2(N)).LT.100.0) GO TO 21                                       MOCS0304
      IF (ABS(P2(N)).GT.ABS(2.*P1(N))) P2(N) = 2.*P1(N)                       MOCS0305
   21 CONTINUE                                                                MOCS0306
      Q(N) = QRT + XLAM/2.*(P2(N) - PRT) - XGAM                               MOCS0307
      CALL ZINT(2,A2(N),P2(N))                                                MOCS0308
      CALL ZINT(3,A2(N),C2(N))                                                MOCS0309
      U2(N) = Q(N)/A2(N)*AO(1)/AO(N)                                          MOCS0310
      QB2 = 1./(AO(1)*CO(1)*R2 + AO(1)*XL*DT/2./CV)*(PC1 - PB + AO(1)*        MOCS0311
     2   XL/CV*(VM + DT/2.*(Q(N) + Q1(N) - QB)))                              MOCS0312
      XPSI = EL2*(QB2 - QB)/DT                                                MOCS0313
   20 CONTINUE                                                                MOCS0314
      VM = VM + DT/2.*(Q(N) + Q1(N) - QB2 - QB)                               MOCS0315
      QB1 = QB                                                                MOCS0316
      QB = QB2                                                                MOCS0317
C                                                                             MOCS0318
C        UPSTREAM BOUNDARY CONDITIONS (X=0)                                   MOCS0319
C                                                                             MOCS0320
      CLT = C1(1)                                                             MOCS0321
      ULT = U1(1)                                                             MOCS0322
      DELCL = DELC(1)                                                         MOCS0323
      DO 30 K=1,2                                                             MOCS0324
```

```
      XLT = XLT1(X(1),DT,U2(1),C2(1),DELC(1))                          MOCS0325
      QLT = YINT(X(1),XLT,Q1(1),Q1(2))                                 MOCS0326
      AIT = YINT(X(1),XLT,A1(1),A1(2))                                 MOCS0327
      AOL = YINT(X(1),XLT,AO(1),AO(2))                                 MOCS0328
      CFL = YINT(X(1),XLT,CF(1),CF(2))                                 MOCS0329
      DPXL = YINT(X(1),XLT,DPX(1),DPX(2))                              MOCS0330
      DELCL = YINT(X(1),XLT,DELC(1),DELC(2))                           MOCS0331
      DADXL = YINT(X(1),XLT,DADX(1),DADX(2))                           MOCS0332
      DCDXL = YINT(X(1),XLT,DCDX(1),DCDX(2))                           MOCS0333
      CALL ZINT(1,ALT,PLT)                                             MOCS0334
      CALL ZINT(3,ALT,CLT)                                             MOCS0335
      ULT = QLT/ALT*AO(1)/AOL                                          MOCS0336
      CALL SHEAR (ALT,ULT,CFL,FL,AOL)                                  MOCS0337
      CALL SHEAR (A2(1),U2(1),CF(1),F2,AO(1))                          MOCS0338
      HL = DPXL + 2.*PLT*DCDXL                                         MOCS0339
      H2 = DPX(1) + 2.*P2(1)*DCDX(1)                                   MOCS0340
      GL = ALT*ULT*DADXL                                               MOCS0341
      G2 = A2(1)*U2(1)*DADX(1)                                         MOCS0342
      XA = .5*(A2(1)*(F2 + H2) - DELC(1)*C2(1)*G2 + AOL/AO(1)*         MOCS0343
     2    (ALT*(FL + HL) - DELCL*CLT*GL))*DT - .5*(Q(1) + AO(1)/AOL*QLT)MOCS0344
     3    *(1. - AOL/AO(1))                                            MOCS0345
      XB = BETA/2.*(A2(1)*(U2(1) + DELC(1)*C2(1))/C2(1)**2 + ALT*AOL/  MOCS0346
     2    AO(1)*(ULT + DELCL*CLT)/CLT**2)                              MOCS0347
      Q(1) = ((PA -PEU)/XKP - PLT + (QLT - XA)/XB)/(1./XB + XC)        MOCS0348
      P2(1) = PLT + (Q(1) - QLT + XA)/XB                               MOCS0349
      CALL ZINT (2,A2(1),P2(1))                                        MOCS0350
      CALL ZINT(3,A2(1),C2(1))                                         MOCS0351
      U2(1) = Q(1)/A2(1)                                               MOCS0352
   30 CONTINUE                                                         MOCS0353
C                                                                      MOCS0354
C        CALCULATE HEAD LOSS PARAMETER DUE TO FLOW SEPARATION          MOCS0355
C                                                                      MOCS0356
      KOLD = KFD                                                       MOCS0357
      AMAX = 0.                                                        MOCS0358
      AMIN = 2.                                                        MOCS0359
      DO 41 K=2,MN                                                     MOCS0360
```

```
      IF (A2(K).LE.AMAX) GO TO 40                                       MOCS0361
      AMAX = A2(K)                                                      MOCS0362
      KMAX = K                                                          MOCS0363
 40   IF (A2(K).GE.AMIN) GO TO 41                                       MOCS0364
      AMIN = A2(K)                                                      MOCS0365
      KMIN = K                                                          MOCS0366
      KFD = K                                                           MOCS0367
      IF (KFD.GT.KSTP) KFD = KSTP                                       MOCS0368
 41   CONTINUE                                                          MOCS0369
      IF (((KFD/2)*2).EQ.KFD) GO TO 42                                  MOCS0370
      KFD = KFD + 1                                                     MOCS0371
 42   IF (KFD.EQ.KOLD) GO TO 44                                         MOCS0372
      IF (KFD.GT.KOLD) GO TO 43                                         MOCS0373
      U2(KOLD) = UFD                                                    MOCS0374
      U1(KOLD) = UFD                                                    MOCS0375
      P2(KOLD) = PFD                                                    MOCS0376
      A2(KOLD) = AFD                                                    MOCS0377
      A1(KOLD) = AFD                                                    MOCS0378
      Q(KOLD) = UFD*AFD*AO(KOLD)/AO(1)                                  MOCS0379
      Q1(KOLD) = Q(KOLD)                                                MOCS0380
      CALL ZINT (3,AFD,C2(KOLD))                                        MOCS0381
 43   UFD = U2(KFD)                                                     MOCS0382
      PFD = P2(KFD)                                                     MOCS0383
      AFD = A2(KFD)                                                     MOCS0384
 44   CONTINUE                                                          MOCS0385
      XLMB = 1. - ((1. - AO(KMIN)*A2(KMIN)/AO(KMAX)/A2(KMAX))**2/       MOCS0386
     2    (1. - (AO(KMIN)*A2(KMIN)/AO(KMAX)/A2(KMAX))**2))              MOCS0387
C                                                                       MOCS0388
C        SOLUTION USING CHARACTERISTIC EQUATIONS UP TO K=KFD             MOCS0389
C                                                                       MOCS0390
      DO 56 K=2,MN                                                      MOCS0391
      IF (K.EQ.(KFD+1)) GO TO 60                                        MOCS0392
      NX = 0                                                            MOCS0393
      CRT = C1(K)                                                       MOCS0394
      URT = U1(K)                                                       MOCS0395
      CLT = C1(K)                                                       MOCS0396
```

```
      ULT = U1(K)                                                       MOCS0397
      DELCR = DELC(K)                                                   MOCS0398
      DELCL = DELC(K)                                                   MOCS0399
50    IF (U1(K).GE.(DELC(K)*C1(K))) GO TO 51                            MOCS0400
      XLT = XLT1(X(K),DT,U2(K),C2(K),DELC(K))                           MOCS0401
      ALT = YINT(X(K),XLT,A1(K),A1(K+1))                                MOCS0402
      QLT = YINT(X(K),XLT,Q1(K),Q1(K+1))                                MOCS0403
      CFL = YINT(X(K),XLT,CF(K),CF(K+1))                                MOCS0404
      AOL = YINT(X(K),XLT,AO(K),AO(K+1))                                MOCS0405
      DPXL = YINT(X(K),XLT,DPX(K),DPX(K+1))                             MOCS0406
      DCDXL = YINT(X(K),XLT,DCDX(K),DCDX(K+1))                          MOCS0407
      DADXL = YINT(X(K),XLT,DADX(K),DADX(K+1))                          MOCS0408
      DELCL = YINT(X(K),XLT,DELC(K),DELC(K+1))                          MOCS0409
      GO TO 52                                                          MOCS0410
51    XLT = XLT1(X(K),DT,U2(K),C2(K),DELC(K))                           MOCS0411
      ALT = YINT(X(K-1),XLT,A1(K-1),A1(K))                              MOCS0412
      QLT = YINT(X(K-1),XLT,Q1(K-1),Q1(K))                              MOCS0413
      CFL = YINT(X(K-1),XLT,CF(K-1),CF(K))                              MOCS0414
      AOL = YINT(X(K-1),XLT,AO(K-1),AO(K))                              MOCS0415
      DPXL = YINT(X(K-1),XLT,DPX(K-1),DPX(K))                           MOCS0416
      DCDXL = YINT(X(K-1),XLT,DCDX(K-1),DCDX(K))                        MOCS0417
      DADXL = YINT(X(K-1),XLT,DADX(K-1),DADX(K))                        MOCS0418
      DELCL = YINT(X(K-1),XLT,DELC(K-1),DELC(K))                        MOCS0419
52    XRT = XRT1(X(K),DT,U2(K),C2(K),DELC(K))                           MOCS0420
      ART = YINT(X(K-1),XRT,A1(K-1),A1(K))                              MOCS0421
      QRT = YINT(X(K-1),XRT,Q1(K-1),Q1(K))                              MOCS0422
      CFR = YINT(X(K-1),XRT,CF(K-1),CF(K))                              MOCS0423
      AOR = YINT(X(K-1),XRT,AO(K-1),AO(K))                              MOCS0424
      DPXR = YINT(X(K-1),XRT,DPX(K-1),DPX(K))                           MOCS0425
      DCDXR = YINT(X(K-1),XRT,DCDX(K-1),DCDX(K))                        MOCS0426
      DADXR = YINT(X(K-1),XRT,DADX(K-1),DADX(K))                        MOCS0427
      DELCR = YINT(X(K-1),XRT,DELC(K-1),DELC(K))                        MOCS0428
      CALL ZINT (1,ALT,PLT)                                             MOCS0429
      CALL ZINT (1,ART,PRT)                                             MOCS0430
      CALL ZINT(3,ART,CRT)                                              MOCS0431
      CALL ZINT(3,ALT,CLT)                                              MOCS0432
```

```
      URT = QRT/ART*AO(1)/AOR                                                  MOCS0433
      ULT = QLT/ALT*AO(1)/AOL                                                  MOCS0434
      CALL SHEAR (ALT,ULT,CFL,FL,AOL)                                          MOCS0435
      CALL SHEAR (ART,URT,CFR,FR,AOR)                                          MOCS0436
      HL = DPXL + 2.*PLT*DCDXL                                                 MOCS0437
      H2 = DPX(K) + 2.*P2(K)*DCDX(K)                                           MOCS0438
      GL = ALT*ULT*DADXL                                                       MOCS0439
      G2 = A2(K)*U2(K)*DADX(K)                                                 MOCS0440
      HR = DPXR + 2.*PRT*DCDXR                                                 MOCS0441
      GR = ART*URT*DADXR                                                       MOCS0442
53    CALL SHEAR (A2(K),U2(K),CF(K),F2,AO(K))                                  MOCS0443
      CRR = 1./CRT/DELCR + 1./C2(K)/DELC(K)                                    MOCS0444
      CLL = 1./CLT/DELCL + 1./C2(K)/DELC(K)                                    MOCS0445
      XU2 = U2(K)                                                              MOCS0446
      XA2 = A2(K)                                                              MOCS0447
      U2(K) = (CRR*URT + CLL*ULT + 2.*ALOG(ART/ALT) - DT*(2.*(F2 + H2)         MOCS0448
     2   /DELC(K)/C2(K) + (FR + HR)/DELCR/CRT + (FL + HL)/DELCL/CLT            MOCS0449
     3   + GR/ART - GL/ALT))/(CRR + CLL)                                       MOCS0450
      A2(K) = ALT*EXP(CLL/2.*(U2(K) - ULT) + DT/2.*((F2 + H2)/DELC(K)/         MOCS0451
     2   C2(K) + (FL + HL)/DELCL/CLT - G2/A2(K) - GL/ALT))                     MOCS0452
      CALL ZINT (3,A2(K),C2(K))                                                MOCS0453
      IF (NX.GE.5) GO TO 54                                                    MOCS0454
      NX = NX + 1                                                              MOCS0455
      IF (NX.EQ.1) GO TO 50                                                    MOCS0456
      IF (ABS((XA2 - A2(K))/A2(K)).GE.0.01) GO TO 50                           MOCS0457
      IF (ABS((XU2 - U2(K))/U2(K)).LE.0.01) GO TO 55                           MOCS0458
      GO TO 50                                                                 MOCS0459
54    WRITE (6,200) XA2, A2(K)                                                 MOCS0460
200   FORMAT (10X,'ITERATION REQUIREMENTS NOT SATISFIED, XA2 = ',              MOCS0461
     2   F7.3,' A2(K) = ',F7.3)                                                MOCS0462
55    Q(K) = U2(K)*A2(K)*AO(K)/AO(1)                                           MOCS0463
      CALL ZINT(1,A2(K),P2(K))                                                 MOCS0464
      TCHK = DX/(U2(K) + DELC(K)*C2(K))                                        MOCS0465
      IF (TCHK.LT.TCHKM) TCHKM = TCHK                                          MOCS0466
56    CONTINUE                                                                 MOCS0467
      GO TO 70                                                                 MOCS0468
```

```
C                                                                       MOCS0469
C         SOLUTION USING DIFFERENCE EQUATIONS BEGINNING AT K=KFD        MOCS0470
C                                                                       MOCS0471
 60    AFD1 = AFD                                                       MOCS0472
       UFD1 = UFD                                                       MOCS0473
       KLT = KFD + 1                                                    MOCS0474
       KLS = KFD + 2                                                    MOCS0475
       DO 65 KIT=1,3                                                    MOCS0476
       NDEL = 1                                                         MOCS0477
       DO 62 K=KLS,MN                                                   MOCS0478
       IF (NDEL.EQ.1) GO TO 61                                          MOCS0479
       CALL SHEAR (A2(K),U2(K),CF(K),F2,AO(K))                          MOCS0480
       IF (K.LE.KMAX) YLAM = XLMB                                       MOCS0481
       IF (U2(K).LE.0.0) YLAM= 1.0                                      MOCS0482
       IF (K.GT.KMAX) YLAM = 1.0                                        MOCS0483
       U2(K) = U1(K) - DT*(YLAM*(U2(K+1)**2 - U2(K-1)**2)/4./DX +       MOCS0484
      2    BETA/CO(1)**2*(CO(K+1)**2*P2(K+1) - CO(K-1)**2*P2(K-1))/2./DX MOCS0485
      3    + DPX(K) + F2)                                              MOCS0486
       IF (U2(K).LE.0.0) U2(K) = 0.0                                    MOCS0487
       NDEL = 1                                                         MOCS0488
       GO TO 62                                                         MOCS0489
 61    A2(K) = A1(K) - DT/2.*(AO(K+1)*A2(K+1)*U2(K+1) - AO(K-1)*A2(K-1)* MOCS0490
      2    U2(K-1))/DX/AO(K) + QL(K)*DT*XL/CO(1)/AO(K)                  MOCS0491
       IF (A2(K).LT.0.0) A2(K) = 0.5*A2(K-2)                            MOCS0492
       NDEL = 2                                                         MOCS0493
 62    CONTINUE                                                         MOCS0494
       YLAM = XLMB                                                      MOCS0495
       CALL SHEAR (A2(KLT),U2(KLT),CF(KLT),F2,AO(KLT))                  MOCS0496
       U2(KLT) = U1(KLT) - DT*(YLAM*(U2(KFD+2)**2 - UFD**2)/4./DX +     MOCS0497
      2    BETA/CO(1)**2*(CO(KFD+2)**2*P2(KFD+2) - CO(KFD)**2*PFD)/2./DX MOCS0498
      3    + DPX(KLT) + F2)                                            MOCS0499
       IF (U2(KLT).LE.0.0) U2(KLT) = 0.0                                MOCS0500
       AFD = AFD1 - DT/2.*(AO(KLT)*A2(KLT)*U2(KLT) - AO(KFD-1)*A2(KFD-1) MOCS0501
      2    *U2(KFD-1))/DX/AO(KFD) + QL(KFD)*DT*XL/CO(1)/AO(KFD)        MOCS0502
       IF (AFD.LT.0.0) AFD = 0.5*A2(KFD)                                MOCS0503
       A2(KLT) = .5*(A2(KFD+2) + AFD)                                   MOCS0504
```

```
      CALL ZINT (1,A2(KLT),P2(KLT))                                     MOCS0505
      Q(KLT) = A2(KLT)*U2(KLT)*AO(KLT)/AO(1)                            MOCS0506
      UFD = .5*(U2(KLT) + U2(KFD-1))                                    MOCS0507
      CALL ZINT (1,AFD,PFD)                                             MOCS0508
      DO 63 KR=KLS,MFND,2                                               MOCS0509
      K = KR + 1                                                        MOCS0510
      A2(K) = .5*(A2(K+1) + A2(K-1))                                    MOCS0511
      CALL ZINT (1,A2(K),P2(K))                                         MOCS0512
 63   Q(K) = A2(K)*U2(K)*AO(K)/AO(1)                                    MOCS0513
      DO 64 KR=KFD,MFND,2                                               MOCS0514
      K = KR + 2                                                        MOCS0515
      CALL ZINT (1,A2(K),P2(K))                                         MOCS0516
 64   U2(K) = .5*(U2(K+1) + U2(K-1))                                    MOCS0517
 65   CONTINUE                                                          MOCS0518
      NDEL = 1                                                          MOCS0519
      DO 67 K=KLT,MN                                                    MOCS0520
      CALL ZINT (3,A2(K),C2(K))                                         MOCS0521
      IF ((K/2)*2.NE.K) GO TO 66                                        MOCS0522
      Q(K) = A2(K)*U2(K)*AO(K)/AO(1)                                    MOCS0523
 66   TCHK = DX/(U2(K) + DELC(K)*C2(K))                                 MOCS0524
      IF (TCHK.LT.TCHKM) TCHKM = TCHK                                   MOCS0525
 67   CONTINUE                                                          MOCS0526
 70   CONTINUE                                                          MOCS0527
C                                                                       MOCS0528
C        PUNCHED OUTPUT OF CONDITIONS AT PROGRAM TERMINATION            MOCS0529
C                                                                       MOCS0530
 80   WRITE (7,250) A2, Q                                               MOCS0531
 250  FORMAT (8F10.5)                                                   MOCS0532
      STOP                                                              MOCS0533
      END                                                               MOCS0534
```

```
C
C       ***************************************************************
C
C       SUBROUTINE SHEAR (A, U, XMU, FF, AO)
C
C       THIS SUBROUTINE PROVIDES VALUES FOR FLOW RESISTANCE.
C       THE APPROPRIATE COMPUTATIONAL FORM IS SELECTED BY
C       CONSIDERING THE BOUNDARY LAYER THICKNESS AND REYNOLDS
C       NUMBER OF THE FLOW LOCALLY.
C
C       ***************************************************************
C
      COMMON/CHEAR/RHO, T, DT, XL, QI, CO , NO
      IF ((U*A).GT.(2.*QI)) NQ = 1
      IF (NQ.GE.1) GO TO 200
      GO TO 214
  200 DE = 4.*(XMU*T*XL/RHO/CO)**.5
      IF(A - .27)201, 201, 202
  201 D = (2.*A*AO/3.141)**.5
      GO TO 203
  202 D = (4.*A*AO/3.141)**.5
  203 RE = ABS(RHO*CO*U*D/XMU)
      R = D/2.
      IF(RE - 4000.)204, 204, 205
  204 IF(DE - R)206, 206, 207
  205 IF(A - .27)208, 208, 209
C
C       TURBULENT FLOW IN COLLAPSED TUBE
C
  208 FF = .3164/4.*(2.*3.141/(AO*A))**.5*RHO*CO**2 /RE**.25*U**3 /(U**2
     1 )**.5
      GO TO 215
C
C       TURBULENT FLOW IN OPEN TUBE
C
  209 FF = .3164/4.*(3.141/AO)**.5*RHO*CO**2 /(A*RE**.25*(U**2 )**.5)*U*
```

SHEA0001 SHEA0002 SHEA0003 SHEA0004 SHEA0005 SHEA0006 SHEA0007 SHEA0008 SHEA0009 SHEA0010 SHEA0011 SHEA0012 SHEA0013 SHEA0014 SHEA0015 SHEA0016 SHEA0017 SHEA0018 SHEA0019 SHEA0020 SHEA0021 SHEA0022 SHEA0023 SHEA0024 SHEA0025 SHEA0026 SHEA0027 SHEA0028 SHEA0029 SHEA0030 SHEA0031 SHEA0032 SHEA0033 SHEA0034 SHEA0035 SHEA0036

```
     2*3                                                                SHEA0037
      GO TO 215                                                         SHEA0038
 206  IF(A - .27)210, 210, 211                                          SHEA0039
C                                                                       SHEA0040
C      DEVELOPING BOUNDARY LAYER FLOW IN COLLAPSED TUBE                 SHEA0041
C                                                                       SHEA0042
 210  FF = (32.*CO**3/XL/AO/A/XMU*RHO/T)**.5*XMU*U                      SHEA0043
      GO TO 215                                                         SHEA0044
C                                                                       SHEA0045
C      DEVELOPING BOUNDARY LAYER FLOW IN OPEN TUBE                      SHEA0046
C                                                                       SHEA0047
 211  FF = 4.*(CO**3/XL/AO/XMU*RHO/T)**.5*XMU*U/A                       SHEA0048
      GO TO 215                                                         SHEA0049
 207  IF(A - .36)212, 212, 213                                          SHEA0050
C                                                                       SHEA0051
C      FULLY DEVELOPED LAMINAR FLOW IN COLLAPSED TUBE                   SHEA0052
C                                                                       SHEA0053
 212  FF = 70.*XMU*CO*U/AO/A                                            SHEA0054
      GO TO 215                                                         SHEA0055
C                                                                       SHEA0056
C      FULLY DEVELOPED LAMINAR FLOW IN OPEN TUBE                        SHEA0057
C                                                                       SHEA0058
 213  IF (A.GE.1.0) GO TO 214                                           SHEA0059
      FF = 8.*3.141*XMU*CO*U/AO/A**2                                    SHEA0060
      GO TO 215                                                         SHEA0061
 214  FF = 8.*3.141*XMU*CO*U/AO/A                                       SHEA0062
 215  FF2 = 8.*3.141*XMU*CO*U/AO/A                                      SHEA0063
      IF (ABS(FF2).GT.ABS(FF)) FF = FF2                                 SHEA0064
      FF = XL*FF/RHO/CO**2                                              SHEA0065
      RETURN                                                            SHEA0066
      END                                                               SHEA0067
```

```
C                                                                       ZINT0001
C       ***************************************************************ZINT0002
C                                                                       ZINT0003
        SUBROUTINE ZINT (L, YA, PC)                                     ZINT0004
C                                                                       ZINT0005
C       USING ONE OF THREE DIFFERENT RELATIONSHIPS, THIS                ZINT0006
C       SUBROUTINE DETERMINES CORRESPONDING VALUES OF A, P, OR C.       ZINT0007
C                                                                       ZINT0008
C       ***************************************************************ZINT0009
C                                                                       ZINT0010
      DIMENSION AUX1(10),AUX2(10),AUX3(10)                              ZINT0011
      COMMON A(25), BETA                                                ZINT0012
      COMMON/CINT/P(25), C(25)                                          ZINT0013
      IF (L.EQ.2) GO TO 306                                             ZINT0014
      IF (YA.GE.0.7) GO TO 304                                          ZINT0015
      IF (YA.LE.0.02512) GO TO 302                                      ZINT0016
C                                                                       ZINT0017
C       DETERMINE VALUE OF C OR P CORRESPONDING TO A PARTICULAR         ZINT0018
C       VALUE OF A                                                      ZINT0019
C                                                                       ZINT0020
C       TABULATED FUNCTIONS                                             ZINT0021
C                                                                       ZINT0022
      IF(L.EQ.1) GO TO 301                                              ZINT0023
      CALL IVP (A,0,C,25,YA,3,0.05,PC,AUX1,IER1)                        ZINT0024
      GO TO 310                                                         ZINT0025
  301 CALL IVP (A,0,P,25,YA,3,0.05,PC,AUX2,IER2)                        ZINT0026
      GO TO 310                                                         ZINT0027
C                                                                       ZINT0028
C       SIMILARITY REGION                                               ZINT0029
C                                                                       ZINT0030
  302 IF(L.EQ.1) GO TO 303                                              ZINT0031
      PC = (1.5/YA**1.5*BETA)**.5                                       ZINT0032
      GO TO 310                                                         ZINT0033
  303 PC = -1./YA**1.5                                                  ZINT0034
      GO TO 310                                                         ZINT0035
C                                                                       ZINT0036
```

```
C         LINEAR REGION                                                  ZINT0037
C                                                                        ZINT0038
 304  IF (L.EQ.1) GO TO 305                                             ZINT0039
      PC = (BETA/0.235*EXP(YA/0.235))**.5                               ZINT0040
      GO TO 310                                                         ZINT0041
 305  PC = EXP(YA/0.235)                                                ZINT0042
      GO TO 310                                                         ZINT0043
C                                                                       ZINT0044
C         DETERMINE VALUE OF A CORRESPONDING TO A PARTICULAR VALUE OF P ZINT0045
C                                                                       ZINT0046
 306  IF (PC.LE.-251.) GO TO 307                                        ZINT0047
      IF (PC.GE.19.7) GO TO 308                                         ZINT0048
C                                                                       ZINT0049
C         TABULATED FUNCTION                                            ZINT0050
C                                                                       ZINT0051
      CALL IVP (P,0,A,25,PC,3,0.05,YA,AUX3,IER3)                        ZINT0052
      GO TO 310                                                         ZINT0053
C                                                                       ZINT0054
C         SIMILARITY REGION                                             ZINT0055
C                                                                       ZINT0056
 307  YA = 1./(-PC)**.667                                               ZINT0057
      GO TO 310                                                         ZINT0058
C                                                                       ZINT0059
C         LINEAR REGION                                                 ZINT0060
C                                                                       ZINT0061
 308  YA = 0.235*ALOG(PC)                                               ZINT0062
 310   CONTINUE                                                         ZINT0063
      RETURN                                                            ZINT0064
      END                                                               ZINT0065
C                                                                       ZINT0066
C         *****ALTERNATE FORM USED FOR LATEX TUBES**********************ZINT0067
C                                                                       ZINT0068
      SUBROUTINE ZINT (L, YA, PC)                                       ZINT0069
C                                                                       ZINT0070
C         USING ONE OF THREE DIFFERENT RELATIONSHIPS, THIS              ZINT0071
C         SUBROUTINE DETERMINES CORRESPONDING VALUES OF A, P, OR C.     ZINT0072
```

```
C                                                                       ZINT0073
C     ********************************************************          ZINT0074
C                                                                       ZINT0075
      DIMENSION AUX1(10),AUX2(10),AUX3(10)                              ZINT0076
      COMMON A(62), XK, BETA                                            ZINT0077
      COMMON/CINT/P(62),C(62)                                           ZINT0078
      IF (L.EQ.2) GO TO 306                                             ZINT0079
      IF (YA.GE.1.1054) GO TO 304                                       ZINT0080
      IF (YA.LE.0.165) GO TO 302                                        ZINT0081
C                                                                       ZINT0082
C        DETERMINE VALUE OF C OR P CORRESPONDING TO A PARTICULAR        ZINT0083
C        VALUE OF A                                                     ZINT0084
C                                                                       ZINT0085
C        TABULATED FUNCTIONS                                            ZINT0086
C                                                                       ZINT0087
      IF(L.EQ.1) GO TO 301                                              ZINT0088
      CALL IVP (A,0,C,62,YA,5,0.05,PC,AUX1,IER1)                        ZINT0089
      GO TO 310                                                         ZINT0090
  301 CALL IVP (A,0,P,62,YA,5,0.05,PC,AUX2,IER2)                        ZINT0091
      GO TO 310                                                         ZINT0092
C                                                                       ZINT0093
C        SIMILARITY REGION                                              ZINT0094
C                                                                       ZINT0095
  302 IF(L.EQ.1) GO TO 303                                              ZINT0096
      PC = (1.5/YA**1.5*BETA)**.5                                       ZINT0097
      GO TO 310                                                         ZINT0098
  303 PC = -1./YA**1.5                                                  ZINT0099
      GO TO 310                                                         ZINT0100
C                                                                       ZINT0101
C        LINEAR REGION                                                  ZINT0102
C                                                                       ZINT0103
  304 IF (L.EQ.1) GO TO 305                                             ZINT0104
      PC = (YA*BETA/XK)**.5                                             ZINT0105
      GO TO 310                                                         ZINT0106
  305 PC = (YA - 1.0766)/XK                                             ZINT0107
      GO TO 310                                                         ZINT0108
```

```
C                                                                       ZINT0109
C        DETERMINE VALUE OF A CORRESPONDING TO A PARTICULAR VALUE OF P  ZINT0110
C                                                                       ZINT0111
 306  IF (PC.LE.-15.) GO TO 307                                         ZINT0112
      IF (PC.GE.60.) GO TO 308                                          ZINT0113
C                                                                       ZINT0114
C        TABULATED FUNCTION                                             ZINT0115
C                                                                       ZINT0116
      CALL IVP (P,0,A,62,PC,5,0.05,YA,AUX3,IER3)                        ZINT0117
      GO TO 310                                                         ZINT0118
C                                                                       ZINT0119
C        SIMILARITY REGION                                              ZINT0120
C                                                                       ZINT0121
 307  YA = 1./(-PC)**.667                                               ZINT0122
      GO TO 310                                                         ZINT0123
C                                                                       ZINT0124
C        LINEAR REGION                                                  ZINT0125
C                                                                       ZINT0126
 308  YA = 1.0766 + XK*PC                                               ZINT0127
 310   CONTINUE                                                         ZINT0128
      RETURN                                                            ZINT0129
      END                                                               ZINT0130
C                                                                       ZINT0131
C        ***************************************************************ZINT0132
C                                                                       ZINT0133
```

APPENDIX D:

EXPERIMENTS FOR DETERMINING THE STRUCTURAL PROPERTIES OF COLLAPSING VESSELS

In an earlier discussion we developed the theoretical approach to the analysis of tube collapse. The characteristic most sought after was the constitutive expression relating vessel cross-sectional area to transmural pressure, termed the "tube law." This appendix includes a discussion of the experiments that were conducted to examine the validity and limitations of the existing theories. The results are analyzed in a way that will help us to predict the constitutive relation for tubes of known geometry and composition.

The techniques available to use for obtaining this information fall into two general categories:

- Direct determination of the pressure-volume and hence pressure-area law by means of absolute volume/area/linear dimension and transmural pressure measurements.

- Deduction of this relationship from wave speed measurements which determine the slope of the P-α curve at a particular transmural pressure [see Eq. (3)].

A number of complicating factors arise when measuring wave speeds, including (1) dispersion or frequency dependence; (2) different propagation speeds for competing modes of wave propagation; and (3) interference due to wave reflections. Therefore we chose to use the former method.

When using the direct measurement method, problems arise when

estimating the wave speed using the derivative of an experimental curve. For this reason and for the benefit of all the results, much care was taken to design an apparatus with high precision.

The Experimental Apparatus

The apparatus is shown in Fig. 41. Illustrated here is the ram mechanism for volume changes, the vertical chamber to enclose the collapsible tube and the pressure varying and sensing equipment. The internal pressure is held constant by maintaining a consistent fluid level in the capillary tube while the external pressure is varied by raising or lowering the fluid reservoir. The ram which translates by way of a 32 thread/inch leadscrew measures the volume changes (to ± 10 $\mu\ell$) necessary to maintain a constant internal pressure. The pressures are recorded by observing the fluid level in two manometers using a cathetometer. The pressure can be determined to within ± 0.05 cm H_2O. The two independent hydraulic circuits for the internal and external systems are shown in the drawing.

Analysis of the Experimental Results

The results one obtains using this apparatus are complicated by the need to attach the collapsible tube to rigid supports inside the fluid chamber. As the tube collapses two problems arise.

First, in boundary regions adjacent to each of the two supports, the tube undergoes a transition from what appears to be a zone of uniform

collapse to a cross-section equal to that of the supporting structure. Within this boundary region the cross-sectional area varies longitudinally and is determined, in part, by the tension in the tube wall. The measured volume changes, ΔV_m , represent the sum of changes in a uniform tube essentially void of all end effects, ΔV , plus a volume change which is influenced by the presence of the two boundary regions, ΔV_b ; i.e., $\Delta V_m = \Delta V + \Delta V_b$.

Second, if the tube is constrained longitudinally, the wall tension increases as the vessel collapses. The variations in wall tension are easily eliminated by mounting the tube vertically within a chamber containing the same fluid as that inside the tube (to negate the effect of hydrostatic pressure gradients) and allowing the lower support, designed to be slightly negatively buoyant, to float freely, thus providing a constant longitudinal wall tension.

The effects associated with the boundary regions pose a more difficult problem. These, too, can be compensated for, however, in the following way. If a complete pressure-volume experiment is performed on two lengths of the same piece of tubing and if the boundary regions occupy less than the length of the shorter tube, then the end effects can be subtracted out because they should be identical in the two experiments. Using the terms defined earlier, the change in volume of the uniform tube, ΔV, is

$$\Delta V = \Delta V_{m_1} - \Delta V_{m_2} = \Delta V_1 + \Delta V_b + \Delta V_2 - \Delta V_b \qquad \text{(D-1)}$$

Here, ΔV represents the volume change taking place in a tube of length

$(L_1 - L_2)$ which is not influenced by the presence of rigid supports as shown in the sketch.

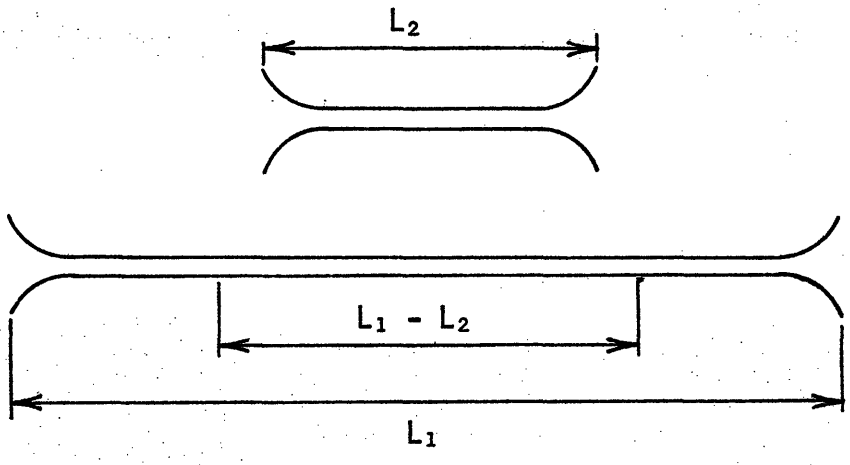

The raw data from these experiments was obtained in the form of (i) ram position; and (ii) transmural pressure (p_{tr}). The first step in the analysis of the data was to express the results in terms of $\Delta V_m/\Delta p_{tr}$ for each of the two tubes. The curves of $\Delta V_m/\Delta p_{tr}$ were smoothed numerically using the method of cubic splines and the difference,

$$\left.\frac{\Delta V_m}{\Delta p_{tr}}\right|_1 - \left.\frac{\Delta V_m}{\Delta p_{tr}}\right|_2 ,$$

was determined at the values of p_{tr} for one set of data, the corresponding values from the associated data being determined by interpolation. The result, using Eq. (D-1), is $\Delta V/\Delta p_{tr}$, the corrected value.

Next we postulate that for the range of transmural pressures within the similarity range of the theoretical result (see Chapter VIII) the relationship between pressure and area is

$$p_{tr} = -K_p(x)\left(\frac{A}{A_0}\right)^{-3/2} , \qquad (D\text{-}2)$$

where, according to the theory, $K_p(x) = \frac{E[h(x)/R]^3}{12(1-\nu^2)}$. For generality, we let h , the tube wall thickness, be a function of x , thus making K_p a function of x as well.

Equation (D-2) can be solved for A and integrated to give volume:

$$V = \int_0^L A\,dx = A_0(-p_{tr})^{-2/3}\left[\frac{E}{12R^2(1-\nu^2)}\right]^{2/3}\int_0^L h^2(x)dx \qquad (D\text{-}3)$$

from which we obtain

$$\frac{dV}{dp_{tr}} = \frac{2}{3}A_0\frac{\left[\frac{E}{12R^2(1-\nu^2)}\right]^{2/3}}{(-p_{tr})^{5/3}}\int_0^L h^2(x)\,dx . \qquad (D\text{-}4)$$

Replacing the differential term in Eq. (D-4) by the difference terms obtained experimentally, we can show that

$$\frac{\Delta V}{\Delta p_{tr}} \cong \frac{2}{3}A_0\frac{\left[\frac{E}{12R^2(1-\nu^2)}\right]^{2/3}}{(-p_{tr})^{5/3}}\left[\int_0^{L_1} h^2(x)\,dx - \int_0^{L_2} h^2(x)\,dx\right]$$

or, since tube 2 is a shortened version of tube 1,

$$\frac{\Delta V}{\Delta p_{tr}} \cong \frac{2}{3}A_0\frac{\left[\frac{E}{12R^2(1-\nu^2)}\right]^{2/3}}{(-p_{tr})^{5/3}}\int_0^{L_1-L_2} h^2(x)\,dx , \qquad (D\text{-}5)$$

where $h(x)$ is the wall thickness of the portion of tube 3 left over when tube 2 is cut from it.

Plotting $\Delta V/\Delta p_{tr}$ against $\frac{2}{3}(L_1-L_2)(-p_{tr})^{-5/3}$ should produce a straight line of slope

$$A_0\left[\frac{E}{12R^2(1-\nu^2)}\right]^{2/3}\frac{\int_0^{L_1-L_2} h^2(x)\,dx}{L_1-L_2},$$

if our previous assumption in writing Eq. (D-2) is valid. The actual curve fitting is done using the method of least squares and in each case a straight line gave an excellent fit to the experimental data.

The analysis up to and including Eq. (D-5) is completely general in terms of the functional form of $h(x)$. Therefore, regardless of how $h(x)$ varies, the experimental data should still be reducible by the method described above. One discrepancy should be noted, however. It was assumed initially that ΔV_b was identical for the two experiments. The value of $H(x)$ within the boundary region might, however, influence this quantity and prevent the cancellation necessary for the subsequent analysis. We felt that the small errors associated with this problem would not warrant a more detailed description of the boundary region but might in cases where the variations in $h(x)$ become much larger than those encountered in our experiments.

Returning to the data analysis procedure, upon obtaining the slope of the previously described curve, the actual volume of the uniform tube

can be computed using the expression:

$$V = A_0(-p_{tr})^{-2/3}\left[\frac{E}{12R^2(1-\nu^2)}\right]^{2/3}\frac{1}{L_1-L_2}\int_0^{L_1-L_2} h^2(x)\,dx \qquad (D\text{-}6)$$

up to the point which marks the upper bound of the similarity range (i.e., the range of pressures for which the straight line fit occurs).

The pressure-volume relation can be extended beyond this point simply by using the values of $\Delta V/\Delta p_{tr}$ in the following expression:

$$V = V_S + \int_{p_{tr_S}}^{p_{tr}} \frac{dV}{dp_{tr}}\,dp_{tr} \cong V_S + \sum_{n=1}^{N} \Delta V \quad , \qquad (D\text{-}7)$$

where the subscript "S" denotes a point in the similarity range. The resulting value of V corresponding to $p_{tr} = 0$ yields a value for A_0

$$A_0 = \frac{V}{L_1 - L_2} \quad . \qquad (D\text{-}8)$$

Knowing A_0, we can compute an experimental value for K_p using the slope from Eq. (D-5). (We actually compute an estimate of

$$\frac{E}{12R^2(1-\nu^2)}\,\frac{1}{L_1 - L_2}\int_0^{L_1-L_2} h^2(x)\,dx \quad .)$$

This is an averaged value of $K_p(x)$ and, if our definition of K_p is

correct,

$$K_{p_{exp}} = K_{p_{calc}} = \frac{E}{12R^2(1-\nu^2)} \frac{1}{L_1-L_2} \int_0^{L_1-L_2} h^2(x)\, dx \qquad (D\text{-}9)$$

where the integral in $K_{p_{calc}}$ is evaluated from the actual $h(x)$.

For the tubes used in these experiments, the wall thickness varied in an approximately linear fashion. The tubes were formed from a dipping process which accounts for this variation. If the wall thickness is expressed as $h(x) = h_0 + h_1 \frac{x}{L_1-L_2}$, the integral in (D-9) can be evaluated, giving

$$K_{p_{calc}} = \frac{E}{12R^2(1-\nu^2)} \left(h_0^2 + h_0 h_1 + \frac{h_1^3}{3} \right)^{3/2} \qquad (D\text{-}10)$$

Discussion

Table 7 summarizes the tube measurements and the experimental results. Because of the tedious nature of the experiments and the difficulty in developing the proper technique, only three sets of usable data were obtained. The agreement between the calculated and experimental values of K_p is good, however, considering that the measurement of wall thickness contains an error of $\pm 5 \times 10^{-4}$ cm . The effect of this error is amplified when we see that the wall thickness appears in the equation for K_p raised to the third power.

Figures 7 and 8 present all three sets of data on a normalized basis:

$$P = \frac{p_{tr}}{K_{p_{exp}}}$$

$$\alpha = \frac{A}{A_0} \quad .$$

Once again, the similarity region is clearly defined as all data fits well to a line having a slope of -3/2 on the log-log scale. Figure 8 illustrates the departure of the curves as we approach the range of positive transmural pressures. Since radial stretch and not bending are the dominant influences for this range, we would expect this departure. In fact, we can predict the slope of this portion of the curve using the results of Chapter VIII, where the relationship between pressure and area (or volume) is given by Eq. (54). The values of A_0 chosen in this way are also given in Table 7.

In between the similarity zone and the region of positive transmural pressures lies the portion of the curve encompassing intermediate collapsed states. In this region, the tube shape and area are primarily determined by the bending stiffness of the wall but are strongly affected by, for example, the shape of the unstressed tube and the presence of an elastic medium surrounding the tube. The effect of the surrounding medium is most pronounced in this region because large deformations occur over relatively minute changes in transmural pressure. We will consider this problem in more detail in the discussion of venous compliance found in Chapter XI.

Biographical Note

During my first eighteen years, beginning in 1950, I led a healthful, enjoyable life on the shores of Lake Superior in Northern Wisconsin. For college, I travelled to Evanston, Illinois and Northwestern University, where I remained for four years--long enough to earn a B.S. degree in Mechanical Engineering. I have my father's employers, Interlake Steamship Co., to thank for their generosity in providing complete financial support during my stay at NU.

Having never lived on the East Coast and possessing a certain curiosity of those who did, I moved on to Cambridge to attend MIT for graduate work in Mechanical Engineering. My first year yielded considerable confusion and an S.M. degree. My thesis and several publications were written on a novel opto-acoustic technique of measuring atmospheric pollutants.

Perhaps a much more notable accomplishment was my finding and eventually marrying Judy Brown, a native of Massachusetts.

I continued at MIT in search of a doctorate through the trauma of qualifying exams and the rigors of teaching the undergraduate fluid mechanics course. My interests during more recent years have focused on the field of biomedical fluid mechanics, in particular the investigation of biological flows through systems of collapsible vessels. My plans for the future are to continue doing research of this same general type in either an academic or clinical environment.